TABLE OF CONTENTS

WOOD

1 **DAS KONZEPT DER HOLZ „RAFFINERIE“**
H. Harms

9 **ASSESSING FUNGAL DECAY OF SPRUCE AND BEECH WOOD USING NEAR INFRARED SPECTROSCOPIC TECHNIQUES**
K. Fackler, M. Schwanninger, C. Gradinger, B. Hinterstoisser, and K. Messner

14 **THE INFLUENCE OF BEECH WOOD STORAGE ON THE PRODUCTION AND PROPERTIES OF REGENERATED VISCOSE FIBRES**
A. Promberger, H. K.Weber , C. Gradinger, K. Messner, and H. Sixta

PULP COOKING PROCESS

24 **PROBLEME DER UMSETZUNG NEUER TECHNOLOGIEN IN DIE INDUSTRIELLE PRAXIS, DARGESTELLT AM BEISPIEL DES ALKALISCHEN SULFITVERFAHRENS MIT AQ UND METHANOL - ASAM**
H.-L. Schubert

32 **COMPREHENSIVE KINETIC STUDY OF DELIGNIFICATION, CARBOHYDRATE DEGRADATION, CELLULOSE CHAIN SCISSIONS, AND HEXENURONIC ACID REACTIONS DURING KRAFT PULPING OF *EUCALYPTUS GLOBULUS***
H. Sixta and E. W. Rutkowska

46 **STUDIES ON PREHYDROLYIS SULFITE - STATEGIES TO MITIGATE THE EFFECTS OF LIGNIN DEACTIVATION DURING PREHYDROLYSIS**
M. Fasching, G. Kandioller, A. Griebl, and H. Sixta

56 **CALCULATION OF PHYSICAL PROPERTY DATA OF THE SYSTEM MGO-SO2-H2O AND THEIR IMPLEMENTATION IN ASPEN PLUS®**
K. Schöggl, M. Steindl, A. Friedl, H. K. Weber, and H. Sixta

PULP

63 **COMPARATIVE REMOVAL OF HEMICELLULOSES FROM PAPER PULPS USING NITREN, CUEN, NAOH, AND KOH**
J. Puls, R. Janzon, and B. Saake

71 **BLEICHE VON SAUREM FICHTENSULFITZELLSTOFF UNTER EINSATZ VON OZON**
O. Kordsachia und A. Reinhard

85 **CRYSTALLINITY DETERMINATION OF NATIVE CELLULOSE – COMPARISON OF ANALYTICAL METHODS**
T. Röder, J. Moosbauer, M. Fasching, A. Bohn, H.-P. Fink, T. Baldinger, and H. Sixta

PAPER

90 **A NOVEL DESTRUCTIVE APPROACH FOR 3D PAPER STRUCTURE ANALYSIS**
M. Wiltsche, M. Donoser, and W. Bauer

96 **A REVIEW OF IMAGE ANALYSIS BASED METHODS TO EVALUATE FIBER PROPERTIES**
U. Hirn and W. Bauer

106 **MAPPING OF THE AGING STATUS IN HISTORICAL PAPER BY FLUORESCENCE LABELING OF OXIDIZED GROUPS AND PH MEASUREMENTS**
U. Henniges, J. Smolle, T. Rosenau, P. Kosma, and A. Potthast

REGENERATED CELLULOSE

111 **SEC IN CELLULOSE XANTHATE ANALYSIS**
A. Rußler, A. Potthast, T. Rosenau, B. Saake, J. Puls, H. Sixta, and P. Kosma

116 **SPUNBOND CELLULOSE**
M. J. Hayhurst

124 **CELLULOSE MELTBLOWN NONWOVENS USING THE LYOCELL-PROCESS**
H. Ebeling, H.-P. Fink, M. Luo, and H.-G. Geus

132 **CRYSTALLINITY DETERMINATION OF MAN-MADE CELLULOSE FIBERS – COMPARISON OF ANALYTICAL METHODS**
T. Röder, J. Moosbauer, M. Fasching, A. Bohn, H.-P. Fink, T. Baldinger, and H. Sixta

137 **AEROCELL - AEROGELS FROM CELLULOSIC MATERIALS**
J. Innerlohinger, H. K. Weber, and G. Kraft

144 **BEITRAG ZUR STRUKTUR VON LYOCELLFASERN, ERSPONNEN AUS AMINOXIDHYDRATEN BZW. IONISCHEN FLÜSSIGKEITEN**
C. Michels und B. Kosan

154 **CELLULOSE PROCESSING WITH CHLORIDE-BASED IONIC LIQUIDS**
G. Bentivoglio, T. Röder, M. Fasching, M. Buchberger, H. Schottenberger, and H. Sixta

DAS KONZEPT DER HOLZ „RAFFINERIE“

Haio Harms

Lenzing AG, Werkstraße 1, 4860 Lenzing, Austria

Es ist erstaunlich, aber noch immer ist nicht ausreichend bekannt, dass Holz eine der wichtigsten Primärressourcen für die österreichische Wirtschaft ist. 47% des Bundesgebietes sind von Wald bedeckt. Ein großer Teil dieser Flächen lässt sich nur forstlich wertschöpfend nutzen, da im Gegensatz zu anderen Nutzpflanzen Wald nur sehr geringe Anforderungen an Klima und Fruchtbarkeit der Böden hat. Von 3,9 Mio. ha Nutzwaldfläche werden jährlich rund 16 Millionen Festmeter Holz geerntet.

Rund 260.000 Menschen beziehen ihr direktes Einkommen aus der Holzproduktion und Holzverarbeitung. Indirekt aber sichert dieser Bereich die Lebensgrundlage für viel mehr Österreicher. Die Arbeitsplätze liegen dabei im Bereich von Dienstleistern im ansonsten mit sicheren Arbeitsplätzen nicht gut versorgten ländlichen Raum. Darüber hinaus lebt eine überraschende Anzahl von arbeitsintensiven Industriezweigen von der Weiterverarbeitung der primären Holzprodukte (Verpackung, Druck, Textil, Hygiene, ...). Den Investitionen dieser kapitalintensiven Branchen wiederum verdankt eine Vielzahl von diversifizierten und Know-how-intensiven Engineering- und Anlagenbau-Unternehmen ihre für Österreich überraschende, oftmals weltweit führende Position.

Tatsache ist, dass es sich bei Holz und Holzverarbeitung um einen der wichtigsten Sektoren unserer Volkswirtschaft handelt. Österreich ist einer der größten Schnittholzproduzenten Europas und weltweit einer der wichtigsten Exporteure von Zellstoff und Zellstoffprodukten. Mit einem Produktionswert von etwa 10 Mrd. € (etwa 4% der österreichischen Wirtschaftsleistung) wird ein Exportüberschuss von 3,3 Mrd. € erwirtschaftet (Abb. 1). Der Großteil davon stammt aus der chemischen „Veredelung“ des Holzes, rund 15% allein von der Lenzing AG und den österreichischen Weiterverarbeitern der Lenzinger Fasern. Lenzing bezieht rund 95% des österreichischen Buchenindustrieholzes.

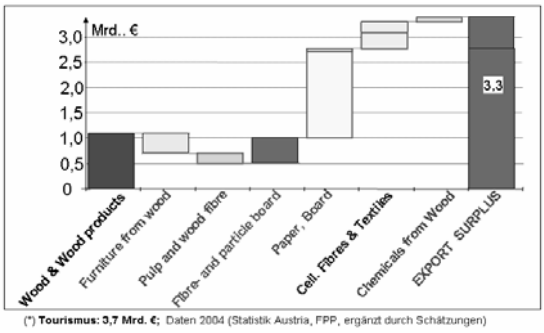

Abbildung 1. Exportüberschuss Österreichs im Bereich Holz und Holzverarbeitung [1].

Damit ist der Sektor im klassischen Tourismusland Österreich gemeinsam mit dem Fremdenverkehr an erster und zweiter Stelle in der Bedeutung für die Zahlungsbilanz: Holz ist der wichtigste „Bodenschatz“ Österreichs!

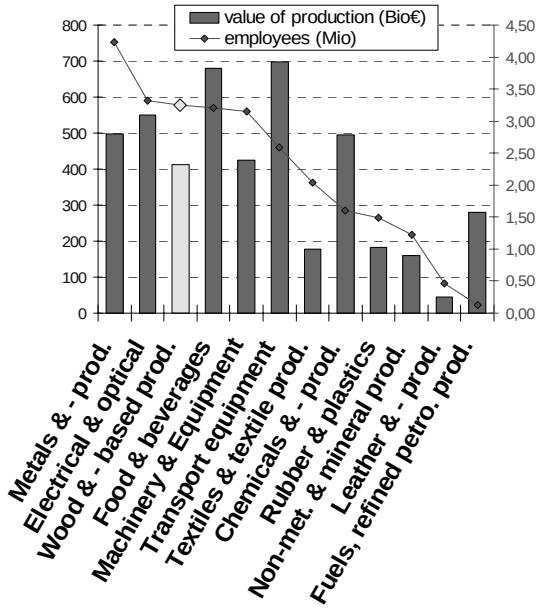

Abbildung 2. Industrial sectors EU(15) 2001 [1].

Wenn auch nicht ganz so ausgeprägt, so stimmt dieses Bild aber ebenfalls für die gesamte EU. Ausgehend von einer bewaldeten Fläche von rund 24% des EU Territoriums boten die Industrien des Forst-Clusters schon im Jahr 2001 bereits für fast 3,5 Mio. Mitarbeiter Arbeit in von KMU's dominierten Branchen und darüber hinaus Einkommen für rund 12 Mio. Forstbesitzer vorwiegend in rein ländlichen Gebieten. In der Beschäftigung ist dies mit rund 12% die dritte Stelle hinter der Metall- und Elektroindustrie (Abb. 2). Mit 400 Mrd. € werden etwa 9% des europäischen Produktionswertes erwirtschaftet.

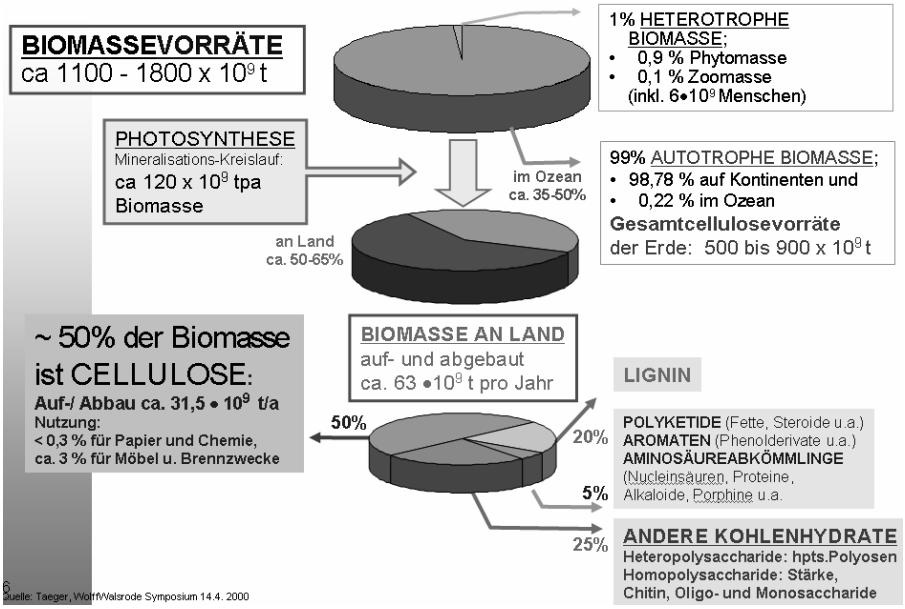

Abbildung 3. Zusammensetzung der Biomassevorräte auf der Erde [2].

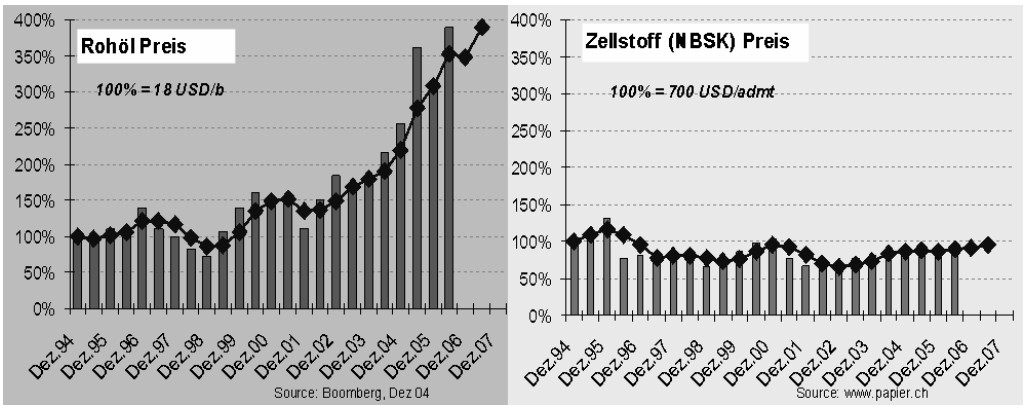

Abbildung 4. Preisverlauf von Rohöl und Zellstoff [1].

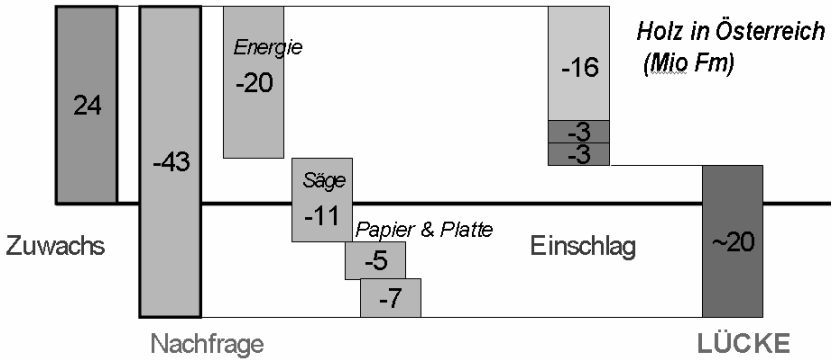

Abbildung 5. Holzbilanz Österreich 2010 [1].

Als Rohstoffquelle ist Holz ebenfalls einzigartig. Es stellt den Großteil der weltweiten Biomassevorräte von rund 1500 Milliarden Tonnen (Abb. 3). Durch Photosynthese werden jährlich etwa 10% davon neu gebildet, wovon rund die Hälfte zu Land entsteht. Großteils sind das diverse lignocellulosische Verbundmaterialien, das wichtigste davon ist Holz! Weltweit gesehen ist dieses im Überschuss vorhanden. Nur ein Bruchteil des jährlichen Zuwachses wird wertschöpfend verwertet.

Ganz anders ist die Situation bei Erdöl. Seit Mitte der 80-er Jahre übersteigt der Verbrauch das Auffinden zusätzlicher Lagerstätten: die Vorräte schrumpfen! Aus einer Nachhaltigkeitsperspektive ist dies kein haltbarer Zustand. Der in den letzten Jahren beobachtbare drastische Anstieg der Ölpreise (Abb. 4) wurde zwar durch weltpolitische Ereignisse ausgelöst, ist aus diesem Blickwinkel aber auch langfristig makroökonomisch durchaus nachvollziehbar. Ein analog drastischer Preisanstieg von Holz und holzbasierenden Produkten war hingegen bisher noch nicht zu beobachten.

Man kann davon ausgehen, dass die direkte thermische Verwertung in den industrialisierten Ländern, in denen eine fast unbegrenzte Nachfrage nach preislich günstigen Energiequellen und kein entsprechender Holzüberschuss gegeben ist, regional zu einer Verknappung führen wird und dass sich der Holzpreis weitgehend am thermischen Wert des Erdöls orientieren wird. Dies wird jedoch nicht in Ländern mit Holzüberangebot im Tropengürtel der Fall sein!

Die derzeit von der Politik betriebene, marktverzerrende Subvention der energetischen Nutzung von Holz beschleunigt aber die angesichts der Erdölpreise unvermeidliche Verknappung dieses Rohstoffes noch zusätzlich und schafft damit weitere Wettbewerbsnachteile für die stoffliche Nutzung.

Die Nachfrage nach Energieholz wird infolgedessen von 1993 bis 2010 allein in Österreich von 8,5 auf rund 20 Millionen Festmeter steigen (Abb. 5). Die österreichische Nutzwaldfläche (dzt. 3,9 Mio. ha) müsste nahezu doppelt so groß sein, um die derart gestiegene gesamte Holznachfrage aus inländischer Produktion decken zu können (6 fm/ha).

Den politisch Verantwortlichen scheint nicht klar zu sein, dass dies schon jetzt einen erneuten Migrationsschub von betroffenen Industrien mit relativ niedrigerer Wertschöpfung in Regionen auslöst, in denen keine Versorgungsengpässe bei kostengünstigem Industrieholz vorherzusehen sind. Die Abwanderung beispielsweise der kapitalintensiven Unternehmen der Papier und Zellstoffindustrie ist naturgemäß ein nur langsamer Prozess, der mit reduziertem Instandhaltungsaufwand und unterlassenen Ersatzinvestitionen der heimischen Produktionsstandorte beginnt. Sehr bald aber ist er irreversibel.

Unabhängig von dieser energetischen Perspektive ist das grundsätzlich neue Preisszenario aber für nahezu alle organisch-chemischen Produkte, die in überwältigender Mehrzahl auf Erdöl basieren, von ausschlaggebender Bedeutung.

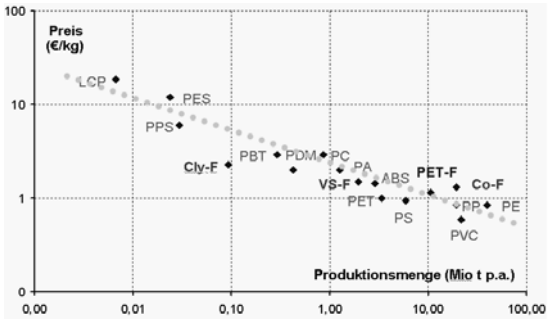

Abbildung 6. Preis versus Produktionsmenge polymerer Werkstoffe [1].

Für polymere Werkstoffe auf der gesamten Skala von Massenprodukten bis hin zu hochfunktionalen Spezialmaterialien gilt, dass das mittelfristige Marktpotential streng von deren Preisniveau bestimmt ist (Abb. 6).

Neue Produkte müssen in dieser Skala zwar erst ihren Platz finden, doch scheint klar, dass ein nachhaltig gestiegenes Ölpreisniveau neue Materialien, Chemikalien und Energieträger auf Basis Holz

und Cellulose in bisher noch nicht vorstellbarem Ausmaß erwarten lässt. Es ist mit grundlegenden Änderungen der Verbrauchsmuster zu rechnen. In der Vergangenheit konnte beispielsweise der weltweit mit der Bevölkerung und dem Lebensstandard steigende Faserbedarf (derzeit rund 65 Mio. Tonnen mit etwa 2 - 3% Steigerung im Jahr) durch vollsynthetische, auf Erdöl basierende Fasern gedeckt werden (Abb. 7). Baumwolle, deren Produktion auf sehr begrenzt verfügbares fruchtbares Ackerland angewiesen ist, hat laufend Marktanteile verloren.

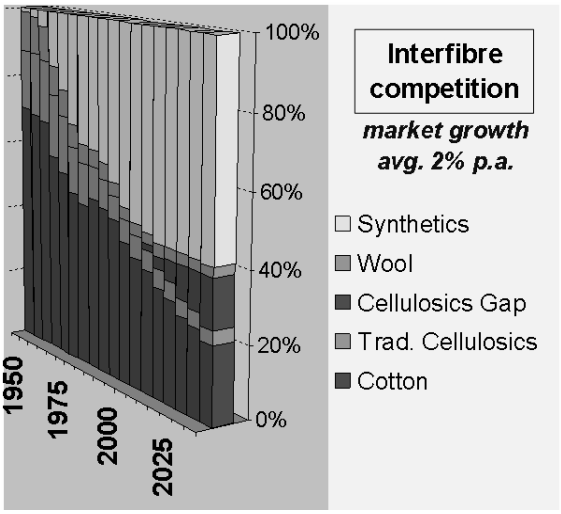

Abbildung 7. Versorgung des Weltfasermarktes [1].

Nun lassen sich in Textilien die Eigenschaften von Cellulosefasern durch Synthetics nicht wirklich ersetzen. Selbst bei gleichbleibenden Preisen wird deshalb die Nachfrage nach Cellulosefasern bei geschätzten 30-40% des Fasermarktes bleiben. Verstärkt durch eine langfristige Verschiebung des Erdölpreisniveaus ist abzusehen, dass es zu einer massiven Angebotslücke bei Cellulosics und damit zu hervorragenden Chancen für qualitativ gleichwertige Cellulosefasern auf Basis Holz kommen wird. Hier ist wohl auch die Ursache dafür zu finden, dass ein weltweit bei chemischen Halbfertigprodukten eher kleines Unternehmen wie Lenzing in den letzten Jahrzehnten mit der Lyocelltechnologie so außerordentliche Anstrengungen unternommen hat, in grundlegend neue Produkte auf diesem Gebiet zu investieren. Schlüssel für die physiologisch hervorragenden Eigenschaften der Cellulose ist ihre Fähigkeit, Feuchtigkeit aufzunehmen, zu speichern und abzugeben. Bei nicht absorbierenden Materialien wie Polyester, kondensiert die Feuchtigkeit als Wasserfilm auf der Faseroberfläche. Cellulosefasern hingegen absorbieren die Feuchtigkeit: wenn sie zu 100% feucht sind, wurde das gesamte Wasser im Inneren der Faser durch deren Porenstruktur aufgenommen (Abb. 8). Das Wassermanagement ist der Schlüssel für den Tragekomfort und wurde als Hightech-Funktionalität für Textilien bionisch entwickelt. Es ist verantwortlich für die hohe Wärmekapazität und -isolation, für die aktive Feuchte- und Thermoregulation. All das resultiert auch in neutralen elektrische Eigenschaften (relevant für Elektrostatik, -smog) und in einem für Hygiene und Geruch bedeutsamen stark gehemmten Bakterienwachstum.

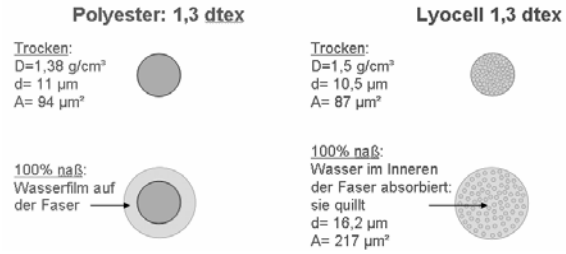

Abbildung 8. Wasseraufnahmevermögen von Lyocellfasern und Polyesterfasern im Vergleich [3].

Holz und seine Inhaltsstoffe sind viel zu wertvoll, um allein als Träger von Primärenergie genutzt zu werden. Die stoffliche Nutzung bringt den Mehrwert. Den Energiewert kann man nach dem Einsatz als Konsumartikel noch immer durch thermische Verwertung gewinnen.

In Abb. 9 kann man am Beispiel eines Hemdes aus Cellulosefasern sehen, dass der Preis des Rohstoffes für den des Endproduktes nur untergeordnete Bedeutung hat: nur 3,5% des Endverkaufspreises eines Hemdes ist vom Faserpreis bestimmt. Die Differenz ist Wertschöpfung über mehrere Schritte aufwendiger Weiterverarbeitungsprozesse. Während die Arbeitsintensität steigt, sinken Technolo-

gie- und Kapitalintensität von Stufe zu Stufe. Der Druck zur Abwanderung in Billiglohnländer ist daher in der Konfektion am größten. Die Endverbrauchermärkte für „High-end"- Produkte sind hingegen vorrangig in den westlichen Industriestaaten zu finden.

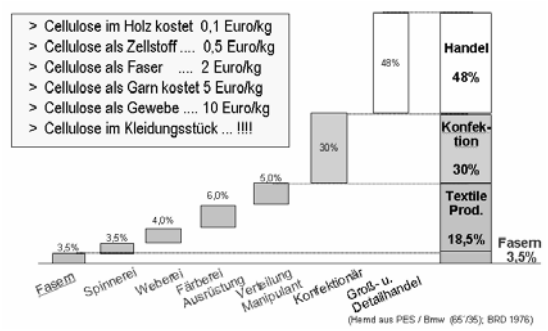

Abbildung 9. Wertschöpfungskette bei cellulosischen Textilfasern auf Basis Holz [4].

Eine Fraktionierung des Holzes mit darauf folgenden getrennten Nutzungsstrategien für die einzelnen chemischen Bestandteile ist sinnvoll! Dem entspricht die „best practice" heutiger Zellstoff-Fabriken, bei denen die Cellulose als festes polymeres Ausgangsmaterial für weitere stoffliche Nutzung gewonnen und das in der Kochlauge gelöste Lignin verbrannt wird. Der Brennwert von Lignin, das viele aromatische Gruppen beinhaltet und etwa 30% des Holzes ausmacht, beträgt 25–26 MJ/kg. Cellulose und Hemicellulosen - reine Kohlehydrate - hingegen haben mit 16–18 MJ/kg einen um 1/3 niedrigeren Brennwert.

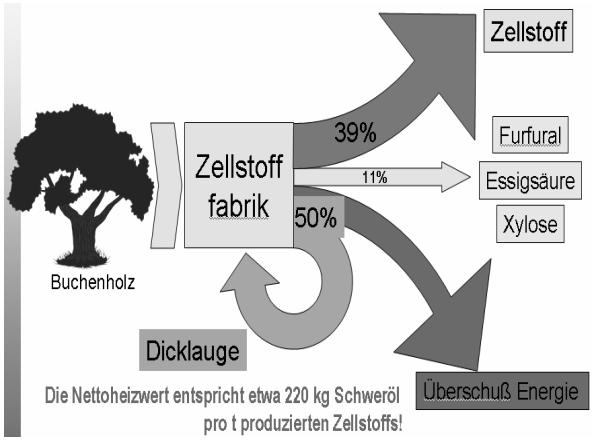

Abbildung 10. „Holzraffinerie" in Lenzing.

Lenzing ist schon seit langem den Weg eines systematischen Ausbaus der stofflichen Nutzung der Rohstoffquelle Holz gegangen und hat damit eine sehr kompetitive Kostenposition erreichen können.

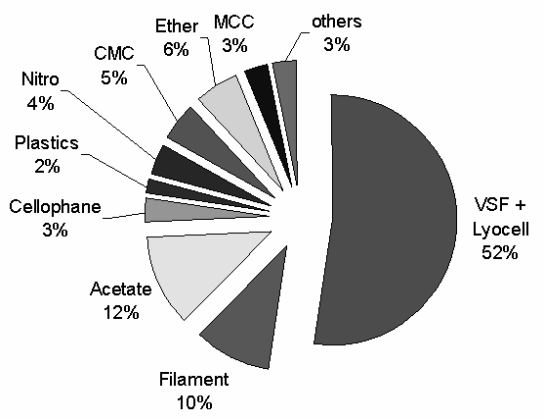

Abbildung 11. Einsatzgebiete Chemiezellstoff.

In der Lenzinger „Holzraffinerie" (Abb. 10) werden neben dem Hauptprodukt „reine Cellulose" (Chemiezellstoff) für Chemiefasern ganz gezielt eine Reihe von Feinchemikalien auf Basis der Hemicellulosen gewonnen. Der stofflich genutzte Rohstoffanteil konnte derart um rund 25% gesteigert werden. Rund 50% der verbleibenden Biomasse werden derzeit noch thermisch verwertet, wodurch die gesamte Lenzinger Zellstoff- und Faserproduktion energetisch nahezu autark ist.

Die Suche nach Mitteln und Wegen, Basischemikalien auch aus alternativen Rohstoffen herzustellen, hat infolge des nachhaltig gestiegenen Preisniveaus von Rohöl voll eingesetzt. Dabei führt kein Weg an der unvergleichlichen Basis lignocellulosischer Substrate – in erster Linie Holz – vorbei. Es ist zu erwarten, dass es in vorhersehbarer Zukunft auch zu einem Durchbruch bei den noch gegebenen Herausforderungen der Entwicklung und Umsetzung geeigneter Technologien des Holzraffinerie-Konzepts kommen wird. Diese sind Voraussetzung für einen Quantensprung bei der stofflichen Nutzung auch der nicht cellulosischen Holzinhaltsstoffe.

Der wichtigste Holzbestandteil ist Cellulose. Diese ist unbestritten das auch mengenmäßig weltweit wichtigste organische Polymer. Sie ist die Gerüstsubstanz der gesamten pflanzlichen Natur und wird von ihr im „Hochleistungs-Verbundwerkstoff“ Holz beispielsweise als leistungsfähige Verstärkungsfaser eingesetzt. Cellulose ist ein multifunktionales, polymorphes Molekül und hat ein Struktur- und Eigenschaftsspektrum, das bisher von keinem synthetischen Polymer erreicht wird.

Schon heute werden weltweit etwa 4 Mio. t unterschiedlichster Spezialitäten im Jahr aus „Dissolving” Zellstoff hergestellt (Abb. 11). Es handelt sich dabei um Chemikalien und Werkstoffe für eine Vielzahl von segmentierten Märkten in Hightech Anwendungen.

Die größte Bedeutung dabei haben heute Regeneratcellulosefasern, die entweder nach dem Viscoseverfahren auf dem Wege einer Derivatisierung oder nach dem oben bereits angesprochenen Lyocellverfahren durch Direktlösung in N-Methyl-N-morpholinoxid (NMMO) großtechnisch hergestellt werden.

Regeneratfasern weisen ein unvergleichliches Eigenschaftsspektrum für eine Vielzahl von Anwendungen im Bereich Textilien, Hygieneartikeln und technischen Produkten auf (Abb. 12). Sie sind physiologisch kompatibel, hydrophil, können Wasser aufnehmen und bewirken dadurch ein vergleichsweise verzögertes Wachstum von Mikroorganismen. Sie schmelzen nicht, sind mechanisch, thermisch und chemisch sehr stabil, können andererseits durch geeignete Färbe-, Veredelungs- und Derivatisierungsreaktionen sehr effizient modifiziert werden. Sie bieten mit weich, fließenden Konturen und brillanten Farben eine spezielle, ansprechende Optik und Haptik. Weitere spezifische Eigenschaften der Cellulose ermöglichen darüber hinaus ihren Einsatz beispielsweise als Folien, selektive Trennmembranen und hochporöse Schwammstrukturen.

Abbildung 12. Anwendungen von Cellulosefasern.

Mehrere sehr spezifische Eigenschaften der Cellulose kommen erst nach ihrer Derivatisierung zum tragen. Insbesondere die Fähigkeit feinster Cellulosepulver oder mehr oder weniger wasserlöslicher organischer Äther (Carboxymethyl-, Methyl-, Äthylcellulose, usw.) der Cellulose die Rheologie fluider Systeme gezielt zu beeinflussen, ist der Schlüssel für ihren Einsatz als Verdickungsmittel für Druckfarben, Leime in der Papierindustrie, Kosmetika und Lebensmittel, aber auch als strukturviskoses Additiv in Zement und Mörtel und bei der Erdölförderung.

Celluloseacetate mit den spezifischen Filtrations- und Adsorptionseigenschaften kommen als Fasern in Zigarettenfiltern zum Einsatz. Ihre unübertroffenen optischen Eigenschaften machen sie zum wichtigsten Rohstoff für photographische Filme. Als polymerer Werkstoff bringen sie neben der modischen Gestaltbarkeit auch alle anderen Eigenschaften für mechanisch höchst beanspruchte fragile Brillengestelle mit.

Bei Nitrocellulose kommen Eigenschaften wie Oberflächenaktivität, Schlagzähigkeit, Transparenz und Farbbrillanz insbesondere als brillante Druckfarben und hochwertige Lacke für die Holz-, Metall-, Papierindustrie und als Nagellack zur Geltung.

Hemicellulosen und seltene Zucker (20 bis 30% der Holzsubstanz) liegen bereits heute in großer Menge bei der Zellstofferzeugung gelöst in den diversen Prozessmedien vor. Im beschränkten Um-

fang haben sie dementsprechend auch schon Eingang in eine Reihe interessanter Anwendungen im Lebensmittel-, Pharma- und technischen Bereich gefunden.

Anders ist die Situation bei Lignin, dem dritten Hauptbestandteil des Holzes (30 bis 40% der Holzsubstanz). Über die thermische Verwertung der ligninhaltigen Prozessmedien und ein paar kleinere Anwendungen von Lignosulfonaten und Derivaten von Kraftlignin hinaus wäre der Durchbruch für eine stoffliche Nutzung erst auf der Basis einer großtechnischen Verfügbarkeit schwefelfreien Lignins zu erzielen. Diesbezüglich sehr vielversprechende neue Verfahren sind bisher allerdings im Pilotanlagenstadium stecken geblieben. Der erforderliche Innovationsbedarf und das Umsetzungsrisiko übersteigen, wegen der für einen kommerziellen Betrieb erforderlichen enormen Mindestanlagengrößen, die Möglichkeiten selbst großer Industrieunternehmen.

Es handelt sich um ungewöhnlich komplexe, teure und langfristig zu bearbeitende Probleme, die nur mit einem echt multidisziplinären Ansatz gelöst werden können. Der Engpass liegt dabei im fehlenden Durchbruch im Bereich klassisch chemischer Prozesstechnologien, wie beispielsweise großtechnisch brauchbarer Separationstechnologien für die komplexen Aufschlussmedien. Hier fehlen eine Reihe wichtiger Ergebnisse einer auf derartige Themen orientierten Grundlagenforschung.

Ein Gutteil der ungelösten Probleme liegt im upscaling der entsprechenden Technologien. Aus diesem Grund sind vor einer Implementierung kostspielige und intensive Entwicklungsarbeiten an Demonstrations- und semikommerziellen Anlagen erforderlich. Durch „Puzzle“-Projekte ist der erforderliche Durchbruch nicht zu erzielen!

Um hier weiter zu kommen, gälte es auch, politisch entsprechende Prioritäten und Rahmenbedingungen zu schaffen: Eine geeignete Basis für konzertierte transnationale F&E Anstrengungen scheint in den neuen EU Technologieplattformen „Forest based Industries“ und „Sustainable chemistry“ im Entstehen. Derartige Initiativen wären durch gemeinsame Prioritäten von Seiten der EU und nationalen Fördereinrichtungen zu unterstützen. Die noch immer nicht aus der Gedankenwelt der Forschungsadministrationen verschwundene alleinige Fixierung auf „life sciences“ ist hinderlich. Angesichts der bei der Herstellung von Grundstoffen typischerweise gegebenen ungeheuren Massen von Biomaterialien und den dadurch gegebenen Problemen der Raum/Zeitausbeuten scheint es ausgeschlossen, ökonomisch umsetzbare Lösungen allein mithilfe von „Biotechnologien“ zu finden.

Klare Botschaften von Seiten der Politik wären mit Bezug auf die zukünftige Verfügbarkeit des Rohstoffes Holz in unseren Breiten erforderlich. Die Verunsicherung potentiell Interessierter durch marktverzerrende Subvention der energetischen Nutzung von Holz ist im Begriff, derartige Initiativen im Keim zu ersticken. Es geht um die Willensbildung für ein Konzept, das die energetische erst nach der stofflichen Nutzung vorsieht und außerdem die Förderung des Einsatzes agrarischer Energieträger anstelle von Holz vorsieht. Thermische Verwertung ist leichter regional, in kleineren Einheiten zu organisieren als die weltweit kompetitive Herstellung von Chemierohstoffen.

Zusammenfassend lässt sich feststellen, dass mehrere Trends derzeit die Umsetzung des Konzepts der Holzraffinerie speziell aber eine Renaissance für Produkte aus Regeneratcellulose erwarten lassen.

Die auch logistisch sichere Verfügbarkeit von Holz, nachwachsend, ohne Ansprüche mit Bezug auf Fruchtbarkeit von Böden, Bewässerung, Pestizide, Düngung oder spezielle klimatische Bedingungen ermöglicht wirkliche Nachhaltigkeit für die entsprechenden Produkte, was gerade in Zeiten eines zunehmenden Bewusstseins über die beschränkten Vorräte von Erdöl und den dementsprechend steigen-

den Preisen zunehmend an Bedeutung gewinnt.

Die ausgereiften Technologien und installierten Kapazitäten bei der Zellstofferzeugung, die in den letzten Jahren erfolgte industrielle Umsetzung neuer umweltfreundlicher Weiterverarbeitungstechnologien, insbesondere des Lyocellprozesses und der signifikante wissenschaftliche und technische Fortschritt auf dem Gebiet polymerer Naturstoffe bieten heute signifikant verbesserte Voraussetzungen für die Entwicklung und auch kommerziell erfolgreiche Umsetzung neuer Produkte und Anwendungen auf Cellulosebasis.

Die spezifischen inhärenten Eigenschaften der Cellulose wurden bisher noch von keinem synthetischen Polymer erreicht. Das Eigenschaftspotential ist bislang noch lange nicht in kommerziellen Produkten ausgeschöpft.

Literatur

[1] Vortrag H. Harms, EUROPÄISCHES FORUM ALPBACH: Technologiegespräche 25. Aug. 2006

[2] Vortrag E. Taeger, WolffWalsrode Symposium 14.4.2000

[3] Vortrag M. Abu Rous, K.C. Schuster, EPNOE Summer School in Dornbirn, 25. August 2006

[4] Hemd aus PES/Bmw (65/35); BRD 1976

Lenzinger Berichte, 86 (2006) 9-13

ASSESSING FUNGAL DECAY OF SPRUCE AND BEECH WOOD USING NEAR INFRARED SPECTROSCOPIC TECHNIQUES *

Karin Fackler[1,2], Manfred Schwanninger[3], Cornelia Gradinger[1,2], Barbara Hinterstoisser[1,4], and Kurt Messner[1,2]

[1]Competence Centre for Wood Composites and Wood Chemistry (Wood K plus), St. Peter Strasse 25, A-4021 Linz, Austria

[2]Institute of Chemical Engineering and Applied Biosciences, University of Technology Vienna, Getreidemarkt 9/166, A-1060 Wien, Austria

[3]Department of Chemistry, BOKU-University of Natural Resources and Applied Life Sciences, Muthgasse 18, A-1190 Wien, Austria

[4]Department of Material Sciences and Process Engineering, BOKU - University of Natural Resources and Applied Life Sciences, Peter Jordan Strasse 82, A-1190 Wien, Austria

* This work was presented during the 9th European Workshop on Lignocellulosics and Pulp, August 28th to 30th 2006, Vienna, Austria.

Wood is colonised and degraded by a variety of micro-organisms. The most efficient ones are wood rotting basidiomycetes. On the one hand, the fungal decay processes cause enormous damage on man-made wooden structures, on the other hand, white and brown rot fungi have been identified as potential biotechnological tools to change the properties of wood surfaces and of sound wood. Extensive screening programs were carried out in the past to identify the most active fungal isolates. The screening targets, used by most scientists, were loss of weight and quantification of specific wood components including lignin, as well as cellulose and hemicelluloses by wet lab chemical methods. These methods are time consuming because wood blocks were usually inoculated with the fungal cultures and assayed after 2-3 months. Using near infrared spectroscopy (NIR), changes in the chemical composition of solid spruce or beech wood samples or wood samples after milling can be detected after several days of cultivation with the fungi.

Keywords: *brown rot, white rot, lignin, FT-NIR*

Introduction

The biodegradation of lignocellulose is the domain of wood rotting fungi. Brown rot fungi degrade cellulose and hemicelluloses leaving the lignin more or less undegraded but strongly modified, whereas white rot fungi are able to mineralise all wood constituents simultaneously. However, some selective white rot fungi can remove lignin in preference to cellulose, an ability that makes these fungi interesting for the industrial production of cellulose. The composition and the properties of wood are changed by all of these fungi. However, conventional methods to determine the lignin content of wood are very time consuming and make it difficult to handle large numbers of samples (TAPPI T 222 om-88). Standard deviations of the TAPPI standard method range from 0.4 % w/w to 1.6 % w/w lignin [1]. The limited number of replicate analyses together with relatively high

standard deviations restricts the sensitivity of the method. Therefore, in screening programs for technologically interesting species and strains, the determination of the lignin content of wood samples after fungal decay is carried out after several weeks of colonisation by the fungi, although the treatment time in the technological process may be much shorter. Near infrared (NIR) techniques have been shown to be powerful and rapid tools for the determination of wood components [2–6]. Absorption bands observed in the reflectance spectra of wood arise from overtones and combination bands of vibrations of C-O, O-H, C-H, and N-H which have their fundamental molecular absorption in the mid infrared region. Various constituents give similar absorption signals leading to highly overlapping bands, with the exception of substance classes such as aromatics, which can be related to the amount of lignin [7, 8].

Experimental

Fungal strains

Ceriporiopsis subvermispora CBS 347.63 (Selective white rot), *Trametes versicolor* (Simultaneous white rot on beech, selective on spruce), and *Gloeophyllum trabeum* (brown rot), which had been pre-cultivated on malt extract agar plates, were used in this study.

Cultivation of fungi on wood

Spruce or beech wood veneers (3 cm x 5 cm x 0.1 cm) were steam sterilised for 15 min and soaked for a few seconds in 2 % (w/V) corn steep liquor (CSL, Agrana) containing suspended fungal mycelium (one malt extract agar plate overgrown by the fungus was mixed in 150 ml 2 % (w/V) sterile corn steep liquor in a Waring blender for 30 s at full speed) before they were put in agar dishes (9 cm diameter) with 25 ml water agar (1.5 %) and beech tooth picks to allow growth of the fungi throughout the whole wood surface in a moisture-saturated atmosphere. The samples were incubated at 30°C. After the treatment, the mycelium was washed from the surface and the samples were dried at 50°C for several days. Wood shavings were cultivated according to Fackler et al. [9].

FT-NIR-spectroscopy and data analysis was performed according to Fackler et al. [9]. NIR spectra of wood surfaces were recorded from 10 areas at random positions on the front and back side of the veneers. For the short time cultivation with white rot fungi (Figure 4), the measuring areas were not taken at random positions, but the same five spots on the veneer were measured before the sterilisation of the veneer and after the treatment with the fungal culture.

Results and discussion

NIR-spectra

Figure 1(a) shows NIR reflectance spectra from spruce and beech wood meals. The absorption region between 6020 and 5770 cm^{-1} is attributed to the lignin compound of wood, showing bands deriving from the aromatic ring (C-H) as well as C-H vibrations of methyl groups and methylene groups respectively [10]. To accentuate differences between the spectra, they were transformed into the second derivative mode (Figure 1(b)). The lignin content of the sample can be calculated from the amplitude of the minimum near 5980 cm^{-1}. Additionally, lower lignin contents shift the minimum near 5800 cm^{-1} and 5980 cm^{-1} to higher wavenumbers and the amplitude minimum near 5890 cm^{-1} to lower wavenumbers [11]. The 2^{nd} derivative of the NIR spectrum of spruce shows a high similarity to that of lignin but with a lower intensity and different ratios of the amplitudes, additionally accompanied by small shifts. In beech wood however, the amplitude near 5980

cm^{-1} is influenced not only by lignin but also by the beech xylan. C-H deriving bands of the acetyl groups show minima in the second derivative spectra near 6000 cm^{-1}, 5955 cm^{-1}, 5890 cm^{-1}, and near 5805 cm^{-1}. Thus, in hardwood, the amplitude at 5980 cm^{-1} is not a minimum; but a local maximum between two minima deriving from xylan.

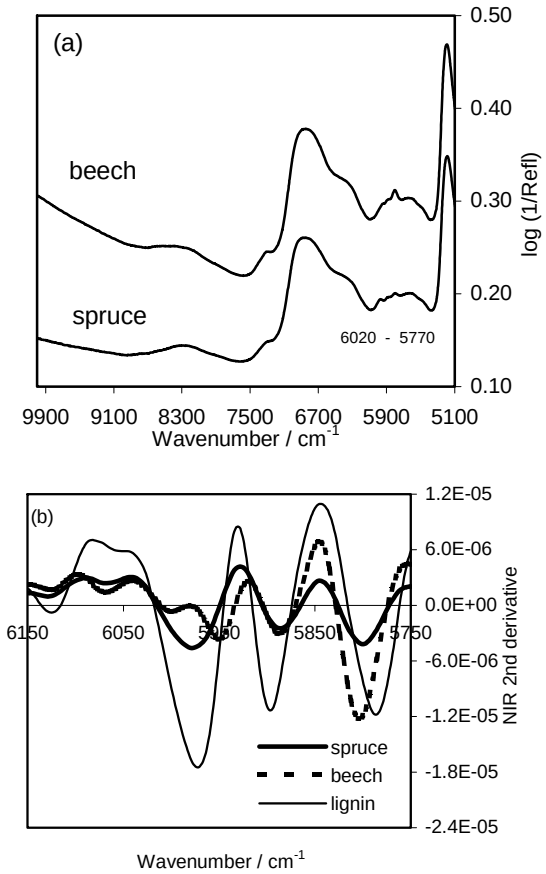

Figure 1. FT-NIR reflectance spectra of beech and spruce wood meals (a) and 2nd derivatives of NIR spectra of spruce, beech, and Klason lignin from beech (b).

Lignin content of wood meals

The lignin content of spruce wood meals from shavings that were modified by the selective white rot fungus *C. subvermispora* was assayed with the NIR method. Figure 2 shows the amplitudes of the NIR spectra in the second derivative mode at 5978 cm^{-1}. The error bars indicate the 95 % confidence interval for the mean value obtained from eight replicate spectra. The differences of the amplitudes refer directly to the relative changes in lignin content from day to day. Schwanninger *et al.* [11] calibrated the NIR-method with the wet-lab method for spruce wood and found a linear correlation ($R^2 = 0.96$) between 23 and 32 % w/w total lignin content. Differences of amplitudes at 5978 cm^{-1} representing a difference in lignin content of 0.6 % w/w can be reliably resolved by the method. The lignin content of spruce subjected to the selective white rot fungus *C. subvermispora* decreases significantly during the first two weeks of cultivation and can be reliably detected after five days. Differences between the consecutive cultivation days 4 to 8 are significant as well, whereas the lignin decreases more slowly from day 9 to 14.

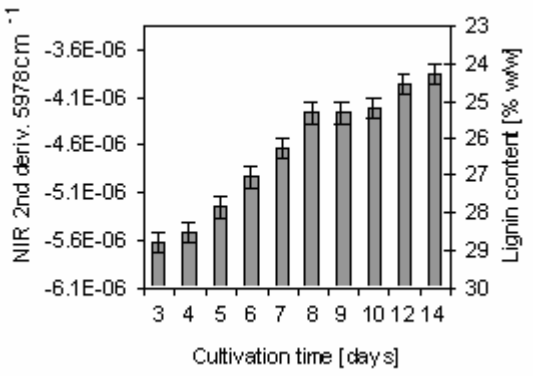

Figure 2. Amplitude of the 2nd derivative of the spectra of meals from white rot modified spruce wood shavings. Error bars indicate the 95 % confidence interval for the mean values.

Lignin content of wood surfaces

Figure 3(a) shows the 2nd derivative of NIR spectra of surfaces of beech wood samples after treatment with wood rotting basidiomycetes for ten weeks. The biggest difference occured again near 5980 cm^{-1}: selective white rot fungi (*C. subvermispora*) decrease the amplitude indicating a decrease of the lignin content. Simultaneous white rot (*T. versicolor*) led only to minor changes of the lignin content, although the weight loss of the sample exceeded 50 %. Due to the selective degradation of the wood polysaccharides, the lignin content of

brown rotted wood (*G. trabeum*) is higher than in the reference sample. A similar picture is presented in Figure 3(b), which shows the surface spectra of spruce wood subjected for ten weeks to selective white rot and brown rot. Changes of the amplitudes and spectral shifts indicate changes in lignin content caused by the fungi.

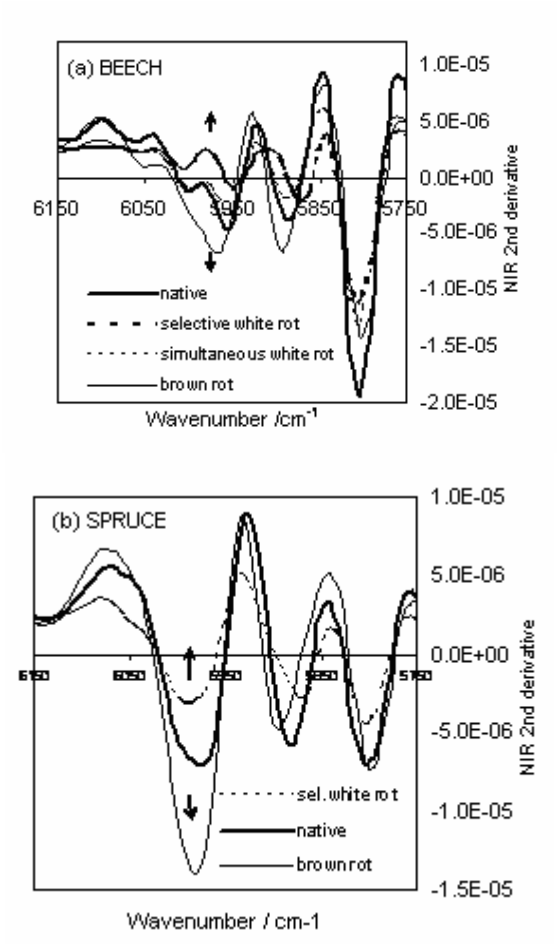

Figure 3. 2nd derivatives of NIR spectra of brown and white rot degraded wood surfaces.(a) beech and (b) spruce.

Depending on the metabolism of the species, the changes in the surface spectra can be detected already after several days. Figure 4 shows the differences in the NIR 2nd derivative amplitude of spruce veneers treated with the white rot fungi *C. subvermispora*, and *T. versicolor* (which degrades lignin selectively on softwoods). Lignin attack by the first fungus is significant already after five days, whereas that of the latter is just above the limit of detection after five days and can be clearly measured after 10 days.

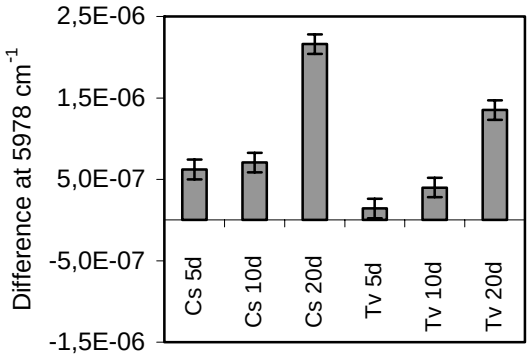

Figure 4. NIR 2nd derivative amplitudes of spruce wood surfaces subjected to two different white rot species (*C. subvermispora* – Cs and *T. versicolor* – Tv) for up to twenty days. Differences between treated and untreated veneers were determined. Error bars indicate the 95 % confidence interval of the mean values.

Conclusions

NIR spectroscopy is a quick and sensitive tool in order to estimate the lignin content of wood after biotechnological modification by brown or white rot fungi. The amplitude of the 2nd derivative of the NIR spectra near 5980 cm^{-1} are linearly correlated to the lignin content of spruce wood determined by wet-lab methods. Differences representing lignin contents smaller than 0.6 % w/w can be reliably detected. Therefore, small changes during short bio-modification times of only a few days, small differences between fungal strains, and even changes during short time fermentations can be determined.

Contrary to the standard methods, samples are not destroyed for the analyses, and apart from drying and milling (if required), no sample preparation is necessary. Using a fibre optic probe, NIR spectra can be recorded directly from the surfaces of wood samples or wood meals. Many spectra can be recorded in one day (one spectrum per minute), and – if required – automatisation of the method is possible.

Acknowledgements

We acknowledge the support of Competence Centre for Wood Composites and Wood Chemistry (Wood K*plus*), funded by the Austrian government and the federal governments of Upper and Lower Austria and Carinthia.

References

[1] Schwanninger, M. and Hinterstoisser, B. (2002) Holzforschung 56, 161 – 166.

[2] Gierlinger, N., Schwanninger, M., Hinterstoisser, B., Wimmer, R. (2002) J. Near Infrared Spectrosc. 10, 203 – 214.

[3] Bailleres, H., Davrieus, F., Pichavant, F. H. (2002) 59, 479 – 490.

[4] Yeh, T-F., Chang, H-M., Kadla, J. F. J. Agricult. Food Chem. (2004) 52,: 1435 – 1439.

[5] Easty, D. B., Berben, S. A., DeThomas, F. A., Brimmer, P. J. Tappi J./Wood Pulp Analysis (1990) 73, 257 – 261.

[6] Schultz, T. P., Burns, D. A.(1990) Tappi Journal, *73*: 209 – 212.

[7] Michell, A. J., Schimleck, L. R (1996) Appita 49, 23 – 26.

[8] Shenk, J. S., Workman, J. J., Westerhaus, M. O. (2001). *In* DA Burns, EW Ciurczak, eds, Handbook of Near-Infrared Analysis. Dekker Inc., New York, 419 – 474.

[9] Fackler, K., Gradinger, C., Hinterstoisser B., Messner, K., Schwanninger M. (2006) Enzyme Microb. Technol. 39, 1476 -1483.

[10] Schwanninger M. and Hinterstoisser B. (2001) 11th ISWPC, International Symposium on Wood and Pulping Chemistry, Nice, Vol. III: 641 – 644.

[11] Schwanninger, M., Hinterstoisser, B., Gradinger, C., Messner, K., Fackler, K. (2004). J. Near Infrared Spectrosc. 12(6), 397 – 410.

Lenzinger Berichte, 86 (2006) 14-23

THE INFLUENCE OF BEECH WOOD STORAGE ON THE PRODUCTION AND PROPERTIES OF REGENERATED VISCOSE FIBRES*

Andrea Promberger[1,2], Hedda K.Weber[1] , Cornelia Gradinger[1,3], Kurt Messner[3], and Herbert Sixta[2]

[1]Kompetenzzentrum Holz GmbH, A-4021 Linz, Austria
[2]Lenzing AG, Department ZF, A-4860-Lenzing, Austria
[3]University of Technology Vienna, 1060 Vienna, Austria

Phone: (+43) 07672-701-3817; Fax: (+43) 07672-918-3817; E-mail: a.promberger@lenzing.com

Beech wood storage under dry and wet conditions has recently been investigated with regard to dissolving pulp quality and shows some benefits for the wet storage form. Determining the influence of different storage conditions on the viscose production and the viscose fibre quality are the major objectives of this work. Additionally, pulp from *Chondrostereum purupureum* infested beech wood and from fresh beech wood as reference were investigated. The performance of different pulp samples in the viscose production gave the best results for the pulp made from fresh beech wood in all mechanical and optical properties. The sample infested with *C. purpureum* gave rather good results having surprisingly little problems and even better results in bleaching compared to samples, which were stored for a long time. The fibres from the latter both wet and dry display the lowest strength properties than derived from the fresh sample. The major differences between the wet and dry storage conditions comprise the optical properties.
Identical bleaching experiments are leading to lower brightness results in the pulp of dry stored beech wood deriving mostly from highly condensed structures, which can also be found in the final regenerated viscose fibre.

Keywords: *beech wood storage, TCF bleaching, dissolving pulp, viscose processability, viscose fibre properties*

Introduction

The quality of viscose fibre is depending on its raw material, which is bleached dissolving pulp. The better part is still made according to the acid sulphite pulping process. There the usage of hardwood, which is cheaper and more available, has gradually increased over the last decade [1]. Fresh beech wood for example is predominately available during the non-growing season, whereas stored wood is used as pulp wood supply for the rest of the year. The seasonal variation of the wood supply significantly affects the delignification of pulp and the optical properties of both, pulp and viscose fibre [2]. Unprotected storage of beech wood (*Fagus sylvatica* L.), which is also used at Lenzing AG, is accompanied by rapid decay from degrading fungi, which has been found to affect the yield and properties of sulphite pulp [3]. The storage of beech wood under water can inhibit the infestation of fungi and other oxidative reactions [4], [5]. This has a positive effect

on the processability of the wood stored under water during the cooking process [1]. These reactions mainly have an impact on the optical properties of the pulp due to the formation of highly condensed substances [6], which can influence the brightness of the pulp. Furthermore, the residual lignin in the pulp, which has already a rather low molecular weight, should not influence the viscose process but it can reduce the brightness of the viscose fibre [7].

The reactivity of the cellulose is another important aspect in viscose production and an important parameter for the evaluation of the dissolving pulp. It is related to the accessibility of the chemicals to the cellulose and is dependent on the structure and morphology of the fibre [8]. Hemicelluloses and low molecular carbohydrates can influence the fibre strength and lower the filterability of the viscose solution while building colloid structures. Further the influence of the extractives concentration can vary the xanthation and filterability of the viscose especially when sulphite pulp is used [7].

This study focused on the impact of the pulp samples made from differently stored beech wood on the production of regenerated viscose fibre. It was first bleached according to TCF conditions following an E(OP)-Z-P sequence to obtain fully bleached dissolving pulp. Afterwards the pulp was converted to viscose solution and finally spun into viscose fibres. The characteristics of the intermediate products and the final fibres were then extensively scrutinized and compared with products deriving from pulp, which was made from fresh beech wood, used as the reference for the experiments.

Experimental

Raw material

Fresh cut beech wood logs (*Fagus sylvatica* L.) have been stored under dry and wet (submerged in water) conditions for 15 months and labelled with DRY and WET, respectively. Fresh beech wood was further inoculated with *Chondrostereum purpureum* (9W C), a widely spread fungus also found at the wood yard, for nine weeks as reported in [9]. Additionally, fresh beech wood logs (FRESH) were used as a reference for all experiments. The logs were chipped and screened and the fraction <7 mm and >3 mm was used for the pulping experiments.

Pulping experiments

The cooking trials were carried out in a 10 L digester with forced circulation and connected to three pressurized pre-heating tanks for the simulation of large-scale operation. The dosage volumes, temperatures, and H-factors were monitored and recorded on-line. The digester and the pressurized tanks were heated by steam injection and/or a heat exchanger. Acid Mg sulphite pulping was carried out according to [2] at a liquor-to-wood ratio of 2.4:1, a total SO_2 charge of 116 g/kg o.d. wood, of which 42% was (true) free SO_2.

Bleaching experiments

Oxygen (O), hot caustic (E), and ozone treatments (Z) were carried out in a medium-consistency high-shear mixer equipped with three differently sized mixing reactors (100 to 500 g o.d.). Mixing conditions were adjusted to guarantee a fluidizing state. The system allowed on-line monitoring and recording of pressure, temperature, pH, and rotor speed. Heating on bottom, side, and top minimized the temperature gradient inside the digester. Peroxide bleaching was carried out in PE-flasks plunged into an agitated water bath. The bleached pulp was

acidified with diluted sulphuric acid prior to testing and analytical characterization.
According to long-term experience, an (E/OP)-Z-P bleaching sequence was chosen. The conditions of the initial E/OP treatment were adjusted to obtain the required purity levels for viscose grade pulp. The E/OP pre-treated pulps were subjected to medium consistency ozone (Z) bleaching. Pre-trials were carried out to determine the amount of ozone necessary to adjust final viscosity to a level of approximately 600 mL/g. The conditions of peroxide (P) bleaching were kept constant (Table 1):

Table 1. Bleaching conditions for the production of fully bleached beech sulphite viscose grade pulps.

Treatment	***Temp.***	***Time***	***Cons.***	***NaOH***	***O_2***	***H_2O_2***	***O_3***
	°C	min	%	g/ kg o.d.	bar	g/kg o.d.	g/kg o.d.
E	85	140	11	40			
OP	90	90	10	20	7 to 4	4.5	
Z	50		10				0.5 - 4
P	65	240	10	5		3	

Additional pulping experiments are carried out analogous to these except the amount of ozone is kept constant and the peroxide concentration is varied from 4.5 to 15 g/kg o.d. to simulate a limited ozone availability.

Steeping
The pulp was steeped in 17.8% sodium hydroxide at a ratio of 1:18 and a temperature of 50°C, which causes fibre swelling and converts the cellulose to sodium cellulose I, also known as alkali cellulose.

Viscose preparation
Viscose preparation and characterization was performed according to a modified method by [10]. The particle analysis was performed with a Pamas device operating according to the light blocking principle.

Viscose fibre production
Viscose fibres were produced on a bench-scale unit imitating the regular production of rayon fibres. Viscose solution was extruded through a 20-hole spinneret into a spinning bath. The fibres were cut to staples with a length of 40 mm before being carefully washed and processed to remove acid, salts and occluded sulphur.

Analytical Methods
Kappa number determination was performed according to T236 cm-85 mod., viscosity according to SCAN-CM 15:88, brightness according to ISO 3688/2470, alkali resistances according to ISO 699 / ZM IV/39/67, carbohydrate composition by total hydrolysis and HPLC separation with anion exchange chromatography with pulsed amperometric detection (AX/EC-PAD), β- and γ-cellulose according to a modified TAPPI method, T203 om-93, copper number according to ZM IV/8/70, carboxylic groups according to *Das Papier* **1965**, *19 (1)*, DCM extractives according to ISO 624, cations by means of ICP after microwave digestion. The single-reflection diamond ATR technique was applied for FTIR analysis. A Bruker IFS 66 spectrometer with a MCT detector was used; resolution 2 cm^{-1}; number of scans 200. Molecular weight distribution (MWD) by size exclusion chromatography (SEC) with multi-angle laser light scattering (MALLS) detection in LiCl/DMAc solution [11] and aging kinetics according to ZM III/19/69 mod. Fibre strength was measured according to an LAG internal standard procedure.

Results and discussion

Bleaching

The first bleaching step is a hot alkaline extraction with a hydrogen peroxide reinforced oxygen delignification (E/OP) without intermediate stage washing. The conditions have been varied with regard to the amount of peroxide as described before. The trend of the brightness is given in Figure 1 correlating the kappa number of the unbleached pulp sample to the increasing peroxide input in the bleaching step.

The fresh and wet samples are determined to have similar bleaching behaviour with an absolute brightness increase of 11.7 and 12.2% ISO, respectively. The results of the dry and inoculated samples, however, show some significant differences. Although both samples indicate the presence of chromophoric substances, which are difficult to remove due to the low effect of the additional amount of peroxide on the brightness level in this bleaching step, the inoculated sample has an even better performance than the fresh beech wood sample. The chromophoric substances, which could be identified as highly condensed aromatic components by UV-microspectrophotometry, are derived mostly from storage compounds in the wood altered during dry storage and possible enzymatic reactions of fungi [6],[2]. The FRESH and WET pulp samples do not have this effect, because the substances are not present in these samples.

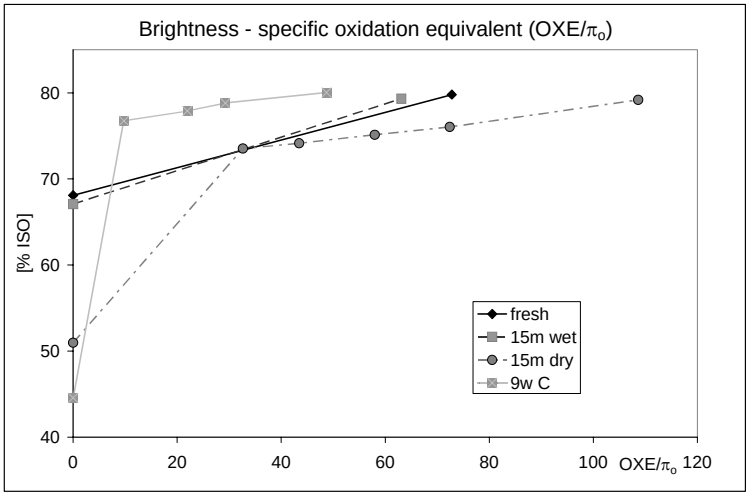

Figure 1. Brightness gain with increasing peroxide input (in OXE = oxidation equivalent) per unbleached kappa number of sulphite pulp from different wood pulps.

Table 2. Data of the ozone bleaching step for E/OP bleached pulp from differently stored beech wood.

Sample	Ozone	**Kappa**	***Δ kappa***	***Chain scission***	***Chain scission/ Δ kappa***
	[kg/t od pulp]	#	#	[$(1/P_j-1/P_o)*1000$]	
FRESH	1.21	0.32	1.22	0.095	0.078
WET	1.20	0.41	1.22	0.071	0.058
DRY	1.20	0.35	1.58	0.086	0.055
9W C	1.20	0.47	1.40	0.073	0.052

The introduction of ozone in acidic environment at 10% consistency is the subsequent bleaching step, followed by a standard alkaline peroxide treatment which is used as a standardized after-treatment. The performance of the ozone treatment with regard to the chain scission and the kappa reduction is compared in Table 2 for all samples.

The behaviour of all pulps in the ozone stage is very similar except for the value of the brightness and the kappa number prior to this bleaching step. An increase of the ozone input, however, can amplify the chain scission drastically. The input of, for example, 3 kg ozone /t oven dried (o.d.) pulp leads to a chain scission to Δ kappa ratio of 0.146 and 0.210 for the FRESH and DRY samples, respectively. According to these results the increase of the ozone concentration to obtain the target brightness particularly in the pulp from dry stored wood might reduce the fibre strength due to the increasing chain scission. The results will be discussed later.

The last step of the bleaching sequence is a peroxide step, which parameters have been kept constant for all experiments. The fully bleached pulp, which will be used for the production of viscose fibres, has been treated according to the (E/OP)-Z-P bleaching sequence. The final results with the most prominent characteristics are displayed in Table 3 and give a good survey of the pulp data before and after the bleaching treatment.

The equivalence of the pulps can only be achieved by varying the amount of bleaching chemicals as already reported elsewhere [2]. The input of the bleaching chemicals for the pulp from dry stored wood is significantly higher than that for the pulp deriving from fresh and wet stored wood. The viscosity of pulp DRY is also lower compared to the other pulp samples because of the reinforced cooking and bleaching experiments, which were necessary to reach the target brightness of >92% ISO. The overall parameters after bleaching, however, are comparable for all TCF bleached viscose pulp samples. The fungal infested pulp has been added to the sample matrix, without further increase of the bleaching chemicals, which results in brightness of 90.9% ISO. This, however, will somewhat influence the optical properties of the final fibres. The degree of purification, expressed as R-values and pentosan content, is slightly lower for the WET and 9W C sample, but still within the normal deviation.

Table 3. Characteristic parameters of unbleached and correlating bleached pulp from differently stored beech wood samples, which are used for the production of viscose fibres.

Parameters	***Units***	***FRESH UNBL.***[1]	***FRESH BL.***[2]	***WET UNBL.***	***WET BL.***	***DRY UNBL.***	***DRY BL.***	***9W C UNBL.***	***9W C BL.***
Chemical charge	OXE	0	591	0	567	0	772	0	590
Kappa number		3.64	0.32	4.33	0.36	8.12	0.21	12.07	0.47
Brightness	% ISO	68.1	92.9	66.5	92.4	51	92.2	44.6	90.9
Viscosity	mL/g	680	615	612	575	567	529	671	624
R_{18}	%	92.1	94.0	91.1	93.8	91.6	94.0	90.8	93.5
R_{10}	%	87.2	89.0	85.4	87.5	85.7	87.5	86.0	88.6
Pentosan	%	-[3]	3.19	-	3.21	-	2.63	-	3.69
Carbonyl groups	µmol/g	39.9	22.0	-	23.0	-	23.0	-	-
Carboxyl groups	µmol/g	28.7	22.7	25.2	23.2	25.2	21.4	55.4	37.3

[1] unbleached, [2] bleached, [3] not determined

Molecular weight distribution

The pulp source must have a high-molecular–weight fraction, which is an essential requirement for the fibres to obtain the desired physical properties of strength and extensibility [12]. Therefore, analyses of the MWD were performed by size exclusion chromatography.
The weight fraction above DP 2000 characterizes the long chain molecules and is comparable for the FRESH and DRY stored samples. The WET and 9W C samples contain insignificant higher percentage of this fraction. The low-chain fraction of DP <50 is also higher for the inoculated sample, which, however, does not correlate to the amount of pentosan present in the pulp. There are no significant influences in the pulp sample deriving from *C. purpureum* infested wood, which also confirms the non-degrading nature of this fungus. The DP_w of the DRY and WET samples are compared to the FRESH sample (Table 4).

Table 4. Molecular weight distribution of viscose grade pulps (GPC).

Wood	DPw	PDI	DP< 50	DP < 200	DP > 2000
			%		
Fresh	1580	6.52	4.6	17.1	22.9
Wet	1445	7.29	5.0	18.7	24.7
Dry	1295	6.74	5.1	18.4	22.6
9w C	1610	8.79	6.4	19.2	26.8

Steeping and Aging

The prerequisite of the viscose fibre production is the complete conversion of the pulp into sodium cellulose I. This is achieved by steeping the dissolving pulp in an aqueous solution containing more than 16% sodium hydroxide. The alkali-soluble hemicelluloses are removed to an extent, which depends mainly on the pulp properties and the reaction conditions. Furthermore, the cellulose is swelling during this steeping procedure.
A defined alkali to cellulose ratio is obtained by pressing the steeped pulp. The alkali cellulose contains 33-35% cellulose and around 16% alkali. The pressed residue is shredded immediately to get a high specific surface, which is important The reaction itself is performed under controlled time and temperature conditions to adjust the desired degree of polymerization of the cellulose. The viscosity of the alkali cellulose from FRESH, WET, DRY, and 9W C is adjusted and finally reaches 231, 241, 238, and 235 mL/g, respectively, after this process. The subsequent xanthation with carbon disulphide and dissolving in an aqueous solution of NaOH is performed to obtain a viscose solution, which contains ~ 5% of sodium hydroxide of the dissolving pulp samples.

Viscose preparation and filterability

The suitability of the dissolving pulp from the differently stored beech wood for the viscose application has been tested by the determination of the filterability performance and the average particle content. The relationship between these two parameters characterizes the quality of the viscose solution. The characteristics of the solutions from the different pulp samples are given in table 5.
The filter value of the viscose gives the best result for the FRESH sample, followed rather surprisingly by the DRY and 9W C sample. The WET sample had the lowest filter value, which also correlates with its result from the particle analysis. They have the highest values for the WET sample compared to the DRY and FRESH sample, which are considerably lower. Again the viscose made from the pulp of dry stored wood has a better performance than the one from the wet stored wood sample. The values of all samples, although varying, are still within the specification range of a typical viscose quality [13], [14].

Table 5. Characteristics of viscose solutions obtained from differently pulp samples.

	Units	*FRESH*	*WET*	*DRY*	*9W C*
Alkali	%	5.21	5.29	5.26	5.21
Cellulose	%	8.56	8.61	8.55	8.59
Sulphur	%	2.22	2.21	2.21	2.20
Ball fall	s	47	54	53	51
Particles	ppm	12.5	23.9	13.9	22.8
Filter value		441	332	404	396

The deviations, which we found, are attributed to the variations within the viscose production process but are insufficient to be ascribed to the storage history of the samples.

Conversion of the viscose solution into fibres

Before the spinning process, the viscose was aged and filtered to eliminate any persistent fibre fragments and gel particles. The final production of viscose fibres was performed on a lab scale spinning machine, where the conditions were adjusted according to the production of a regular viscose rayon staple fibre with a titre of 1.3 dtex. Different stretch levels from 50-80%, in steps of 10%, have been applied to obtain a general view of the strength properties of the fibres. The tenacities as a function of the elongation values in the conditioned fibres are given in Figure 2 for the different stretch levels.

The results show a clear superiority of the reference sample from fresh beech wood. The WET and DRY samples are comparable to each other but well below the fungal infested sample, which is another proof that the fungus does not attack the cellulose chains in the wood.

The work potential, which is the product of the elongation and the tenacity, is listed from the highest to the lowest value as following: FRESH, 9W C, DRY, WET. The changes of the physical properties are significant in the long stored samples. We assume that the cellulose chains alter during this extended storage of more than a year, but the results are still within the required range of the viscose fibre specification.

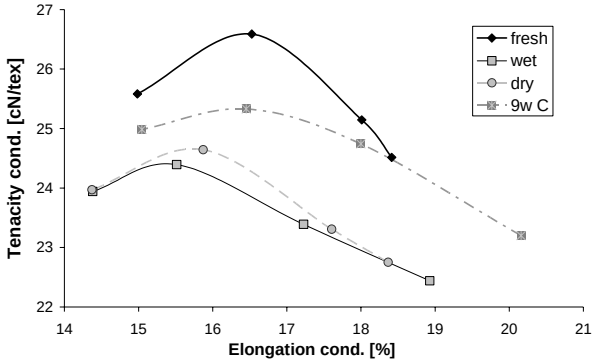

Figure 2. Tenacity versus elongation of regular viscose fibers in the conditioned state made from dissolving pulp from differently stored wood.

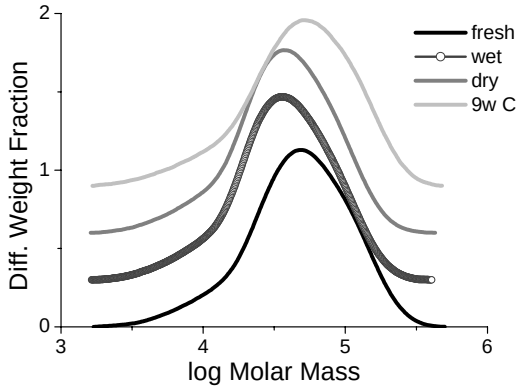

Figure 3. Molecular weight distribution of viscose fibres deriving from sulphite pulp of the differently stored beech wood.

Although the DRY sample was expected to give lower results compared to the WET sample due to the extended bleaching process, the final strength properties show no significant differences. The working potential of the fibres can be verified by

the molecular mass distributions (Table 6), which give again rather similar results for the WET and DRY samples. The viscose fibres from 9W C pulp have a higher proportion in the DP <50 and a similar one in the DP <200 fraction compared to the reference (FRESH). The chromatograms of all fibre samples, which also show that the MWD is significantly narrowed down compared to the dissolving pulp as verified by the decrease of PDI value, is given in Figure 3.

The different storage conditions do not significantly influence the final fibre properties with regard to the different analyses made. However, we can only assume that a long storage period of the wood might alter the cellulose so that the working capacity decreases approximately 10% in comparison to the fibres made from the FRESH sample.

One of the most important characteristics not only of the pulp but also of the final viscose fibre is the optical properties. As already mentioned before and described in other papers the unbleached pulp from dry stored wood has lower brightness compared to the WET and FRESH samples. This is also true for the pulp deriving from fungal infested wood. The two bleaching concepts we investigated give the following brightness results in the final viscose fibres.

The results in Table 7 give the exact results for all pulps processed equally with the same amount of chemicals. The differences can be clearly demonstrated in the brightness level of the final viscose fibre especially in the DRY sample. The optical properties of the fungal infested sample have the lowest value in the unbleached state but can be compensated along the production line. The brightness of the final fibres from 9W C is even two points above the WET sample.

The major differences in the optical properties could be already eliminated in the bleaching step and furthermore during steeping. We assume that the main portion of the residual lignin after bleaching is discharged along with the hemicelluloses in the steeping lye. The dry stored sample, however, has a higher concentration of residual lignin and due to that fact not everything can be discharged. This is represented by the 7% ISO lower brightness compared to the WET sample. We presume that a part of the condensed substances is covalently bonded to the cellulose chain [15]. The results of the DRY and WET samples are compared in Table 8 in case of the reinforced bleaching experiment. The results of the optical characteristics demonstrate that there are no further differences in these properties.

Table 6. Molecular mass distribution of fibres from different pulp sources (GPC).

Pulp		*DP <50 (%)*	*DP <200 (%)*	*DP >2000 (%)*
Fresh	2.05	3.5	31.6	0.2
Wet	1.93	4.7	42.6	-
Dry	1.93	4.8	41.8	-
9w C	2.25	4.4	31.5	0.3

Table 7. Brightness results along the production from unbleached pulp to viscose fibres.

	Unbleached Pulp brightness [%]			*Bleached Pulp brightness [%]*			*Viscose Fibres brightness [%]*		
Sample	R_{457}	Ry	Rz	R_{457}	Ry	Rz	R_{457}	Ry	Rz
FRESH	68.14	75.33	67.74	92.89	94.62	92.65	81.42	87.09	80.82
WET	67.08	74.51	66.67	91.64	94.40	91.28	76.22	82.76	75.65
DRY	50.62	59.01	50.22	88.61	91.60	88.37	68.88	77.05	68.40
9W C	44.57	54.43	44.15	90.91	94.06	90.54	78.49	85.27	77.83

Table 8. Comparison of brightness results from differently stored samples after pulp bleaching and viscose fibre production.

	Bleached Pulp brightness [%]			*Viscose Fibres brightness [%]*		
Sample	R_{457}	Ry	Rz	R_{457}	Ry	Rz
WET	92.36	94.86	92.01	79.62	85.63	78.98
DRY	92.23	94.16	92.03	79.60	85.49	79.00

Conclusions

This survey described the detailed production and the analyses of each production step of pulps deriving from beech wood stored under wet and dry conditions for 15 months and fresh beech wood chips infested with the fungus *C. purpureum*. We can clearly distinguish a draw back in the dry storage form due to an enforced bleaching process with 760 OXE compared to 540 OXE for the wet stored sample, which are necessary to reach the target brightness of 92% ISO. The experiments with equal amounts of bleaching chemicals resulted in a low brightness of 88.6% ISO for the dry samples compared to 91.6% ISO for the wet sample after bleaching. Further experiments determined that the chromophores present in the insufficiently bleached pulp from the sample DRY are still visible in the final viscose fibre and have still a lower brightness compared to WET. The fungal infested sample, however, could be bleached without difficulty, although it had the lowest brightness value in the unbleached state.
The performance of the bleached dissolving pulp, however, is comparable for all samples and the quality parameters are within the standard quality range for viscose fibre. Furthermore the mechanical characteristics were investigated in addition to the optical properties. The stored samples showed a little decrease in the working capacity in comparison to the reference sample. The different storage conditions (dry, wet), however, could not be clearly distinguished but are comparable to each other.

Finally we can state that the fibre quality is not influenced by the storage conditions applied to the beech wood in the first place, when the target brightness of the bleached dissolving pulp is reached. This however is the draw-back of the wood stored under dry conditions, which does need a higher amount of chemicals and increases production costs.

Acknowledgements

Financial support was provided by the Austrian government, the provinces of Lower Austria, Upper Austria and Carinthia as well as by the Lenzing AG. We also express our gratitude to the Johannes Kepler University, Linz, the University of Natural Resources and Applied Life Sciences, Vienna, and the Lenzing AG for their in kind contributions. Furthermore we want to thank Gregor Kraft for the vital discussion.

References

[1] H. Sixta, A. Promberger, G. Koch, C. Gradinger and K. Messner. in International Symposium on Wood Based Materials; Wood composites and Chemistry (Teischinger, A. and Stingl, R., eds.), Vol. 4, special ed., pp. 455-468, Inst. of Wood Science and Technology, Vienna 2002.
[2] H. Sixta, A. Promberger, G. Koch, C. Gradinger and K. Messner, Holzforschung 58 (2004) 14-21.
[3] S.A. Rydholm, Pulping Processes,

Wiley Interscience, New York, 1965.

[4] G. Koch, J. Bauch, J. Puls and J. Welling, ForschungsReport 2 (2001) 30-33.

[5] A. Promberger. in Inst. of Pulp and Paper Science, pp. 191, University of Technology Graz, Graz 2004.

[6] G. Koch, J. Puls and J. Bauch, Holzforschung 57 (2003) 339-345.

[7] K. Götze, Chemiefasern nach dem Viscoseverfahren, 3rd ed., Springer Verlag, Berlin, Heidelberg, 1967.

[8] K.E. Christoffersson, M. Sjöström, U. Edlund, A. Lindgren and M. Dolk, Cellulose 9 (2002) 159-170.

[9] C. Gradinger, K.Messner, A. Promberger and H. Sixta. in 12th International Symposium on Wood and Pulping Chemistry, Vol. 3, pp. 27-30, University of Wisconsin, Madison, Department of Forest Ecology and Management, Madison, USA 2003.

[10] E. Treiber, J. Rehnström, C. Ameen and F. Kolos, Das Papier 16 (1962) 85-94.

[11] N. Schelosky, T. Röder and T. Baldinger, Das Papier 12 (1999) 728-738.

[12] H. Mark, Tappi Section - Paper Trade Journal 34 (1941) 28-35.

[13] H. Sixta, A. Borgards and A. Lima. Lenzing AG, Lenzing 1999.

[14] H. Sixta, H. Harms, S. Dapia, J.C. Parajo, J. Puls, B. Saake, H.-P. Fink and T. Röder, Cellulose 11 (2004) 73-83.

[15] S.Y. Lin and C.W. Dence, Methods in Lignin Chemistry, Vol. 14, first ed., Springer Verlag, Berlin, Heidelberg, New York, 1992.

Lenzinger Berichte, 86 (2006) 24-31

PROBLEME DER UMSETZUNG NEUER TECHNOLOGIEN IN DIE INDUSTRIELLE PRAXIS, DARGESTELLT AM BEISPIEL DES ALKALISCHEN SULFITVERFAHRENS MIT AQ UND METHANOL - ASAM*

Hans-Ludwig Schubert

Voith Paper Fiber Systems GmbH&Co.KG, Escher-Wyss-Straße 25, 88212 Ravensburg/Deutschland
Tel.: +49-571 83 2034; Fax: +49-571 83 2050; E-mail: hans.schubert@voith.com
*Vortrag anlässlich des Festkolloquiums zur Verabschiedung von Herrn Prof. Dr. Dr. h.c. Rudolf Patt am 27. Oktober 2006 in Hamburg

Einleitung

Von Enthusiasmus und Aufbruchstimmung war mein Einstieg in die ASAM-Arbeitsgruppe von Prof. Patt am 1. April 1987 geprägt. Wenig hatte ich mich bis zu diesem Zeitpunkt mit dem neuen Aufschlussverfahren beschäftigt, aber es war leicht, sich von der Begeisterung anstecken zu lassen. ASAM [1-3] steht für das „alkalische Sulfitverfahren mit Anthrachinon und Methanol". Dieses Verfahren mit hohen Ausbeuten an Zellstoff, sehr guten Zellstofffestigkeiten, geringerer Umweltbelastung und einer leichteren Bleichbarkeit der Faserstoffe verglichen mit den konventionellen Verfahren bot alles, was ein vom Umweltgedanken angehauchtes Forscherherz brauchte, um sich zu engagieren.
Fast 20 Jahre später stellt sich mir die Frage, wie ein Verfahren, das nachweislich ein hervorragendes Potential hat [4], um erfolgreich zu sein, industriell gescheitert ist und nie wirklich die Chance bekommen hat, sich durchzusetzen. Dieser Vortag ist der Versuch einer Aufarbeitung, der Versuch Erfahrungen weiter zu geben, der Versuch, den Blick für eine gesamtheitliche Verfahrensentwicklung zu schärfen und die Forderung, nicht zu lange nur auf der Betrachtung von Teilaspekten einer notwendigen Erfolgskette zu verharren.

ASAM-Historie

Die Erfindung von ASAM erfolgte im Jahr 1985 durch die Herren Kordsachia und Patt. Schnell wurde das Potential des Verfahrens klar. Forschungsgelder wurden beantragt und bewilligt. Eine Forschungsgruppe mit bis zu vier zeitgleich arbeitenden Doktoranden beackerte die Themen Aufschluss, Bleiche, Chemikalienrückgewinnung und Reaktionskinetik.
Verhandlungen mit der Industrie begannen 1985 und 1987 gelang es, die beiden Firmen Kraftanlagen Heidelberg und Feldmühle AG für das Projekt zu begeistern. Die gemeinsam errichtete Pilotanlage ging 1989 in Baienfurt in Betrieb und sollte den Beweis antreten, dass ASAM-Zellstoff großtechnisch erzeugt werden kann. Die Produktionskapazität betrug ca. 5 t/Tag.
Die Anlage bestand aus einem Kocher, einer Eindampfanlage für die Schwarzlauge, einer Methanolrückgewinnungsanlage, einer Grobsortierung für den Zellstoff sowie einer 4- stufigen, chlorfreien Bleiche mit Sauerstoff, Ozon und Peroxyd. 1994 wurde die Pilotanlage letztmalig betrieben und 1998 abgerissen.
Mit der Pilotanlage wurde Zellstoff erzeugt, der auf drei industriellen Papiermaschinen erfolgreich getestet wurde (Hagen-Kabel, Hallein, Salach). Der Nachweis, dass der Zellstoff „funktioniert" konnte erbracht werden und die Übertragung der Laborergebnisse aus dem 7 l Drehkocher und den Plastikbeutelbleichen mit 10 bis 100 g Zellstoff in eine

Pilotanlage war erfolgreich. Gleiches galt für die Eindampfbarkeit der Schwarzlauge bis auf hohe Trockengehalte und die Rückgewinnung des beim Aufschluss eingesetzten Methanols aus der Schwarzlauge.
Nicht nachgewiesen werden konnte die Rückgewinnung der Aufschluss-chemikalien Na_2SO_3 und NaOH sowie deren Kreislaufführung, da dieser Teil der notwendigen Verfahrenstechnologie nicht in der Pilotanlage realisiert war. Somit fehlte der Technologie ein wichtiger Meilenstein zum grundsätzlichen Nachweis des Gesamtverfahrens.
1993 entschied sich Kraftanlagen Heidelberg, das Verfahren zu verkaufen. Somit gelangte die Technologie über die Firmen Voest Alpine, Ingersoll-Rand und Austrian Energy an die Firma Beloit. Mit der Insolvenz von Beloit verschwand das ASAM-Verfahren vom Markt der Möglichkeiten.
In der Gesamtzeit der ASAM-Entwicklung wurden 9 Doktor- und 18 Diplomarbeiten zu diesem Thema erarbeitet. Überträgt man diese Zeit in Forschungsjahre, so kann man wohl sagen, dass wenigstens 50 Forscherjahre in diese Entwicklung geflossen sind.
In den 80er und 90er Jahren existierte eine wahre Entwicklungswelle, um Alternativen zur bestehenden Technologie der Zellstofferzeugung zu etablieren. Viele haben versucht, die Zellstoffwelt zu revolutionieren. Genannt seien hier stellvertretend das Alcell-, das Formacell- und das Organocell-Verfahren. Für alle drei Verfahren gab es ebenfalls Pilotanlagen. Diese Verfahren konnten sich ebenfalls nicht durchsetzen und es bleibt die eine Frage: Warum?
Heute stellt sich die Weiterentwicklung des ASAM-Verfahrens, das ASA-Verfahren, diesem Markt der Möglichkeiten. Wie geht diese Geschichte aus?

Die ASAM Forschungsschwerpunkte

Eine Verfahrensentwicklung durchläuft mehrere Phasen. Eine mögliche Einteilung könnte sein:

- Entstehung einer Idee
  Ideenphase
- Erhärtung der Idee
  Bestätigungsphase 1
- Absicherung der Idee
  Grundlagenphase
- Verbesserung der Idee
  Verbesserungsphase
- Prüfung der Idee auf Umsetzbarkeit
  Bestätigungsphase 2
- Umsetzung der Idee in die Praxis
  Umsetzungsphase

Wenn ein Projekt in die industrielle Praxis umgesetzt werden soll, ist die entscheidende Frage: Auf welcher Entwicklungsebene befindet sich das Projekt? Erst mit der Erkenntnis, in welcher Entwicklungsphase sich ein Projekt befindet, kann eine Entscheidung getroffen werden, ob die Umsetzung der Idee in die Anwendung überhaupt möglich ist. Verharrt ein Forschungsprojekt zwischen der Bestätigungsphase 1 und der Verbesserungsphase, kann keine Entscheidung getroffen werden, ob eine Realisierung überhaupt möglich ist.
Zurück zum ASAM Verfahren: Eine Entwicklung startet immer mit der Feststellung, dass ein Produkt oder ein Verfahren nach dessen Erfindung viel versprechende Vorteile aufweist. Diese Idee kann durch Grundlagenforschung entstanden sein. Es ist aber auch möglich, dass eine Neuentwicklung durch das gezielte Variieren bekannter Verfahrens-parameter entsteht. So war es beim ASAM-Verfahren.
Alle Chemikalien, die für das ASAM-Verfahren notwendig sind, waren in der Zellstofferzeugung hinlänglich bekannt. Die Erfindung entstand durch die Kombination dieser bekannten Chemikalien, wobei neue Apparaturen

nicht entwickelt werden mussten. Schon mit den ersten Kochungen gelang es Patt und Kordsachia, einen Zellstoff zu erzeugen, der über Kraftzellstoff ähnliche Festigkeiten verfügte und der ohne die üblichen Geruchsbelästigungen hergestellt werden konnte. Durch die Verwendung von Na_2SO_3 fehlten die gasförmigen und geruchsintensiven Schwefelkomponenten SO_2 sowie H_2S oder Methylmerkaptane. Die Kombination von Sulfit mit Methanol und Anthrachinon hat der ursprünglichen Ingruber-Idee des Alkalischen Sulfit-aufschlusses eine neue Anwendungsmöglichkeit erschlossen. Die Idee ASAM war entstanden.

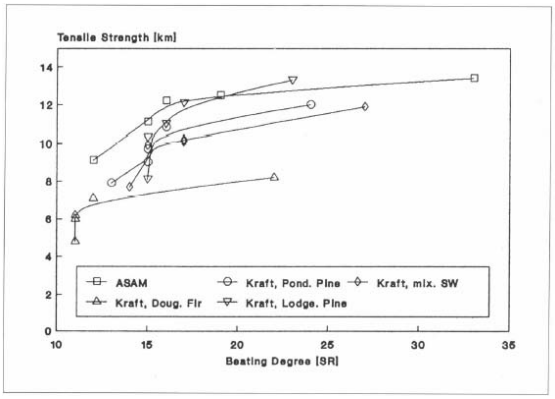

Abb. 1. Festigkeit von ASAM-Zellstoff [5].

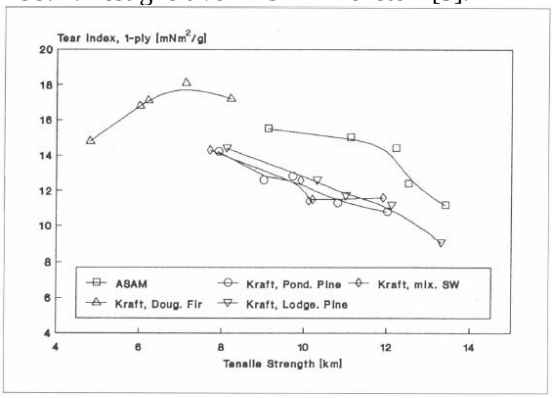

Abb. 2. Festigkeit von ASAM-Zellstoff [5].

Aufgrund dieser Ergebnisse etablierte sich schnell eine Forschung, die vor allem die Optimierung des Aufschlussprozesses und die Entwicklung einer chlorfreien Bleiche zum Ziel hatte. Es wurden verschiedenste Holzarten (Fichte, Kiefer, Pappel, Birke, Eukalyptus, Buche, etc.) aufgeschlossen. Zellstoffe mit verschiedenen Kappazahlen wurden erzeugt und hinsichtlich Ausbeute, erzielbaren Festigkeiten und Splitter-gehalten untersucht. Die Bleiche der Zellstoffe wurde mit unterschiedlichsten Chemikalien durchgeführt und eine Feinoptimierung mittels der Bestimmung von Zellstoffviskositäten versucht. Diese erzielten Produktqualitäten (Festigkeiten, Ausbeuten und Weißgrade der Zellstoffe) überzeugten die Firmen Kraftanlagen Heidelberg und Feldmühle AG, eine Pilotanlage zu errichten. Detaillierte Produkteigenschaften wurden betrachtet.

Was passiert beim ASAM-Verfahren eigentlich? Es wurde versucht, die Aufschlusskinetik aufzuschlüsseln, Lignin zu isolieren, funktionelle Gruppen und topochemische Vorgänge zu bestimmen. Grundlagen wurden bei der ASAM-Forschung intensiv bearbeitet.

Ein weiterer Arbeitsbereich war die Charakterisierung der Schwarzlauge. Grundlagenarbeiten waren Versuche zur Ablaugenpyrolyse. Auf der Produktebene beschäftigte man sich mit den Ablaugenviskositäten und Heizwerten.

Erst mit der Entscheidung zum Bau einer Pilotanlage begann die grundlegende Auseinandersetzung mit dem Prozess, wobei durch den ausgewählten Standort Rahmenbedingungen vorgegeben waren, die für die Gesamtprozessumsetzung nicht optimal waren: Das Werk Baienfurt (damals Feldmühle AG) verfügte über eine Zellstofferzeugung nach dem sauren Magnesiumsulfitverfahren. Somit konnten die ASAM- Ablaugen auf Natriumbasis nicht in Baienfurt direkt entsorgt werden. Es wurde nur die Faserlinie mit Eindampfung und Methanolrück-gewinnung, aber nicht auch die Rückgewinnung für die anorganischen Chemikalien realisiert. Die eingedampfte Schwarzlauge wurde zu einem Kraft-zellstoffwerk transportiert und dort der Chemikalienrückgewinnung zugeführt. Mit dieser Entscheidung war es folglich nur bedingt möglich, den Gesamtprozess darzustellen.

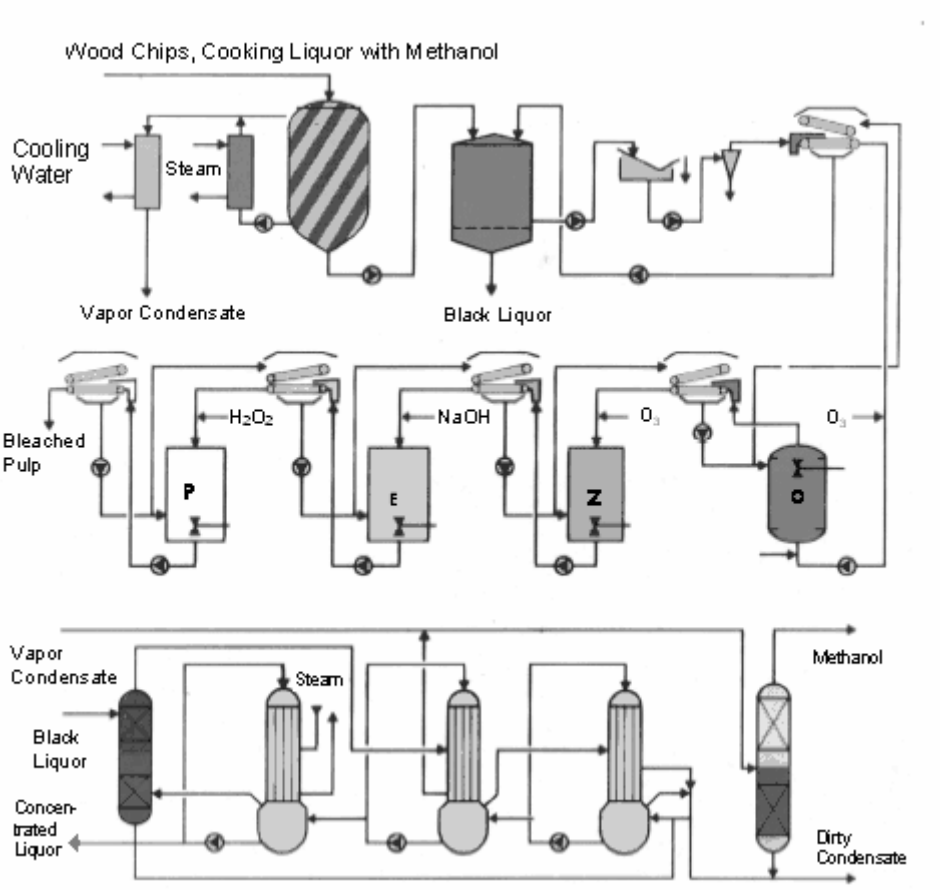

Abb. 3. Flowdiagramm ASAM-Pilotanlage.

Das Wassersystem der Anlage wurde nach dem Gegenstromprinzip im geschlossenen Kreislauf ausgeführt, d. h. neben neuen Verfahren für den Aufschluss des Holzes und die Bleiche der erzeugten Zellstoffe wurde mit der Schließung des Wasserkreislaufes eine bis dahin nicht bekannte Komplizierung des Prozesses der Zellstofferzeugung realisiert. Erfahrungen bezüglich der Auswirkungen des Gegenstromprinzips auf das Bleichergebnis lagen weder aus dem Labor noch aus der industriellen Praxis vor.

Die ASAM-Anlage war so konzipiert, dass praktisch alle Prozessdaten händisch ermittelt werden mussten. Der Automatisierungsgrad war sehr gering und entsprechend schwierig war es, den ASAM-Prozess auf Basis der Pilotanlagenergebnisse zu bilanzieren. Fokus der Pilotanlage war das Produkt, d. h. der Nachweis der Zellstoffqualitäten und nicht das Funktionieren des Gesamtprozesses zur Herstellung von ASAM-Zellstoff inklusive aller Nebenprodukte.

Die Betrachtung des gesamten Prozesses ist entscheidend dafür, ob es gelingt, frühzeitig zu erkennen, ob ein Verfahren realisierbar ist oder nicht. Durch die Betrachtung des Gesamtprozesses können richtungweisende Forschungsschwerpunkte entstehen, die bei bloßer Betrachtung des Produktes nicht erkennbar sind. Damit ist die Prüfung des Prozesses auf Umsetzbarkeit für die potentiellen Anwender von erheblich höherer Bedeutung als nur gute Produkteigenschaften.

Die Bewertung von Produktqualitäten ist einfach. Die Bewertung eines Prozesses bzw. die Einbindung eines neuen Produktes in einen Produktionsprozess ist erheblich komplexer. Ein entsprechender Forschungsschwerpunkt existierte bei ASAM nicht oder er kam zu spät in den

Fokus der Verfahrensentwickler.
Ob der ASAM-Prozess bei einer Investition von 500 Mio. € eine nachhaltige Wirtschaftlichkeit für den Betreiber darstellt oder ob der Prozess überhaupt möglich war, konnte lange nicht nachgewiesen werden. Erst mit der Erstellung der Jaakko-Pöyry-Studie im Jahre 1997, wurde klar, dass ASAM diese Alternative ist. Zu diesem Zeitpunkt war das Verfahren 8 Jahre alt und die Verfahrensumsetzung bereits drei Mal, schon in der Verhandlungsphase, gescheitert.
Wird der Gesamtprozess erst betrachtet, wenn über eine Investition entschieden werden soll, kommt es häufig zu Verzögerungen auf den Entscheidungswegen, da offene Fragen erst durch Forschungsarbeiten beantwortet werden müssen. Diese Forschungsaktionen lassen ein Verfahren altern und reduzieren den Enthusiasmus des Investors für das Produkt, da zu diesem Zeitpunkt investitionsentscheidende Grundlagen nicht vorliegen.
Teilweise kann die dann notwendige Forschung dazu führen, dass sich Produkteigenschaften verschlechtern, weil sich das Verfahren in der industriellen Wirklichkeit anders als im Labor realisieren lässt.
Beispiele für Prozessforschungsaufgaben ASAM waren:

- Auswirkung der Chemikalienkreislaufführung auf das Aufschlussergebnis
- Auswirkung der Wasserkreislaufschließung auf Aufschluss- und Bleichergebnis
- Rückgewinnung des Methanols und Verschleppung von Methanol in nachfolgende Prozessstufen
- Tallöl- und Tallseifenabscheidung

Leider sind derartige Forschungsthemen im Labor kaum oder gar nicht durchführbar, eher unspektakulär und nur selten dazu geeignet, Renommee zu erwerben. Das Fazit des ASAM-Entwicklungsweges ist, dass sehr lange lediglich auf das Produkt Zellstoff fokussiert wurde. Erst sehr spät setzte eine Prozessbetrachtung ein.
Entscheidend für die erfolgreiche Umsetzung einer Idee ist jedoch, wann und wie schnell werden die Schwachpunkte für die industrielle Umsetzung einer Idee erkannt. Dieser Aufgabe sollte sich jeder Verfahrensentwickler möglichst früh bei einem neuen Prozess stellen.

Rahmenbedingungen

Um ein neues, kapitalintensives Verfahren in den Markt zu bringen, braucht es optimaler Rahmenbedingungen, ohne die eine Markteinführung nicht erfolgreich sein kann.
Voraussetzungen für die Markteinführung sind eine gute oder bessere Produktqualität als die der bisherigen Technologien. Gleiches gilt für die Wirtschaftlichkeit und die Umweltverträglichkeit des Verfahrens.
In mindestens einem dieser Punkte sollte ein neues Verfahren so große Vorteile haben, dass einer Verfahrenseinführung aus diesem Grund nichts entgegen spricht. Zudem braucht jedes neue Verfahren einen Anwender, der den Mut aufbringt, dieses neue Verfahren auch tatsächlich zu testen. Diese vier Voraussetzungen sind die Basis, um mit einem neuen Verfahren an den Markt heranzutreten.
Diese Basis ist allerdings nicht die Gewähr, dass eine Neuentwicklung tatsächlich eine Chance hat, umgesetzt zu werden, denn erforderlich für die nächsten Schritte zum Erfolg sind ein umfangreiches Wissen über den Gesamtprozess und ein tragbares Personalkonzept, um diese neue Technologie tatsächlich umsetzen zu können.
Das Wissen um den Gesamtprozess beinhaltet, dass alle wesentlichen Parameter des erforderlichen Verfahrens zur Herstellung des neuen Produktes betrachtet worden sind, die sich aufgrund

der neuen Produktherstellung verändern. Dies bedeutet, dass während der Forschung darauf geachtet werden muss, nicht nur das Produkt zu verbessern, sondern dass auch die Machbarkeit der Erzeugung geprüft wurde. Eine Einbettung der Forschungsaktivitäten in die Gesamtprozessgestaltung muss frühzeitig erfolgen.

Tabelle 1. Bewertung von Einführungsvoraussetzungen für neue Verfahren

Was	**Basis**	**Erforderlich**	**Entscheidend**
Gute Produktqualität	**X**		
Wirtschaftlichkeit des Verfahrens	**X**		
Umweltverträglichkeit	**X**		
Lead Customer (Anwender)	**X**		
Wissen über Gesamtprozess		**X**	
Personalkonzept		**X**	
Finanzkonzept			**X**
Prozessumsetzungskonzept			**X**
Risikobetrachtung			**X**
Risikoübernahme			**X**

Ein Personalkonzept für die Umsetzung einer Technologie ist ebenfalls erforderlich. Eine Betrachtung des Gesamtprozesses, welcher zur Erzeugung des neuen Produktes erforderlich ist, kann nur mit einer interdisziplinär besetzten Personaldecke gelingen. Nur mit den richtigen Personalressourcen ist eine effektive Umsetzung möglich.

Es muss ein machbares Projektumsetzungskonzept entwickelt werden, in das das Wissen um den Gesamtprozess einfließt. Auf Basis dieses Projektumsetzungskonzeptes sollte eine Risikobetrachtung durchgeführt werden, und die Machbarkeit des Verfahrens zur Erzeugung des neuen Produktes wird klar.

Danach kann ein Finanzierungskonzept und ein Konzept zur Risikoübernahme erstellt werden, womit die reale Machbarkeit eines Verfahrens möglich wird.

Projektunabhängige Einflussfaktoren

Es gibt neben den beeinflussbaren Projektfaktoren auch jene, die durch Dritte einem Projekt aufgezwungen werden und die nur schwer oder nicht entkräftbar sind. Die 1997 erschiene JP-Studie [4] weist das ASAM-Verfahren als einzige erkennbare Alternative zum Kraftverfahren aus. Für einen Versuch, das Verfahren umzusetzen, war es zu diesem Zeitpunkt allerdings schon zu spät. Was hat die Barriere so hoch gehoben, dass die Einführung des ASAM Verfahrens praktisch unmöglich geworden ist?

Zum einen gab es Verfahren am Markt, deren Einsetzbarkeit für die Papier- und Zellstoffindustrie nur bedingt Erfolg versprach. Die Verfahren auf Basis organischer Lösungsmittel wie Alcell, Acetosolv und Natural Pulping konnten nur bedingt durch die damit erzeugten Zellstoffe überzeugen. Alle diese Verfahren waren nur für einige Rohstoffarten geeignet. Die so produzierten Zellstoffe wiesen keine positiven Unterscheidungsmerkmale zu bereits am Markt verfügbaren Produkten auf. Es gelang nicht, Zellstoffverbraucher nachhaltig für diese Produkte zu gewinnen.

Die Wirtschaftlichkeit dieser Verfahren auf der Basis von Lösungsmitteln zur Zellstofferzeugung konnte nur dargestellt werden, in dem aus Ablaugen Produkte generiert wurden, für die es zu dem damaligen Zeitpunkt keinen Markt gab.

Beim Organocell Verfahren ist die Sachlage anders. Den Entwicklern dieses Verfahrens ist es gelungen, Investoren für den Bau einer großtechnischen Anlage in Kelheim zu begeistern. Leider gelang es den Planern und Betreibern dieser Anlage nicht, dauerhafte und stabile Betriebszustände zu erreichen, so dass der Betreiber 1993 Insolvenz anmelden musste [6]. Die Übertragung der Entwicklung vom Pilot- in den Großmaßstab scheiterte. Aufgrund der erzielten Produktqualitäten

und des Anlagenzustandes ließ sich anschließend kein Investor finden, der die Anlage in Kelheim mit dem Organocell-Verfahren weiter betreiben wollte. Eine Investition im Wert von mehreren 100 Mio. € musste letztlich abgeschrieben werden. Die Anlage wurde abgerissen.
Es ist müßig, jedes Detail, welches zum Scheitern der Organocell-Großanwendung geführt hat, aufzulisten. Nach meinen Informationen sind die Gründe vielfältig. Sicher ist, dass auch produktions-technische Gründe für das Scheitern des Projektes mitverantwortlich waren [6]. Übertragen auf das ASAM-Verfahren, war das Scheitern des Organocell-Prozesses ein schwerer Rückschlag oder eine Katastrophe. Die Pleite dokumentierte nachhaltig für potentielle Investoren, wie realistisch das Scheitern eines neuen Verfahrens ist, wenn es von der Demonstrations- in die Anwendungsphase übertragen wird.
Ein Erfolg des Organocell-Verfahrens, damit ist gemeint, dass reibungslose Funktionieren der errichteten Anlage und die Erzeugung verwertbarer Zellstoffe, hätte sicherlich einen positiven Schub für das ASAM-Verfahren bedeutet. So ging der Schuss nach hinten los.

Einführungswege

Um das Risiko der Einführung eines neuen Verfahrens zu reduzieren, ist es erforderlich zu prüfen, ob eine Umstellung einer bestehenden Produktionsanlage möglich ist oder ob Teilprozesse in großtechnischen Anlagen nachgestellt werden können.
Dies ist natürlich bei Verfahren zur Erzeugung von Zellstoff, die organische Lösungsmittel verwenden, erschwert, da alle kommerziellen Anlagen auf diese Chemikalien in ihren Prozessen verzichten. Hiermit hatten alle hier genannten Verfahren ein Einführungs-hemmnis. Der Bau von Pilotanlagen mit hierauf spezialisierten Techniken war zwingend erforderlich, wobei jeweils nur die Faserlinien in Demonstrationsanlagen realisiert wurden. Die Gesamtverfahren wurden nicht betrachtet.
Hinzu kommt, dass bei einigen Verfahren zusätzlich neue Rückgewinnungs-technologien für Aufschlusschemikalien erforderlich waren. Auch dies konnte in „konventionellen Anlagen“ nicht ausprobiert werden.
Risikoarme Umsetzungswege sind somit solche, die ermöglichen, dass neue Verfahren in bestehenden Anlagen zumindest teilweise geprüft werden können, auch wenn hierzu vorübergehend technologische Kompromisse eingegangen werden müssen. Sind solche Wege nicht gegeben, erhöht sich das Risiko so weit, dass eine Einführung dieser neuen Technologie grundsätzlich nicht gegeben ist. Hierüber sollte sich jeder Entwickler und Forscher im Klaren sein.
Beim Bau einer Pilotanlage ist darauf zu achten, dass der Gesamtprozess abgebildet wird, so dass wirklich eine Verfahrensbilanzierung ermöglicht wird. Nur so kann es gelingen, die Verfahrensprobleme zu erfahren und Prozesskreisläufe nachzuvollziehen. Scalingeffekte können gesehen werden, so dass eine realistische Risikoabschätzung vor einer Verfahrenseinführung in die Großtechnik möglich ist.
Abschließend sollte darauf geachtet werden, dass die erzeugten Produktmengen so groß sind, dass das Zielprodukt für Anwendungstests bei den Weiter-verarbeitern in ausreichender Menge bereitgestellt werden kann. Erfolgt dies nicht, werden sonst nur immer wieder offene Fragen auftreten, die einer Markteinführung des Produktes entgegen-stehen.

Zusammenfassung

Produktentwicklungen verlaufen in verschiedenen Phasen

- Entstehung einer Idee
- Erhärtung der Idee
- Absicherung der Idee
- Verbesserung der Idee
- Prüfung der Idee auf Umsetzbarkeit
- Umsetzung der Idee in Praxis

Wird die Prüfung der Umsetzbarkeit zu spät oder gar nicht während der Forschung betrachtet, führt dies häufig zu einem Scheitern bei der Überführung eines Verfahrens in die industrielle Praxis. Es ist somit erforderlich, dass die Forschung sich verstärkt um die Prüfung der Umsetzbarkeit und die Betrachtung des Gesamtprozesses bemüht, wenn eine erfolgreiche Projektumsetzung gewünscht ist.
Neben diesen von der Forschung vorzubereitenden Aktivitäten ist es selbstverständlich, dass jedes Verfahren Erfordernisse erfüllt, wie eine verbesserte Produktqualität, Wirtschaftlichkeit oder Umweltverträglichkeit. Entscheidend für eine Verfahrensumsetzung sind jedoch ebenso Finanzierungskonzepte, Personalkonzepte, eine Risikobetrachtung sowie die Bereitschaft eines Investors zur Risikoübernahme.
Beim Bau von Demonstrationsanlagen ist darauf zu achten, dass das Gesamtverfahren so weitgehend wie möglich abgebildet werden kann, damit möglichst wenig offene Fragen nach dieser Phase übrig bleiben.
Das ASAM-Verfahren ist trotz des bescheinigten Potentials nicht in die industrielle Praxis überführt worden. Der Grund war sicherlich nicht der ASAM-Zellstoff.

Literatur

[1] Patt, R.; Kordsachia, O.: Herstellung von Zellstoffen unter Verwendung von alkalischen Sulfitlösungen mit Zusatz von Anthrachinon und Methanol. Das Papier **40**, 1986, 10 V1-V8.

[2] Schubert, H.-L.; Fuchs, K.; Patt; R. Kordsachia, O.; Bobik, M.: Der ASAM Prozess – Eine industriereife Zellstofftechnologie. Das Papier **47**, 10A, 1993, V6-V15.

[3] Schubert, H.-L.; Kordsachia, O.; Shackford, L.; Shin, N.-H.: High Yield and Easy Bleachability – The ASAM Process. Proc. Tappi, Breaking the Yield Barrier, 1998, Atlanta, 241-246.

[4] Jaakko Pöyry Deutschland GmbH, Umweltverträgliche Holzaufschlußverfahren, Schriftenreihe „Nachwachsende Rohstoffe“ Band 8, Landwirtschaftsverlag GmbH 48165 Münster, 1997.

[5] Schubert, H.-L.: Pilot Plant Cooking of Softwood. Kraftanlagen Heidelberg, ASAM Report 1, 1990.

[6] Wagner, U.; Scheper K.: Flächenrecycling am Beispiel des kontaminierten Werksgeländes der Zellulosefabrik in Kelheim: DU Diederichs + Partner, Gutenbergstraße 13, 82178 Puchheim, 2006, www.stmugv.bayern.de/de/aktuell/download/boden/35.pdf.

Lenzinger Berichte, 86 (2006) 32-45

COMPREHENSIVE KINETIC STUDY OF DELIGNIFICATION, CARBOHYDRATE DEGRADATION, CELLULOSE CHAIN SCISSIONS, AND HEXENURONIC ACID REACTIONS DURING KRAFT PULPING OF *EUCALYPTUS GLOBULUS*

Herbert Sixta[1], Ewa Wiktoria Rutkowska[2]
[1] Lenzing AG Pulp Research, Werkstraße 1, 4860 Lenzing, Austria
[2]Kompetenzzentrum Holz GmbH, St.-Peter-Str. 25, A-4021 Linz, Austria

Eucalyptus globulus **represents one of the most suited fibre sources for the production of a wide range of high quality papers and high-purity dissolving pulps. The optimization of kraft pulping covering both continuous and batch processes demands kinetic models suitable for advanced control and offline optimization of the cooking operation.**

Quite recently, an improved kinetic model structure for softwood kraft cooking has been published, which considers varying alkali and temperature profiles during the cooking [1]. Unfortunately, most alkaline cooking models are based solely on softwood [2, 3]. This work contributes to an improved kinetic model for kraft cooking of *Eucalyptus globulus* suitable for advanced control of modern displacement cooking processes such as the continuous batch cooking process (CBC). After impregnation where the initial lignin has been removed, the bulk and residual delignification have been studied in a batch reactor as a function of the [OH^-], [HS^-], ionic strength, [Na^+], and temperature. The underlying kinetic expressions are similar to those used in the Andersson model also including a mechanism for determining the distribution of lignin and carbohydrate species 2 and 3 as a function of the cooking conditions. The kinetic equations were successfully validated against experimental data from a pilot plant digester applying conventional batch cooks.

Furthermore, the formation of hexenuronic acid bound to the xylan backbone and its degradation / dissolution were described by a consecutive first-order reaction. In agreement to other studies, the temperature and the effective alkali charge revealed a strong influence on the hexenuronic acid content in the pulp while the effect of sulfidity proved to be insignificant. The role of ionic strength on the HexA content remained unclear. An increase in the ionic strength resulted in a higher maximum HexA content shifted to a higher kappa number (about 58), but with progressive delignification to a kappa number typical for unbleached *E. globulus* kraft pulp (about 15), the HexA content decreased to a level more than 20% lower as compared to pulps cooked at lower ionic strength.

Keywords: *E. globulus, CBC pulping, reaction kinetics, hexenuronic acid*

Introduction

The majority of kinetic studies have been performed with softwoods. So far, only basic informations about the kinetics of *E. globulus* kraft pulping are available. Santos et al. [4] developed expressions for the initial and the bulk delignification phase. His work was continued by Gilarranz et al. [5] who investigated the

residual phase and also modeled the lignin conversion value at the transition point from the bulk to the residual phase. However, none of the presented models was able to meet all necessary requirements for modeling *E. globulus* CBC kraft pulping. CBC is a new pulping method, which allows to change the alkali profile and other important reaction conditions during the cooking process [6]. The model of choice seems to be the model proposed by Andersson et al. [1]. This model considers the influence of varying cooking conditions by introducing an appropriate algorithm for determining the distribution of lignin and carbohydrate species 2 and 3 as a function of the relevant cooking conditions. The aim of this study was to develop a comprehensive kinetic model for kraft pulping of *E. globulus* based on the concept of Andersson to provide an appropriate tool for the optimization of cooking processes in practice.

Characteristic for hardwood kraft pulps is their relatively high content of hexenuronic acid groups (HexA) linked to the xylan backbone. Different to softwood pulping, in hardwood pulping the decrease in HexA content seems to occur only at very low kappa numbers, normally not achieved during commercial pulping processes [7]. The presence of HexA in hardwood kraft pulps contributes to 25 - 30% of the pulp kappa number and thus explains the low efficiency of oxygen delignification of hardwood kraft pulps. Recently, some efforts have been made to better understand the mechanisms of both the HexA formation and HexA degradation/ dissolution [7-11]. So far, it is agreed that the HexA reactions are mainly dependent on temperature and alkali charge, which concludes that a considerable decrease in HexA contents can only be achieved when high temperatures and high alkali charges are applied.

The present work proposes a simplified kinetic model that describes the formation of HexA from 4-*O*-methyl-α-D-glucuronic acid (MeGlcA) and the degradation/ dissolution of HexA during kraft pulping of *E. globulus*. Moreover, the influence of effective alkali concentration, the sulfidity of the cooking liquor and the ionic strength, expressed as sodium ion concentration, on the HexA concentration profiles are exemplified.

Experimental

For the kinetic studies *E. globulus* chips received from ENCE, M'Bopicua, Uruguay, with an average thickness of 4 mm were further cut in the laboratory. After screening their average dimensions were reduced to 9.6 mm in length, 4.9 mm in width and 1.9 mm in thickness. The wood chemical composition was as follows: 22.1 % Klason lignin (KL) (T 222 om-98), 4.6 % acid soluble lignin (T om-250), 47.3 % cellulose (C), 2.2 % glucomannan (GM), 21.8 % 4-*O*-methylglucuronoxylan (X) (AEC with PAD detection after total hydrolysis with H_2SO_4) and 2.0% resins and ash (T 211 om-93; ISO 14453:1997). The hexenuronic acid (HexA) content in the pulp was determined by a selective hydrolysis of the glycosidic linkage between the hexenuronic acid group and the xylan chain followed by oxidation and conversion to a coloured compound for colorimetric determination [12]. The kappa number <20 was determined according to T236 cm-85, and >20 according to SCAN-C 1:00, the viscosity according to SCAN 15:88. The cooking liquors were prepared from NaOH(s), $Na_2S.H_2O$(s), and NaHS(s). The sodium concentration was adjusted by gravimetric addition of NaCl. Effective and residual alkali concentrations were analyzed according to SCAN-N 30:85 and sulfidity according to SCAN-N 31:94.

Prior to the kinetic investigations, the wood was subjected to a uniform

impregnation stage in a 10 L-digester at 100 °C for 60 min with [OH^-] = 0.37 mol/L, [HS^-] = 0.16 mol/L, [Na^+] = 1.5 mol/L at a L/S ratio of 10:1. With a yield loss of 6.5%, the composition of the impregnated wood changed to 18.9 % KL, 47.1 % C, 0.7 % GM, 17.9 % X, and 1.5 % resins and ash. KL can be calculated from kappa number by a factor of 0.183 (18.9/103.3).

After drainage of the impregnation liquor, the chips were transferred to a 400 ml-Parr reactor to proceed with the kinetic investigations. The stainless steel pressure vessel was provided with an external heating system and measurement and control of both pressure and temperature. The temperature was increased at a rate of about 5 °C per minute to the preset cooking temperature. The heating-up time and any deviation from the target cooking temperature were corrected for isothermal conditions using the following expression:

$$t_{T_0} = \int_{t_{T_1}}^{t_{T_0}} Exp\left(-\frac{E_A}{R}\left[\frac{1}{T_t} - \frac{1}{T_{T_0}}\right]\right) \cdot dt \qquad (1)$$

in which T_t is the temperature during heating-up, T_0 the target temperature, t_{T0} the reaction time at target temperature (corrected for isothermal conditions), and E_A the activation energy which was assumed to be 134 kJ/mol. The numerical integration can be carried out by just adding the terms as follows using an Excel sheet (Eq. 2).

The experiments were accomplished at an L/S ratio of 40:1 in order to keep constant concentration of chemicals throughout the cooks. Time series at four different temperature levels (140, 150, 160, and 170°C), five different [OH^-] levels (0.1, 0.27, 0.52, 0.94 and 1.23 mol/L), three different [HS^-] levels (0.17, 0.29, 0.64 mol/L) and three different [Na^+] levels (0.8, 1.5 and 2.5 mol/L) were conducted to provide the necessary database for the evaluation of the kinetic models for delignification, carbohydrate degradation and cellulose chain scissions. For the kinetic investigations of both, HexA formation and HexA degradation/ dissolution, the conditions given in Table 1 were applied.

$$t_{T_{0,n}} = t_{T_{0,n-1}} + \left(t_{T_{t,n}} - t_{T_{t,n-1}}\right) \cdot \left(Exp\left(-\frac{E_A}{R}\left[\frac{1}{T_{t,n}} - \frac{1}{T_0}\right]\right) + Exp\left(-\frac{E_A}{R}\left[\frac{1}{T_{t,n-1}} - \frac{1}{T_0}\right]\right)\right) \Big/ 2 \qquad (2)$$

Results and discussion

Kinetics of delignification and carbohydrate degradation

The general structure of the delignification and carbohydrate degradation models is derived from the model introduced by Andersson et al. [1]. The advantage of this model is that it accounts for any subsequent changes in cooking conditions as occurring in industrial batch and continuous cooking processes (see also [13]). It is commonly agreed that the single wood species such as lignin (L) and (CH) can be divided into three species with different reactivity (L1, L2, L3 and CH1, CH2, CH3) representing their different chemical and supramolecular composition.

Table 1. Cooking conditions of *E. globulus* kraft cooking used for the kinetic investigation of HexA formation and HexA degradation/dissolution.

Parameter	Units	Changed Parameters				Const. Parameter
Temperature	°C	140	150	160	170	160
[OH^-]	mol/L	0.10	0.52	1.23		0.52
[HS^-]	mol/L	0.17	0.28	0.64		0.28
[Na^+]	mol/L	0.80	1.50	2.50		1.50

The model is based on the assumption that all species react in parallel throughout the cook. Assuming that a great part of species 1 (L1, CH1) is easily degraded during impregnation it is suggested to consider only species 2 and 3 (L2, L3, CH2, CH3) for both delignification and carbohydrate degradation models. In the case of nonisothermal industrial cooks, the initial chemical wood composition (L_0, CH_0) has to be used as starting values to account for the overall consumption of active cooking chemicals ($[OH^-]$, $[HS^-]$).

A general rate equation for both lignin and carbohydrate degradation can be expressed according to Eq. 3.

$$\frac{dW_{i,j}}{dt} = -k_{W_i,j} \cdot W_{i,j} \qquad (3)$$

for W_i = L for lignin and CH for the sum of carbohydrates comprising cellulose (C), glucuronoxylan (X) and glucomannan (GM), for j = species 2 and 3 for both L and CH and for k = rate constants.

The general solution for these first-order rate equations is given in Eq. 4:

$$W_{i,tot} = \sum_{j=2}^{3} W_{i,j}^{0} \cdot Exp\left(-k_{W_i,j} \cdot t\right) \qquad (4)$$

for W^0_i = L and CH concentrations after impregnation for the evaluation of the kinetic models and initial wood composition for modelling of industrial cooks.

The dependency of the rate expressions, $k_{Wi,j}$, on the reaction conditions can be described according to Eq. 5:

$$k_{W_i,j} = A_{W_i,j} \cdot Exp\left[\frac{EA_{W_i,j}}{R} \cdot \left(\frac{1}{443} - \frac{1}{T}\right)\right] \cdot \left(\left[OH^-\right]^a \left[HS^-\right]^b \left[Na^+\right]^c + k_r\right) \qquad (5)$$

for A = pre-exponential factor, EA = activation energy [kJ/mol], R = gas constant [kJ/(mol.K)], a, b, c, are constants and k_r a rate constant reflecting the observation of carbohydrate degradation even at very low alkali concentrations.

The experimental results have been fitted by nonlinear regression using Scientist® as data fitting software. Scientist employs a least squares minimization procedure based on a modification of Powell's algorithm. The fitting yields the results shown in Table 2.

Please note, that similar to Andersson et al., the pre-exponential factors A were modified by a "factor" reflecting the (not considered) differences between constant composition cooks and industrial pulping.

Table 2 shows that the activation energies are in the range reported for kraft pulping, except in the case of carbohydrate degradation of species 3, whose activation energy is significantly higher as published for the same reaction in spruce (174.6 kJ/mol compared to 144 kJ/mol reported by Andersson et al. [1]). Moreover, the kinetic order of the hydroxide ion concentrations, particularly for L3 and CH3, are far higher as reported in the literature [13]. The large order for $[OH^-]$ in the case of L3 may be attributed to its simultaneously high dependency on $[Na^+]$. The results from the kinetic study confirm that an increase in the ionic strength

Table 2. Kinetic constants for delignification and carbohydrate degradation of *Eucalyptus globulus.*

Component	L_0		CH_0	A	EA	a	b	c	factor	k_r
	% odw	kappa#	% odw	1/(M*min)	kJ/mol					1/min
Lignin including HexA										
L1*	3.2									
L2	17.1	93.5		0.4527	131.4	0.63	0.32	-0.63	1.3	0.00
L3	1.8	9.8		0.0402	133.0	1.47	0.00	-0.68	0.5	0.00
CH1*			5.6							
CH2			15.3	0.2415	140.9	1.54	0.00	0.00	1.0	0.11
CH3			50.3	0.0031	174.6	2.35	0.00	0.00	2.0	0.00

*calculated from mass balance

decreases the rate of delignification considerably as shown for birch by Lindgren and Lindström [14] and in Figure 1.

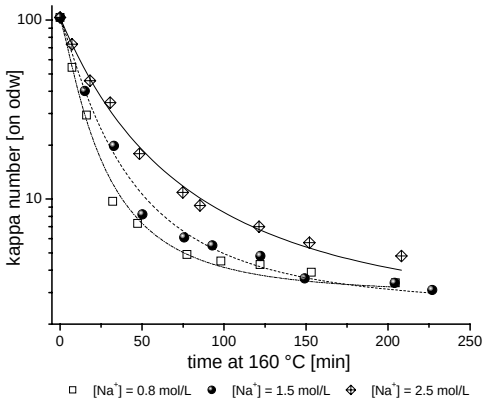

Figure 1. Course of kappa number during kraft pulping at 160 °C, constant [OH^-] = 0.52 mol/L, [HS^-] = 0.28 mol/L and increasing [Na^+].

Changes in ionic strength, however, exhibit no significant influence on carbohydrate degradation.

To allow for changes in the main reaction conditions such as [OH^-], [HS^-], [Na^+] and temperature, the distribution model proposed by Andersson et al. [1] has been implemented in our cooking model. This model shows that the species W_2 and W_3 interchange reversibly and that the equilibrium between both species is dependent on certain reaction conditions. The intersection is the level of wood component where W_2 equals W_3 and is termed W*. Multiple regression analysis provides an expression for W* as a function of the reaction conditions. The expressions for L* and CH* are given in Eq. 6 and 7, respectively, in which the temperature T is expressed in °C.

Figure 2 illustrates the dependency of the extracted intersections L* on the [OH^-], [Na^+] and [HS^-].

Surprisingly, no clear influence of L* on temperature has been observed, while CH* was clearly influenced by temperature and [OH^-] but not by [HS^-] and [Na^+].

The way of determining the proportions of W2 and W3 follows the procedure given by Andersson et al. [1, 13].

Kinetics of cellulose chain scissions

The kinetics of carbohydrate degradation, observed as viscosity loss or cellulose chain scissions, can be followed by a very simple approach with reasonable precision. Equation 8 describes the cellulose chain scissions as a function of temperature, effective alkali and sodium ion concentrations and time.

$$L* = 0.001487 \cdot \left(\left[OH^-\right] + 0.025\right)^{-0.625} \cdot \left(\left[HS^-\right] + 0.045\right)^{-0.308} \cdot \left(\left[Na^+\right] + 5.0\right)^{4.106} \quad (6)$$

$$CH* = 55.44 + 68.45 \cdot \left[OH^-\right] - 0.48 \cdot T \cdot \left[OH^-\right] \quad (7)$$

$$\left(\frac{1}{DP_{n,t}} - \frac{1}{DP_{n,0}}\right) = A \cdot Exp\left(-\frac{EA_C}{R}\frac{1}{T}\right) \cdot \left[OH^-\right]^d \cdot \left[Na^+\right]^e \cdot t \quad (8)$$

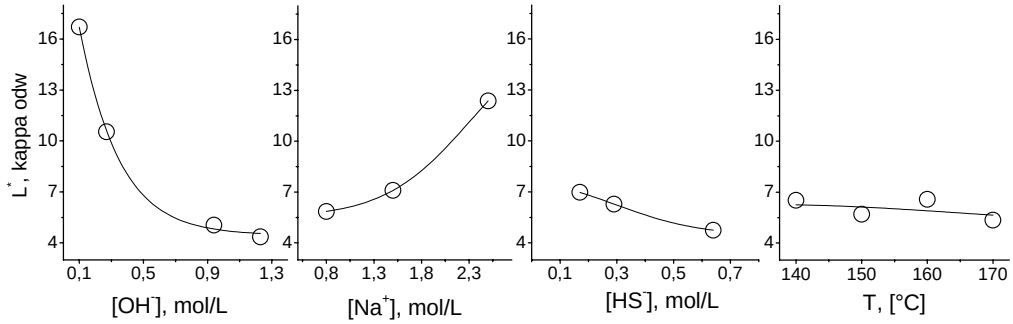

Figure 2. L* as a function of [OH^-]-,[Na^+], [HS^-] and temperature.

$$D = 0.057 \cdot \sqrt{T} \cdot Exp\left(-\frac{2452.4}{T}\right) \cdot \left(0.00364 \cdot \kappa\# + 0.13 \cdot \left[OH^-\right]^{0.55} + 0.58\right) \quad (9)$$

Using this simple expression, it is permissible to use DPv, calculated from intrinsic viscosity according to SCAN-CM-15:88, instead of DP_n. Nonlinear regression using least square minimization procedure yields the coefficients for the applied kinetic model shown in Table 3:

Table 3. Kinetic constants for chain scissions during kraft pulping of *E. globulus*.

Model Parameter	Units	
$DP_{n,0}$		4900
ln A	1/(M*min)	36.48
EA_c	kJ/mol	180.3
d		1.08
e		0.74

Unlike to carbohydrate degradation, an increase in ionic strength at a given [OH^-] is connected with an increase in cellulose degradation. It may be speculated that the presence of high [Na^+] promotes chain cleavage due to a better accessibility of the glycosidic linkages.

Effective concentration of cooking chemicals

Chip dimensions and the level of cooking chemical concentrations in the bulk liquor influence the concentration profiles of the cooking chemicals within the wood. The [OH^-], [HS^-] and [Na^+] across the chip thickness (one-dimensional chip model) were calculated by using the diffusivity parameters of McKibbins solving Fick's second law of diffusion corrected with respect to pH and lignin content [15, 16], where D is the diffusion coefficient in cm^2min^{-1} and T the temperature in K.

The reactive cooking chemicals, [OH^-] and [HS^-], are transported from the bulk phase to the boundary layer and finally through the water layer of the cell wall and pit membrane structure under the influence of their concentration gradient in the entrapped and free liquor. The model considers only the diffusion of alkali in a one-dimensional wood chip through the chip thickness (radial direction). The diffusion of [OH^-] is described by Fick's second law of diffusion. The concentration of the active cooking chemicals in the entrapped liquor (bound liquor) must be determined to provide the necessary data for a reliable kinetic study which may be used to predict the course of pulping reactions in pilot or even commercial digesters.

At the beginning of the cook, at $t = t_0$, the average [OH^-] in the entrapped liquor depends on the wood density (ρ_{dc}) and the moisture content (MC_W) of the wood according to Eq. 10:

$$\left[OH^-\right]_{EL} = \left(1 - \frac{MC_w}{(100 - MC_w) \cdot \left(\frac{1}{\rho_{DC}} - \frac{1}{1.53}\right)}\right) \cdot \cdot \left[OH^-\right]_{FL} \quad (10)$$

where FL is the free or bulk liquor, EL the entrapped or bound liquor.

During pilot plant or industrial cooking, where L/S ratios range between 2.5 and 5, the concentration of cooking chemicals decreases as a result of the consumption of chemicals by the reaction products. Thus consumption of active cooking chemicals must be considered to predict the extent of delignification and carbohydrate degradation accurately. The specific consumptions of [OH^-] were determined as 0.20 NaOH/kg degraded lignin and 0.45 kg NaOH/kg degraded carbohydrates, respectively, which are only slightly higher as reported by Christensen et al. for similar reactions of softwood components [17].

The concentration profiles for the effective alkali in both free (FL) and entrapped (EL) liquors (average concentration) during a conventional batch kraft cook using *Eucalyptus urograndis* as a raw material have been calculated by the model. Additionally, the minimum EA concentration in the center of the 4 mm-chip (CC) is shown in Figure 3.

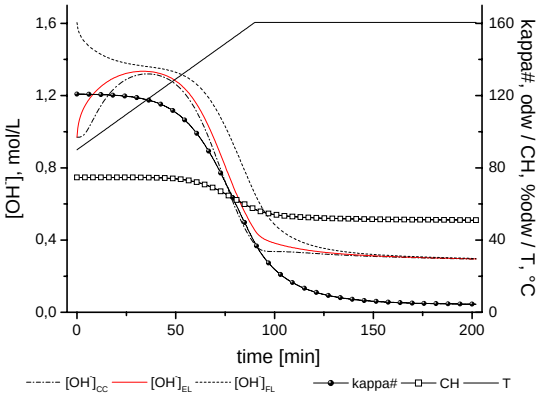

Figure 3. Course of effective alkali concentrations in the free (FL) and entrapped cooking liquor (EL) during a conventional *E. globulus* kraft cook. The conditions were taken from pilot plant cooking (KA440): chip thickness 4.0 mm, chip moisture content, MC_W = 35%, chip density, ρ_{DC} = 0.50; $[OH^-]_{t=t0}$ = 1.60 mol/L, $[HS^-]_{t=t0}$ = 0.245 mol/L, L/S = 3.15 kg/kg.

The EA concentration in the bound liquor reveals an increase during the first third of the heating-up phase, approaching the maximum value after 33 min at 115 °C, indicating that diffusion is the dominating process. The effective alkali, however, is rapidly consumed by the chemical reactions which start heavily in the second third of the heating-up period. The EA concentration inside the chips approaches that outside the chips only after 30 min reaction time at cooking temperature. The calculated residual EA concentration (after t = 90+112 = 202 min) of 0.300 mol/L agrees perfectly with the experimentally determined residual EA concentration of 0.296 mol/L.

Validation of the Model

One of the key advantages of the distribution model from Andersson is that it accounts for changes in the reaction conditions appropriately.

Therefore, in a first set of experiments the influence of a sudden increase of $[OH^-]$ from 0.1 mol/L to 1.0 mol/L after a reaction time of 45 min at 160 °C and a L/S ratio of 40:1 on the course of the degradation of wood components was simulated. Figure 4 displays the comparison between predicted and experimentally determined kappa numbers. Even though only a few experiments were carried out so far, the correspondence between calculated and measured kappa numbers is satisfactory. The (calculated) course of $[OH^-]$ in both the bound liquor and the chip centre is quite comparable due to the high L/S ratio.

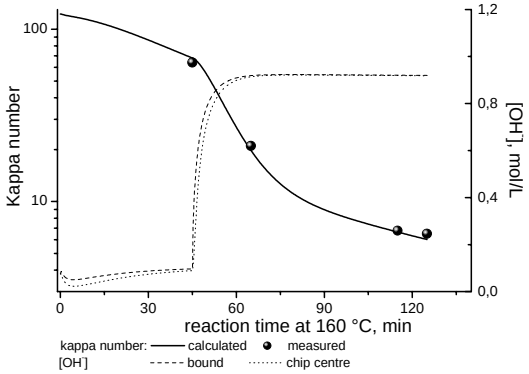

Figure 4. Comparison of predicted and experimentally determined kappa numbers in the course of kraft pulping of *E. globulus*. Constant cooking conditions: L/S = 40:1, $[HS^-]$ = 0.30 mol/L, $[Na^+]$ = 1.5 mol/L, T = 160 °C, cooking liquor as a function of H factors during batch kraft.

The aim of the second set of experiments was the prediction of the unbleached pulp quality derived from *E. globulus* kraft pulping using a conventional batch process. The mean thickness of the industrial chips was 4.0 ± 1.5 mm and the chips had a moisture content of 35%. The cooking trials were carried out in a 10-L digester with forced liquor circulation. After a short steaming phase (8 min, final temperature 98 °C), white liquor was introduced to a total L/W ratio of 2.96 L/kg. The effective alkali charge was set to 19% on od wood. The sulfidity was 26.5% resulting in initial $[OH^-]$ and $[HS^-]$ of 1.60 mol/L and 0.245 mol/L, respectively. The conventional batch cooking procedure was characterized by a heating-up time of 90 min to a cooking temperature of 160 °C. Four cooks were performed comprising H-factors of 300, 450, 600, and 800. Figure 5 illustrates an acceptable correspondence between simulated and experimentally

determined kappa numbers and viscosity values. Even though the modelling of viscosity is based on a very simple approach, the viscosity is predicted more precisely as compared to the kappa number. The latter reduces only by 3.5 units when increasing the H-factor from 300 to 800. The low change in kappa number during a significant prolongation of cooking time may be attributed to a progressive precipitation of dissolved lignin.

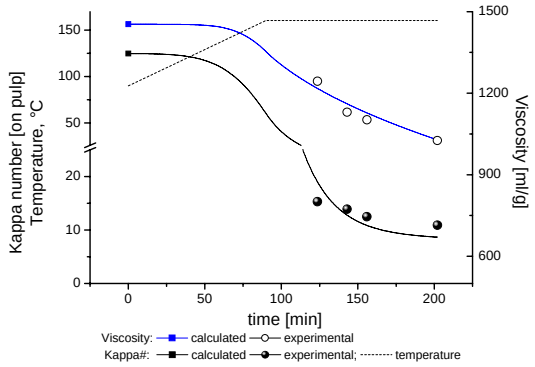

Figure 5. Measured and predicted kappa numbers and viscosities and calculated [OH^-] in the free and bound liquor as a function of H-factors of conventional batch kraft cooking of *E. globulus*.

Formation and degradation /dissolution of hexenuronic acid (HexA) in pulp during kraft pulping

Hexenuronic acid (4-deoxyhex-4-enuronic acid or HexA) is formed from 4-*O*-methyl-α-D-glucuronic acid (MeGlcA) after β-elimination of methanol during the preliminary cooking stages. HexA contributes to the kappa number (11.6 mmol of HexA corresponds to 1 kappa unit) [18] and causes an increased brightness reversion of pulp and paper [19]. The HexA concentration profiles in softwood differ significantly from those reported in hardwood pulping [7]. The formation of HexA in softwood pulping is very fast, and their degradation/dissolution of HexA starts already in the bulk phase of the cook [20]. Gustavsson et al. investigated the influence of hydroxyl ion [OH^-] concentration, hydrogen sulphide ion [HS^-] concentration, ionic strength [Na^+] and temperature, on the degradation/ dissolution of HexA in kraft pulping of spruce [21]. According to a simplified kinetic model, the rate of HexA removal increases with increasing [OH^-], increasing [Na^+], increasing [HS^-], and increasing cooking temperature. Taking the delignification kinetics into account, this translates into a reduced HexA content at a given corrected kappa number (the kappa number of HexA is subtracted) by applying a high [OH^-], a high [Na^+], a low temperature, and a low [HS^-].

It is widely agreed that the HexA content of hardwood pulps increases during the initial phases of bulk delignification and does not decrease until very low kappa numbers are attained [7]. Because the pulp will not cook to such low kappa number in mill practice, HexA content of hardwood pulps is significantly higher as compared to softwood pulps. Both the lower HexA formation and the delayed HexA reduction rates in conventional kraft pulping of hardwood as compared to softwood has been attributed to the higher EA consumption in the early stages of cooking due to a higher demand for neutralization of the formed hydroxycarbxylic acids originated from the degradation of hemicelluloses. This clearly indicates that hydroxide ion concentration and the temperature level are decisive parameters controlling the HexA concentration both in the pulp and in solution.

The decrease of MeGlcA in pulp through HexA formation or the cleavage of methylglucuronic acid and subsequently the cleavage of HexA from the xylan backbone can be described by a consecutive reaction kinetics (Eq. 11):

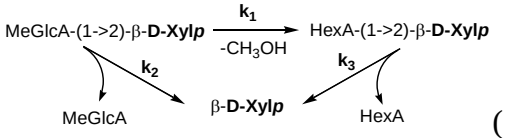

(11)

Quite recently, this reaction scheme has been proposed by Daniellson et al. [10]. In their study the MeGlcA and HexA contents of pulp xylan and of dissolved xylan were investigated at constant [OH^-]

(0.4 mol/L) and [HS^-] (0.2 mol/L) at a L/S ratio of 75:1 and three different levels of temperature (140 °C, 150 °C and 160 °C) as a function of reaction times. According to their findings, the degree of substitution of MeGlcA and HexA in dissolved xylan was higher than in the pulp xylan.

In this report, the HexA content of the pulp was followed as a function of temperature, [OH^-], [HS^-] and ionic strength [Na^+]. The net formation of HexA bound to the xylan backbone and its degradation/dissolution are described by a consecutive first-order reaction according to the reaction scheme in Eq. 12 (For simplicity, the MeGlcA and HexA contents of the dissolved xylan were not considered):

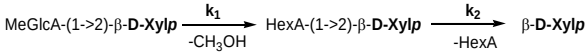

(12)

The change of the HexA content of pulp xylan is controlled by both the MeGlcA and the HexA concentrations, as shown in Eq. 13:

$$\frac{d[HexA]}{dt} = k_1 \cdot [MeGlcA] - k_2 \cdot [HexA] \quad (13)$$

The initial conditions are [HexA] = 0 at t = 0 and [MeGlcA] = $[MeGlcA]_0$ at t = 0.
The solution of this differential equation is expressed in Eq. 14:

$$[HexA] = \frac{k_1 \cdot [MeGlcA]_0}{(k_2 - k_1)} \cdot (Exp(-k_1 t) - Exp(-k_2 t)) \quad (14)$$

An initial concentration of 4-*O*-methyl-α-D-glucuronic acid (MeGlcA) in pulp xylan of 166 mmol/kg wood was estimated by assuming a molar ratio between MeGlcA and xylose of 0.1378 : 1 reported by Evtuguin et al. [22] and the experimentally determined xylan content of 16.0 wt% (od wood). Figure 6 displays the course of HexA contents in pulp as a function of reaction time for the different temperature levels. It shows the typical pattern of successive first-order reactions.

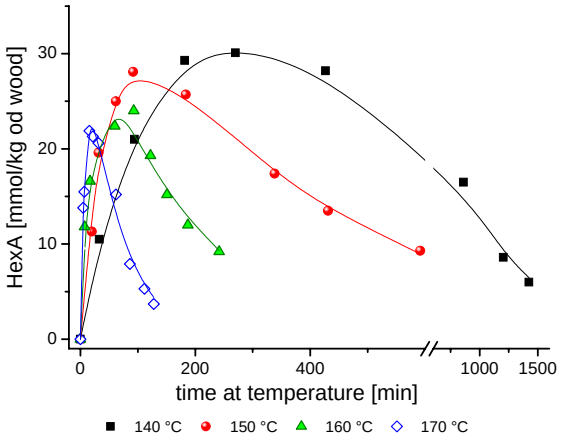

Figure 6. The effect of temperature on HexA contents of the pulp xylan at constant cooking chemical concentrations of [OH^-] = 0.52 mol/L, [HS^-] = 0.28 mol/L and [Na^+] = 1.5 mol/L. Experimental values vs. model predictions for the HexA contents.

The model parameters originate from nonlinear regression analysis of the experimental results using Scientist® as data fitting software. The values of the rate constants are shown in Table 4 together with the energies of activation.

Table 4. Model parameters used in Eqs. 12 - 14.

temperature [°C]	k_1 [min^{-1}]	k_2 [min^{-1}]
140	0.0019	0.0058
150	0.0040	0.0135
160	0.0078	0.0329
170	0.0192	0.0927
EA [kJ/mol]	116.5	140.3
ln A [min^{-1}]	27.6	35.6

The energies of activations for HexA formation (116.5 kJ/mol) and HexA degradation/dissolution (140.3 kJ/mol) listed in Table 4 are quite comparable to those reported by Danielsson et al. [10] although, differently to our investigations, they considered the HexA content of the sum of the pulp xylan and the dissolved xylan. In contrast, the corresponding activation energies for HexA formation and HexA degradation reported by Simao at al. [8, 9] were at a significantly lower level (92 and 110 kJ/mol, respectively) also compared to the activation energies for degradation of carbohydrates and

delignification (see Table 2 and [1]) indicating that, with increasing temperature, the HexA side groups will be progressively degraded while the carbohydrate and lignin contents in the pulp remain less affected. However, the results are not comparable because their approach with respect to experimental conditions and the proposed reaction scheme was somewhat different.

Following the HexA content of the pulp as a function of the kappa number it can be seen that the HexA degradation/dissolution exceeds the HexA formation only at kappa numbers below 15 (on pulp), even though the [OH^-] is kept constant at 0.52 mol/L which is illustrated in Figure 7.

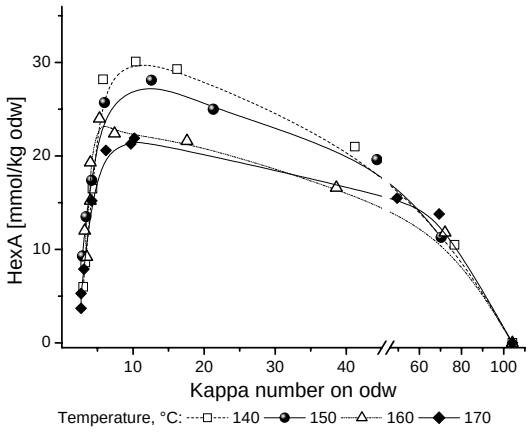

Figure 7. The effect of temperature on the amount of HexA vs. kappa number (on dry wood). Constant cooking conditions: [OH^-] = 0.52 mol/L, [HS^-] = 0.28 mol/L, [Na^+] = 1.5 mol/L.

In agreement with the results of the kinetic investigations (Table 2 and 4, the HexA content in pulp xylan at a given kappa number decreases with increasing temperature.

It is widely accepted that the level of hydroxyl ion concentration controls both the formation of HexA by the elimination of the 4-*O*-methoxyl group and the degradation/dissolution of HexA by alkaline cleavage of HexA from the xylan backbone or by dissolution of HexA linked to the xylan chain. In their kinetic study Simao et al. reported rather high reaction orders on the hydroxyl ion concentration, the order for degradation/dissolution being higher than for HexA formation indicating a lowering of the HexA content in the pulp xylan when increasing the effective alkali concentration during residual delignification [8]. The strong influence of [OH^-] on the HexA concentration profiles has been confirmed in our study as illustrated in Figure 8.

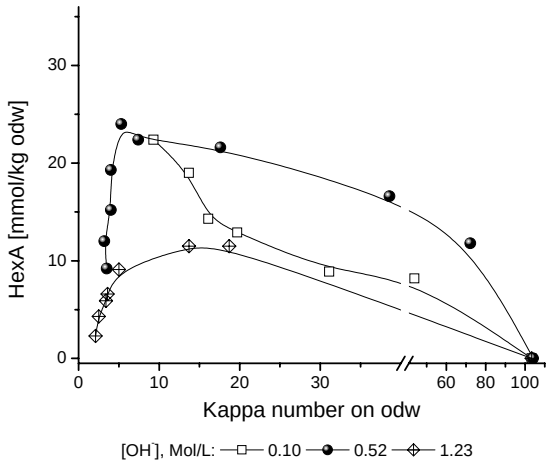

Figure 8. The effect of [OH^-] on the amount of HexA vs. kappa number (on dry wood). Constant cooking conditions: Temperature = 160 °C, [HS^-] = 0.28 mol/L, [Na^+] = 1.5 mol/L.

Interestingly, the HexA content in pulp continues to rise for kappa numbers below 15 at an effective alkali concentration of only 0.10 mol/L, as demonstrated in Figure 8. This may be explained by the observation that at a low hydroxyl ion concentration re-precipitation of HexA-Xylan fractions dominates over alkali-induced splitting of the HexA side chain. Unfortunately, the highest HexA content in the unbleached pulp, kappa number 12 to 20, occurs at a medium [OH^-] of 0.52 mol/L, typical for modern displacement cooks. Obviously, this level of effective alkali concentration is not yet sufficient to favour the cleavage of the HexA side chain. It needs more than twice the [OH^-] to keep the HexA content at a low level (around 10 mmol/kg wood). However, such conditions are known to decrease pulp yield, particularly the hemicelluloses

content and thus deteriorate pulp strength.
In agreement with other authors, the sulfidity of the cooking liquor displays not a noticeable influence on the HexA concentration profiles [9, 23]. However, when plotting the HexA content in pulp against the kappa number, the sulfidity appears to affect the HexA content (Figure 9).

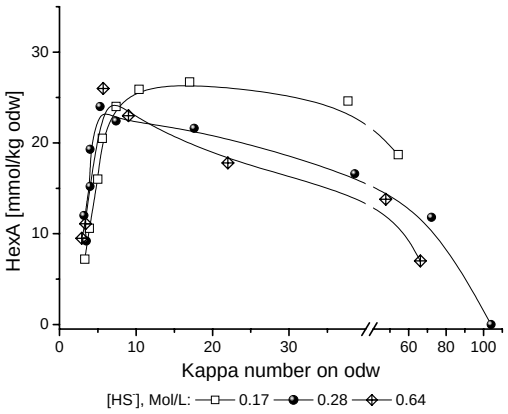

Figure 9. The effect of [HS^-] on the amount of HexA vs. kappa number (on dry wood). Constant cooking conditions: Temperature = 160 °C, [OH^-] = 0.52 mol/L, [Na^+] = 1.5 mol/L.

The effect of sulfidity may be attributed to its accelerating influence on the delignification rate rather than on a direct involvement in the HexA reactions.
An increase in ionic strength from 1.5 mol/L to 2.5 mol/L leads to a dramatic increase of the maximum HexA content in the pulp at a kappa number of about 35 on dry wood (corresponding to a kappa number of about 58 on dry pulp) as depicted in Figure 10. The shift of the maximum HexA content to considerably higher kappa numbers can be attributed to the negative impact of a high ionic strength on the delignification rate (see Figure 1 and Table 2).

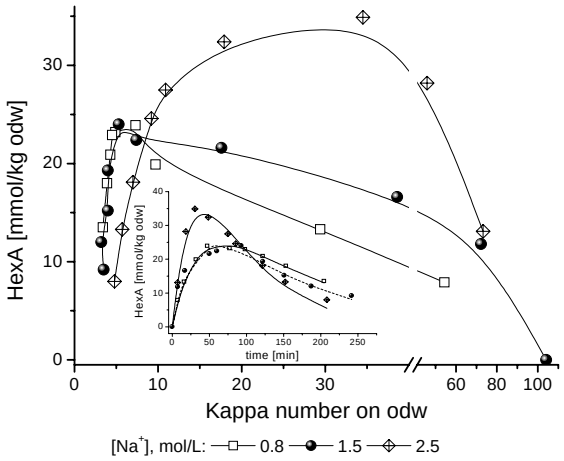

Figure 10. The effect of ionic strength, expressed as [Na^+], on the amount of HexA vs. kappa number (on dry wood). Constant cooking conditions: Temperature = 160 °C, [OH^-] = 0.52 mol/L, [HS^-] = 0.28 mol/L.

The small figure inside Figure 10 reveals that the maximum HexA content in pulp appears after the same reaction time while the level is almost 40% higher as compared to the HexA content at lower levels of ionic strengths, 1.5 mol/L and 0.8 mol/L, respectively. A closer examination shows that both reaction rates increase with increasing ionic strength (Figure 11).

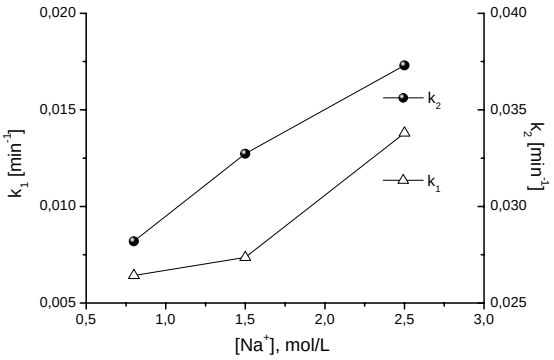

Figure 11. Reaction rates of HexA formation (k_1) and HexA degradation/dissolution (k_2) vs. ionic strength, expressed as [Na^+]. Constant cooking conditions: Temperature = 160 °C, [OH^-] = 0.52 mol/L, [HS^-] = 0.28 mol/L.

An increase in ionic strength, expressed as [Na^+], was found to promote the rate of HexA degradation also in kraft pulping of Norwegian spruce [21]. It may be speculated that the HexA formation reaction (k_1) is favoured over the cleavage

reaction of MeGlcA from the xylan backbone with increasing [Na^+]. Adequate model experiments have be undertaken to elucidate the reason for the increase of both HexA formation and degradation rates along with an increase in ionic strength.

Conclusions

The proposed kinetic model adequately describes the performance of lignin and carbohydrate degradation and cellulose chain scissions during kraft pulping of *E. globulus*. For the first time also the influence of [Na^+] was considered in a comprehensive kinetic pulping model. The good correspondence between predicted and experimentally determined unbleached pulp parameters confirms the suitability of the distribution model introduced by Andersson et al. for offline optimization studies of industrial kraft cooks.
Furthermore, the formation of HexA bound to the xylan backbone and its degradation/dissolution were described by a consecutive first-order reaction. Unfortunately, the results were not very encouraging and confirmed the results of other authors in broad terms in a sense that the HexA content cannot be reduced to low levels by choosing appropriate cooking conditions without simultaneously deteriorating pulp quality and decreasing pulp yield. The energies of activation for the formation of HexA, the degradation/dissolution of HexA, and the delignification of *E. globulus* during kraft pulping were found to be 116.5, 140.3, and 131.4 (L2) or 133.0 kJ/mol (L3), respectively. The differences in activation energies indicate that cooking at higher temperature may be advantageous to achieve a lower HexA content in the pulp. A very high alkali concentration, especially in the later parts of the cook, is necessary to substantially decrease the HexA content. Such cooking conditions, however, are known to degrade the carbohydrates, particularly the hemicelluloses, and consequently to decrease pulp yield and pulp strength. The role of ionic strength, expressed as [Na^+], on the HexA content is not yet elucidated. An increase in the ionic strength resulted in a higher maximum HexA content shifted to a higher kappa number (about 58), but with progressive delignification to a kappa number typical for unbleached *E. globulus* kraft pulp (about 15), the HexA content decreased to a level more than 20% lower as compared to pulps cooked at lower ionic strength.

However, more work has to be conducted to create an understanding of the reactions of the single wood components including the different hemicellulose substances, molecular and supramolecular structure of cellulose and alien substances such as resins and inorganic components.

References

[1] Andersson, N., D.I. Wilson, and U. Germard, *An Improved Kinetic Model Structure for Softwood Kraft Cooking.* Nordic Pulp and Paper Research Journal, 2003. **18**(2): p. 200-209.

[2] Smith, C., *Studies of the mathematical modelling, simulation, and control of the operation of a Kamyr continuous digester for the kraft process*. 1974, Purdue University: West Lafayette, Indiana, USA.

[3] Christensen, T., *A mathematical model of the kraft pulping process*, in *Purdue Laboratory for Applied Industrial Control*. 1982, Purdue University: West Lafayette, Indiana.

[4] Santos, A., et al., *Kinetic Modeling of Kraft Delignification of Eucalyptus globulus.* Ind. Eng. Chem. Res., 1997. **36**: p. 4114-4125.

[5] Gilarranz, M.A., et al., *Kraft Pulping of Eucalyptus globulus: Kinetics of Residual Delignification.* Ind. Eng. Chem. Res., 2002. **41**: p. 1955-1959.

[6] Hepp, M.D., *Process for continuously guiding liquids when digesting pulp in a digester*, in *European Patent Specification*. 1997, EP 0891 438 B1: Europe.

[7] Chai, X.-S., et al., *The Fate of Hexenuronic Acid Groups During Kraft Pulping of Hardwoods.* Journal of Pulp and Paper Science, 2001. **27**(12): p. 403-406.

[8] Simao, J.P., et al., *Heterogeneous kinetic model for the methylglucuronic and hexenuronic acids reactions during kraft pulping of Eucalyptus globulus.* Ind. Eng. Chem. Res., 2005. **44**: p. 2997-3002.

[9] Simao, J.P., et al., *Evolution of methylglucuronic and hexenuronic acid contents of Eucalyptus globulus pulp during kraft delignification.* Ind. Eng. Chem. Res., 2005. **44**: p. 2990-2996.

[10] Danielsson, S., K. Kisara, and M.E. Lindström, *Kinetic Study of Hexenuronic and Methylglueuronic Acid Reactions in Pulp and in Dissolved Xylan during Kraft Pulping of Hardwood.* Industrial Engineering Chemical Research, 2006. **45**: p. 2174-2178.

[11] Daniel, A.I.D., et al., *Hexenuronic acid contents of Eucalyptus globulus kraft pulps: Variation with pulping conditions and effect on ECF bleachability.* Tappi, 2003. **2**(5): p. 3-8.

[12] Gellerstedt, G. and J. Li, *An HPLC method for the quantitative determination of hexeneuronic acid groups in chemical pulps.* Carbohydrate Research, 1996. **294**: p. 41-51.

[13] Sixta, H., *Handbook of Pulp*. Vol. 1. 2006: Wiley-VCH Verlag GmbH&Co. KGaA. 212.

[14] Lindgren, C.T. and M.E. Lindström, *Kinetics of the bulk and residual delignification in kraft pulping of birch and factors affecting the amount of residual phase lignin.* Nordic Pulp and Paper Research Journal, 1997. **12**(2): p. 124-134.

[15] McKibbins, S., *Application of Diffusion Theory to the Washing of Kraft Cooked Wood Chips.* Tappi Journal, 1960. **43**(10): p. 801-805.

[16] Gustafson, R.R., et al., *Theoretical Model of the Kraft Pulping Process.* Ind. Eng. Chem. Process Des. Dev., 1983. **22**(1): p. 87-96.

[17] Christensen, T., L.F. Albright, and T.J. Williams, *A kinetic mathematical model for the kraft pulping of wood.* Tappi Proceedings - Annual Meeting, 1983: p. 239-246.

[18] Li, J. and G. Gellerstedt, *The contribution to kappa number from hexeneuronic acid groups in pulp xylan.* Carbohydrate Research, 1997. **302**: p. 213-218.

[19] Granström, A., et al., *Variables affecting the thermal yellowing of TCF-bleached birch kraft pulps.* Nordic Pulp and Paper Research Journal, 2001. **16**(1): p. 18-23.

[20] Chai, X.-S., S.H. Yoon, and J. Li, *The fate of hexenuronic acid groups during alklaine pulping of lobolly pine.* Journal of Pulp and Paper

Science, 2001. **27**(12): p. 407.

[21] Gustavsson, C.A.-S. and W.W. Al-Dajani, *The influence of cooking conditions on the degradation of hexenuronic acid, xylan, glucomannan and cellulose during kraft pulping of softwood.* Nordic Pulp and Paper Research Journal, 2000. **15**(2): p. 160-167.

[22] Evtuguin, D.V., et al., *Characterization of an acetylated heteroxylan from Eucalyptus globulus Labill.* Carbohydrate Research, 2003. **338**: p. 597-604.

[23] Chai, X.-S., S.-H. Yoon, and J. Li, *The fate of hexenuronic acid groups during alkaline pulping of lobolly pine.* Journal of Pulp and Paper Science, 2001. **27**(12): p. 407-411.

Lenzinger Berichte, 86 (2006) 46-55

STUDIES ON PREHYDROLYIS SULFITE - STATEGIES TO MITIGATE THE EFFECTS OF LIGNIN DEACTIVATION DURING PREHYDROLYSIS

Mario Fasching[1], Gottfried Kandioller[1], Andreas Griebl[1], and Herbert Sixta[2]

[1] Kompetenzzentrum Holz GmbH, St.-Peter-Str. 25, 4021 Linz, Austria
[2] Department Zellstoff-Forschung, Lenzing AG, Werksstrasse 1, A-4860 Lenzing, Austria
Phone: (+43) 07672-701-3788; Fax: (+43) 07672-918-3788; E-mail: m.fasching@lenzing.com

Multistage pulping combining a prehydrolysis stage with a bisulfite pulping step is prevented by the deactivation of lignin during the prehydrolysis against subsequent sulfite pulping. Several approaches were studied to either prevent the deactivation during the prehydrolysis stage or to mitigate the negative impact by the inclusion of a third pulping stage between prehydrolysis and sulfite pulping. Sulfonation by hydrogen sulfite solutions and alkaline extraction were studied as intermediate steps between prehydrolysis and sulfite pulping. The usage of ß-naphthol and SO_2 as additives in the prehydrolysis stage was examined for the ability to prevent condensation reactions during prehydrolysis.

Keywords: *pulp, lignin, sulfite pulping, prehydrolysis*

Introduction

The pulping industry has to continuously improve its performance to maintain economic profitability. This is especially important in highly industrialized countries with high wages and high environmental standards. At the same time the existing pulping processes are already highly optimized with respect to the main product pulp. One strategy to further increase pulping performance and to facilitate by-product usage is multi stage cooking. Multistage cooking enables more selective pulping processes than one stage cooking. It facilitates the cheap production of high quality pulp and is necessary to achieve a good separation of the different wood components. The alkaline prehydrolysis Kraft process is well established. During aqueous prehydrolysis acetic acid is liberated and in the resulting acid environment a large fraction of the hemicelluloses may be dissolved. Attempts to develop a similar prehydrolysis sulfite process have been undertaken in the past [1-6]. In these experiments reduced susceptibility of the wood in relation to subsequent sulfite pulping was an obstacle that could only be partially overcome by choosing rather impracticable conditions (e.g. buffered solutions combined with low temperatures) during the prehydrolysis [1, 2]. Several explanations for the observed behavior have been put forward by these early investigators, some of these hypotheses (like a physical agglomeration of small lignin particles during the prehydrolysis [5]) are no longer consistent with today's understanding of wood structure. A sound scientific description of the processes responsible for the observed failures is still missing. Recently we started to re-evaluate the introduction of a prehydrolysis step into a sulfite pulping sequence [7]. We established a prehydrolysis kinetic for the prehydrolysis of beech wood and used this data to

perform prehydrolysis experiments with varying conditions while always achieving the same prehydrolysis intensity, using the P-factor concept [8, 9]. Both, increased condensation degree and an increased number of free phenolic hydroxyl groups were found in the lignin isolated after prehydrolysis. Not surprisingly, the delignification efficiency in subsequent sulfite pulping was drastically decreased by the prehydrolysis treatment. However, we found that at the same overall prehydrolysis intensity a short prehydrolysis at high temperatures is strongly favorable against a longer prehydrolysis at lower temperature in respect to subsequent delignification. The introduction of an intermediate alkaline extraction between prehydrolysis and sulfite cooking (to remove reactive lignin species) resulted in an even stronger and - up till now - difficult to understand deactivation of the lignin with respect to subsequent sulfite pulping. In the present work we evaluated four additional strategies to overcome the strong deactivation of wood by prehydrolysis with regard to subsequent sulfite pulping. The studied strategies were (I) intermediate sulfonation, (II) intermediate alkaline extraction at varying temperatures, (III) ß-naphthol as additive during prehydrolysis, and (IV) SO_2 as additive during (very mild) prehydrolysis.

Experimental

Chemicals

Fine chemicals were purchased from Sigma-Aldrich or Merck, SO_2 (l), 99.99 %, was supplied by Linde. Fully deionised water was used for all experiments.

Wood chips

Freshly cut beech wood (*Fagus sylvatica* L.) was ground in frozen condition and fractionated with a Retsch mesh. The residue of the widest-meshed sieve (3.55 mm) was used for the experiments.

Pulping

The experiments were carried out in a lab-scale Parr reactor station with a reactor volume of 450 ml. The steel reactors had each a stirrer, a temperature sensor, and a heating mantle. The indicated starting material (30 g dry matter) was placed in the reactor together with enough water to achieve a total liquid-to-wood ratio of 10:1 (including wood moisture). A process control system was used to perform different pulping stages (prehydrolysis, alkaline extraction, or acid magnesium bisulfite pulping). The reactions were stopped by rapid external cooling with ice. The solid residues were filtered off and washed with water. The residues were stored in wet condition in sealed plastic bags for further processing.

Prehydrolysis (P): Chips were submitted to water-prehydrolysis in the sealed reactor at the conditions indicated in the text. For the calculation of the P-factor from the recorded temperature / time data an activation energy (E_a) of 125.6 kJ/mol was used [10]. To produce sufficient amounts of prehydrolysis residue for subsequent processing, selected prehydrolysis experiments were done in a 10 l digester with forced circulation. In each of those trials 800 g wood (dry mater) was processed; all other conditions were as described above. When the prehydrolysis was performed in the presence of ß-naphthol, the additive (4% ß-naphthol calculated on dry wood) was dissolved in hot water used for the prehydrolysis. Two prehydrolyses were performed that deviated from the concept of constant prehydrolysis intensity: The same amounts of wood and water as described above were used in the reactor system for these prehydolyses but a temperature of 105 °C was applied for 180 minutes. In one of these prehydrolyses 1.5% SO_2 (calculated on total amount of water in the reaction vessel) was added.

Alkaline extraction (Ex): Extractions were done in the reactor system applying

aqueous NaOH (0.5 mol/l) as base for the times and temperatures indicated in the text. Immediately after these experiments a "mud-phase" was separated from the liquor.

Sulfonation (Sulf): For the sulfonation step an aqueous solution of sodium (hydrogen) sulfite (0.5mol/l) at pH 6, which is a solution dominated by the hydrogen sulfite species, was applied in the reactor system at 135 °C for the times indicated in the text.

Acid sulfite cooking (S): A modern variation of acid magnesium bisulfite cooking, including addition of liquid SO_2, was applied with the following parameters: 0.75 mol/l total SO_2, 42 % free SO_2, 148 °C cooking temperature. The process was controlled by the automated process control system to achieve the H-factor of 200. For the H-factor calculation an activation energy (E_a) for delignification of 110 kJ/mol was used. The solid phase obtained in the sulfite cooking stage was sorted into a "pulp" and a "shives" fraction by suspending the residue in 300 ml water (rapid stirring) and passing the suspension through a sieve (mesh aperture 1 mm) with the help of approximately 50 l water from a water hose. The "shives" fraction remaining in the sieve was analyzed separately, whenever sufficient material was obtained.

Analytical Methods

Kappa numbers were determined according to TAPPI test method T236 cm-85, carbohydrate composition by total hydrolysis and HPLC separation with pulsed amperometric detection (PAD). Dry matter contents were determined by drying in a vacuum oven at 105 °C. Cited lignin contents for solid substrates always comprise Klason lignin and acid soluble lignin (according to TAPPI test method T222 om-98). Lignin contents of liquid phases were calculated from UV/Vis spectra recorded at pH 4.5. An absorption coefficient of 110 l/(g*cm) at 205 nm for dissolved lignin (Tappi-UM-250) and of 35 l/(g*cm) at 233 nm for dissolved lignosulfonates (Lignin Institute test method T-500) was used.

Results and discussion

A note on the "shives" fraction

In some of our experiments a considerable amount of "shives" was separated from the pulp after the final acid bisulfite cooking. As was already noted in reference [7] the "shives" fraction described in our work should not be confused with "shives" obtained in a technological process. Also, Kappa numbers only describe the "pulp" fractions and are therefore no adequate parameter for delignification in these experiments. Therefore, and to quantify also the other wood components correctly, the "shives" and "pulp" fractions were analyzed separately for lignin and carbohydrates, whenever enough material was obtained to do so. Then an overall lignin and carbohydrate content for the total solid phase ("pulp" + "shives") was calculated.

(I) Intermediate Sulfonation

One of the early attempts to overcome the limitations of prehydrolysis sulfite aimed to reestablish the reactivity lost during prehydrolysis in an intermediate sulfonation step. This approach (partially in combination with other techniques) was described by Lautsch [2]. The original procedure described by Lautsch involved the treatment of the prehydrolysed wood with aqueous solutions of sodium or magnesium sulfite at varying concentrations and pH values. The preceding prehydrolyses were performed at various conditions, mostly at low temperatures and with the addition of SO_2 or mineral acids. We applied the most promising of this sulfonation conditions (0.5 M $NaHSO_3$, pH = 6) to our prehydrolysed wood samples. In contrast to Lautsch we performed prehydrolyses at

comparable high temperatures but in much shorter times. Indeed, we found the reactivity of the lignin (as measured by delignification ability of subsequent bisulfite pulping) nearly, but not completely, restored, see Table 1. The pulp with a kappa number of 17 obtained by the sequence prehydrolysis (170 °C) – sulfonation – sulfite cooking (P_{170}-Sulf-S) was (together with the pulp obtained from prehydrolysis at 190 °C and subsequent sulfite pulping, P_{190}-S [7]) our first indication that acid magnesium bisulfite pulping could be successfully performed after prehydrolysis with the desired prehydrolysis intensity. However, when both favorable processes (prehydrolysis at 190 °C for a very short time and intermediate sulfonation) were combined no further improvement in delignification could be achieved: After prehydrolysis at 190 °C, subsequent sulfonation and bisulfite cooking yielded a pulp with quite the same Kappa number (19) as that obtained by the same pulping sequence but with prehydrolysis at only 170 °C (Kappa 17). Therefore, while sulfonation caused a decrease in kappa number of 17 points when the prehydrolysis was performed at 170 °C, only a Kappa number decrease of 8 points was realized for prehydrolysis at 190 °C.

Although this sulfonation was quite successful in restoring the reactivity of the lignin with regard to subsequent acid bisulfite pulping, it is not feasible for any practical purposes due to the long sulfonation time. Unfortunately, exploratory experiments performed with wood subjected to prehydrolysis at 190°C seem to underline the necessity of this long sulfonation time, see Table 1. When the sulfonation time was reduced by 50 % from 8 hours to 4 hours, only an insignificant increase in pulping performance, as compared to not performing any sulfonation at all, was observed. To elucidate the mechanisms of this sulfonation procedure we tried to establish a mass balance for the major wood components during this step, see Table 2. To quantify the loss of wood substance during the treatment we followed the approach described in our previous report [7]. Therefore, in Table 2 we cite both, the dissolved amounts calculated from differences between the two solid phases (starting material and product) as well as the amount of wood components actually detected in the liquor generated during sulfonation. Since no significant glucan losses were detected, only the results for xylan and lignin removal are given in Table 2. Clearly, sulfonation is accompanied by massive lignin removal. If 5% of initial wood substance are removed as lignin during the sulfonation this equals 20% of the lignin initially present in the wood and more than a quarter of the lignin still present before the sulfonation. Thus, one should properly speak of a neutral sulfite cooking step, rather than of a sulfonation. However, the interpretation would go too far in ascribing the beneficial effects of the sulfonation only to this partial lignin dissolution. In the first place, very considerable lignin dissolution was also achieved during alkaline extraction but the total impact of alkaline extraction on the pulp quality was negative non the less. Secondly, we followed the reaction by elemental analysis. If one assumes the sulfur content measured thus to be located only in the lignin moieties, these values can be converted to degrees of substitution, see Table 3. For this calculation an empiric formula for beech wood lignin prior to sulfonation of $C_9H_{7.16}(OCH_3)_{1.36}$ according to Nimz was assumed [11] and the increase of molecular weight by the sulfonation itself was considered. The results from these calculations show that, with the time for sulfonation reduced by 50%, also the degree of sulfonation was accordingly decreased.

Table 1. The Influence of intermediate sulfonation on pulping performance.

Sequence	T (pre-hydrolysis)	t (Sulf.)	Total Yield	Kappa	Xylan		Glucan		Lignin	
	°C	h	%		%		%		%	
			wood		pulp	wood	pulp	wood	pulp	wood
S	-	-	45	8	9	4	85	45	1.8	0.5
P-S	170	-	48	34	8	4	81	39	4.9	2.3
	190	-	47	27	8	4	88	42	4.2	2.0
P-Sulf-S	170	8	46	17	10	5	91	42	2.8	1.3
	190	4	47	25	8	4	87	41	3.6	1.7
	190	8	46	19	7	3	88	40	3.1	1.4

Lignin, xylan, and glucan composition of final pulp cited as % in pulp and calculated on initial wood components (% wood). There were only insignificant amounts of "shives" obtained in these experiments, P: prehydrolysis, Sulf: sulfonation, S: acid magnesium bisulfite cooking.

Table 2. Xylan and lignin loss during sulfonation.

T (prehydrolysis)	t (Sulf.)	Xylan		Lignin	
°C	h	%		%	
		difference	liquor	difference	liquor
170	8	2	ND	6	ND
190	4	3	2	5	7
190	8	4	2	6	9

% of initial wood substance

Table 3. Elemental composition of wood prior and after sulfonation.

Sequence	T (prehydrolysis)	t (Sulf.)	C	H	N	S	Degree of sulfonation
	°C	h	% (w/w)				% (propylphenyl units)
wood	-	-	46.5	5.85	0.10	0.00	--
P	170	-	48.4	5.93	0.08	0.00	--
P	190	-	48.5	6.10	0.09	0.00	--
P-Sulf	190	4	44.9	5.93	0.09	0.66	16
P-Sulf	190	8	44.3	5.88	0.09	1.42	37

(II) Intermediate Alkaline Extraction at Varying Temperatures (P-Ex-S)

Prehydrolysis of beech wood reduces the susceptibility of lignin towards subsequent acid bisulfite pulping and consequently produces pulp with an increased kappa number. One possible approach to limit this negative effect is an intermediate alkaline extraction (Ex) to remove reactive lignin species formed during prehydrolysis. In the first part of this project [7] we tested an alkaline extraction at 120 °C for 30 minutes as intermediate stage between prehydrolysis and sulfite pulping. However, these studies showed that the reduced lignin content of the P-Ex treated wood could not be translated into improved kappa numbers of pulps produced by subsequent acid bisulfite pulping. In fact the alkaline extraction inactivated the residual lignin even further towards acid sulfite treatment and delignification performance decreased as compared to sulfite cooking immediately after prehydrolysis (P-S). In the current work we tried to find conditions for the alkaline extraction that still maintain any beneficial effects (removal of reactive lignin species) but avoid the inactivation of the lignin structures. In a first stage we aimed to elucidate the temperature dependence of the amount of lignin removed during alkaline extraction. Beech wood prehydrolysed at 170 °C was subjected to alkaline extraction for 30 min at temperatures ranging from 70 °C to 140

°C. As can be seen in Table 4 the extents of lignin and xylan extraction were both temperature dependent.

Table 4. Influence of temperature on lignin and xylan extraction during alkaline extraction of prehydrolysed (170 °C) beech wood.

T (alkaline extraction)	Extracted Lignin	Extracted Xylan
°C	% (w/w) of prehydrolysed wood	
70	4.3	1.1
100	7.2	0.8
120	7.3	0.8
140	17.3	0.6

The amount of extracted lignin increased from 4.3% to 17.3% with extraction temperature rising from 70 °C to 140 °C, while the amount of removed xylan actually decreased slightly. In the next step, we used the mildest studied extraction conditions in a full P-Ex-S pulping sequence. However, the achieved delignification was inferior, both compared to the direct sulfite cooking of prehydrolysed wood, as well as compared to wood extracted at 120 °C, see Table 5. These results clearly indicate that an intermediate alkaline extraction is not a feasible way to improve the susceptibility of prehydrolysed wood towards subsequent acid bisulfite pulping.

(III) ß-Naphthol as Additive During Aqueous Prehydrolysis

ß-Naphthol was suggested by Lora as an additive to prevent lignin condensation in prehydrolysis treatments followed by subsequent alkaline pulping [12-14]. This was based on extensive screening experiments that showed ß-naphthol to be the most suitable substance to prevent condensation during prehydrolysis [15]. This was assessed by determining the amount of lignin that could be extracted with dioxan / water after an aqueous prehydrolysis. ß-Naphthol is believed to scavenge the active species generated during prehydrolysis by reaction with its hydroxyl groups. The ß-substituted naphthols generated thus are non reactive for further condensation reactions [16, 17]. It was our aim to a.) test if this mechanism also applies to beech wood and b.) test the reactivity of wood prehydrolysed in the presence of ß-naphthol in subsequent bisulfite pulping.

Table 5. Results of acid magnesium bisulfite pulping experiments from beech wood prehydrolysed at 170 °C and subsequently extracted with NaOH at different temperatures.

Sequence	T (alkaline extraction)	Kappa	Shives	Lignin	Xylan
	°C		% w/w (pulp + shives)		
P-S	-	34	1	4.94	8.3
P-Ex-S	70	57	73	ND	8.5
	120	48	18	8.73	5.8

a.) Aqueous prehydrolysis of beech wood with ß-naphthol as additive: Beech wood was subjected to aqueous prehydrolysis at 170 °C (P Factor = 348) with and without the addition of 4% ß-naphthol. The prehydrolysed wood was milled and extracted with dioxin / water 9:1. The amount of extractives obtained in this way increased by a factor of two when ß-naphthol was added during the prehydrolysis, that is from 7.6% to 13.3% w/w of prehydrolysed wood. The solvent was removed from the dioxin / water extract and IR spectra were recorded from the residues. While the residue obtained from prehydrolysis without ß-naphthol showed a typical MWL (Milled Wood Lignin) spectrum, two additional bands at 750 and 815 cm^{-1}, respectively, were visible in the residue derived from wood prehydrolysed in the presence of ß-naphthol. These bands were observed by Lora in the dioxin / water extract from aspen milled wood lignin that had been prehydrolysed in the presence of ß-naphthol [17] and can be assigned to ß-substituted naphthol derivatives formed during prehydrolysis.

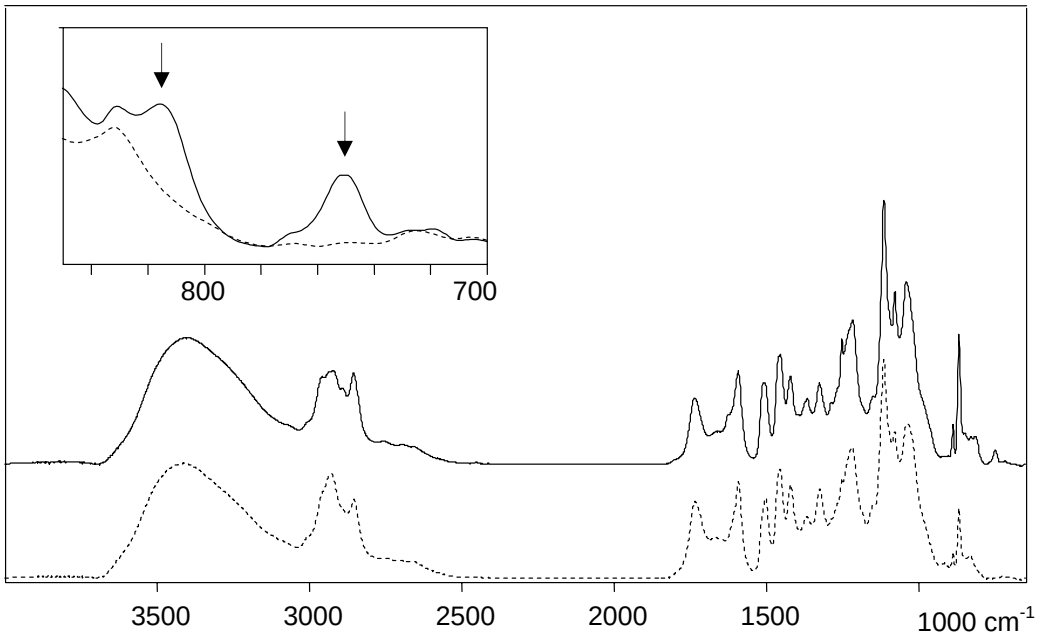

Figure 1. IR spectra of dioxan / water extractives from wood prehydrolysed at 170 °C for 30 min in the presence (full line) and without (dashed line) ß-naphthol. The inset clearly shows the additional bands at 750 and 815 cm^{-1}, respectively.

Thus, the condensation preventing effect of ß-naphthol was clearly observed for the prehydrolysis of beech wood at 170 °C.

b.) Sulfite pulping of wood prehydrolysed in the presence of ß-naphthol: Wood subjected to prehydrolysis with and without ß-naphthol as described above was used in standard acid magnesium bisulfite pulping experiments. Table 6 summarizes the principal results of the pulping experiments. As may be seen from Table 6 delignification performance for wood prehydrolysed in the presence of ß-naphthol was even inferior to that obtained by pulping the wood hydrolyzed in pure water. One reason for this observed deterioration instead of the expected improvement could be that ß-naphthol remaining in the prehydrolysed wood forms condensed structures in subsequent sulfite pulping. To test this hypothesis we included an alkaline extraction step after the prehydrolysis in the pulping sequence. By an intermediate extraction with aqueous sodium hydroxide any remaining ß-naphthol should be removed. On the other hand the negative impact of such an alkaline extraction between prehydrolysis and sulfite pulping was already known from our previous experiments. Therefore, one could expect both negative and positive effects by such a treatment. Our results showed indeed that the incorporation of an alkaline extraction step improved the pulping performance when ß-naphthol was used in the prehydrolysis. This is contrary to the behavior of wood prehydrolysed without ß-naphthol. In this case the alkaline extraction had a negative impact on subsequent sulfite pulping. However, the pulping performance achieved by this treatment is still inferior to prehydrolysis (without ß-naphthol) directly followed by sulfite pulping (P-S) and barely reaches the delignification performance by the sequence prehydrolysis (without ß-naphthol) – alkaline extraction – sulfite pulping (P-Ex-S), see Table 6.

Considering the usually strong negative impact of intermediate alkaline extraction these results may be explained in two ways: (a) The addition of ß-naphthol to the prehydrolysis has no positive effect. The negative effects of ß-naphthol addition derive solely from un-reacted ß-naphthol

that may be removed in the alkaline reaction, thus yielding the same result as prehydrolysis without ß-naphthol followed by alkaline extraction.
Or, (b) the positive influences of ß-naphthol during the prehydrolysis are cancelled by negative impacts that can not be overcome by removing un-reacted ß-naphthol in the alkaline extraction. Especially, ß-naphthol could react during the prehydrolysis with the very structure necessary for successful delignification in the acid bisulfite pulping. Considering the proofed success of ß-naphthol to scavenge reactive species (demonstrated both by the increased amount of extractives and by the observation of ß-substituted naphthols in the extractives) this seems to be the more plausible hypothesis. Like the results of intermediate alkaline extraction this shows again that a certain pulping step may be useful per se but not compatible with subsequent acid bisulfite pulping.

(IV) Mild Prehydrolysis and SO_2 as Additive During Prehydrolysis

Even in earlier works [1-4] several descriptions can be found how the inactivation of wood by aqueous hydrolysis in regard to subsequent acid sulfite pulping was overcome by using various acids as additives in the prehydrolysis step. Sometimes the term "buffered solutions" is used in connection with these attempts, even if only completely dissociating mineral acids were used. Also, one has to be careful which data to compare: Described prehydrolysis procedures might be so mild that subsequent sulfite pulping is surely successful because there is simply no significant prehydrolysis intensity reached or, cooking liquors might be used in the prehydrolysis that would lead rather to sulfite pulping than to prehydrolysis. To overcome the first of these problems in our work described so far we have used prehydrolysis with identical prehydrolysis intensities as measured by the P-factor concept. In the experiments described below we had to deviate from this principle to evaluate the usefulness of some proposed pulping sequences. We studied a very mild prehydrolysis at only 105 °C, a mild prehydrolysis but with addition of SO_2, and application of the intermediary sulfonation to both prehydrolyses. The conditions of the prehydrolyses involved in this comparative study are given in Table 7, while the performances in subsequent standard acid magnesium bisulfite pulping experiments (with and without intermediate sulfonation) are presented in Table 8. The very mild prehydrolysis at only 105 °C for 3 hours achieved no significant prehydrolysis intensity (i.e. removal of xylan) at all. Not surprisingly, there were no negative effects in subsequent sulfite pulping. When the same prehydrolysis conditions were used but 1.5% SO_2 were added to the water (as suggested by Lautsch [2]) significant removal of xylan was achieved, however, subsequent sulfite pulping showed the same negative effects known from our more severe prehydrolysis conditions.

Table 6. Results of acid magnesium bisulfite pulping experiments from beech wood pre-hydrolyzed at 170°C with and without β-naphthol and subsequently extracted with NaOH at various temperatures.

Additive in prehydrolysis	Sequence	T (alkaline extraction)	Kappa	Shives	Lignin	Xylan
		°C		% w/w (pulp + shives)		
none	P-S	-	34	1	4.94	8.3
	P-Ex-S	120	48	18	8.73	5.84
β-naphthol 4% w/w on wood	P-S	-	64	34	9.81	8.76
	P-Ex-S	70	51	72	10.18	8.64
	P-Ex-S	100	57	71	10.38	7.13
	P-Ex-S	140	53	65	8.76	6.40

Table 7. Prehydrolysis conditions and achieved intensity.

Type	T	t	SO_2	Yield	Wood material removed	
					Xylan	Lignin
	°C	min	%	% (wood)	% (initial wood material)	
A	170	30	-	75	9	6
B	105	180	-	97	0	1
C	105	180	1.5	71	10	8

Table 8. Pulping Performances of variously pretreated materials.

Sequence	Pre-hydrolysis	t (Sulf.)	Total Yield	Kappa	Xylan	Glucan	Lignin
		h	% (wood)			% (pulp)	
S	-	-	45	8	9	85	1.0
P-S	A	-	48	34	8	81	4.9
	B	-	45	7	9	86	1.0
	C	-	45	27	7	87	4.0
P-Sulf-S	A	8	46	17	10	91	2.8
	B	8	48	8	13	88	1.5
	C	8	46	18	8	91	3.1

This negative impact could be overcome by an intermediate sulfonation step yielding pulps of Kappa 18. However, the same delignification may be more easily achieved by a short prehydrolysis (without SO_2) at 170 °C followed by sulfonation. Therefore, it seems that some of the suggested additives had solely the effect of achieving the desired prehydrolysis effect at lower temperatures.

As may be also seen from Table 7, prehydrolysis in the presence of SO_2 leads to extensive delignification during the prehydrolysis, even more than our standard prehydrolysis at 170 °C, thus deviating from our goal to perform the removal of xylan during prehydrolysis.

Conclusions

Intermediate alkaline extraction and the addition of ß-naphthol are not compatible with subsequent sulfite pulping. It is possible to reach sufficient delignification in a three stage prehydrolysis – sulfonation – bisulfite cooking process. The massive removal of lignin in the sulfonation step might not be a severe problem for actual process design, because probably the liquor of the sulfonation step would be processed further with the spent liquor from the actual sulfite pulping. However, the long times necessary for successful sulfonation (at least at the studied conditions) prohibit the application of this sequence on a technical scale for obvious economical reasons. In spite of the disappointing results described here for the system involving aqueous SO_2 as an additive during prehydrolysis, it may well be possible to develope stronger buffered systems (also incorporating $MgHSO_3$ or some other base) that indeed are able to prevent the negative impacts of prehydrolysis. These systems may well be valuable additions to the technique of sulfite cooking but considering the huge amount of delignification during prehydrolysis, these systems should rather be called multistage sulfite pulping with varying pulping liquor composition and are therefore not in the line of this investigation, that aims to separate, as cleanly as possible, the hemicelluloses from the remaining wood components prior to the proper delignification stage.

Acknowledgements

Financial support was provided by the Austrian government, the provinces of Lower Austria, Upper Austria, and Carinthia as well as by the Lenzing AG. We also express our gratitude to the Johannes Kepler University, Linz, the University of Natural Resources and

Applied Life Sciences, Vienna, and the Lenzing AG for their in kind contributions. We also would like to thank Jairo Lora for helpful discussions.

References

[1] W. Lautsch, Über die Vorhydrolyse von Buchenholz mit Puffergemischen und über Aufschlußversuche nach dem Sulfitverfahren. Holz 1942**,** 5/6, 119-128.

[2] W. Lautsch, Über die Gewinnung von lignin- und pentosanarmen Zellstoffen durch Vorhydrolyse und mehrstufigen Sulfitaufschluß. Holz 1943**,** 6, 148-151.

[3] A. J. Corey, J. M. Calhoun, and O. Maass, A further study of the pretreatment of wood in aqueous solutions. Canadian Journal of Research 1937**,** 15, (B), 168-185.

[4] A. J. Corey, and O. Maass, The influence of hydrogen-ion concentration with pretreatment of wood on its subsequent delignification. Canadian Journal of Research 1935**,** 13B, 289-295.

[5] A. J. Corey, and O. Maass, The influence of the preheating of wood in water on the rate of delignification by sulfite liquor. Canadian Journal of Research 1935**,** 13, (B), 149-155.

[6] W. Overbeck, and H. Mülller, Über die Vorhydrolyse verschiedener Hölzer mit Wasser unter Druck und die damit verbundene Veränderung der Holzbestandteile, insbesondere des Lignins. Berichte 1942**,** 75, (5), 547-555.

[7] M. Fasching, A. Griebl, G. Kandioller, A. Zieher, H. Weber, and H. Sixta, Prehydrolysis Sulfite Revisited. Macromolecular Symposia 2005**,** 223, 225-238.

[8] A. J. Kerr, and V. D. Harwood, Prehydrolysis-kraft pulping of New Zealand beech. Appita 1976**,** 30, (2), 135-142.

[9] C. K. Lin. Prehydrolysis-alkaline pulping of sweetgum wood. PhD-Thesis, North carolina State University, Raleigh, NC 27650, USA, 1979.

[10] H. Sixta. Zellstoffherstellung unter Berücksichtigung umweltfreundlicher Aufschluß- und Bleichverfahren am Beispiel von Chemiezellstoffen. Habilitation, Technical University of Graz, Graz, 1995.

[11] H. Nimz, Das Lignin der Buche - Entwurf eines Konstitutionsschemas. Angew. Chem. 1974**,** 86, (9), 336-344.

[12] M. Wayman, and J. H. Lora, Delignification of wood by autohydrolysis and extraction. Tappi 1979**,** 62, (9), 113-114.

[13] J. H. Lora, and M. Wayman, Delignification of wood by autohydrolysis and extraction. Tappi 1978**,** 61, (6), 47-50.

[14] J. H. Lora, and M. Wayman, Autohydrolysis-extraction: a new approach to sulfur-free pulping. Tappi 1978**,** 61, (12), 88-89.

[15] M. Wayman, and J. H. Lora, Aspen autohydrolysis. The effects of 2-naphthol and other aromatic compounds. Tappi 1978**,** 61, (6), 55-57.

[16] J. H. Lora, and M. Wayman, Simulated autohydrolysis of aspen milled wood lignin in the presence of aromatic additives. Changes in molecular weight distribution. Journal of Applied Polymer Science 1980**,** 25, (4), 589-96.

[17] M. Wayman, and J. H. Lora, Simulated autohydrolysis of aspen milled wood lignin in the presence of aromatic additives: Structural modifications. Journal of Applied Polymer Science 1980**,** 25, (10), 2187-94.

Lenzinger Berichte, 86 (2006) 56-62

CALCULATION OF PHYSICAL PROPERTY DATA OF THE SYSTEM MgO-SO_2-H_2O AND THEIR IMPLEMENTATION IN ASPEN PLUS®*

Karl Schöggl[1], Michael Steindl[1], Anton Friedl[2], Hedda K. Weber[1], and Herbert Sixta[3]

[1]Kompetenzzentrum Holz GmbH, St.-Peter-Str. 25, 4021 Linz, Austria; phone: +43 7672 701-3181
[2]Vienna University of Technology, Getreidemarkt 9/166, 1060 Vienna, Austria
[3]Lenzing R&D, Werkstrasse 1, 4860 Lenzing, Austria

* Parts of this work were presented during the 9th European Workshop on Lignocellulosics and Pulp (EWLP) 28th-30th August, Vienna, Austria and during the 17th International Congress of Chemical and Process Engineering 27th-31th August 2006, Prague, Czech Republic

The recovery of the cooking chemicals of a standard chemical pulping process is of main economical and environmental interest. In a magnesium based sulphite pulp mill, venturi scrubbers are installed to absorb SO_2 from the exhaust gas. An aqueous magnesium hydroxide solution is added as an absorbing agent. It is essential to calculate the chemical equilibrium of the system MgO–SO_2– H_2O to optimise the absorption process. The equilibrium calculations are based on the standard module "flash" ,which is included in Aspen Plus®.

This module can be used to calculate the vapour liquid equilibrium and the solid substance precipitation. The activity coefficient model "Electrolyte–Non–Random–Two–Liquid" (Elec-NRTL) is used to calculate the equilibrium under real conditions.

The solubility of both $MgSO_3$-hydrates, $MgSO_3 \cdot 6H_2O$ and $MgSO_3 \cdot 3H_2O$, as well as the influence of the $MgSO_4$ on the solubility of the two $MgSO_3$ - hydrate types has to be considered and, therefore, new procedures were developed, which allow a better adjustment of the used property data sets. The results of the calculations done with the new procedures were compared with literature data. Problems of the internal data management are described.

Keywords: p*rocess simulation, phase equilibrium, property data, recovery*

Introduction

In addition to the well known wet desulphurization technique based on a calcium washing solution, processes based on magnesium are used in special areas, for example in the absorptive chemical recovery systems of the magnesium sulphite based pulp and paper production processes.

In contrast to the electrolyte system CaO-SO_2-H_2O, literature data for the system MgO-SO_2-H_2O are rare.

The primary reactions taking place during the Lenzing AG´s desulphurization process attached to the pulp mill are shown by the equations (1) – (6).

$$MgO + H_2O \rightleftharpoons Mg(OH)_2 \rightleftharpoons MgOH^+ + OH^- \quad (1)$$

$$MgOH^+ + OH^- \rightleftharpoons Mg^{2+} + 2OH^- \quad (2)$$

$$SO_2(aq) + 2H_2O \rightleftharpoons H_3O^+ + HSO_3^- \quad (3)$$

$$HSO_3^- + H_2O \leftrightharpoons H_3O^+ + SO_3^{2-} \quad (4)$$

$$Mg^{2+} + 2HSO_3^- \leftrightharpoons Mg(HSO_3)_2 \quad (5)$$

$$Mg^{2+} + SO_3^{2-} + xH_2O \leftrightharpoons MgSO_3.xH_2O \quad (6)$$

An overview of the main reactions of the system MgO - SO_2 - H_2O is shown in Figure 1.

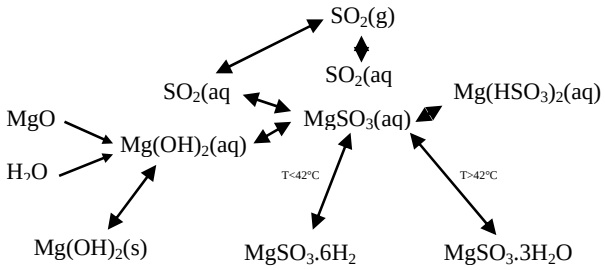

Figure 1. Reaction scheme of the system MgO – SO_2 – H_2O.

Additionally the following parameters had to be taken into account during the development of the model:

- precipitation of the produced solids,
- phase transition of different hydrate types at working conditions,
- the SO_2 partial pressure over the solution,
- the influence of the magnesium sulphate concentration on the solubility of the sulphite hydrates.

In order to build up an accurate model of a desulphurization process based on the magnesium system the quality of the used property data is of high relevance.

Used Software

The fundamental model was developed with the commercial steady state, equilibrium based simulation tool Aspen Plus® V11.1 (service pack 1). Basic data for the electrolyte system MgO-SO_2-H_2O were also taken from the simulation tools data base. The implemented activity coefficient model Elec-NRTL was used because of the non ideal behaviour of the system. Further improvement by implementation of new data was necessary to enhance the model quality. This was done by routines prepared with Compaq Visual Fortran 6®. For runtime linking Microsoft Visual C^{++} 6.0 SP5® libraries have been used.

All simulations were done with a reactor and a single standard flash unit. The schematic structure is shown in Figure 2. As input streams the components MgO, SO_2 and water were defined. The temperature was controlled directly in the flash unit. As usual for flash units two output flows – one vapour and one liquid flow - were defined, where the liquid flow also contains possible precipitated solids.

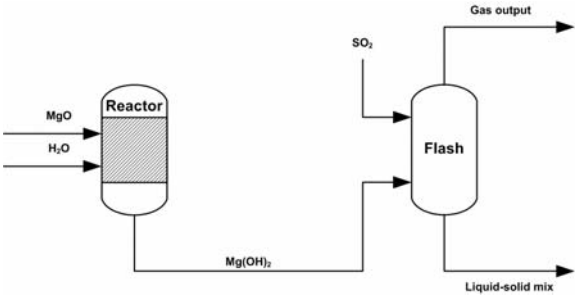

Figure 2. Schematic structure of the fundamental Aspen Plus® model.

Data Base (Literature and Simulation tool)

Literature data for the system MgO-SO_2-H_2O

The solubility of magnesium hydroxide in water and aqueous solutions is reported in several publications. A review was published by Lambert [1]. The solubility of magnesium hydroxide is also dependent on its structure. Both, the precipitation of the hydroxide from salt solution and the hydration of MgO lead to the formation of an amorphous magnesium hydroxide

designated in the literature as “labile” or “active”. Aging the amorphous form changes it to the thermodynamically stable, well crystallized form, which is less soluble, called the “stable” or “inactive” form. The difference in solubility of these different forms may be perceptible in precise measurements.

All required data for the calculation of the solubility of $Mg(OH)_2$ have been taken from Lambert [1] and Lide [2].

Under the assumption that the reaction enthalpy follows a linear dependency between two measurement points the solubility product for $Mg(OH)_2$ can be calculated from equation (7)

$$\frac{\partial \ln K}{\partial T} = \frac{\Delta H_R^o(T)}{RT^2} \qquad (7)$$

Several sources were necessary to obtain a basic property data set for the system MgO-SO_2-H_2O.

SO_2 partial pressure data for unsaturated $MgSO_3$ solutions were obtained from Hagisawa [3] and Markant et al. [4], for saturated solutions data from Kuzminykh et al. [5] have been used.

Research on the formed magnesium sulphite hydrates was performed by Hagisawa [3], Nývelt [6], Söhnel and Rieger [7] and Steindl et al. [8]. All of them observed two hydrate types being formed at working conditions of approximately 65°C. Below temperatures of 42°C magnesium sulphite hexahydrate $MgSO_3 \cdot 6H_2O$ is the stable equilibrium solid phase (Hagisawa [3], Nývelt [6]), above this temperature the trihydrate $MgSO_3 \cdot 3H_2O$. However, the metastable hexahydrate often starts crystallising at temperatures higher than the transition temperature of 42°C. The two hydrate types differ in their solubility, which was reported by several authors (Hagisawa [3], Lowell et al. [9], Söhnel and Rieger [7], Broul et al. [10]). Figure 3 shows the solubility data for magnesium sulphite hexa- and trihydrate, respectively.

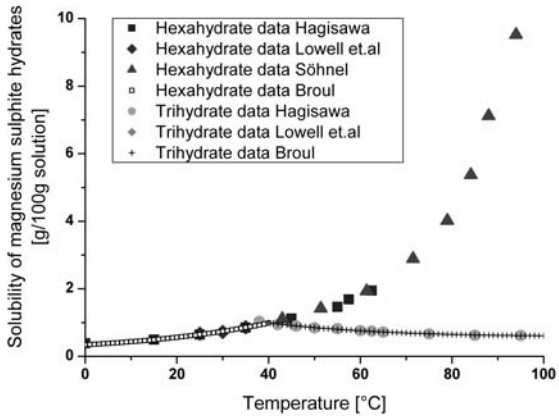

Figure 3. Solubility of magnesium sulphite hydrates.

Further research on the magnesium sulphite solubility was done by Hagisawa [3], Nývelt [6], Lowell et al. [9] and Pinaev et al. [11] and showed a significant connection of the magnesium sulphate concentration with the solubility behaviour in the way that raising sulphate concentrations increase the solubility of the sulphite.

Data simulation tool

The implemented data of the simulation tool were checked by several simulation runs. Therefore, sensitivity analyses on the implemented property data for the system MgO-SO_2-H_2O were done concerning the solubility behaviour of the different magnesium sulphite hydrates when varying the temperature and the input concentration.

Comparison between literature data and implemented data

The comparison between the literature data and the implemented data showed several discrepancies. Significant deviations compared to literature data were obtained (Figure 4) because of a wrongly calculated dependence of the phase transition starting

point on the initial $MgSO_3$ concentration by Aspen Plus®. Also the influence of the magnesium sulphate concentration on the magnesium sulphite solubility showed significant deviations compared to the literature (Figure 5). Although the SO_2 partial pressure for the system SO_2-H_2O is in good agreement with literature, the SO_2 partial pressure over solutions with $MgSO_3$ differed significantly compared to the literature data (Figure 6).

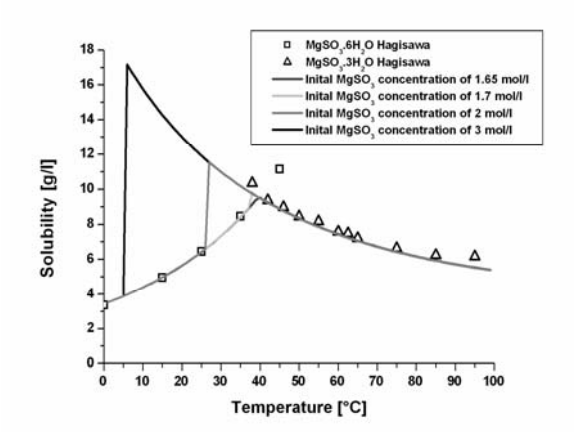

Figure 4. The solubility of magnesium sulphite hydrates calculated by Aspen Plus® (lines) compared with literature data from Hagisawa [3](symbols).

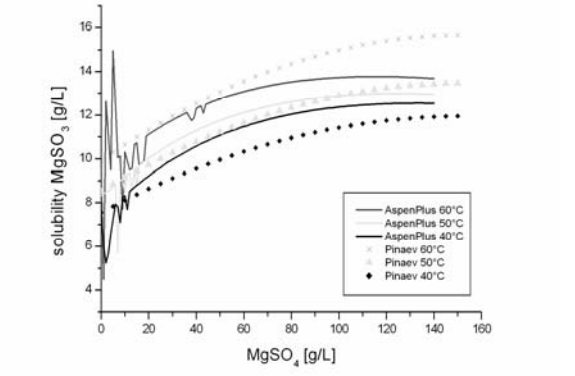

Figure 5. The solubility of magnesium sulphite hydrates as function of MgSO4 - concentration calculated by Aspen Plus® compared with literature data from Pinaev et al. [11].

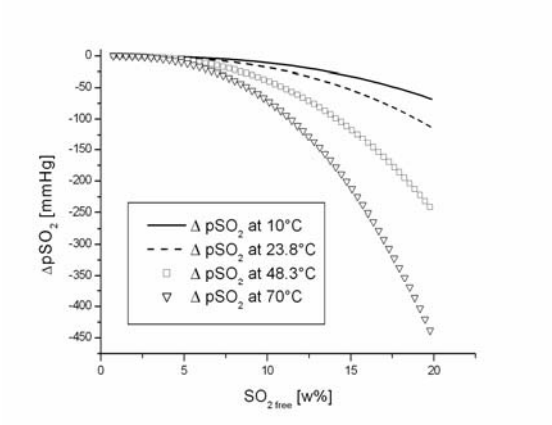

Figure 6. Deviation between calculated and measured data from Kuzminykh et al. [5] of the partial pressure over saturated magnesium sulphite solutions as a function of temperature.

Implementation procedure

The discrepancies described above require a possibility to adjust new data for the purpose of improving the model.
Therefore, Compaq Visual Fortran 6® based routines were developed in order to implement advanced data from literature. The approach was to readout the data derived within the simulation tool procedure and compare it with the literature data sets. If no significant deviation could be observed the same value was used for calculation. By observable deviations the value obtained from literature data was derived for the operation parameters and written back to the simulation tool.

The fitting functions used were developed by data regressions from the literature data for the following property data sets.

- Dissociation of the magnesium hydroxide,
- Solubility of the magnesium sulphites,

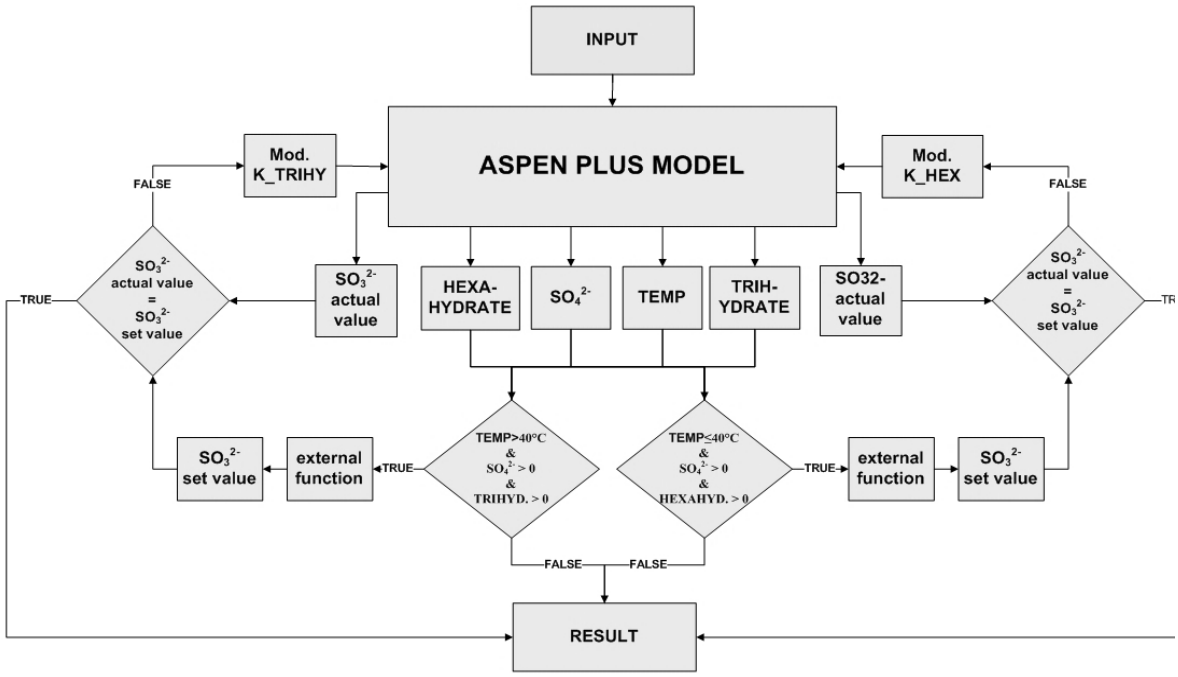

Figure 7. Schematic data flow diagram for calculation of the $MgSO_3$ solubility depending on the $MgSO_4$ concentration.

- Dependency of the magnesium sulphite solubility on the magnesium sulphate concentration,
- Equilibrium partial pressure of SO_2 over saturated and unsaturated magnesium sulphite solutions, respectively.

The schematic structure of the dataflow for correcting the solubility of magnesium sulphite as a function of magnesium sulphate content is shown in Figure 7.

Results

The Aspen Plus® calculation results, derived with the new routines, are in good agreement with to the literature data.

With these procedures it is now possible to implement new experimental data from the recovery plant. This opens new ways to raise the models prediction accuracy significantly.

Unfortunately, the new procedure worked trouble free only with a single absorption stage in Aspen Plus®. By using it with a multi-stage absorption model internal data conflicts were generated. These problems can be led back to the Aspen Plus® stepwise calculation procedure and its internal data structure.

To improve the calculation precision for a multi-stage absorption model a completely revised property data set including all interaction parameters for the activity coefficient model Elec-NRTL would be necessary.

The following figures show comparisons between Aspen Plus® calculation results done with the adjusted property data set and literature data

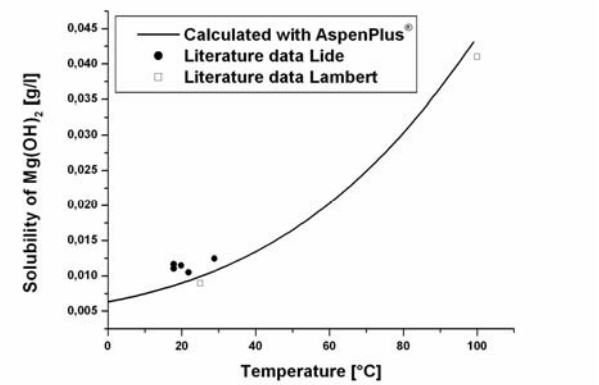

Figure 8. Solubility of magnesium hydroxide in water**.**

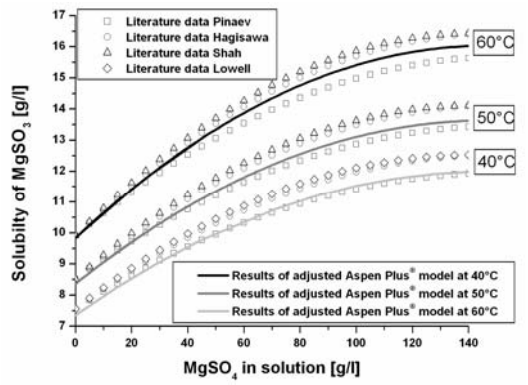

Figure 9. Comparison between literature data of $MgSO_3$ solubility and results calculated with the adjusted Aspen Plus® model.

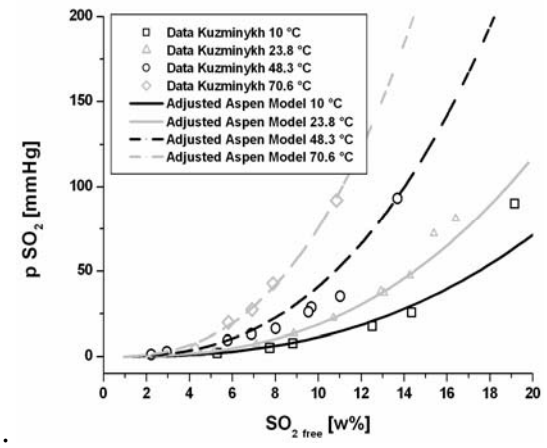

.

Figure 10. Comparison between literature data of SO_2 partial pressure over saturated magnesium sulphite solutions and results calculated with the adjusted Aspen Plus® model.

Conclusions

A new implementation procedure to adjust and expand the property data set of a single stage model for MgO-SO_2-H_2O was successfully developed. The model quality was raised significantly with this basic implementation concept and the use of literature data.

Because of the problems with the internal data conflicts, the development of a new model, based on a specialized simulation tool for the pulping industry was started. This new simulation basis allows better interventions into the program structure. Hence, the successful implementation of the new findings is also possible for multi - stage absorption models with the new simulation tool.

Acknowledgements

Financial support was provided by the Austrian government, the provinces of Lower Austria, Upper Austria and Carinthia as well as by the Lenzing AG. We also express our gratitude to the Johannes Kepler University, Linz, the University of Natural Resources and Applied Life Sciences, Vienna, and the Lenzing AG for their in kind contributions.

List of symbols

INPUT input values for the system
Mod. K_TRIHY modified solubility constant of Magnesium Sulfite Trihydrate
Mod. K_HEX modified solubility constant of Magnesium Sulfite Hexahydrate
HEXAHYDRATE content of Magnesium Sulfite Hexahydrate
TRIHYDRATE content of Magnesium Sulfite Trihydrate
TEMP Temperature
SO_3^{2-} actual value content of SO_3^{2-} ions at actual conditions
SO_4^{2-} content of SO_4^{2-} ions

References

[1] I. Lambert, Solubility Data Series, Alkaline Earth Hydroxides in water and aqueous solutions **1992**, Vol. 52.

[2] D. R. Lide, Handbook of Chemistry and Physics, CRC Press, **2001**.

[3] H. Hagisawa, Studies of Magnesium Sulphite, Bull. Inst. Phys. Chem. Res. **1933**, 12, 976.

[4] H. P. Markant, R. A. McIlroy and R. E. Matty, Absorption Studies - MgO-SO2 Systems, Tappi **1962**, 45, 849.

[5] I. N. Kuzminykh and M. D. Babushkina, Equilibrium between Sulfur Dioxide and Magnesium Bisulfite Solutions, Zhurnal Prikladnoi Khimii **1957**, 3, 495.

[6] J. Nývlt, Solubilities of Magnesium Sulfite, Journal of Thermal Analysis and Calorimetry **2001**, 66, 509.

[7] O. Söhnel and A. Rieger, Solubilities of Magnesium Sulfite Hydrates, Journal of Chemical and Engineering Data **1994**, 39, 161.

[8] M. Steindl, T. Röder, R. Simharl, M. Harasek, A. Friedl and H. Sixta, Online Raman monitoring of the phase transition of magnesium sulphite hydrate, Chemical Engineering and Processing **2005**, 44, 471.

[9] P. S. Lowell, F. B. Meserole and T. B. Parsons in Precipitation chemistry of magnesium sulfite hydrates in magnesium oxide scrubbing, Vol. Radian Corp.,Austin,TX,USA. FIELD URL, **1977**, 377.

[10] M. Broul, J. Nývlt and O. Söhnel, Solubility in inorganic two-component systems, Academia - Czechoslovak Academy of Sciences, Prague, **1979**.

[11] V. A. Pinaev, Mutual solubility of Magnesium Sulfite, Bisulfite and Sulfate, Zhurnal Prikladnoi Khimii **1964**, 37, 1361.

Lenzinger Berichte, 86 (2006) 63-70

COMPARATIVE REMOVAL OF HEMICELLULOSES FROM PAPER PULPS USING NITREN, CUEN, NAOH, AND KOH*

Juergen Puls, Ron Janzon, and Bodo Saake

Federal Research Centre of Forestry and Forest Products, Institute for Wood Chemistry and Chemical Technology of Wood, D-21031-Hamburg, Germany, Phone: (+49) 040-73962-514; Fax: (+49) 040-73962-599; E-Mail: jpuls@holz.uni-hamburg.de

* This work was presented during the 7th International Symposium "Alternative Cellulose“ 6th-7th September 2006, Rudolstadt, Germany and dedicated to Prof. Dr. Dr. h.c. Rudolf Patt on the occasion of his retirement

Xylans were selectively removed from paper grade pulps by nitren extraction in order to produce dissolving pulps. The impact of nitren charge on the removal of hemicelluloses was demonstrated for a birch and mixed softwood kraft pulp. The 95% purity level could easily be reached for the birch kraft pulp. Softwood glucomannans were almost insoluble under the investigated extraction conditions applying nitren. Accordingly softwood pulps seem to be less suited for the nitren process.

Furthermore, the selectivity of nitren extraction was compared with cuen. Nitren turned out to be much more selective in xylan removal, whereas cuen also dissolved part of the cellulose, when this solvent was applied at concentrations, which were needed to reach dissolving pulp purity.

Nitren was also tested in its xylan extraction capability in comparison with sodium and potassium hydroxide. Extraction of a xylan-rich birch kraft pulp with nitren resulted into a pulp of highest purity (96% cellulose content), which could not be obtained applying KOH and NaOH. In the case of a eucalyptus kraft pulp, however, nitren and sodium hydroxide extraction resulted into a product of more or less the same cellulose content (97%). With a beech sulfite pulp as the starting material highest purities with regard to the cellulose content were obtained applying 10% sodium hydroxide (97.5%), whereas the nitren procedure yielded into a pulp of 96.5% cellulose content. This was due to the inability of the nitren procedure to remove 2.7% mannan, which was present in the initial paper pulp from beech.

The residual nickel content in all pulps could be removed by a special washing procedure applying lactic acid.

Keywords: *carbohydrate composition, cuen, dissolving pulp, extraction, glucomannan, nitren, paper grade pulp, xylan*

Introduction

Dissolving-grade pulps are high-value, intensively bleached pulps with special quality requirements. Cellulose contents of 90-99% are necessary to produce regenerated cellulose fibres and cellulose derivatives. Accordingly, the hemicellulose content in dissolving pulps is low (0.5-10%), as well as the residual lignin and extractives content (below 0.2%) [1].

With a view on the worldwide pulp production capacity of about 150 x10^6 tons per year, the production of dissolving

pulps represents only a niche market of totally 2.5% of the global chemical pulp production. This market situation and the high price difference between both pulp categories rises the question, why paper grade pulps cannot be converted into dissolving pulps in an economically feasible process by selective removal of the hemicelluloses.

In this context, enzymatic hydrolysis of hemicelluloses from paper grade pulps with xylanases and mannanases was investigated by Puls et al. [2] and Christov and Prior [3], but the obtained purity levels were not satisfactory. Alkaline extraction could also be a conceivable solution, as this technique is the basis of most analytical procedures for the isolation and characterisation of hemicelluloses [4]. Accordingly dissolving pulps are frequently purified by hot or cold caustic extractions [5]. It is well known that the extraction potential of 10% sodium hydroxide towards pulps is often higher than applying 18% sodium hydroxide, whereas potassium hydroxide is usually used as extraction medium in 18% concentration. NaOH, LiOH, and KOH are equally powerful extractants for xylans. For the extraction of mannan however, KOH is less effective, whereas NaOH and LiOH have a similar potential [6].

Stimulated by investigations of Burger et al. [7], Kettenbach et al. [8], and Saalwächter et al. [9] a new process for the upgrading of paper pulp into dissolving pulp was recently patented by Rhodia Acetow GmbH [10]. The inventors claimed that nitren, a metal complex of tris(2-aminoethyl)amine and nickel(II)-hydroxide (Figure 1), selectively removes hemicelluloses from paper grade pulps. The cellulose content of a eucalyptus kraft pulp could be improved from 81% to 96% by a two-stage extraction with a 3% nitren solution. Moreover, xylans of high purity could be precipitated by lowering the pH value to 4.

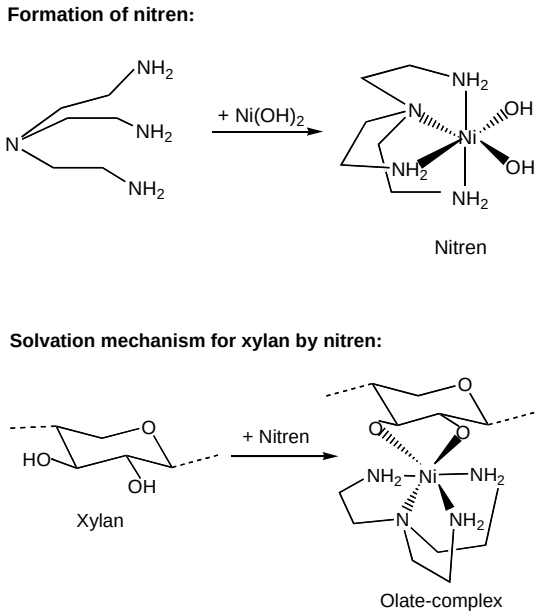

Figure 1. Constitution of nitren and its complexation with xylan in aqueous solution [10].

Another metal complex, cuen, has been known as a potential cellulose solvent for a long time [11,12,13]. It would be interesting to know about the performance of cuen for hemicellulose extraction in comparison with nitren, when being used at the same concentration level.

In the present study the extraction performance of nitren should be explored for a set of paper pulp samples, namely a high-xylan and a low-xylan hardwood kraft pulp in comparison to a softwood kraft pulp and a sulfite beech pulp. This performance should be compared with the extraction result, when Cuen is being used. In addition selected pulps should also be extracted with NaOH and KOH and the results with regard to purity should be compared with those after nitren extraction.

An important issue is also the question on the residual nickel content of the obtained pulps.

Experimental

Paper pulp samples

The starting pulp samples were a eucalyptus kraft pulp (SAPPI, Enstra mill), beech sulfite pulp (M-REAL, Stockstadt), mixed softwood kraft pulp (ZPR, Blankenstein), and birch kraft pulp (M-REAL, Örnsköldsvik). Prior to extraction the four starting pulps had the following carbohydrate compositions (cellulose, xylan and mannan): eucalyptus kraft pulp (84.7%, 14.3%, and 0.5%), beech sulfite pulp (87.0%, 10.3%, and 2.7%), softwood kraft pulp (84.1%, 6.3%, and 8.2%), and birch kraft pulp (75.4%, 24.1%, and 0.4%).

Extraction of the pulps

The preparation of the nitren solution and further characteristics of the starting pulps have been described in a previous study [14].

Prior to the extraction procedure pulp sheets were disintegrated in water, centrifuged and climatised to approximately 93% dry content. All extractions were carried out in 20 g-scale in polyethylene bottles for 1h at 30°C on a temperature-controlled roller mixer. The nitren extractions were conducted with 3%, 5%, or 7% nitren solutions whereas for alkaline extractions 10% NaOH and 14% KOH concentrations were used. The liquor to pulp ratio (L/P ratio) was varied between 10:1 and 20:1. Extracts were separated from the pulps by vacuum filtration over a sintered glass crucible (G1). Then the pulp was washed in three steps with 2% sodium hydroxide, 5% lactic acid (nitren extraction), or 20% acetic acid (alkaline extraction), and hot water. Finally the pulp was air dried at 20°C and 65% humidity and the yield was determined gravimetrically.

Pulp analysis

The carbohydrate composition of the pulps was determined according to [15] and [16], applying a 2-step hydrolysis with H_2SO_4. Subsequently the monosaccharides were detected by borate complex anion exchange chromatography. The results were not corrected for sugar losses and water addition during hydrolysis. The residual nickel content of the extracted pulps was measured by ICP-analysis after hydrolysis with 65% nitric acid in a microwave oven.

Results and discussion

Comparison of extraction behaviour of different pulps applying nitren

As a first step nitren was tested for its extraction efficiency for the four selected pulps, applying 3%, 5% and 7% nitren at a liquor to pulp ratio (L/P) of 10:1 at 30°C and a residence time of 60 min. In an earlier study [14] using a hardwood kraft pulp it had been concluded that time and temperature were rather insensitive for the process. After 5 min the mobilisation of the xylan was more or less completed. A prolongation of the extraction to 120 min resulted in only a minor further reduction of the xylose content in the extracted pulp. The differences in xylan content at various temperatures between 20 and 40°C were only marginal, but the effect was significant in favour of lower temperatures. For an industrial application cooling is very costly, and consequently, nitren extraction should be conducted at ambient temperatures. Under industrial conditions, it also seems unrealistic, that short extraction times of dried pulp sheets can be done in a reproducible way. Thus, all following investigations were performed at a reaction time of 1 h.

The total nitren charge can be varied by the L:P ratio as well as by the nitren concentration in solution. The nitren charge was a decisive factor regarding xylan removal and pulp purity. The combination of a high nitren concentration and a low liquor to pulp ratio was most effective for xylan removal. However, a high liquor to pulp ratio with a lower

nitren concentration proved to be more selective and minimised cellulose degradation as well [14].

Figure 2 illustrates the carbohydrate composition of birch kraft pulp applying 3%, 5%, and 7% nitren at a liquor to pulp ratio of 10:1. The purity of the pulp was increased from 93.9% glucose for 5% nitren up to 95.9% glucose for 7% nitren. Accordingly the purity level of viscose grade pulps could be reached with 5% nitren, while 7% nitren charge was needed to obtain high quality grades, which might be suitable e.g. for production of cellulose acetate.

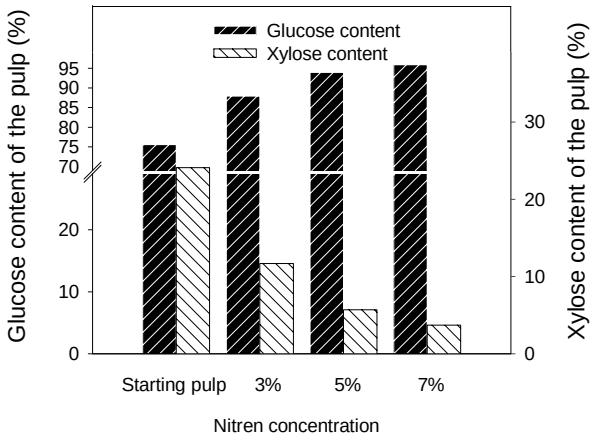

Figure 2. Influence of extraction with 3%, 5%, and 7% nitren on the carbohydrate composition of birch kraft pulp (L/P=10:1, T=30°C, t=60min).

In comparison with nitren extraction of the softwood kraft pulp the most important observation is that nitren hardly solubilised mannan in the examined concentration range (Figure 3). The mannan content of the softwood pulp decreased only slightly from 6.3% (initial paper pulp) to 5.6% after extraction with 7% nitren.
This observation can be explained by the differences in the configuration of the hydroxyl groups, which are in trans configuration for ß-D-glucans and ß-D-xylans, while they are in cis configuration for ß-D-mannans. It is most likely that for the dissolution of polysaccharides with

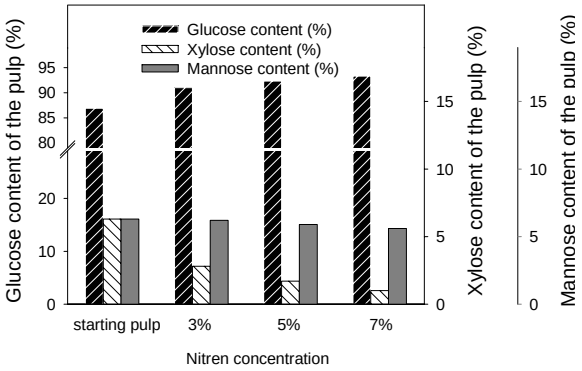

Figure 3. Influence of extraction with 3%, 5%, and 7% nitren on the carbohydrate composition of softwood kraft pulp (L/P=10:1, T=30°C, t=60min).

nitren a trans configuration of the involved hydroxyl groups is required. The xylan content of extracted softwood pulps continuously decreased with increased nitren concentrations analogously to the experiments with hardwood kraft pulps. After extraction with 7% nitren, a cellulose content of 91.4% (softwood pulps) could be achieved for the softwood kraft pulp. This calculation takes into account the glucose content belonging to galactoglucomannans.

Comparison of nitren and cuen extractions
In this comparison the advantage of nitren compared to cuen for selective xylan removal from birch kraft pulp should be verified. Cuen (copper ethylendiamine complex) is a well known cellulose solvent for its viscosimetrical determination of the degree of polymerization [11-13]. Increasing charges of nitren and cuen between 20% and 100%, based on pulp, were used at a liquor to pulp ratio of 20:1 at 30°C for 1 hour (Figure 4).

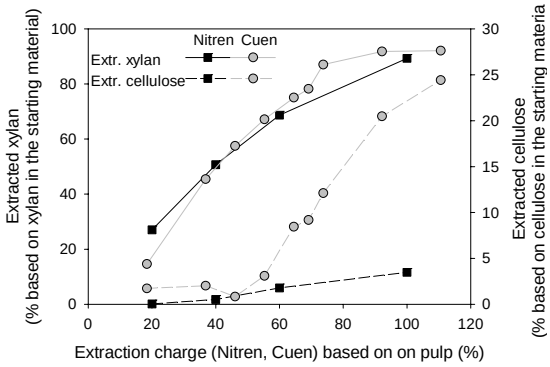

Figure 4. Impact of nitren and cuen on dissolved xylan and cellulose from birch kraft pulp (L/P=20:1, T=30°C, t=60min.

Both solvent systems seemed to be equally well suited for xylan extraction. About 90% of the xylan present in the birch kraft pulp could be removed using both systems at extraction charges of 90%, based on pulp. However nitren turned out to be much more selective from a charge of 60% on. As can be visualized from Figure 4 substantial quantities of cellulose (>20%) were dissolved at those cuen charges, which were necessary for xylan removal in order to obtain dissolving pulp qualities, whereas cellulose dissolution, initiated by nitren, was always <5%.

Comparison of nitren, sodium hydroxide, and potassium hydroxide extractions

In the final investigations on the potential of nitren extraction of hemicelluloses from paper pulps in comparison to the potential of NaOH and KOH (Figures 5-7) only hardwood paper pulps were included due to the inability of nitren for glucomannan mobilisation. A comparatively high liquor to pulp ratio of 20:1 was chosen for the alkaline media in order to take advantage of the full potential of the extractants. The nitren extraction was performed with 5% and 7% nitren concentration. From reasons of comparison with earlier results (Figures 2-4) liquor to pulps ratios of 10:1 and 20:1 were applied. NaOH was applied at 10% concentration, whereas KOH was applied at 14% concentration.

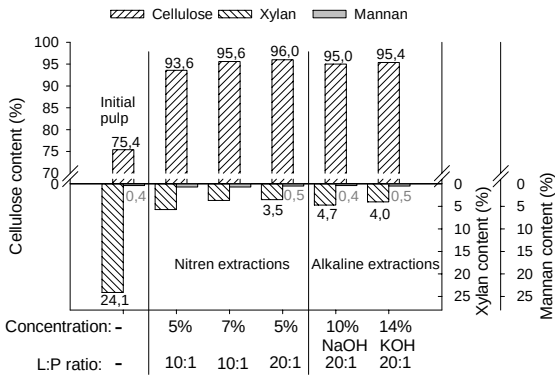

Figure 5. Carbohydrate composition of birch kraft pulp after nitren and alkaline extraction (T=30°C, t=60min).

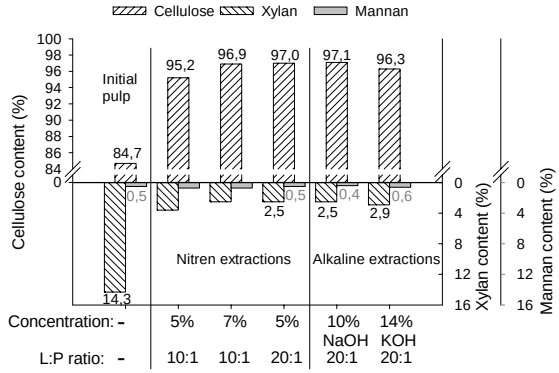

Figure 6. Carbohydrate composition of eucalyptus kraft pulp after nitren and alkaline extraction (T=30°C, t=60min).

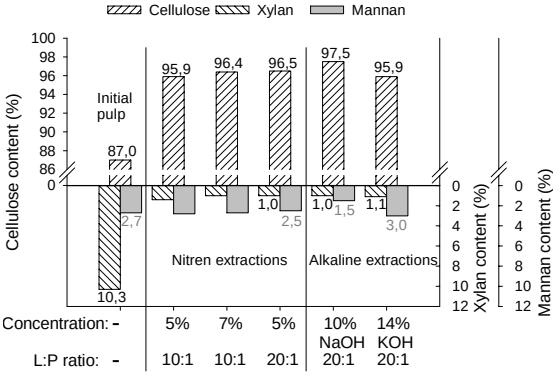

Figure 7. Carbohydrate composition of beech sulfite pulp after nitren and alkaline extraction (T=30°C, t=60min).

Figure 5 illustrates the carbohydrate composition of the extracted birch kraft pulp in comparison to the starting material. The cellulose content of 75.4% in the initial pulp was raised to 96% after 5% nitren extraction (20:1). This purity could not be obtained using NaOH or KOH. The cellulose content of the pulp after 14% KOH extraction was increased to 95.4%, whereas extraction with 10% NaOH resulted in 95% purity.

The cellulose content of the eucalyptus sulfate pulp (84.7% cellulose, 14.3% xylan) could be raised to 97% by nitren extraction at a nitren charge of 5% and a liquor to pulp ratio of 20:1 (Figure 6). This grade in purity could also be achieved with 10% NaOH (96.1% cellulose) and 14% KOH (96.3%).

Comparing the efficiency of nitren and alkali extraction of the beech sulfite pulp (88% cellulose, 10% xylan, 2% mannan) it becomes clear that alkaline extraction resulted in a slightly higher purity (97.5%) compared to nitren extraction (best result 96.5% cellulose, see Figure 7). The comparatively high amount of mannan (2.7%) in the starting material was unfavourable, since this hemicellulose component could not be removed by nitren extraction, whereas sodium hydroxide was most efficient to mobilize mannan besides of xylan. The early results of Hamilton and Quimby [7] and Scott and Pinchot [17] on the better performance of sodium hydroxide for mannan extraction compared to potassium hydroxide could be confirmed.

Reflecting the results from the comparative extraction experiments it can be concluded carefully that nitren is a favourable extraction agent for paper pulps with a high xylan content. As a rule these are kraft paper pulps containing xylans, which have been stabilized under alkaline pulping conditions [18], hindering their complete mobilisation by applying alkali. Nitren, however is capable remove more than 90% of the initial xylan content. These polysaccharides can be utilized elsewhere [19]. Surprisingly by alkaline extraction the eucalyptus kraft pulp could also be upgraded to the required purity of 97.1% cellulose content. The starting material had a lower xylan content. This could be due to the normally lower xylan content in eucalyptus wood chips, compared to beech and birch. Eventually the eucalyptus kraft pulp had been produced according to a modified kraft process, in order prevent a reprecipitation of the initially dissolved lignin and xylan proportion onto the fiber surface [20, 21]. Due to the acid pulping conditions sulfite pulps excel by their lower hemicellulose content [22]. The xylan proportion (10.3%) in the beech sulfite pulp could be removed by nitren as well as by alkali. Highest grades in purity were obtained applying sodium hydroxide. This was due to the fact that sodium hydroxide could mobilize both, xylan and mannan, whereas nitren was rather selective in xylan removal (Figure 7).

Conclusions

Nitren is a very selective solvent for xylans. This could be demonstrated, when nitren was used in the same concentration range as cuen and when softwood pulps were the starting materials. Cuen also dissolved considerable proportions of cellulose at concentrations, which were necessary to reach a cellulose content >95% whereas nitren was rather selective. Glucomannans were almost insoluble in the investigated concentration range, when nitren was used. Thus pulps with a high glucomannan content, e.g. softwood pulps, are not suitable raw materials for the nitren process, particularly not if the production of high purity dissolving pulp is envisaged. The extraction of hardwood pulps from both the kraft and the sulfite processes is well suited for the production of high purity dissolving pulps.

The total amount of nitren applied was the primary factor for adjusting the degree of xylan removal. Applying the most economic liquor to pulp ratio of 10:1 and 5% nitren, the cellulose content of hardwood kraft pulps could be raised up to 94-96%. Cellulose contents of 96-97% could be achieved by extracting with 7% nitren solutions. Hardwood sulfite pulps could be upgraded to 96% cellulose content, even at lower nitren charges of 5%. Provided the case that a high value application can be found for the extracted xylan, kraft pulps might be preferable due to their higher xylan content. If dissolving pulp is the product of higher value, sulfite pulps seem to be superior, because higher pulp yields can be obtained with lower nitren concentrations. However a slightly higher purity could be obtained, when sodium hydroxide was applied as extraction agent. This was due to the fact that nitren was unable to mobilize the residual mannan content in the beech sulfite pulp.

Acknowledgements

SAPPI, M-REAL, and ZPR are thanked for the provision of paper pulp samples.
The skilful technical assistance of Mrs. Nicole Erasmy, Mr. Jan Benthien, Mr. Eugen Pauls, and Mr. Thomas Schwarz is gratefully acknowledged. The authors are indebted to Dr. Armin Stein of Rhodia Acetow for helpful discussions. Financial support for this research was provided by AiF (German Federation of Industrial Research Associations "Otto von Guericke" e.V., AIF project 13892N).

References

[1] Kordsachia, R. Patt, H. Sixta, 1999. Cellulosegewinnung aus verschiedenen Rohstoffen. Das Papier 53, 96-108.

[2] J. Puls, J.L. Lin, H.-U. Körner, 1987. Non-traditional analytical techniques and enzymatic treatments of pulps. In: Proceedings of 1987 Tappi International Dissolving Pulps Conference. Tappi Press, Atlanta, 39-42.

[3] L.P. Christov and B.A. Prior, 1996. Repeated treatments with *Aureobasidium pullulans* hemicellulases and alkali enhance biobleaching of sulphite pulps. Enzyme Microb. Technol. 18, 244-250.

[4] D. Fengel and G. Wegener, Wood - Chemistry, Ultrastructure, Reactions. Walter de Gruyter, Berlin, 1984.

[5] S.A. Rydholm, Pulping Processes. Interscience Publishers, John Wiley & Sons, New York, 1965.

[6] J.K. Hamilton and G.R. Quimby, 1957. The extractive power of lithium, sodium, and potassium hydroxide solutions for the hemicelluloses associated with wood cellulose and holocellulose from western hemlock. Tappi J. 40, 9, 781-786.

[7] J. Burger, G. Kettenbach, P. Klüfers, 1995. Coordination equilibria in transition metal based cellulose solvents. Macromol. Symp. 99, 113-126.

[8] G. Kettenbach, P. Klüfers, P. Mayer, 1997. Deprotonation patterns of disaccharides in coordinating cellulose solvents: A status report. Macromol. Symp. 120, 291-301.

[9] K. Saalwächter, W. Burchard, P. Klüfers, G. Kettenbach, P. Mayer, D. Klemm, S. Dugarmaa, 2000. Cellulose solutions in water metal complexes. Macromolecules 33, 4094-4107.

[10] G. Kettenbach and A. Stein, 2002. Verfahren zur Abtrennung von Hemicellulosen aus hemicellulose-haltiger Biomasse sowie die mit dem Verfahren erhältliche Biomasse und Hemicellulose. DE 10109502 A1.

[11] G. Jayme, 1974. Anwendungs-

möglichkeiten von EWNN und Cadoxen in der Cellulosechemie. Das Papier 28, 12, 528-533.

[12] H. Huckfeld and A. Sczostak, 1995. Die Temming-Methode zur Viscositätsbestimmung an Linters-Cellulosen . Das Papier 49, 315-325.

[13] J. Burger, G. Kettenbach, P. Klüfers, 1995. Coordination equilibria in transition metal based cellulose solvents. Macromol. Symp. 99, 113-126.

[14] R. Janzon, J. Puls, B. Saake, 2006. Upgrading of paper-grade pulp into dissolving pulps by nitren extraction: Optimisation of extraction parameters and application to different pulps. Holzforschung 60, 347-354.

[15] M. Sinner, M.H. Simatupang, H.H. Dietrichs, 1975. Automated quantitative analysis of wood carbohydrates by borate complex ion exchange chromatography. Wood Sci. Technol. 9, 307-322.

[16] M. Sinner and J. Puls, 1978. Non-corrosive dye reagent for detection of reducing sugars in borate complex ion-exchange chromatography. J. Chromatogr. 156, 197-204.

[17] R.W. Scott and G. Pinchot, 1989. Influence of cations and borate on the alkaline extraction of xylan and glucomannan from pine pulps. J. Appl. Polym. Sci. 38, 907-914.

[18] S. Danielsson and M.E. Lindström, 2005. Influence of birch xylan adsorption during kraft cooking on softwood pulp strength. Nord. Pulp Pap. Res. J. 20, 436-441.

[19] K. Schwikal, Th. Heinze, A. Ebringerová, K. Petzold, 2006. Cationic xylan derivatives with high degree of functionalization. Macromolecular Symposia, 232, 49-56.

[20] A. Meller, 1965. The retake of xylan during alkaline pulping. Holzforschung 19, 118-124

[21] K. Kovasin, and P.O. Tikka, 1993. Low-kappa kraft pulping and its advantages. Paperi ja Puu 75, 491-497.

[22] J. Puls, 1995. Zum Schicksal der Hemicellulosen in holzchemischen Prozessen. In: Abwässer aus der Zellstoffindustrie und der Lederverarbeitung, Schriftenreihe Biologische Abwasserreinigung (B. Weigert ed.), Vol. 5, 77-87, 1995.

Lenzinger Berichte, 86 (2006) 71-84

BLEICHE VON SAUREM FICHTENSULFITZELLSTOFF UNTER EINSATZ VON OZON

Wo sollte die Z-Stufe innerhalb einer TCF-Bleichsequenz angeordnet werden?

Othar Kordsachia[1] und Armin Reinhard[2]

[1]Bundesforschungsanstalt für Forst- und Holzwirtschaft, Institut für Holzchemie und chemische Technologie des Holzes, Leuschnerstraße 912, D-21031 Hamburg, Phone: (+49) 040-7395354; Fax: (+49) 040 73962599; E-mail: o.kordsachia@holz.uni-hamburg.de

[2] SCA Hygiene Products GmbH, Sandhofer Straße 176, D-68305 Mannheim, Deutschland, Phone: (+49) 0621-7783317; Fax: (+49) 0621 7782348; E-mail: armin.reinhard@sca.com

Zusammenfassung

Unter der Fragestellung, wo eine Ozonstufe innerhalb einer TCF-Bleiche idealerweise eingesetzt werden sollte, wurde ein nach dem sauren Magnesiumbisulfitverfahren industriell erzeugter Fichtenzellstoff in drei unterschiedlichen Ozonbleichsequenzen gebleicht. Dabei wurde die Ozonbehandlung als erste Bleichstufe (A-Z-Q-P_{NaOH}), als mittler Bleichstufe zwischen zwei Peroxidbleichstufe (P_{MgO}-A-Z-Q-P_{NaOH}) und auch als Endbleichstufe (P_{MgO}-A-Z) durchgeführt. Als Refenrenz diente eine ozonfreie TZF-Bleiche (P_{MgO}-A_Q-P_{NaOH}). Der Zielweißgrad wurde mit 90 % ISO vorgegeben.

Die Untersuchungen haben gezeigt, dass der Einsatz von Ozon, insbesondere unter Kostengesichtspunkten, eine erwägenswerte Möglichkeit darstellt, Fichtensulfitzellstoff auf einen hohen Weißgrad zu bleichen. Die ohne Ozoneinsatz durchgeführte Referenzbleiche zeigte jedoch andererseits, dass es auch ohne Einsatz von Ozon möglich ist, Fichtensulfitzellstoff, auch mit P_{MgO}-Eingangsstufe, mit akzeptablem Peroxideinsatz auf einen Weißgrad von 90 % ISO zu bringen. Die Frage, an welcher Stelle Ozon innerhalb der Bleichsequenz am vorteilhaftesten eingesetzt werden sollte, kann anhand dieser Untersuchungen natürlich nicht abschließend geklärt werden. Überraschend gute Ergebnisse wurden mit der Ozonbleiche als erste Bleichstufe erhalten, aber auch die zwischengeschaltete Ozonstufe zwischen P_{MgO}- und P_{NaOH}-Stufe liefert gute Ergebnisse. Insbesondere kann der Ozoneinsatz in diesem Fall mit etwa 0,3-0,4 % gering gehalten werden, so dass auf eine einfache Ozonbleichtechnologie zurückgegriffen werden könnte. Die Anwendung der Ozonbehandlung als letzte Bleichstufe liefert indes schlechtere Ergebnisse, weil hohe Ozoneinsatzmengen benötigt werden, die Zellstofffasern stark angegriffen werden, was sich negativ auf die Reißfestigkeit auswirkt, und auch die Weißgradstabilität gering ist. Diese Bleichvariante kann daher bei Erwägung einer industriellen Umsetzung ausgeschlossen werden. Insbesondere die Bleichvariante mit zwischengeschalteter Ozonstufe bietet noch Optimierungsmöglichkeiten durch Abstimmung der Bleichstufen aufeinander. Beispielweise könnte der Peroxideinsatz in der Eingangsstufe verringert werden, da anschließend noch zwei weitere Bleichstufen zur Erzielung eines hohen Weißgrades zur Verfügung stehen. Eine andere Option ist, den Holzaufschluss bei höherer Kappazahl abzubrechen, um so bessere Festigkeitseigenschaften zu erzielen.

Einleitung

Aufgrund großer Fortschritte in der Ozonerzeugung kann Ozon heutzutage verhältnismäßig günstig produziert werden. Da Ozon zudem eine sehr hohe Delignifierungseffizienz aufweist, stellt Ozon nunmehr eine sehr attraktive und konkurrenzfähige Bleichchemikalie dar. Die Ozonbleiche von Zellstoffen ist mittlerweile eine etablierte, ausgereifte

Technologie. Dies offenbart sich, wenn man sich die Liste der in der industriellen Zellstoffbleiche bereits installierten Ozonbleichanlagen anschaut [1]. Es fällt auf, dass die Ozonbleiche vor allem genutzt wird, um Sulfatzellstoffe zu bleichen. Der Ozonbleiche kommt dabei in sehr unterschiedlichen TCF- und ECF-Bleichsequenzen im wesentlichen die Funktion zu, nach der Sauerstoffdelignifizierung verbliebene, schwer abbaubare Restligninstrukturen zu zerstören und dadurch die Endbleichbarkeit drastisch zu verbessern. In ECF-Bleichsequenzen ist der Ozoneinsatz zum einen deshalb attraktiv, weil der AOX- und der OX-Wert deutlich verringert werden. Zum anderen können durch den Ozoneinsatz erhebliche Mengen an Chlordioxid eingespart werden, was insbesondere bei eingeschränkter Produktionskapazität an Chlordioxid von Bedeutung ist. Berücksichtigt man zudem die höhere Effizienz des Ozons gegenüber Chlordioxid, dann ist die Ozonbleiche auch in Hinblick auf die Bleichkosten attraktiv. Ein gravierender grundsätzlicher Nachteil der Ozonbleiche ist jedoch die geringere Selektivität des sehr aggressiven Ozons. Um allzu hoher Festigkeitsverluste zu vermeiden, sollte daher der Ozoneinsatz auf 0,5 %/otro Zellstoff limitiert werden. In der ECF-Bleiche hat es sich bewährt, Ozon in einer kombinierten (ZD)-Stufen einzusetzen, da die der Ozonstufe ohne Zwischenwäsche direkt nachfolgende Chlordioxidbehandlung den Zellstoff gegen die alkalische Peelingreaktion stabilisiert, die ansonsten zu einem weiteren Kohlenhydratabbau und zu deutlichen Festigkeitsverlusten führt. Wegen des hohen Substitutionsfaktors von Ozon zu Wasserstoffperoxid können in der TCF-Bleiche von Sulfatzellstoffen erhebliche Mengen an H_2O_2 durch den Ozoneinsatz eingespart werden, wodurch sich auch in diesem Fall ein Kostenvorteil ergibt. Oftmals ist es auch erforderlich, Ozon einzusetzen, um bei Anwendung einer TCF-Bleiche die gestellten Weißgradanforderungen überhaupt erfüllen zu können. Bevorzugt wird Ozon eingesetzt, um Laubholzsulfatzellstoffe zu bleichen. Die mit dem Ozoneinsatz verbundenen Festigkeitsverluste sind geringer als bei der Bleiche von Nadelholzzellstoff und können auch eher akzeptiert werden. Ein weiterer Vorteil der Ozonbleiche von Laubholzsulfatzellstoffen besteht darin, dass Ozon Hexenuronsäuren sehr wirkungsvoll zerstört.

Die industrielle Ozonbleiche von Sulfitzellstoffen stellt bisher eine umstandsbedingte Ausnahme dar. In früheren Arbeiten konnte gezeigt werden, dass Sulfitzellstoffe sehr gut auf eine Ozonbehandlung ansprechen und die damit einhergehenden Festigkeitsverluste, trotz eines starken Abfalls der Viskosität, geringer sind als bei Sulfatzellstoffen [2-7]. Dennoch wurde die Ozonbleiche wegen der hohen Kosten zumeist nicht in Erwägung gezogen, zumal es sich sehr bald herausstellte, dass Sulfitzellstoffe wegen ihrer leichten Bleichbarkeit unter ausschließlicher Verwendung von Wasserstoffperoxid auf ausreichend hohe Weißgrade gebleicht werden können. Da Ozon aber mittlerweile recht günstig hergestellt werden kann, könnte der Ozoneinsatz in der Bleiche von Sulfitzellstoffen eine unter wirtschaftlichen Aspekten sehr interessante Alternative darstellen, zumal man davon ausgehen kann, dass auch in diesem Fall dadurch erhebliche Mengen an Wasserstoffperoxid eingespart werden können, insbesondere wenn ein hoher Weißgrad angestrebt wird. Ozon stellt als starkes Delignifizierungsmittel eine gute Ergänzung zum Wasserstoffperoxid dar, weil dessen Delignifizierungsvermögen beschränkt ist.

Den Untersuchungen zum Einsatz von Ozon in der Bleiche von aus Fichtenholz hergestellten Magnesiumbisulfitzellstoffen lag die Zielsetzung zugrunde, die Einsatzmöglichkeiten von Ozon grundlegend zu prüfen. Gerade im Falle der Bleiche von Magnesiumbisulfitzellstoffen ist die Kombination der Ozonstufe mit einer mit MgO als Bleichalkali durchgeführten ersten P-Stufe (P_{MgO}-Stufe) besonders interessant, zum einen weil dadurch die Abwasserbelastung drastisch verringert werden kann, zum anderen weil eine P_{MgO}-Stufe weit weniger effizient ist als eine mit NaOH betriebene Peroxidbleiche und somit die Ozonbleiche wesentlich dazu beitragen kann, hohe Weißgrade zu erzielen. Vor allem sollte ermittelt werden, an welcher Stelle Ozon innerhalb der Bleichsequenz am besten eingesetzt werden sollte. Ozon kann als starkes Bleichmittel sowohl in der ersten Bleichstufe, in einer Zwischenstufe oder

prinzipiell auch in einer Endbleichstufe eingesetzt werden. Die Vor- und Nachteile dieser verschiedenen Anwendungsmöglichkeiten sind unter anderem auch abhängig von der Beschaffenheit des zu bleichenden Zellstoffes und den gestellten Anforderungen.

Material & Methoden

Für die Untersuchungen stand ein industriell nach dem sauren Magnesiumbisulfitverfahren erzeugter Fichtenzellstoff, sowohl ungebleicht als auch P_{MgO}-gebleicht, zur Verfügung. Die Zellstoffeigenschaften dieser Ausgangsstoffe sind in der Tabelle 1 aufgeführt.

Tabelle 1. Daten der Ausgangsstoffe.

	Kappazahl [-]	Weißgrad [% ISO]	GVZ [ml/g]
ungebleicht	19,1	58,3	1092
P_{MgO}-gebleicht	7,6	73,9	1122

Die Ozonstufe wurde als Hochkonsistenzbleiche bei einer Stoffdichte von etwa 40 % durchgeführt. Der Stoff wurde zunächst mit Schwefelsäure auf einen pH-Wert von unter 3,0 angesäuert, dann – ohne Zwischenwäsche - in einer Wäscheschleuder entwässert und in einem Scheibenrefiner in zwei Durchgängen aufgeflufft. Die Ozonbleiche erfolgte bei einer Temperatur von 50 °C mit einem Stoffeinsatz von jeweils 50 g in einem rotierenden 4l-Rundkolben, dem kontinuierlich ein ozonhaltiger Gasstrom bis Erreichen der vorgegebenen Ozoneinsatzmenge zugeführt wurde. Nach der Ozonbehandlung wurde der Zellstoff jeweils gründlich mit entionisiertem Wasser gewaschen. In den Komplexbildnerstufen (Q) wurde der Zellstoff standardmäßig für 30 min bei 60 °C und 3 % Stoffdichte mit 0,1 % DTPA behandelt. Es erfolgte keine pH-Wert-Einstellung, der pH-Wert schwankte zwischen 4,2 und 4,4. Davon abweichend wurde in der ozonfreien Referenzbleiche eine A_Q-Stufe zwischen der P_{MgO}- und der P_{NaOH}-Stufe durchgeführt. In diesem Fall wurde der pH-Wert mit Schwefelsäure auf unter 3,0 erniedrigt und ebenfalls 0,1 % DTPA zugesetzt. Die Peroxidbleichversuche wurden konventionell bei 10 % Stoffdichte im Wasserschüttelbad durchgeführt. Die jeweils angewendeten Bleichbedingungen sind dem Ergebnisteil zu entnehmen.

Am ungebleichten Zellstoff wurde die folgende Bleichsequenz angewendet:

- A-Z-Q-P_{NaOH}

Die weiteren Bleichuntersuchungen wurden am bereits P_{MgO}-vorgebleichten Zellstoff durchgeführt. Folgende Bleichsequenzen wurden dabei berücksichtigt:

- P_{MgO} --- A-Z
- P_{MgO} --- A-Z-Q-P_{NaOH}
- (P_{MgO} --- A-Z-Q-P_{MgO})
- P_{MgO} --- A_Q-P_{NaOH} (Referenz)

Ozonbehandlung als initiale Bleichstufe

Der Einsatz von Ozon in der ersten Delignifizierungsstufe kommt bei der Bleiche von Sulfatzellstoffe eigentlich nicht in Frage. Bereits der hohe Säurebedarf zur Einstellung des erforderlichen niedrigen pH-Wertes spricht gegen diese Vorgehensweise. Zudem ist der Festigkeitsverlust der Sulfatzellstoffe, trotz eines verhältnismäßig hohen Restligningehaltes, sehr beträchtlich, vor allem bei Nadelholzzellstoffen. Die Sauerstoffdelignifizierung ist eindeutig zu bevorzugen und industriell gängig.

Nach dem sauren Magnesiumsulfitaufschluss liegt eine andere Ausgangslage vor. Eine Sauerstoffdelignifizierung ist nicht sinnvoll. Nach saurem Sulfitaufschluss ist die Kappazahl in der Regel niedrig, was die Effizienz der Sauerstoffstufe herabsetzt. Des Weiteren ist die Sauerstoffdelignifizierung aufgrund der hohen Ausgangsweiße dieser Zellstoffe nicht mit einem Anstieg, sondern mit einem Abfall des Weißgrades verbunden, so dass in den nachfolgenden Bleichstufen kein oder nur wenig Wasserstoffperoxid eingespart werden kann. Saure Sulfitzellstoffe reagieren zudem sehr empfindlich auf eine alkalische Behandlungsstufe unter scharfen Bedingungen, so dass eine Sauerstoffstufe, vor allem wenn MgO als Alkaliquelle bei hoher Bleichtemperatur eingesetzt wird, zu starken Ausbeute- und Festigkeitsverlusten führt. Es hat sich auch gezeigt, dass der Einsatz von Sauerstoff in der Peroxidbleiche nicht wirklich effektiv ist. Eine sauerstoffverstärkte Peroxidstufe bewirkt zwar

einen stärkeren Kappazahlabbau, und damit leider auch eine höhere Abwasserbelastung, aber die Peroxideinsparung und der mögliche zusätzliche Weißgradgewinn sind sehr bescheiden und rechtfertigen den höheren Aufwand nicht.

Dahingegen ist die Ozonbleiche von Sulfitzellstoffen in Bezug auf die Ausbeute- und Festigkeitseinbußen weniger kritisch. Da Sulfitzellstoffe gut auf die Ozonbehandlung ansprechen, ist die erreichbare Delignifizierung sehr hoch, ohne dass es, auch bei hohem Ozoneinsatz, zu derart drastischen Festigkeitsverlusten wie bei der Ozonbleiche von Sulfatzellstoffen kommt.

In den Untersuchungen zum Einsatz von Ozon in der ersten Bleichstufe wurden zunächst Vorversuche mit geringen Zellstoffeinsatzmengen von 50 g durchgeführt. Zur Festlegung der optimalen Ozoneinsatzmenge für einen abschließenden Bleichversuch in größerer Charge wurde der Ozoneinsatz in 0,2 %-Schritten zwischen 0,6 und 1,4 % variiert. Nach anschließender Q-Stufe wurde dann jeweils eine P_{NaOH}-Stufe durchgeführt, wobei zum Teil die Bleichparameter variiert worden, um den Bleicheffekt zu verbessern. Den Einfluss steigender Ozoneinsatzmengen auf Kappazahl, Weißgrad, Zellstoffviskosität (GVZ) und Ozonverbrauch zeigen die Abbildungen 1-4.

Diese Voruntersuchungen bestätigen die hohe Effektivität der Ozonbleiche von Sulfitzellstoffen. Auch bei hohen Ozoneinsatzen über 1 %/otro Zellstoff wurde eine noch hohe spezifische Delignifizierung erreicht (Abb.1). Die Bleichwirkung des Ozons beruht auf der weitgehenden Ligninentfernung. Hohe Weißgrade werden daher in einer Ozonbleichbehandlung erst dann erzielt, wenn der Restligningehalt sehr gering ist. Auch nach dem maximalen Ozoneinsatz von 1,4 % lag die Kappazahl noch bei 4,5, was den noch niedrigen Weißgrad von 68,5 % ISO erklärt (Abb. 2). Ein wesentlicher Vorteil bei Anwendung der Ozonbleichbehandlung als erste Bleichstufe besteht darin, dass das Ozon in hoher Rate mit dem Lignin reagiert (Abb. 3). Daher wird auch bei hoher Ozoneinsatzmenge ein hoher Ozonumsatz erhalten (Abb. 4). Die Zellstoffviskosität wird daher in weit geringerem Maße verringert als bei der Anwendung einer Ozonstufe in einer nachfolgenden Stufe an einem Zellstoff mit geringerem Restligningehalt

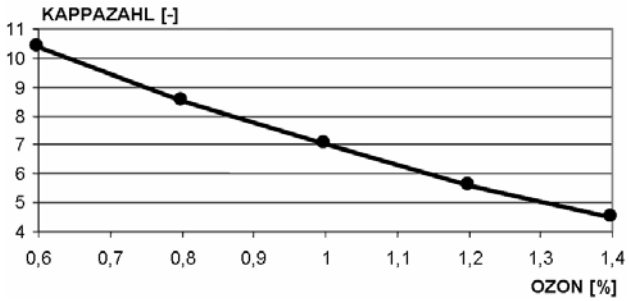

Abbildung 1. Delignifizierung in Abhängigkeit vom Ozoneinsatz. *Ausgangsstoff: ind. Fichtensulfitzellstoff, ungebleicht, Ausgangskappazahl 19,1*

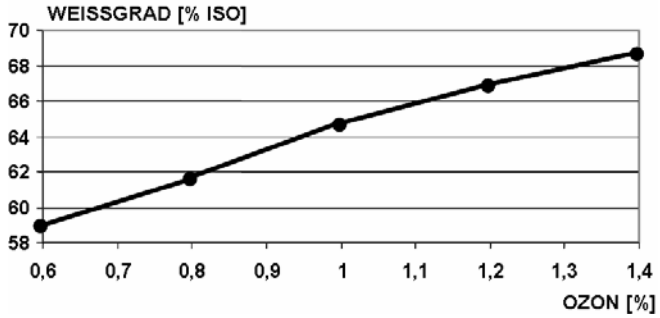

Abbildung 2. Weißgradentwicklung mit steigendem Ozoneinsatz. *Ausgangsstoff: ind. Fichtensulfitzellstoff, ungebleicht, Ausgangsweißgrad 58,3 % ISO*

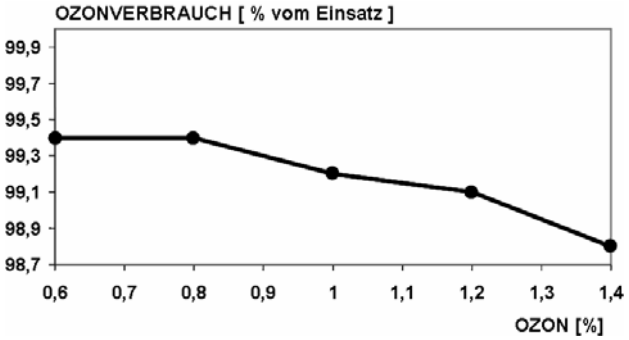

Abbildung 3. Ozonumsetzung versus Ozoneinsatz.

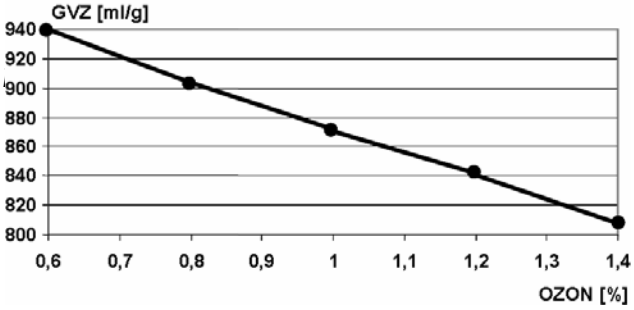

Abbildung 4. Abnahme der Zellstoffviskosität mit Erhöhung der Ozoneinsatzmenge. *Ausgangsstoff: ind. Fichtensulfitzellstoff, ungebleicht, Ausgangsviskosität 1092 mg*

In der abschließenden P_{NaOH}-Stufe betrug der Peroxideinsatz konstant 2 %. Mit steigendem Ozoneinsatz in der vorangegangenen Z-Stufe nahm der Peroxidverbrauch stetig ab und lag bei Ozoneinsätzen über 1 % unterhalb von 50 % (Abb. 5). Die Peroxidstufe erbrachte einen nochmaligen starken Kappazahlabbau (Abb. 6).

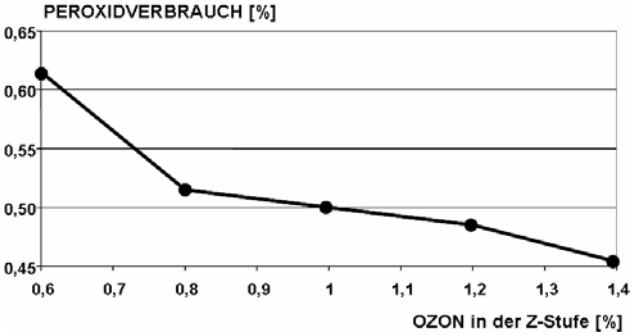

Abbildung 5. Peroxidverbrauch in der abschließenden P_{NaOH}-Stufe abhängig vom Ozoneinsatz.
P-Stufe: 1,5 % H_2O_2 , 1,5 % NaOH, 0,2 % $MgSO_4$, 70 °C, 240 min, 10 % Stoffdichte.

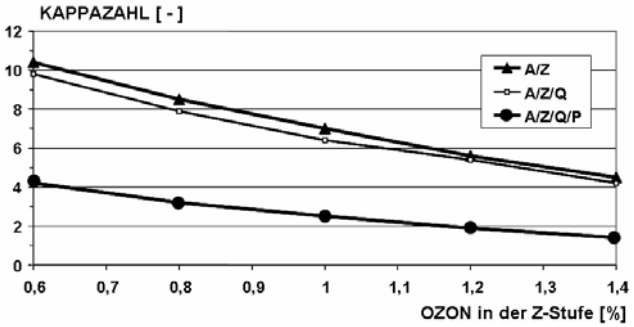

Abbildung 6. Delignifizierung in der abschließenden P_{NaOH}-Stufe abhängig vom Ozoneinsatz.
*P-Stufe: 1,5 % H_2O_2 , 1,5 % NaOH, 0,2 % $MgSO_4$, 70 °C, 240 min, 10 % Stoffdichte. Ausgangskappazahl 19,*1

Der in dieser Stufe erreichte hohe Delignifizierungsgrad von deutlich über 50 % kann darauf zurückgeführt werden, dass das Lignin in der Ozonstufe bereits stark oxidiert wird und so die aromatischen Ligninstrukturen aufgebrochen werden. Dadurch ist dann Wasserstoffperoxid in der Lage, das Lignin weiter abzubauen. Mit der Delignifizierung geht ein starker Weißgradanstieg um 20 bis 25 Weißgradpunkte einher (Abb. 7). Der deutliche Anstieg der Viskosität der ozongebleichten Zellstoffproben in der Q-P_{NaOH}-Endbleiche um fast 100 Einheiten (Abb. 8) kann darauf zurückgeführt werden, dass nach der Ozonbleiche an nicht mit Natriumborhydrid stabilisierten Zellstoffen eine zu niedrige Viskosität ermittelt wird, da ozonbehandelte Zellstoffe unten den stark alkalischen Bedingungen der Viskositätsmessung in Cuen einem DP-Abbau durch stattfindende β-Elimierungsreaktionen unterliegen [8]. Dieser fortgesetzte Abbau der Celluloseketten tritt normalerweise auch in einer der Ozonstufe folgenden alkalischen Bleichstufe auf. Durch eine reduzierende Alkaliextraktion mit Zusatz von $NaBH_4$ kann dieser Kettenlängeabbau wirkungsvoll unterdrückt werden [9]. Auch eine der Z-Stufe nachfolgende Behandlung mit Komplexbildner sowie der Zusatz von Magnesiumsulfat in der abschließenden P-Stufe stabilisieren die Cellulose gegen weitere Schädigung, indem auf den Celluloseabbau katalytisch wirkende Schwermetalle entfernt bzw. inaktiviert werden.

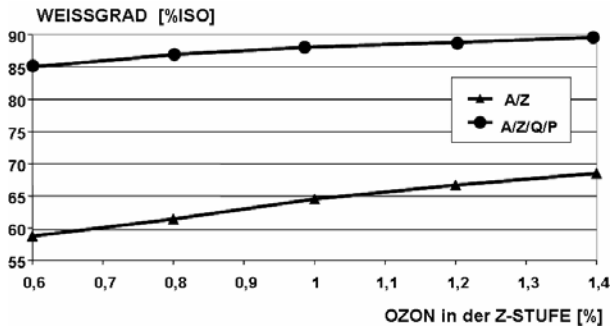

Abbildung 7. Weißgradanstieg in Z- und P-Stufe in Abhängigkeit vom Ozoneinsatz.
P-Stufe: 1,5 % H_2O_2 , 1,5 % NaOH, 0,2 % $MgSO_4$, 70 °C, 240 min, 10 % SD. Ausgangsweißgrad 58,3 % ISO

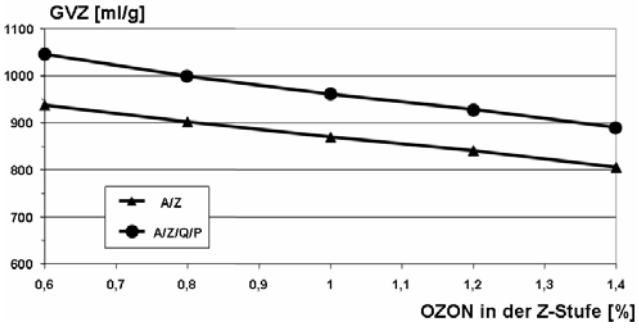

Abbildung 8. Viskosität nach Z- und P-Stufe in Abhängigkeit vom Ozoneinsatz.
P-Stufe: 1,5 % H_2O_2 , 1,5 % NaOH, 0,2 % $MgSO_4$, 70 °C, 240 min, 10 % SD. Ausgangsviskosität 1092 ml/g

Ein weiterer Grund dafür, dass der endgebleichten Zellstoff höhere Viskositätswerte aufweist, ist der hohe Feinstoffanteil saurer Sulfitzellstof-

fen, vor allem nach weit geführtem Aufschluss. Unter alkalischen Bleichbedingungen werden verstärkt Hemicellulosen und kurzkettige Cellulosefragmente aus dieser Feinstofffraktion gelöst, wodurch es zu einem Anstieg der Zellstoffviskosität kommt.
Basierend auf diesen Voruntersuchungen wurde die Bleiche anschließend mit größerer Zellstoffcharge (250 g) durchgeführt, um eine ausreichende Zellstoffmenge für die Bestimmung der Festigkeitseigenschaften des endgebleichten Zellstoffes zur Verfügung zu haben. Für die Bleiche in größerer Charge wurden 1,2 % Ozon eingesetzt. Wie im Vorversuch konnte anschließend mit 2 % H_2O_2 und einer Bleichdauer von 4 Stunden der Zielweißgrad von 90 % ISO erreicht werden. Trotz des hohen Ozoneinsatzes wurde die Zellstoffviskosität in dieser Bleichsequenz mit initialer Ozonbleichstufe nur um 160 ml/g reduziert und somit eine noch überraschend hohe Viskosität von 930 ml/g erhalten (Tabelle 2).

Ozonbehandlung als Zwischenstufe

Der Ozoneinsatz als Zwischenstufe innerhalb der Bleichsequenz, wie bei der Bleiche von Sulfatzellstoffen üblich, bietet auch bei der Bleiche von Sulfitzellstoffen gewisse Vorteile. Die Ozoneinsatzmenge kann gering gehalten werden, was die Anwendung der einfacheren MC-Bleichtechnologie zulässt und eine zu starke Faserschädigung vermeiden sollte. Nach initialer P_{MgO}-Bleichstufe ist eine Ozonbehandlung besonders vorteilhaft, weil diese Stufe gut in die Bleichsequenz eingepasst werden kann.
Ohnehin ist eine Absäuerung auf einen niedrigen pH-Wert erforderlich, um im Falle einer P_{NaOH}-Endbleichstufe in zu hoher Konzentration störende Magnesiumionen aus dem Zellstoff herauszuwaschen.
Des Weiteren wird die Wirksamkeit der nachfolgenden Peroxidbleiche durch die Ozonbehandlung stark erhöht, da nach Ozonierung gut durch Wasserstoffperoxid abbaubare Ligninstrukturen vorliegen. Insofern kann diese zwischengeschaltete Ozonbleiche auch als Aktivierungsstufe für die P-Endbleichstufe angesehen werden.
Wie zuvor bei Einsatz von Ozon in der ersten Bleichstufe wurden zunächst Vorversuche mit kleinen Zellstoffchargen von 50 g durchgeführt. Der Ozoneinsatz wurde dabei im Bereich von 0,4 bis 1,4 %/otro Zellstoff variiert. Trotz der niedrigen Kappazahl des für diese Versuchsserie eingesetzten, bereits industriell P_{MgO}-vorgebleichten Zellstoffes wurden auch sehr hohe Ozoneinsätze bis 1,4 % otro Zellstoff gewählt, um über diese Vorversuche auch gleich Aussagen zu bekommen, wie hoch der Ozoneinsatz sein muss, wenn diese Ozonbehandlung als letzte Bleichstufe angewendet wird. Aus der Abbildung 9 geht hervor, dass Ozon ein sehr effektives Delignifizierungsmittel für den P_{MgO} vorgebleichten Fichtensulfitzellstoff darstellt. Bereits 0,4 % Ozon sind ausreichend, um die Kappazahl von 7,6 auf unter 2 zu reduzieren. Mit Erhöhung des Ozoneinsatzes bis auf 0,6 % geht eine weitere Delignifizierung auf eine Kappazahl von unter 0,5 einher. Mit weiter gesteigertem Ozoneinsatz wird dann keine zusätzliche Reduzierung der Kappazahl mehr erreicht.

Tabelle 2. Bedingungen und Ergebnisse der Bleichsequenz mit initialer Ozonstufe.

Stufe	O_3 [%]	H_2O_2 [%]	NaOH [%]	Zeit [min]	Temp. [°C]	SD [%]	Weiß-grad [% ISO]	Kappa-zahl [-]	GVZ [ml/g]	CSB [kg/t]
-							58,3	19,1	1092	
A	-	-	-	10	50	3	58,6	17,7	1009	4,1
Z	1,2	-	-	30	50	40	66,2	5,5	850	18,7
Q	-	-	-	30	60	3	66,2	5,3	859	5,7
P_{NaOH}	-	2,0	1,5	240	70	10	90,0	2,0	934	28,8

Trotz stagnierenden Kappazahlabbaus steigt aber der Weißgrad mit Erhöhung der Ozoneinsatzmenge über 0,6% hinaus noch deutlich an. Zur Erzielung eines Weißgrades von 90 % ISO waren 1% Ozon erforderlich (Abb. 10). Wegen des niedrigeren Ligningehaltes wurde in der nach der P_{MgO}-Stufe durchgeführten Ozonbleiche, auch bei niedriger Ozoneinsatzmenge, eine wesentlich schlechtere Ozonumsetzung erzielt als in der Ozonbleiche des ungebleichten Zellstoffes (Abb. 11). Der niedrige Ligningehalt des vorgebleichten Zellstoffes ist auch als wesentliche Ursache für den starken Viskositätsabfall mit steigendem Ozoneinsatz zu sehen (Abb. 12).

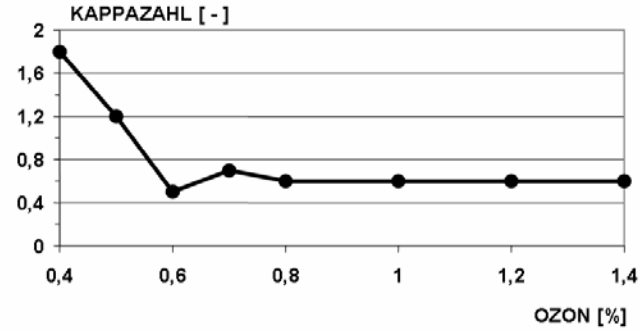

Abbildung 9. Delignifizierung in der Z-Stufe. *Ausgangsstoff: industrieller Fichtensulfitzellstoff, P_{MgO} -vorgebleicht, Kappazahl 7,6*

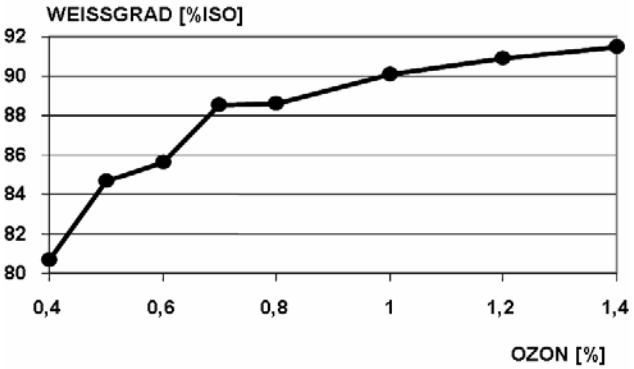

Abbildung 10. Bleicheffekt der Z-Stufe. *Ausgangsstoff: industrieller Fichtensulfitzellstoff, P_{MgO} -vorgebleicht, Weißgrad 73,9 % ISO*

Wird die Ozonbehandlung als Zwischenstufe eingesetzt, muss Ozon somit wesentlich vorsichtiger dosiert, um eine zu starke Faserschädigung zu vermeiden. Trotz des starken Viskositätsabfalls liegt die Viskosität des Zellstoffes bei moderatem Ozoneinsatz noch auf durchaus akzeptablem Niveau. Dies liegt an der hohen Viskosität des eingesetzten, P_{MgO}-vorgebleichten Zellstoffs. Dass dieser Zellstoff trotz sehr intensiver Delignifizierung in dieser initialen Bleichstufe sogar eine höhere Viskosität aufwies als der ungebleichte Zellstoff, ist auf die bereits oben angesprochene Feinstoffentfernung in einer alkalischen Bleichbehandlungsstufe zurückzuführen.

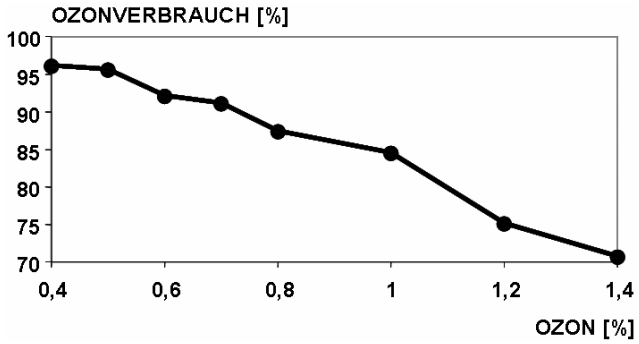

Abbildung 11. Ozonumsetzungsrate bei steigendem Ozoneinsatz. *Ausgangsstoff: industrieller Fichtensulfitzellstoff, P_{MgO} -vorgebleicht*

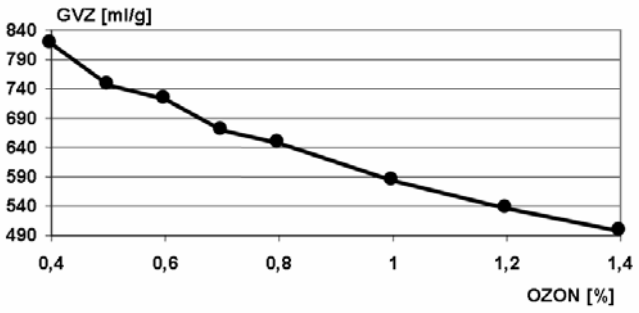

Abbildung 12. Viskositätsabbau in der Z-Stufe. *Ausgangsstoff: industrieller Fichtensulfitzellstoff, P_{MgO} -vorgebleicht, Viskosität 1122 ml/g*

Die Zellstoffe, die mit Ozoneinsatzmengen von 0,4 bis 0,8 % behandelt worden waren, wurden anschließend einer weiteren Bleichbehandlung unterzogen. Nach einer Komplexbildnerbehandlung erfolgte eine Peroxidendbleichstufe, die entweder mit NaOH oder mit MgO als Alkaliquelle durchgeführt wurde. Der Peroxideinsatz betrug 0,5 bzw. 1 %, wovon jeweils nur etwa 40% verbraucht wurden. Dabei erwies sich – wie erwartet – NaOH als das wesentlich wirksamere Bleichalkali. Aus der Abbildung 13 geht hervor, dass bei abschließender P_{NaOH}-Stufe mit 0,5 % H_2O_2 ein Ozoneinsatz von 0,4 % ausreichend war, während bei einer P_{MgO}-Endbleiche 0,6 % Ozon erforderlich waren, um den Zielweißgrad von 90% ISO mit 1 % H_2O_2-Einsatz zu erreichen. Die dabei auftretenden

Verluste an Zellstoffviskosität waren, unabhängig von der gewählten Alkaliquelle, sehr gering. Die Variante mit abschließender P_{NaOH}-Stufe lieferte aber wegen des geringeren Ozonbedarfs zur Erreichung des Zielweißgrades von 90 % ISO eine höhere Endviskosität. Die Verwendung von MgO als Bleichalkali in der letzten Bleichstufe hat den Vorteil, dass auch das in dieser Bleichstufe anfallende Bleichfiltrat über den Kochsäurekreislauf entsorgt werden könnte. Der erforderliche höhere Ozoneinsatz sowie die geringere Reinheit der P_{MgO}-endgebleichten Zellstoffproben sprechen allerdings gegen diese Variante, weshalb nachfolgend nur die Ergebnisse in der Tabelle 3 aufgeführt werden, die in der Bleichvariante mit abschließender P_{NaOH}-Stufe erhalten wurden.

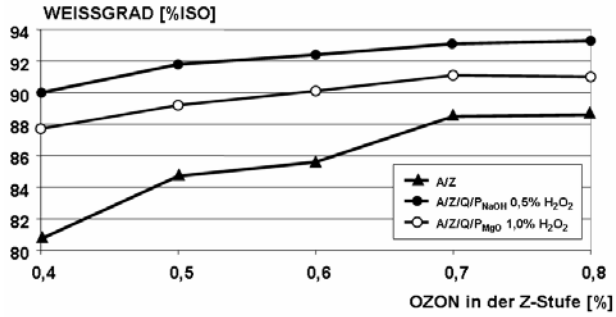

Abbildung 13. Einfluss der Ozoneinsatz auf den Endweißgrad nach P_{NaOH}- bzw. P_{MgO}-Stufe.
Ausgangsstoff: industrieller Fichtensulfitzellstoff, P_{MgO} - vorgebleicht, Weißgrad 73,9 ISO
P_{NaOH} : 1 % H_2O_2 , 0,8 % NaOH, 0,2 % $MgSO_4$, 70 °C, 120 min, 10 % Stoffdichte
P_{MgO} : 0,5 % H_2O_2 , 1,5 % MgO, 80 °C, 120 min, 10 % Stoffdichte

Tabelle 3. Bedingungen und Ergebnisse der Bleichsequenz mit zwischengeschalteter Ozonstufe.

Beim Vergleich der verschiedenen Bleichalternativen wurde daher auch nur diese Bleichvariante berücksichtigt. Der bei Bleiche in großer Charge erzielte höhere Endweißgrad von 91,5% ISO sowie die leicht erniedrigte Zellstoffviskosität sind auf eine effizientere Ozonbehandlung gegenüber dem Vorversuch zurückzuführen. Demzufolge kann festgestellt werden, dass ein Ozoneinsatz von 0,3 %/otro Zellstoff ausreichend gewesen wäre. Da die P_{NaOH}-Stufe in dieser Bleichsequenz unter sehr milden Bedingungen durchgeführt wurde, war die nicht über Filtratrückführung entsorgbare CSB-Fracht aus dieser Stufe deutlich niedriger als zuvor bei der Bleiche mit initialer Z-Stufe.

Ozonbehandlung als Endbleichstufe

Es ist prinzipiell denkbar, dass die Ozonbehandlung als abschließende Bleichstufe durchgeführt wird. Diese Variante sollte hier mitgetestet werden, obwohl es nicht sinnvoll erscheint, ein aggressives, wenig selektives Bleichchemikal am Ende einer Bleichsequenz einzusetzen, weil mit einem starken Kohlenhydratatabbau gerechnet werden muss. Auch die verstärkte Bildung von Carbonylgruppen und die dadurch hervorgerufene schlechte Weißgradstabilität sprechen gegen eine solche Vorgehensweise. Andererseits ist bekannt, dass ozongebleichte Zellstoffe über ein hohes Faserbindungsvermögen und somit über eine recht hohe Reißfestigkeit verfügen. Durch eine anschließende alkalische Behandlungsstufe wird dieses hohe Bindungsvermögen jedoch beträchtlich abgebaut, womit eine deutliche Abnahme der Reißfestigkeit einhergeht.

Stufe	O_3 [%]	H_2O_2 [%]	NaOH [%]	MgO [%]	Zeit [min]	Temp. [°C]	SD [%]	Weiß-grad [%ISO]	Kappa-zahl [-]	GVZ [ml/g]	CSB [kg/t]
P_{MgO}		*3*		*1,5*	*240*	*80*	*10*	*73,9*	*7,6*	*1122*	*~40*
A	-	-	-	-	10	50	3	77,4	7,1	1112	1,6
Z	0,4	-	-	-	-	50	41,5	85,3	1,2	783	18,3
Q	-	-	-	-	30	60	3	84,5	-	803	3,5
P_{NaOH}	-	0,5	0,8		120	70	10	91,5	0,5	781	10,4

Mit dem Fokus auf ein hohes Faserbindungsvermögen, einen sehr geringen Bedarf an Wasserstoffperoxid sowie eine nahezu abwasserfreie Bleiche könnte diese Ozonendbleichstufe aber unter bestimmten Umständen akzeptiert werden.

Die unter Kapitel 4 beschriebenen Vorversuche zur Ozonbehandlung eines bereits P_{MgO}-vorgebleichten Zellstoffes bestätigen, dass eine abschließende Z-Stufe zu einem starken Kohlenhydratabbau führen. Wenn der Ozonbehandlung keine weitere Bleichstufe nachfolgt, ist es erforderlich, den Zellstoff extrem weit zu delignifizieren, um über den Ligninabbau den geforderten Endweißgrad zu erreichen. Da dafür in den Vorversuchen ein Ozoneinsatz von 1% erforderlich war, wurde wiederum diese Ozoneinsatzmenge gewählt, um den Zellstoff in größerer Charge mit Ozon endzubleichen. Aufgrund besserer Ozonumsetzung in der Bleichreaktion wurde ein höherer Weißgrad gegenüber dem Vorversuch erhalten, wobei die Viskositätsverluste in noch einigermaßen akzeptablen Grenzen gehalten werden konnten (Tabelle 4).

Ozonfreie Referenzbleiche

Wegen der leichten Bleichbarkeit von Sulfitzellstoffen ist es, wie bereits zuvor erwähnt, nicht erforderlich, Ozon in einer peroxidbasierten TCF-Bleiche einzusetzen. Die TCF-Bleiche von Fichtensulfitzellstoff auf einen hohen Weißgrad nur unter Einsatz von Wasserstoffperoxid ist aber wesentlich erschwert, wenn die erste Bleichstufe unter Verwendung von technischem Magnesiumoxid durchgeführt wird.

In der Endbleiche muss daher ein erheblicher Aufwand betrieben werden, wenn ein hoher Endweißgrad erzielt werden soll.

In Vorversuchen wurde zunächst der erforderliche Peroxideinsatz nach vorangegangener A_Q-Stufe ermittelt. Zum Erreichen eines Weißgrades von annähernd 90 % ISO waren demnach unter den angewendeten Bleichbedingungen 3 % Wasserstoffperoxid erforderlich. In der Referenzbleiche mit größerer Charge wurde der Zielweißgrad jedoch nicht ganz erreicht (Tabelle 5). Hinsichtlich der hohen Einsatzmenge an Wasserstoffperoxid ist zu berücksichtigen, dass nur ein Viertel des Peroxideinsatzes verbraucht wurde und somit der Peroxideinsatz bei Rückführung des Bleichfiltrates drastisch reduziert werden könnte. Im Vergleich zu den Ozonbleichsequenzen lieferte die Referenzbleiche eine wesentlich höhere Viskosität, nachteilig ist aber die wesentlich höhere Restkappazahl. Auffällig ist der hohe Weißgradanstieg um fast 8 Punkte in der A_Q-Stufe. In zuvor an einem anderen Fichtensulfitzellstoff durchgeführten Bleichuntersuchungen konnte gezeigt werden, dass die Zugabe des Komplexbildners in dieser Absäuerungsstufe wegen der mit dem technischen MgO eingeschleppten Schwermetalle notwendig ist, um das in der nachfolgenden Stufe eingesetzte Wasserstoffperoxid zu stabilisieren und einen hohen Endweißgrad zu erreichen. Wegen der geringen Alkalinität einer solchen Bleichstufe und der starken Peroxidzersetzung, bedingt durch den hohen Schwermetallgehalt technischer MgO-Qualitäten, ist eine P_{MgO}-Stufe weit weniger effektiv als eine P_{NaOH}-Stufe, sowohl hinsichtlich Delignifizierung und Bleicheffekt als auch in Hinblick auf die Reinheit des endgebleichten Zellstoffs.

Tabelle 4. Bedingungen und Ergebnisse der Bleichsequenz mit Ozonbleichstufe.

Stufe	O_3 [%]	H_2O_2 [%]	NaOH [%]	MgO [%]	Zeit [min]	Temp. [°C]	SD [%]	Weißgrad [%ISO]	Kappazahl [-]	GVZ [ml/g]	CSB [kg/t]
P_{MgO}		*3*		*1,5*	*240*	*80*	*10*	*73,9*	*7,6*	*1122*	*~40*
A	-	-	-	-	10	50	3	77,4	7,1	1112	1,6
Z	1,0	-	-	-	-	50	41,4	90,7	0,6	611	41,4

Tabelle 5. Bedingungen und Ergebnisse der Referenzbleiche ohne Ozoneinsatz.

Stufe	O_3 [%]	H_2O_2 [%]	NaOH [%]	MgO [%]	Zeit [min]	Temp. [°C]	SD [%]	Weißgrad [%ISO]	Kappazahl [-]	GVZ [ml/g]	CSB [kg/t]
P_{MgO}		*3*		*1,50*	*240*	*80*	*10*	*73,9*	*7,6*	*1122*	*~40*
A_Q	-	-	-	-	30	60	3	81,6	7,1	1130	2,7
P_{NaOH}	-	3,0	2,25		240	70	10	89,2	5,0	1128	18,6

Abschließender Vergleich der Bleichalternativen

In der Tabelle 6 werden die durchgeführten Ozonbleichsequenzen in Bezug auf die erreichte spezifische Delignifizierung und die Selektivität gegenübergestellt. Bei dieser Betrachtungsweise schneidet die Bleichsequenz mit initialer Z-Stufe außerordentlich gut ab. Trotz des höchsten Ozoneinsatzes und der weitgehende Delignifizierung liefert die Bleichsequenz A-Z-Q-P_{NaOH} den geringsten Viskositätsverlust. Bei hoher spezifischer Delignifizierung (Δkappa/0,1 % O_3) wird die mit Abstand höchste Selektivität (Δkappa/Δvisk./100) erhalten.

In der Bleichsequenz mit Ozonzwischenstufe, P_{MgO}-A-Z-Q-P_{NaOH}, wurde aufgrund des geringen Ozoneinsatzes die höchste spezifische Delignifizierung erzielt, allerdings bei deutlich geringerer Selektivität. Eine höhere Selektivität ist durch Verringerung des Ozoneinsatzes erzielbar. Der hohe Endweißgrad bei Anwendung sehr milder Bedingungen in der P_{NaOH}-Stufe deutet darauf hin, dass auch eine geringere Ozoneinsatzmenge in dieser Bleichsequenz ausreicht.

Die Bleichvariante mit Ozonbehandlung als Endbleichstufe, P_{MgO}-A-Z, erfordert einen hohen Ozoneinsatz, wenn ein hoher Endweißgrad erreicht werden soll. Dadurch bedingt ist der Viskositätsabbau extrem hoch, was sowohl hinsichtlich der spezifischen Delignifizierung als auch der Selektivität zu den schlechtesten Werten führt. Diese Gegenüberstellung bestätigt nochmals, dass die Ozonbehandlung bevorzugt an Sulfitzellstoffen mit noch hohem Ligningehalt vorgenommen werden sollte. Dahingegen muss eine Ozonendbleichstufe aufgrund der geringen Effektivität und Selektivität mit großer Skepsis betrachtet werden.

Auch in Hinblick auf die Einsatzmengen an Bleichchemikalien schneidet die Bleichsequenz mit initialer Ozonstufe sehr gut ab, vor allem kann gegenüber der ozonfreien Referenz die höchste Einsparung an Wasserstoffperoxid erzielt werden (Tabelle 7). Auch wenn die Möglichkeit der Peroxideinsparung durch Filtratrecycling hier nicht berücksichtigt wird, kann festgestellt werden, dass eigentlich alle Ozonbleichsequenzen wegen des hohen Einsparpotentials an Wasserstoffperoxid und Bleichalkali unter Wirtschaftlichkeitsaspekten interessant sind.

Tabelle 6. Selektivität und spezifische Delignifizierung in den Z-Stufen.

Bleichsequenz	Ozon [%]	Δ visk.	Δ kappa	spez. Del. (Δ kappa/0,1 % O_3)	Selektivität (Δ kappa/Δ visc./100)
A-Z-Q-P_{NaOH}	1,2	242	13,6	1,1	5,6
P_{MgO}-A-Z-Q-P_{NaOH}	0,4	329	5,9	1,48	3,5
P_{MgO}-A-Z	1,0	511	6,5	0,65	1,3

Mit einer Einsparung von 2,5 % Wasserstoffperoxid durch Einsatz von 0,4 % Ozon weist die Bleichvariante mit Ozonzwischenstufe dabei den höchsten Substitutionsfaktor Ozon zu Wasserstoffperoxid auf.

Tabelle 7. Einsatzmengen an Bleichchemikalien.

Bleichsequenz	O_3 [%]	H_2O_2 [%]	NaOH [%]	MgO [%]
A-Z-Q-P_{NaOH}	1,2	2,0	1,5	-
P_{MgO}-A-Z-Q-P_{NaOH}	0,4	3,5	0,8	1,5
P_{MgO}-A-Z	1,0	3,0	-	1,5
P_{MgO}-A_Q-P_{NaOH}	-	6,0	2,25	1,5

Die Zusammenfassung der wichtigsten Bleichergebnisse in Tabelle 8 zeigt nochmals einige signifikante Unterschiede zwischen den getesteten Bleichalternativen auf.
Auch wenn in der ozonfreien Bleiche der Zielweißgrad von 90 % ISO nicht ganz erreicht wurde, kann dennoch festgestellt werden, dass es mit Anwendung aller Bleichsequenzen möglich ist, diesen Endweißgrad mit vertretbarem Bleichaufwand zu erreichen.
Hinsichtlich der thermischen Weißgradstabilität gibt es jedoch deutliche Unterschiede. Bei nachfolgender Peroxidbleiche zeigen ozongebleichte Zellstoffe eine gute thermische Weißgradstabilität. In beiden Fällen wurde lediglich eine Weißgradreversion um 2 Punkte festgestellt.
Eine deutlich stärkere thermische Vergilbung wurde nach der Referenzbleiche ohne Ozoneinsatz erhalten.
Die mit Abstand schlechteste thermische Weißgradstabilität wurde – wie erwartet - für die Bleiche mit Ozonendbleichstufe erhalten, da die durch die Reaktion des Ozons mit den Kohlenhydraten gebildeten Carbonylgruppen nicht durch anschließende Peroxidbleiche eliminiert wurden. Da die lichtinduzierte Weißgradreversion vor allem vom Restligningehalt des gebleichten Zellstoffes abhängt, kann davon ausgegangen werden, dass auch diesbezüglich die Bleichsequenzen mit initialer oder zwischengeschalteter Ozonstufe gegenüber der ozonfreien Bleichsequenz Vorteile liefern, denn diese weist die mit Abstand höchste Kappazahl auf.
Der wesentliche Vorteil der Referenzbleiche kann darin gesehen werden, dass sie sehr selektiv verläuft und somit praktische keine Viskositätsverluste auftreten. Demzufolge liegt die Viskosität deutlich höher als für die mit Ozoneinsatz gebleichten Zellstoffe.
Auch in Bezug auf die Höhe der aus den Bleichsequenzen resultierenden CSB-Frachten sind deutliche Differenzen feststellbar, die auch auf die Unterschiede in der Bleichausbeute schließen lassen. Der starke Ozonangriff auf die Kohlenhydrate in der Ozonstufe bei niedrigem Restligningehalt des Zellstoffes resultiert in hohen CSB-Belastungen, vor allem für die P_{MgO}-A-Z, aber auch für die P_{MgO}-A-Z-Q-P_{NaOH}-Sequenz.
Wenn man unterstellt, dass alle Bleichfiltrate aus den Bleichstufen, in denen keine Natronlauge als Bleichalkali eingesetzt wurde, restlos in den Kochereikreislauf zurückführbar sind, verbleibt als Restbelastung nur die CSB-Fracht aus den P_{NaOH}-Stufen.

Tabelle 8. Zusammenstellung wesentlicher Bleichergebnisse.

Bleichsequenz	Weißgrad [% ISO]	Weißgrad nach Vergilbung* [% ISO]	Kappa-zahl [-]	GVZ [ml/g]	CSB [kg/t]	CSB Restfracht [kg/t]
A-Z-Q-P_{NaOH}	90,0	88,2	2,0	934	57,3	28,8
P_{MgO}-A-Z-Q-P_{NaOH}	91,5	89,4	0,5	781	73,8	10,4
P_{MgO}-A-Z	90,7	81,0	0,6	611	83,0	0,0
P_{MgO}-A_Q-P_{NaOH}	89,2	83,6	5,0	1128	61,3	18,6

* 1 Stunden bei 100 °C und 100 % rel. Luftfeuchtigkeit (entspr. der früheren Tappi-Methode T 260)

Diese CSB-Restfracht ist nach einer initialer Ozonstufe besonders hoch, da wegen des hohen Ozoneinsatzes viel Lignin und auch viele Kohlenhydrate in der unter recht scharfen Bedingungen geführten Peroxidendbleichstufe in Lösung gehen. Die geringe Belastung für die Bleichsequenz mit Ozonzwischenstufe kann auf den viel geringeren Ozoneinsatz und den sehr schonenden Bedingungen der nachfolgenden P-Stufe zurückgeführt werden.

An den Ausgangsstoffen sowie den in größerer Charge gebleichten Zellstoffen wurden die papiertechnologischen Eigenschaften geprüft. Die Papierprüfung erfolgte jeweils an den ungemahlenen Zellstoffen sowie nach einer Mahldauer von 1, 2, 5, 10 und 20 min in einer Jokromühle. Aus den Abbildungen 14 und 15 wird ersichtlich, dass alle Bleichbehandlungen zu einer deutlichen Verringerung der statischen Festigkeiten führten. Der ungebleichte Zellstoff weist vor allem im niedrigen Mahlgradbereich ein deutlich besseres Bindungspotential auf. So liegt die Reißlänge des ungemahlenen Ausgangszellstoffes bereits über 5 km, während die gebleichten Proben Reißlängen von nur 2,4 bis 3,5 km im ungemahlenen Zustand aufweisen. Dies zeigt deutlich, dass das Bindungsvermögen der Fasern durch die Bleichbehandlung abnimmt, weil Feinstoff entfernt und sehr bindungsfähige, hemicellulosenreiche Wandschichten von der Oberfläche abgeschält werden. Nach Bleichbehandlung ist eine kurze, 2-5-minütige Mahlung erforderlich, um die Reißlänge des ungebleichten, ungemahlenen Zellstoffes zu erreichen.

In Bezug auf die Reißfestigkeit der gebleichten Zellstoffe ist eine klare Differenzierung möglich. Der ohne Ozoneinsatz gebleichte Referenzzellstoff sowie der mit Ozon in der ersten Bleichstufe gebleichte Zellstoff weisen die besten Reißlängen auf. Etwas niedriger liegt die Reißlänge des Zellstoffes, die unter Anwendung der Bleichsequenz P_{MgO}-A-Z-Q-P_{NaOH} gebleicht wurde. Der P_{MgO}-A-Z-gebleichte Zellstoff weist die niedrigste Reißfestigkeit auf. Die Staffelung der gebleichten Zellstoffe hinsichtlich der Reißfestigkeit steht im Einklang mit den entsprechenden Viskositätswerten. Allerdings hätte man aufgrund dieser Werte eine stärkere Differenzierung in der Reißfestigkeit erwarten können. Offensichtlich wird das Bindungspotential der Faseroberflächen durch Ozonbehandlung erhöht, wodurch die Faserschwächung teilweise kompensiert wird.

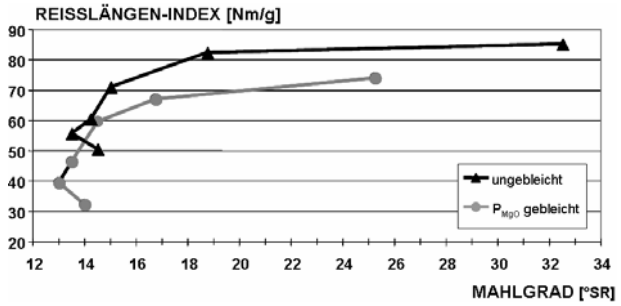

Abbildung 14. Reißfestigkeit der Ausgangsstoffe.

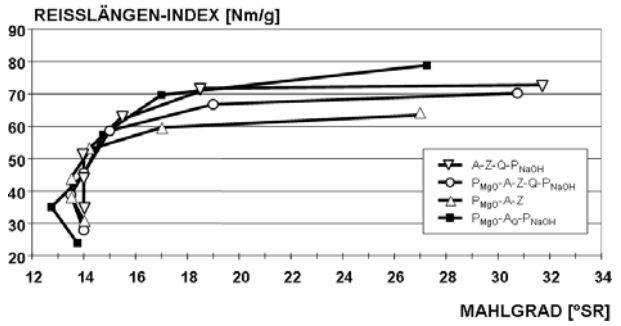

Abbildung 15. Reißfestigkeit der gebleichten Stoffe.

Eine entsprechende Differenzierung zwischen den unterschiedlich gebleichten Zellstoffen ist in Bezug auf die Durchreißfestigkeit nicht erkennbar. Alle Zellstoffe liegen in der Durchreißfestigkeit nahezu auf einheitlichem Niveau. Wegen des bereits angesprochenen Verlusts an Bindungsfähigkeit durch die Bleichbehandlung weisen der MgO-vorgebleichte Stoff und die endgebleichten Proben im niedrigen Mahlbereich gegenüber dem ungebleichtem Ausgangszellstoff eine niedriger Reißfestigkeit, aber andererseits eine höhere Durchreißfestigkeit auf. Mit zunehmender Mahlung tritt aber eine starke Angleichung ein (Abb. 16 und 17).

Erstaunlich gute Festigkeiten liefert die Bleichsequenz A-Z-Q-P_{NaOH}. Trotz hohen Ozoneinsatzes von 1,2 %/atro Zellstoff werden die Fasern offensichtlich nur im geringen Maße geschädigt, weil das eingesetzte Ozon ganz überwiegend mit dem Lignin reagiert. Wie

bereits die hohe Viskosität des Zellstoffes andeutete, wird die Cellulose daher nur wenig abgebaut. Ein weiterer Abbau der oxidierten, gegen eine nachfolgende Alkalibehandlung sensibilisierten Cellulose kann durch die zwischengeschaltete Komplexbildnerbehandlung und durch Zusatz von Magnesiumsulfat in der P_{NaOH}-Stufe vermieden werden.

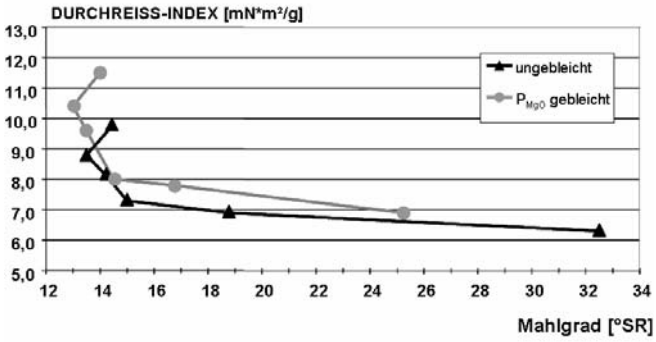

Abbildung 16. Durchreißfestigkeit der ungebleichten und des P_{MgO}- vorgebleichten Zellstoffs.

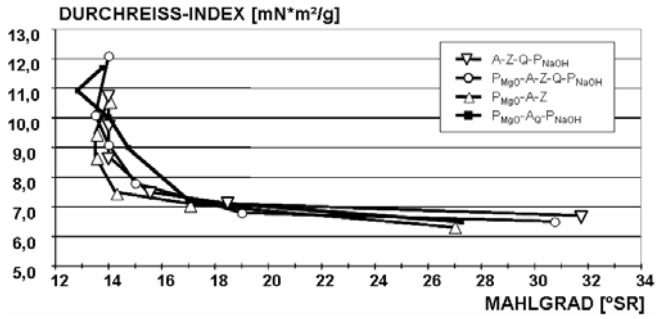

Abbildung 17. Durchreißfestigkeit der ungebleichten und des P_{MgO}-vorgebleichten Zellstoffs.

Bewertung/Schlussfolgerungen

Diese Untersuchungen belegen, dass der Einsatz von Ozon eine interessante Option darstellt, Fichtensulfitzellstoff auf hohe Weißgrade zu bleichen. Zwecks besserer Beurteilung der in dieser Untersuchung angewendeten Bleichvarianten werden deren Vor- und Nachteile in den nachfolgenden Tabellen 9-12 aufgelistet.

Die Frage, ob und an welcher Position Ozon innerhalb der Bleiche von Fichtensulfitzellstoff eingesetzt werden sollte, kann anhand dieser Untersuchungen natürlich nicht abschließend geklärt werden. Trotz des begrenzten Versuchsumfangs konnten jedoch wesentliche Stärken und Schwächen der verschiedenen Bleichsequenzen herausgearbeitet werden.

Tabelle 9. Vor- und Nachteile der Bleichsequenz mit initialer Ozonstufe, A-Z-P_{MgO}.

⊕	**Z-Stufe: hohe spez. Delignifizierung und Selektivität**
⊕	**geringer Bleichchemikalieneinsatz**
⊕	**geringe Bleichstufenanzahl**
⊕	**hohe Zellstofffestigkeit**
⊖	**hoher Ozoneinsatz, HC-Technologie erforderlich**
⊖	**geringe Flexibilität**
⊖	**relativ hohe CSB-Restbelastung**

Tabelle 10. Vor- und Nachteile der Bleichsequenz mit Ozonzwischenstufe, P_{MgO}-A-Z-Q-P_{NaOH}.

⊕	**geringer Ozoneinsatz, MC-Technologie anwendbar**
⊕	**sehr flexibel, hohe Bleichreserve (HYP-Verfahren)**
⊕	**sehr hohe Weißgrade erzielbar**
⊕	**sehr niedriger Restligningehalt**
⊖	**hohe Bleichstufenanzahl, hoher Investitionsaufwand**
⊖	**Ozonbleichstufe ziemlich unselektiv**
⊖	**verminderte Festigkeitseigenschaften**
⊖	**Integration der Z-Stufe in bezug auf Filtratführung problematisch**

Tabelle 11. Vor- und Nachteile der Bleichsequenz mit Ozonendbleichstufe, P_{MgO}-A-Z.

⊕	**geringe Bleichstufenanzahl**
⊕	**kein NaOH-Einsatz, geringe CSB-Restbelastung**
⊕	**Erhöhung der initialen Nassfestigkeit**
⊖	**hoher Ozoneinsatz, HC-Technologie erforderlich**
⊖	**geringe Flexibilität**
⊖	**geringe Ozonselektivität**
⊖	**starke Faserschädigung, geringe Zellstofffestigkeiten**
⊖	**geringe Weißgradstabilität**
⊖	**schlechte Schmutzpunktentfernung**

Tabelle 12. Vor- und Nachteile der Bleichsequenz ohne Ozonbleichstufe, P_{MgO}-AQ-P_{NaOH}.

⊕	**geringer DP-Abbau, gute Festigkeitseigenschaften**
⊕	**industriell etablierte Bleichsequenz, geringes Risiko**
⊖	**hoher Chemikalieneinsatz, hohe Betriebskosten**
⊖	**limitierter maximaler Weißgrad**
⊖	**hoher Restligningehalt, mäßige Weißgradstabilität**
⊖	**lange Bleichdauer**

Aufgrund der Fortschritte in der Ozonerzeugungstechnologie und der doch sehr positiven Ergebnisse bei Ozoneinsatz in der ersten oder zweiten Bleichstufe kann diese Untersuchung somit zumindest als Anreiz gesehen werden,

verstärkt über den Einsatz von Ozon auch für die Bleiche von Sulfitzellstoffen nachzudenken.
Bei der Bewertung der Bleichergebnisse muss allerdings berücksichtigt werden, dass die im Labor durchgeführte Ozonbleiche unter nahezu optimalen Bedingungen abläuft. Vor allem wird eine massive Faserschädigung dadurch vermieden, dass mit einem sehr gut aufgeflufften und damit sehr gut für das Ozongas zugänglichen Zellstoff gearbeitet wurde. Weiterhin wurde der Zellstoff nach jeder Bleichstufe gründlich mit deionisiertem Wasser gewaschen, so dass negative Effekte durch Filtratbelastung (carry over) vermieden wurden. Unter industriellen Bedingungen muss daher vor allem bei hohem Ozoneinsatz mit einem schlechteren Bleichergebnis gerechnet werden.
Unter diesem Aspekt erscheint es sinnvoll, mit niedrigem Ozoneinsatz zu arbeiten, weshalb die Ozonbleichvariante mit Ozonzwischenstufe wohl zu favorisieren ist. Diese Bleichsequenz ist zwar relativ aufwändig, weist aber eine Reihe interessanter Vorteile auf (Tab 10). Vor allem verfügt die Bleichsequenz P_{MgO}-A-Z-Q-P_{NaOH} über ein hohe Bleichreserve, die dazu genutzt werden kann, den Holzaufschluss bei höherer Kappazahl abzubrechen, um dadurch Zellstoffe mit besseren Festigkeitseigenschaften zu erzeugen, wie dies insbesondere bei Anwendung des HYP-Verfahrens der Fall ist [10].

Literatur

[1] H. Sixta (Editor) *Handbook of Pulp*, Wiley-VCH, Weinheim, 2006, Volume 2, Ozone Delignification, 777-853

[2] Soteland N., Bleaching of Chemical Pulps with Oxygen and Ozone. Pulp and Paper Magazine 74 (1974) 90-96

[3] Wang D. K-L., Patt R., Delignifizierung von Buchen- und Fichtensulfitzellstoffen unter Verwendung von Ozon. Das Papier 38 (1984), 245-254

[4] Patt R., Wang D. L.-K., Kordsachia O., Chlorfreie Bleiche von Sulfitzellstoffen. Das Papier 38 (1984), V7-V16

[5] Lindqvist B., Marklund A., Ozone Bleaching of Sulfite Pulps, Svensk Papperstidning (1984) 6, 54-64

[6] Soteland N., Carlberg G., Environmentally Acceptable Bleaching of Sulphite Pulp and Hardwood Kraft Pulp. Paperi ja Puu (1987) 832-838

[7] Patt R., Hamnann M., Kordsachia O., The Role of Ozone in Chemical Pulp Bleaching. Holzforschung 45 (1991), 87-92

[8] Godsay M.P., Pearce E.M., Pysico-Chemical Properties of Ozone Oxidized Kraft Pulps. TAPPI Oxygen, Ozone and Peroxide Bleaching Seminar, New Orleans, Proceeding (1984), 55-70

[9] Kordsachia, O., Oltmann E., Wang D.L.-K., Patt R., Untersuchungen zum Einsatz von Natriumborhydrid in der chlorfreien Zellstoffbleiche. Wochenblatt f. Papierfabrikation 118 (1990), 251-254

[10] Patt R., Kordsachia O, Geisenheiner A., Reinhard A., TCF-gebleichte Hochausbeute-Magnesiumbisulfitzellstoffe mit hohen Festigkeiten. IPW (2002) 32-38

Lenzinger Berichte, 86 (2006) 85-89

CRYSTALLINITY DETERMINATION OF NATIVE CELLULOSE – COMPARISON OF ANALYTICAL METHODS*

Thomas Röder[1], Johann Moosbauer[1], Mario Fasching[2], Andreas Bohn[3], Hans-Peter Fink[3], Thomas Baldinger[1], and Herbert Sixta[1]

[1]Department Zellstoff-Forschung, Lenzing AG, Werksstrasse 1, A-4860 Lenzing, Austria
Phone: (+43) 07672-701-3082; Fax: (+43) 07672-918-3082; E-mail: t.roeder@lenzing.com
[2]Kompetenzzentrum Holz GmbH, St.-Peter-Str. 25, A-4021 Linz, Austria
[3]Fraunhofer-Institute for Applied Polymer Research, Geiselbergstraße 69, D-14476 Potsdam-Golm, Germany

* This work was presented during the 9th European Workshop on Lignocellulosics and Pulp (EWLP) 28th-30th August, Vienna, Austria

The crystallinity of cellulose is one of the main structural parameters determining properties like accessibility and reactivity of cellulose. Native cellulose (e.g., wood, pulp, cotton, kenaf, bacteria cellulose) consists of the cellulose I, regenerated cellulose consists of the cellulose II modification.
WAXS (wide angle X-ray scattering) is the standard method for the determination of crystallinity of cellulose samples. This method was established by Hermans and Weidinger in 1949 [1].
Nowadays the information concerning crystallinity of cellulose I can be obtained by other methods as well, e.g. Fourier Transform (FT) Raman, FT-infrared (IR), or solid state ^{13}C-NMR (nuclear magnetic resonance) spectroscopy.
A matrix of cellulose I samples from different sources was investigated using the methods mentioned above. The results were compared with those of the standard WAXS method.

Keywords: *Raman, cellulose, pulp, crystallinity, NMR, WAXS, IR*

Introduction

Depending on the natural source (wood, cotton, bacteria cellulose) and on the manufacturing process the ratio of crystalline and amorphous regions in the cellulose can vary within a wide range. This ratio is an important parameter correlated with accessibility and reactivity of pulps.
In 1949 Hermans and Weidinger [1] published their procedure for crystallinity determination from WAXS data. Up to now quite a number of methods are available for the determination of cellulose crystallinity based on WAXS experiments [2-4]. Today WAXS is still used as the standard method. Nevertheless, WAXS is expensive, time-consuming, and needs well maintained equipment.
The information concerning crystallinity of cellulose can be obtained by other methods as well: solid state ^{13}C-NMR spectroscopy [5], IR spectroscopy [6], and Raman spectroscopy [7].

Experimental

Methods

WAXS measurements were done in symmetric transmission with a two-circle diffractometer D5000 (Fa. Bruker-AXS, Germany). Cu-K_α radiation (with Ge(111) as monochromator) was used (30 mA, 40 kV, 2theta with 4-104° in 0.2° steps). The scattering curves were corrected

concerning absorption, polarization, Compton, and parasitic scattering [3].
NMR experiments were performed on a Bruker 300 MHZ DPX spectrometer equipped with a 7 mm CP-MAS probehead. For ^{13}C CP-MAS experiments 1000 scans with 2k time domain data points were acquired at 26 °C using a contact time of 1 msec, a recycle delay of 3 sec, and a spinning rate of 4000 Hz. The high field peak of adamantan at 29.5 ppm was used for referencing. Prior to Fourier transformation a line broadening of 20 Hz was applied. Dry cellulose I samples were milled to pass a 10 mesh sieve and packed into a 7 mm zirconia rotor. The crystallinity index CrI was calculated from the C-4 region in the ^{13}C CP-MAS spectrum by using CrI = area 93 – 86.5 ppm / (area 93 -86.5 ppm + area 86.5 – 80.6 ppm).
The IR measurements were done in transmission mode (with KBr press technique) in a Bruker IFS 66 (4000 - 550 cm^{-1}, resolution 2 cm^{-1}). Cellulose samples were cut with a scissor (<0.5 mm length). 1.5 g KBr and 5 mg sample were levigated and four pellets of 300 mg were produced and measured [6].
FT-Raman measurements were done with a Bruker IFS66 with Raman module FRA106, Nd:YAG Laser 500 mW; Laser wavenumber 9394 cm^{-1} (1064 nm), liq. N2 cooled Ge-Detektor, 3500-100 cm^{-1}, resolution 4 cm^{-1}, 100 scans, four measurements of each sample. The range between 3500 and 100 cm^{-1} was used for the calibration. A special data pre-treatment was not necessary.
Cellulose fibers (cotton, ramie, cotton linters) were cut with a scissor (<0.5 mm length). 300 mg of the sample was pressed with 6t/cm for approximately 10 min.
Pulps in sheet form didn't need any sample preparation. Like the cut fibers, fluff pulps were pressed with 6t/cm for approximately 10 min.

Materials

Various pulps and samples from other cellulose sources (cotton, ramie, bacteria cellulose), as well as partly amorphous and amorphous (by milling) pulp were used.
Preparation of the milled samples was done with a centrifugal mill ZM100 (Fa. Retsch, Germany) equipped with a 1 mm sieve. The amorphous and the partially amorphous samples were made with a ball mill "Pulverisette 23" (Fa. Fritsch, Germany, equipped with a ZrO_2 refiner filling (grinding beaker with 15 mm ball)).

Results and discussion

WAXS data were used as standard for calibration and comparison. The degree of crystallinity x_c was determined by the method of Ruland-Vonk with the IAP software WAXS 7. Raman and IR data were calibrated with WAXS data.
In general the calibration of IR-data with WAXS showed a good correlation. The results of a former study and the used methods were published by Baldinger et al. [5]. Two different sample series were measured: (1) the old sample matrix from [5] and (2) a new sample matrix.

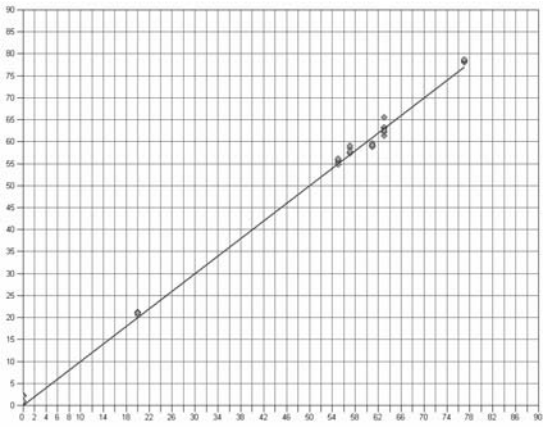

Figure 1. Calibration of Raman crystallinity – old matrix, cross validation: prediction versus reality, rank 4, R^2=99.67, RMSECV=1.39.

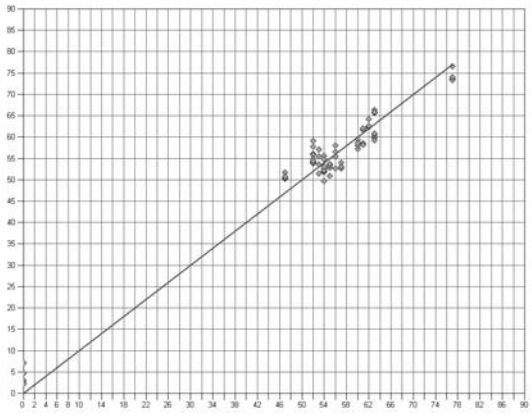

Figure 2a. Calibration of Raman crystallinity – both matrices together; without the milled Avicell and Mg-sul samples, cross validation: prediction versus reality, rank 5, R^2=95.94, RMSECV=2.94.

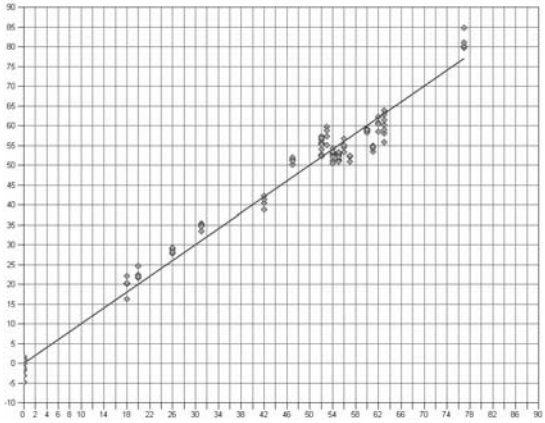

Figure 2b. Calibration of Raman crystallinity – both matrices together, cross validation: prediction versus reality, rank 6, R^2=96.92, RMSECV=3.44.

Table 1. Matrix of cellulose I samples.

Sample, old matrix [6]	x_C WAXS (Golm)	x_C IR	CrI NMR (Lenzing)	x_C Raman [%]		
	[%]	[%]	[%]	Fig.1	Fig. 2a	Fig. 2b
Beech Mg-sul, mi.	0	2		***0***	***0***	***0***
Avicell, mi.	20	19		***20***	(35)	***21***
Beech Mg-sul	55	54	46	***55***	***53***	***54***
Euca-PHK	57	56		***57***	***55***	***54***
Avicell	61	58		***60***	***62***	***59***
Cotton linters (CL)	63	68	63	***63***	***64***	***62***
Bacteria cellulose	63			***63***	***62***	***63***
CL hydrol.	77	76	78	***77***	***76***	***73***
Sample, new matrix						
Softwood PHK	52		48	62	***54***	***54***
Mg/Ca-sul	52		47	58	***54***	***55***
Paper grade pulp	47		47	59	***47***	***47***
Mg-sul	52		46	55	***53***	***52***
Bacteria cellulose	53			61	***53***	***54***
Mg-sul	54		46	56	***53***	***53***
CL	56		57	44	***56***	***57***
Ramie fiber	55		55	57	***54***	***53***
Cotton	54	56		46	***54***	***54***
CL	60		57	72	***59***	***59***
CL	62		56	71	***62***	***61***
mi. Mg-sul, 2 min	31			39	40	***33***
mi. Mg-sul, 4 min	26			33	36	***27***
mi. Mg-sul, 6 min	18			21	31	***19***
mi. Mg-sul, 1h	0			0	12	***0***
Softwood PHK	42		47	33	54	***42***

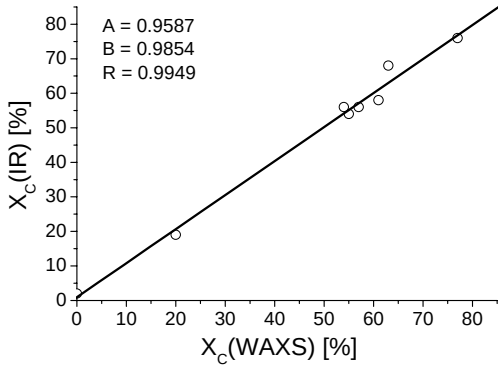

Figure 3a. X_c(IR) versus X_c(WAXS).

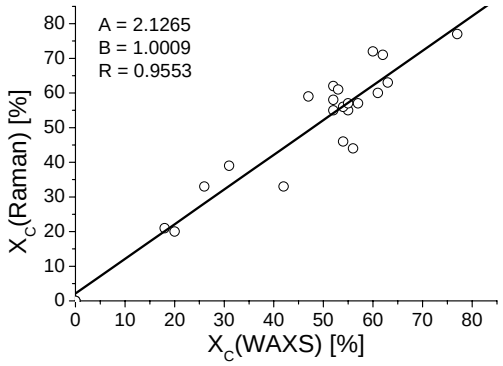

Figure 3b. X_c(Raman) versus X_c(WAXS), Fig.1.

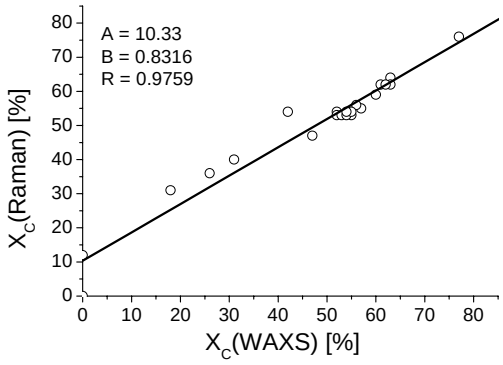

Figure 3c. X_c(Raman) versus X_c(WAXS), Fig. 2a.

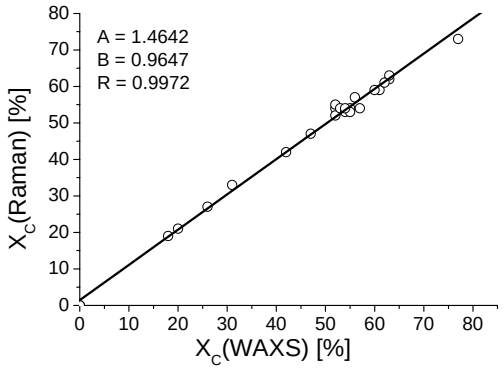

Figure 3d. X_c(Raman) versus X_c(WAXS), Fig. 2b.

One disadvantage of IR is the sensitivity to moisture content of the cellulose samples. Due to this, constant climatic room conditions have to be guarantied the year round. In contrast to IR the Raman method is insensitive concerning water in the sample.

In contrary to NMR WAXS crystallinity comprises also the crystalline areas on the surface. Therefore WAXS typically returns higher values than NMR. The published IR method [6] based on WAXS results, too. So the decision was made using WAXS as standard method for calibration. The best correlation was observed by calibrating the FT-Raman data with WAXS results. Two calibration sets were tested, the old one used for IR-calibration [6] and a new one with old and new samples. The correlation of the old data set (Figure 3b) from Raman and WAXS results is usable. Both together, the old and the new samples (without the milled samples), showed a little better correlation. By using all the samples for calibration, an excellent correlation was found. Figures 1, 2a, and 2b show the result of calibrations. In Figures 3a-3d the correlation of WAXS versus IR (3a) or Raman (3b-3d) crystallinity is shown. Especially for pure cellulose samples like pulp the calibration works well. Difficulties could be observed by analyzing natural fibres (ramie, cotton) without any pre-treatment or extraction step before the measurement. In this case natural impurities can interfere the crystallinity analysis of pure cellulose. To minimize this effect an extraction of resins is recommended. Within the analyzed sample matrix an extraction step was done for those samples before the measurement.

Conclusions

In this study, common spectroscopic methods for crystallinity determination of cellulose I were evaluated and compared with the classical WAXS method. The best correlation was found by using FT-Raman

spectroscopy (Figure 3d). An easy sample preparation, low measuring time, and a rugged calibration are additional benefits of this method. Therefore the use of FT-Raman spectroscopy (calibrated with WAXS) is the fastest, cheapest, and best method to determine the crystallinity of cellulose I in larger sample quantities, e.g. routine analysis.

Acknowledgement

We thank H. Weber and T. Lange (Kplus) for helpful discussions.

References

[1] P. H. Hermans, A. Weidinger. X-ray studies on the crystallinity of cellulose, *J. Polymer Sci.* 4 (1949) 135-144.

[2] W. Ruland. X-ray determination of crystallinity and diffuse disorder scattering, Acta Crystallogr. 14 (1961) 1180-1185.

[3] H.-P. Fink, D. Fanter, and B. Philipp. Wide angle X-ray study of the supermolecular structure at the cellulose I – cellulose II phase transition, Acta Polym. 36 (1985) 1-8.

[4] H.-P. Fink and E. Walenta, X-ray Diffraction Investigations of Cellulose Supermolecular Structure at Processing, Das Papier 12 (1994) 739-748.

[5] W.-D. Herzog, M. Messerschmidt. NMR-Spektroskopie für Anwender, VCH Verlagsgesellschaft, Weinheim, New York, Basel, Cambridge, Tokyo (1995).

[6] T. Baldinger, J. Moosbauer, H. Sixta. Supermolecular structure of cellulosic materials by Fourier Transform Infrared Spectroscopy (FT-IR) calibrated by WAXS and 13 C NMR, Lenzing Berichte, 79 (2000) 15 - 17.

[7] K. Schenzel, S. Fischer, and E. Brendler. New method for determining the degree of cellulose I crystallinity by means of FT Raman spectroscopy, Cellulose 12 (2005) 223-231.

Lenzinger Berichte, 86 (2006) 90-95

A NOVEL DESTRUCTIVE APPROACH FOR 3D PAPER STRUCTURE ANALYSIS

M. Wiltsche[1], M. Donoser[2], and W. Bauer[1]

[1] Institute for Paper, Pulp and Fiber Technology, Graz University of Technology
Kopernikusgasse 24/II, 8010 Graz, Austria
Tel. +43/316/873-7514, Fax +43/316/873-8010, mario.wiltsche@TUGraz.at

[2] Institute for Computer Graphics and Vision, Graz University of Technology
Inffeldgasse 16/II, 8010 Graz, Austria
Tel. +43/316/873-5043, Fax +43/316/873-8010, michael.donoser@TUGraz.at

This paper introduces a new concept for digitization and analysis of the three dimensional paper structure, based on a fully automated microtomy process and light microscopy combined with advanced image analysis algorithms. The concept offers both, a high spatial resolution and a significantly larger sample size than conventional SEM techniques. The concept for digitization is capable of obtaining 3D paper structure data for sample areas in the range of several square millimeters within hours. Application of this concept on 3D analysis of the coating layer and the segmentation of single fibers is presented.

Keywords: *3D, paper structure, destructive, digitization, computer vision*

Introduction

Paper is a heterogeneous material, which consists mainly of fibers, fiber fragments, filler pigments, and in the case of coated papers one or more coating layers. Physical paper properties are strongly influenced by the spatial distribution of these raw materials in the paper sheet.

For coated papers – additionally to detailed description of 3D-microstructure of the base paper – in depth knowledge on the spatial distribution of the coating layer applied to the base paper is of special interest, since variations in this local coating layer thickness are believed to decisively influence print quality. A detailed analysis of the spatial structure of the coating layer also allows a better insight into the interrelations between coating application type, coating process parameters, and coated paper quality parameters.

In the analysis of fibrous networks the possibility of accessing single fibers, and determining their position and orientation within the paper sample, will, for example, allow the 3D analysis of fiber orientation, calculation of spatial mass-distribution, and mechanical behaviour of fiber networks or determination of bonding areas between fibers.

The long term goal of our research work is a complete characterization of the 3D paper structure using light optical measurements combined with advanced image analysis algorithms.

In the following section “Related Research” a brief review of research in the field of 3D paper structure analysis is given. The main challenge is to digitize paper structure with high spatial resolution, sufficient sample sizes and with adequate investment and operating costs.

Our concept for digitizing the 3D paper structure, based on a fully automated microtomy process and light microscopy, is introduced in section “Novel Concept for Digitization”. It combines sufficient spatial resolution and significantly larger sample sizes than conventional light microscopical

or SEM techniques. Image analysis algorithms needed for creation of an accurate, digital 3D representation are also presented. The created data set constitutes the basis for many different applications for extracting characteristics of the 3D paper structure.
Initial applications, which prove the usefulness of the novel concept are presented in section “Results and Discussion”.

Related Research

Furthered by the rapid advances in new measurement techniques in the field of material and medical sciences, significant research activities have been focused on the development of technologies that extract spatial structures of fibers, filler pigments and coating layer to build a three dimensional model of a paper sheet.
Some severely conflicting requirements have to be fulfilled in order to achieve this task:

- High spatial resolution is necessary to be able to detect all main paper components and important structure details. The diameter of the fibers is about 10 µm to 30 µm, their length is in the magnitude of millimeters, the particle size of fillers and coating pigments is below 1 µm. Given the size of these components a resolution at least in the micron range is required.
- Sufficient sample size to get reliable and statistically meaningful results is needed. For every square centimeter of a typical sheet of paper the total number of fibers is 10000 to 100000 [1]. The minimum sample size is determined by the scale of paper non-uniformity itself, therefore at least some square millimeters and ideally one square centimeter should be analyzed.
- The technique should be applicable in “day-to-day” research on commercial paper samples. Hence, measurement time should be at least in the order of hours. Investment and operating costs should also be moderate.

In principle, two main approaches are applied in the analysis of 3D paper structure - non destructive and destructive methods.
Non destructive methods – like confocal laser scanning microscopy (CLSM), microtomography, magnetic resonance imaging (MRI), or ultrasonic microscopy – do not cause any changes in the sample structure during the digitization process. This, of course would be the preferred method, since the analyzed samples would be available for further testing. First applications of CLSM on paper were reported in the late-80s [2]. Limitations of CLSM are the restricted penetration depth and the small sized field of view. X-ray microtomography has also been commonly used in paper research in recent years. There are two different ways of digitizing 3D structures based on microtomography – beam absorption [3] and phase contrast [4]. Present commercial CT scanners based on beam absorption have the disadvantage of a too low spatial resolution and a too low contrast in the obtained images for detailed 3D paper structure analysis [5,6]. Further development will most likely make them the instruments of choice in the near future. Phase contrast based microtomy yields images with impressive spatial resolution and detail [5-7]. Due to the requirement of coherent high-energy synchrotron radiation this approach however is not yet feasible for day-to-day paper analysis. Magnetic resonance imaging (MRI) [8] and ultrasonic microscopy [9] are further potential non-destructive methods, which presently still have the shortcoming of either a too low resolution or a limited penetration depth.
The most commonly used destructive methods for analyzing 3D paper structures are sheet splitting [10,11] and serial sectioning [12,13]. Splitting techniques offer the advantage of rather large sample sizes, but they have the shortcoming, that the splitting process itself considerably influences the analysis results. Serial sectioning via microtome cuts offers a high resolution and good image quality for further analy-

sis, but the method is too time-consuming to make day-to-day application feasible.

Novel Concept for Digitization

None of the current methods presented in the previous section is capable of fulfill all of the three aforementioned requirements. Therefore, a new approach based on automated microtomy and serial sectioning combined with light optical microscopy was developed and a prototype was built. The concept is capable of automatically obtaining 3D paper structure data for sample areas in the range of several square millimeters in the reasonable time span of a few hours at a maximum resolution of $0.16 \times 0.16 \times 0.50\ \mu m^3$. A more detailed description of this technique is given in [14].

Microtomy is a widespread technique with applications in medicine, biology, and material sciences in which uniformly thin sections are cut of embedded specimens for detailed microscopic examination. In order to support internal structures of the specimen during cutting, the specimen has to be embedded in a suitable material. The material used is epoxy resin or glycol methacrylate. Sample preparation follows standard embedding procedures in preparation of paper samples – see for instance [15].

Our prototype comprises a light-optical microscope which is attached to the microtome, see Figure 1. The microscope is fixed on a stage, which is placed in front of the microtome and can be moved with high accuracy in all three dimensions. The system is equipped with a CCD camera for digital imaging.

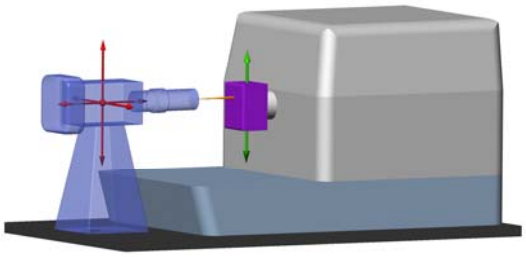

Figure 1. Automated rotary microtome design.

The microtome, light source, CCD camera, and stage are controlled via a PC interface. Repeatedly, slices are cut off the embedded paper sample and the surface is scanned fully automatic. Thus, the digitization is done on the non distorted surface and thereby high accuracy between adjacent slices can be guaranteed.

The field-of-view covered by a single image does not reach the required sample size of at least some square millimeters. Thus, it is necessary to acquire a sequence of adjacent images covering the entire region of interest of the sample, which is possible due to the three-dimensionally moveable microscope. An image analysis algorithm called “Stitching” connects these adjacent images to one composite image. In order to ensure that the assembling can be done properly adjacent images have to overlap each other.

Another problem to cope with is the displacement between subsequent slices due to the limited sample positioning accuracy of the rotary microtome after each cut. These displacements are corrected by means of the second pre-processing step called “Aligning”. Stitching and aligning are described in more detail in [16].

After these initial processing steps a digital 3D representation of the paper sample in terms of a sequence of images is obtained. Figure 2 shows a small cut-out of a digitized 3D woodfree coated paper, which is then subjected to advanced image analysis.

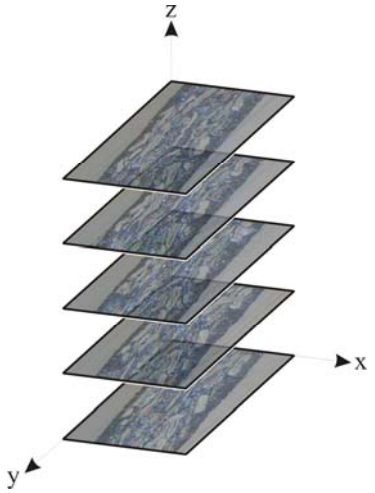

Figure 2. Cut-out of 3D woodfree coated paper structure.

Results and Discussion

Three dimensional analysis of the coating layer

As a first example of possible applications the analysis of the 3D coating layer formation is presented. Image analysis software was developed to automatically detect the coating layer. Segmentation of the coating layer is realized by a 3D color segmentation process in the RGB color space instead of a threshold based algorithm, see [14,17] for a detailed description. The algorithm is three-dimensional, so the decision whether a pixel is classified as coating or not, is based on information coming from the current and also from the adjacent images. Thus, the algorithm delivers both, detailed and robust coating layer recognition.

Figure 3 shows a slice image and the corresponding segmentation result of the 3D color segmentation approach. The coating layer can be identified as a homogeneously colored region at the surface of the coated paper sample in the slice images, see Figure 3(a).

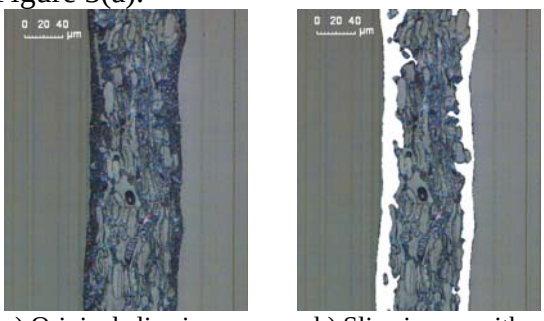

a) Original slice image b) Slice image with segmentation result

Figure 3. Typical result of coating layer segmentation.

Standard parameters like average paper and coating thickness, homogeneity of the coating layer and the portion of the coating layer to the entire paper volume are calculated. In the same step information on the base paper topography under the coating layer is obtained.

Various kinds of interactive 3D visualizations were developed, in order to allow the user to get a better "feel" for the results.

Figure 4 shows the reconstructed surface of a mechanical coated sample. The circular defects are presumably caused due to air bubbles in the curtain coating application.

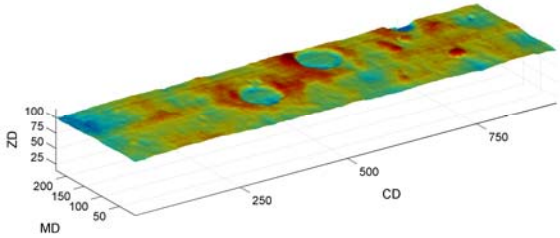

Figure 4. Circular defects in a mechanical coated sample.

Figure 5 shows exemplary results of the local top side coating thickness for a woodfree coated, calendered sample.

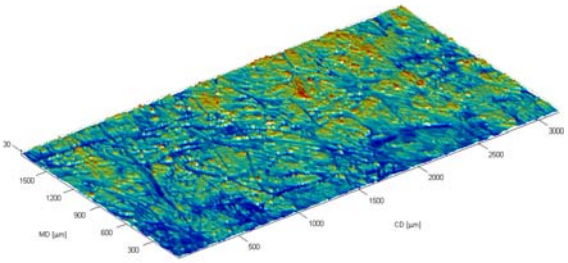

Figure 5. 3D visualization of local top side coating thickness for a woodfree coated, calendered sample.

It can be seen, that fibers near the surface of the base paper cause impressions in the coating layer, thus affecting the local coating thickness. In contrast, local gaps in the base paper surface cause increased values for the local coating thickness.

Three dimensional analysis of the fiber network

Current research focuses on the analysis of the 3D fiber network, based on the digital paper structure data. Due to the complex three-dimensional network of fibers enhanced image analysis methods are required. Algorithms for detection of single fibers in the network and their tracking through the 3D paper structure are currently under development, see [18].

Figure 6 shows a slice image of a kraft paper sample with automatically detected fibers, which are identified as homogene-

ously bright-coloured regions with dark boundaries.

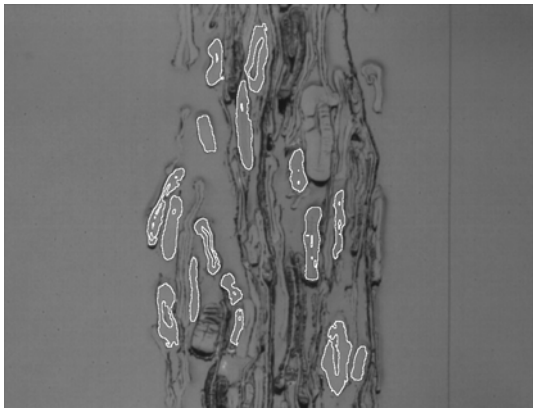

Figure 6. Slice image with automatically detected fibers in a kraft paper sample.

Figure 7 shows 3D visualization of a segmented fiber extracted from a digitized kraft paper sample.

Figure 7. 3D visualization of a detected individual fiber in a kraft paper sample.

Conclusions and Outlook

The concept of automated microtomy has proved to be a feasible concept to obtain digitized 3D paper structure information for sample areas in the range of several square millimeters in a comparatively fast way at high resolution.

First applications of the developed spatial coating layer formation analysis method on various coated paper samples were successfully validated against several other methods and showed the potential of this analysis routine for future applications in the field of coating research [19].

Besides spatial coating layer formation analysis the presented configuration opens a wide range of future research activities, with the main focus being the development of methods for detailed fiber network analysis. From today's point of view, application of the developed methods on various fibrous materials like non-wovens or textiles is promising.

The assessment of fiber transverse dimensions also allow additional insights into the morphology of fibers in pulp samples

Acknowledgements

The authors gratefully acknowledge financial support of Austrian Research Promotion Agency Ltd. (FFG) and from Mondi Business Paper Austria, Mondi Packaging Frantschach, M-Real Hallein, Norske Skog Bruck GmbH, Sappi Gratkorn GmbH, SCA Graphic Laakirchen AG, UPM Steyrermühl and Voith Paper.

References

[1] E. Retulainen, K. Niskanen, and N. Nilsen. Fibers and bonds. In Paper physics, Papermaking Science and Technology, page 59. Fapet Oy, 1998. book 16.

[2] H. Nanko and J. Ohsawa. Mechanisms of fibre bond formation. In Fundamentals of Papermaking, Transactions of the 9th Fundamental Research Symposium, pages 783–830. The Pulp and Paper Fundamental Research Society, 1989.

[3] A. Goel, M. Tzanakakis, S. Huang, S. Ramaswamy, D. Choi, and B.V. Ramarao. Characterization of the three-dimensional structure of paper using x-ray microtomography. In TAPPI Engineering Conference, Atlanta, 2000. TAPPI Press Atlanta.

[4] E.J. Samuelson, P.J. Houen, Ø.W. Gregersen, T. Helle, and C. Raven. Three-dimensional imaging of paper by use of synchrotron x-ray microtomography. In TAPPI International Paper Physics Conference, pages 307–312, San Diego, USA, 1999. TAPPI Press Atlanta.

[5] R. Holmstad, S. Ramaswamy, A. Goel, Ø.W. Gregersen, and B.V. Ramarao. Comparison of 3D structural characteristics of high and low resolution x-ray microtomographic images of paper and board. In Pre-

prints of International Paper Physics Conference, pages 65–69, Victoria, British Columbia, Canada, 2003.

[6] M.A. Knackstedt, C.H. Arns, R. Holmstad, C. Antoine, and Ø.W. Gregersen. Characterisation of 3D structure and transport properties of paper from tomographic images. In Proceedings of the 2004 Progress in Paper Physics Seminar, pages 64–66, Trondheim, Norway, 2004. NTNU, PFI and Tappi Paper Physics Committee.

[7] R. Holmstad, A. Goel, C.H. Arns, M.A. Knackstedt, and Ø.W. Gregersen. Effect of papermaking variables on the detailed 3D paper structure assessed by X-ray microtomography. In Proceedings of the 2004 Progress in Paper Physics Seminar, pages 67–69, Trondheim, Norway, 2004. NTNU, PFI and Tappi Paper Physics Committee.

[8] M.J. Lehmann, E.H. Hardy, J. Meyer, and G. Kasper. Bestimmung der Faserstruktur und Packungsdichteverteilung in Tiefenfiltermedien mittels MRI. Chemie Ingenieur Technik, 75:1283–1286, 2003.

[9] A. Fenster and D.B. Downey. 3-D ultrasound imaging: A review. IEEE Engineering in Medicine and Biology, 15(6):41–51, 1996.

[10] A.-L. Erkkilä, P. Pakarinen, and M. Odell. Sheet forming studies using layered orientation analysis. Pulp & Paper Canada, 99(1):81–85, 1998.

[11] U. Knotzer. Image analysis evaluation of paper structure in z-direction. PhD thesis, University of Technology Graz, 2002.

[12] M. Aronsson. On 3D Fibre Measurements of Digitized Paper. PhD thesis, Swedish University of Agricultural Sciences Uppsala, 2002.

[13] M. Hasuike, T. Kawasaki, and K. Murakami. Evaluation method of 3-d geometric structure of paper sheet. Journal of Pulp and Paper Science, 18(3):J114-J120, May 1992.

[14] M. Wiltsche, M. Donoser, W. Bauer, and H. Bischof, „A New Slice-Based Concept for 3D Paper Structure Analysis Applied to Spatial Coating Layer Formation", Advances in Paper Science and Technology. Transactions of the 13th Fundamental Research Symposium held in Cambridge, p. 853-899. The Pulp and Paper Fundamental Research Society, 2005.

[15] A.R. Dickson. The quantitative microscopic analysis of paper cross-sections: sample preparation effects. Appita Journal, 53(5):362–366, 2000.

[16] M. Donoser, M. Wiltsche, H. Bischof. A New Automated Microtomy Concept for 3D Paper Structure Analysis. In: Proceedings of 9th IAPR Conference on Machine Vision Applications, 2005, p. 76-79, Tsukuba Science City (Japan).

[17] M. Donoser, M. Wiltsche, H. Bischof, and W. Bauer. Paper Coating Layer Analysis Based on Computer Vision Methods. In: Proceedings of 7th International Conference on Quality Control by Artificial Vision, 2005, p. 39-44, Nagoya, Aichi (Japan).

[18] M. Donoser and H. Bischof. Efficient Maximally Stable Extremal Region (MSER) Tracking. Accepted for publication in IEEE Computer Society Conference on Computer Vision and Pattern Recognition 2006, New York (USA).

[19] M. Wiltsche, M. Donoser, and W. Bauer. Coating Application Method and Calendering Influence on the Spatial Coating Layer Formation Obtained by an Automated Serial Sectioning Method. In: Proceedings of 9th TAPPI Advanced Coating Fundamentals Symposium, 2006, p. 413-425, Turku (Finland).

Lenzinger Berichte, 86 (2006) 96-105

A REVIEW OF IMAGE ANALYSIS BASED METHODS TO EVALUATE FIBER PROPERTIES

Ulrich Hirn and Wolfgang Bauer

Institute for Paper, Pulp and Fiber Technology, Graz University of Technology
Kopernikusgasse 24/II, 8010 Graz, Austria. Tel. +43/316/873-7097, ulrich.hirn@TUGraz.at

This review focuses on fiber analysis methods, where the fibers are carried in suspension. They are photographed in a flow cell and their properties are evaluated by digital image analysis.
Three fields of fiber analysis are covered: Fiber morphology, pulp surface chemistry, and chemically induced swelling respectively dissolving behaviour of pulp.
For fiber morphology commercial analyzers were compared. On an absolute level the measurement differences between the analyzers varied from 15% to 40%, for some morphological parameters up to 70%. Still fiber length, width, and curl results are highly correlated, so relative comparison is possible.
An increasing number of publications have recently been devoted to image analysis based evaluation of surface chemistry respectively chemically induced fiber swelling and dissolving. Considering that research effort it can be expected, that numerous innovations in both fields commercial fiber analyzers as well as new machine vision based fiber analysis techniques, can be expected in the next years.

Keywords: *fiber analysis, flow cell, fiber morphology, machine vision.*

Introduction

The rapid development of digital image analysis technology within the last years has lead to a multitude of new applications in the field of fiber assessment. This paper gives a review of analysis methods with special emphasis put on the following:

- Flow cell based methods. That means that the fibers are measured in suspension, the fiber suspension is pumped through a transparent flow cell where the fibers are photographed.
- Application of image analysis. The review focuses on methods applying machine vision to characterize fibers.
- Only methods for fibers in a size range up to a few millimeters of length and 100 µm of width are considered. So the focus lies on pulp analysis, but some methods can also be used for other fiber types.

A Flow cell combined with image analysis is an efficient concept for fiber characterization because the measurement can be carried out in a fully automated manner. Provided that hard- and software are stable enough, such analyzers can be used for online process control, e.g. in the pulp industry. This is the main motivation for the considerable research effort that has taken place in this area within the last years.
In the following the focus has been set on three different aspects of fiber analysis:

- Fiber morphology
- Pulp surface chemistry
- Chemically induced pulp fiber swelling and dissolving.

Fiber Morphology

This section first gives an overview of the fiber properties which are commonly summarized under the term fiber morphology. Then six commercially available fiber morphology analyzers are discussed in detail. At the end of this section a quantitative comparison of measurements from the various analyzers as well as repeatability issues are treated.

An overview of fiber morphology features

The morphology, i.e. the structural appearance, of fibers is commonly described by five parameters: length, width, coarseness, kink, and curl. Fiber length and width are common features which are fairly straightforward to implement for image analysis [8,14,27]. Fiber coarseness is defined as the fiber mass per unit length, usually in microgram per meter fiber length. It is closely related to the fiber wall thickness of tube shaped fibers like wood. Coarseness is normally determined by producing a fiber suspension with well defined solids content and measuring the cumulative fiber length in a defined volume of this suspension.

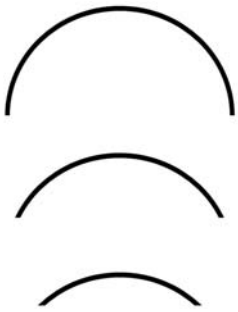

Figure 1. Fibers with different curl but same curvature [11].

Please note, that the arithmetic mean may be a bad measure to characterize a population of fibers, especially when the multitude of elements is small (as it is the case for e.g. pulp). Then the mean value is merely determined by the amount of small particles in the sample. For that reason often the length weighted mean is recommended [3].

Fiber kink and fiber curl provide information about the bending of the fiber. Curl describes the degree of non-straightness of a fiber, it gives no information if a fiber bends gradually or abruptly. A multitude of different mathematical definitions for curl is used [11,12,16,22,28]. The commercial pulp analyzers use varying definitions for curl.

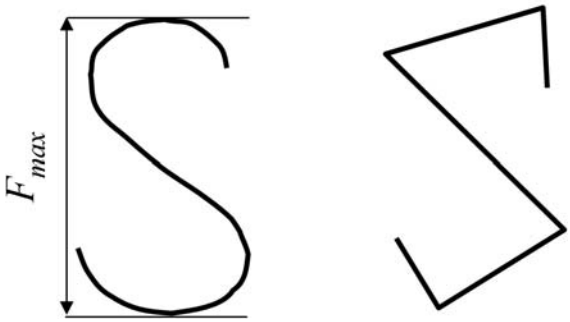

Figure 2. Fibers with different kink but the same curl [11].

Although it is reported that the various definitions for curl are correlated [22] the measurement results can usually not be compared. Figure 1 shows fibers with ascending curl, please note that the curl varies but fiber curvature remains unchanged. That is the case because curl, in contrast to curvature, is a size invariant descriptor. Fiber kink [13] denotes small regions of very high curvature, i.e. sharp bends, along the fiber. It indicates fiber deformations, mostly caused by mechanical damage. A fiber with high kink is shown in Figure 1 on the right side, the fiber on the left side has the same curl (i.e. overall non straightness) but significantly lower kink.

Further fiber characterization parameters are listed in Figure 3. Fibrillation describes the number of fibrils, i.e. fiber wall fragments, sticking out of the surface of pulp fibers.

	CIS 100	FiberLab	Fiber Master	FQA	MorFi	FS200
Fiber length	•	•	•	•	•	•
Curl	•	•	•	•	•	
Kink			•		•	
Flexibility			•			
Fibrillation	•				•	
Coarseness		•	•	•	•	•
Fiber width	•	•	•	•	•	
Fiber wall thickness		•				
Area of Crossection		•				
Shives content			•	•	•	
Fines content		•	•	•	•	(•)
Vessel content			•	•		

Figure 3. Fiber properties measured by six commercially available fiber analyzers.

Fines content denotes the number of small fiber fragments. Unfortunately definitions below which size a particle is considered small differ vary largely between the examined analyzers [2,12,28,30]. Few analyzers evaluate number and size of hardwood vessel cells in the pulp, fiber flexibility, or wall thickness. Finally shives are counted, they are bundles of fibers that were improperly disintegrated during the pulping process.

Flow cell based fiber morphology Measurement

Now six widely used commercial pulp analyzers from different manufacturers are reviewed. They are all based on a rear illumination flow cell and image analysis. The measurements obtainable, hardware concept, and some aspects of image analysis are discussed for each analyzer. An overview of the fiber parameters measured by the devices gives Figure 3, Figure 4 summarizes some technical specifications.

The Galai CIS-100 [2] is also sold under the name Pulp Fibre Analyzer. The flow cell light source is a pulsed flash, images are acquired by a CCD camera. Length, width, and curl of roughly 2000 fibers are measured per pulp sample. The device also gives a value for fiber fibrillation, however neither a definition of this value, nor an empirical verification could be found in the literature.

The Metso FiberLab has two light sources, it uses three optical detectors [30]. That enables it to perform a wide variety of fiber measurements. Images from a low resolution camera are evaluated for fiber length, coarseness, kink, and curl. Fiber width, cell wall thickness, and cross sectional area are measured by a separate high resolution camera. The fiberLab is the only device that offering measurement of these parameters. The third sensor is a light scattering detector used for measurement of smaller particles.

The STFI Fibermaster [12] is a two-camera system providing fine and coarse resolution images. All image processing is hard wired as camera on-chip logic which makes measurements considerably faster than the other systems. The fiber measurement provides length, width, coarseness, kink, and two shape factors for curl. Vessel cells are identified and counted, also shive content is evaluated. The Fibermaster is the only fiber analyzer that provides a measure for fiber flexibility [12]. It follows the principle that shear forces (and thus bending stress imposed on fibers) increase with flow speed in the flow cell channel. Therefore flexibility in Fibermaster measurements is defined as the change of fiber curl at different flow rates in the measurement cell. Large changes of fiber curl upon changes in flow speed indicate high fiber flexibility.

The OpTest Fiber quality analyzer (FQA) has a special flow cell design aimed to to prevent fouling and forming of deposits. Three currents are lead through the cell, only the middle current carries fibers, the currents flowing next to the wall consist of pure water [29]. Transmitted illumination is provided by a circular polarized laser flashlight, opposed to other flow cells which are using linear polarized light. The device measures length, width, coarseness, kink and curl. Fiber width measurement sensitivity is given as 1 µm although camera resolution is 36 µm/pixel, additional resolution is estimated by interpolation. The FQA also measures shives and vessel content.

The Techpap MorFi fiber analyzer [28] has one high resolution camera. Fiber length, width, coarseness, kink and curl are analyzed. The system gives a measure for fiber fibrillation, it is defined as the length of all micro fibrils attached to the fibers in relation to total fiber length. However an empirical verification for this measure can not be found in the literature.

Finally there is the Kajaani FS-200, which has been on the market since the 1980ies [34] and has been widely used since. Its working principle is totally different from the other devices: The sensor is a line camera aligned along the length axis of a capillary, this capillary carries the fiber suspension. The capillary is illuminated with transmitting polarized light, as the fibers are carried along in front of a sensor element, they induce changes in polarization which are detected by the sensor element [30]. So basically the 1-dimensional projection of a fiber is measured. For this reason only fiber length and coarseness can be measured. As the row sensor has a rather low resolution of 50µm/pixel fines measurement is only possible to a limited extent.

Repeatability and comparison of results

Repeatability of the above described fiber analyzers [2,5,8,24] is obviously closely related to processing speed and subsequent total number of fibers analyzed, see Figure 4. Repeatability on a 95% confidence level according to Tappi standard T 1200 sp91 was between 2% and 5% for (length weighted) fiber length and fiber width. For curl and kink repeatability is not as good, it ranges between 6% and 11%. For Coarseness measurement, which additionally contains the error of determining the solids content of the suspension, repeatability is 10% or worse. No repeatability is given for other parameters.

Comparing the results from measuring the same pulp fiber samples using the various pulp analyzers revealed large differences between the devices.

For fiber length the Kajaani FS-200 has a totally different measurement principle than the other devices, mainly because it measures a 1-dimensional projection of the fibers whereas all other systems evaluate 2-dimensional projections. Consequently the FS-200 measures curled and kinked fibers too short. Apart from one publication [24], this result has repeatedly been confirmed in the literature [2,30,33] and was also found by our own investigations [8]. The MorFi system measures even shorter values for fiber length than the Kajaani [5,30] although it uses a 2D. That leads to the conclusion, that the MorFi system also measures fiber length too short.

Deviations in (length weighted) mean fiber length between the systems was around 15% to 20%, so absolute comparison of results is impossible. However, relative comparison of 17 different pulps measured in four analyzers [30] gave highly correlated results. The situation for fiber

	CIS 100	FiberLab	Fiber Master	FQA	MorFi	FS200
Sensor type	2D-CCD	2D-CCD	2D-CCD	2D-CCD	2D-CCD	Row Sensor
Illumination	polar. flash	polar. laser, Xenon light	undis-closed	circular polar. laser flash	undis-closed	polar. light
Optical resolution	15 $\mu m/pix$	10 $\mu m/pix$ 1.5 $\mu m/pix$	26 $\mu m/pix$ 6 $\mu m/pix$	36 $\mu m/pix$	4 $\mu m/pix$	50 $\mu m/pix$
Number of fibers analyzed	2000 to 4000	2000 to 6000	10 000 to 30 000	several 1000	3000 to 6000	20 000
Measurement time	10 min	8 to 10 min	1.5 min	100 per sec.	3 min, 5 min	10 min

Figure 4. Technical specifications of six commercially available flow cell based fiber analyzers.

width was similar, differences in absolute values were up to 40%, still relative comparison is possible because the results are highly correlated.

As mentioned above, different definitions for fiber curl are used by most of the reviewed pulp analyzers. Not surprisingly the curl values between MorFi, Fibermaster, and Fiberlab differed strongly [30], absolute difference was up to 70%. Correlations were still fairly good, thus relative comparison is still possible to some extent.

The analyzers do not recognize fine particles in the same way, which comes from two reasons. First there are great differences in optical resolution, from MorFi with 4 µm/pixel to Kajaani FS-200 with 50 µm/pixel. These differences become most relevant for recognition of small particles. Secondly different rules for classification of fines are implemented. As a consequence they measure different amount of fines, which in turn leads to strong differences in coarseness [30].

It does, however not lead to strong differences in average fiber length, because length weighted fiber length was compared, reducing the influence of fines content [8].

For coarseness not only absolute values differed, correlation was also bad [24, 30] thus the results of coarseness measurements from different pulp analyzers can not be compared. That is mainly due to the fact that for coarseness measurement, apart from the error of differing fines results, additional error for determining the (very low) measurement consistency of the suspension comes into effect.

In conclusion quantitative comparison of the results displayed large differences between the fiber analyzers regarding several perspectives. Hardware concept, image resolution, and illumination vary largely. It can be speculated that the implemented image analysis algorithms might also be very different. Most important however is the fact, that the measurement results are grossly differing, for some fiber properties they do not even reflect relative ranking. All these facts indicate, that developments in this field are far from being finished. Calibration and standardization of these measurements still needs to be accomplished.

Surface chemistry of pulp fibers

A multitude of dyeing or staining schemes exists for microscopic analysis of pulp fiber surface chemistry [3,16]. Some of them are directly observable [4,25], many apply fluorescence [23]. Apart from staining, lignin exhibits strong autofluorescence, when it is excited with light in the wavelength range of 500 nm. This is often combined with Confocal Laser Scanning Microscopy, for example

in order to measure lignin content profiles across the fiber wall [20].
The key point is that many of these microscopic methods have the potential to be adapted for automated, image analysis based measurement in a flow cell.
Several flow cells have been developed for measurement of pitch, i.e. colloids of hydrophobic substances, in pulp suspension. A measurement based on staining with fluorescent dye and laser light was described by [15]. They measure count and size of previously stained resin particles by pumping a colloidal particle suspension through a capillary and evaluating the scattering of laser light. An evaluation of the instrument [35] showed, that reproducible results are obtained, if influenced parameters like for example solids concentration and flow speed are controlled. Flow cytometry of bacteria and wood resin particles are also discussed in [32] and [17]. Fluorescence scattering induced by staining of resin and bacteria is evaluated in a flow cytometer (i.e. a flow cell for cell counting). They find very good correlations between bacterial counts performed in a flow cell and counting of bacteria colonies grown on a laboratory nutrient media. Relations between resin agglomeration and bacteria count as well as interaction with carbonate particles are discussed.
A particularly interesting approach to measure the uniformity of Kappa number on a single fiber basis describes [18]. This method stains the fibers with the metachromatic fluorescent dye Acridine Orange. It has been shown that at low lignin concentrations the stained fibers exhibit a green fluorescence, while at higher lignin content they exhibit a shift to red fluorescence. The ratio of red to green fluorescence correlates well with lignin content. Measurement of fluorescence is realized by picturing and subsequent image analysis of individual fibers in a flow cell.
An interesting approach to combine a set of dyes to characterize different types of chemical fiber surfaces has been published quite recently [4]. They use basic dyes for identification of lignin on the surface, basic phthalocyanine dyes for detection of hemicellulosic surface regions and finally direct dyes, which have an affinity for alpha cellulose. Then they evaluate the effect of different laboratory bleaching sequences on the fiber light absorbancy caused by the varying dyes. Principal component analysis revealed two main components representing lignin content and polarity (hydrophilicity or hydrophobicity).

Chemically induced fiber swelling and dissolving

Since the 1960ies, the swelling and dissolving process of chemical pulp fibers dissolving in chemicals has been examined [10]. Fiber dissolution in chemicals like iron-sodium-tartrate (EWNN), lithium-chlorine/dimethylacetamide (LiCl/DiMAc) or cuproethylenediamine (CUEN) starts with intense swelling and proceeds to increasing disintegration of the fiber. These various stages of disintegration of the fiber have a very specific visual appearance [10], for example see Figure 5. Fiber swelling starts with so called balloon swelling (I) where only limited parts of the fiber are swollen, it proceeds to volume swelling (II) where large parts of the fiber wall are already broken apart. Finally it reaches a phase called gel swelling (III), where the fiber has already widely disintegrated.
It has been quite straightforward to observe, that the presence of specific swelling phenomena at lower chemical concentration is related to the ability to dissolve at higher concentration. So fiber swelling has been observed to assess the adequacy of chemical pulp for viscose production. A quantitative evaluation of swelling and dissolving of pulp fibers in EWNN and LiCl/DiMAc has been

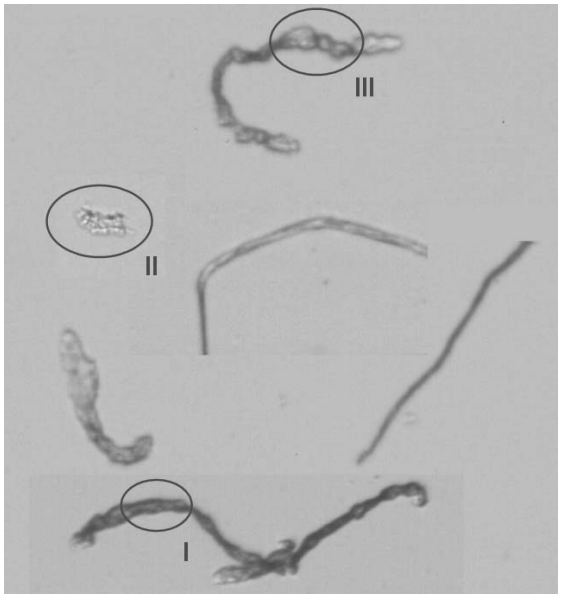

Figure 5. Characteristic types of pulp fiber swelling induced by a chemical agent: Balloon swelling (I), volume swelling (II), gel swelling (III).

implemented [31]. The authors record video images of single fibers dissolving and apply image analysis to evaluate changes in fiber thickness and fiber transparency. Finally they measure the time until the fiber breaks apart. These parameters, together with other laboratory results, are used to quantify swelling and dissolving behaviour.

On the other hand, the swelling behaviour is largely related to the fiber wall structure [26]. The S2 layer of the wood fiber wall, due to its highly aligned fibril structure, is very prone to swelling, whereas the S1 wall layer with its crossed fibril structure restricts fiber swelling [26]. So chemically induced fiber swelling provides an indirect method to evaluate mechanical and chemical damage of the S1 wall, in fiber regions with heavy swelling the S1 is obviously damaged. Such methods use different chemical agents to promote strong fiber swelling. A CUEN based method [21] finds good correlations between beating degree and fiber swelling. This method was adapted at our institute, we evaluate fiber swelling using image analysis and a flow cell [5,6,8,33]. A different swelling chemical, iron-sodium-tartrate (EWNN) is used in [9]. The authors examined fiber swelling, fibrillation, nodes of damage, and curl index by visual inspection of photographs taken at specified time intervals after addition of the swelling chemical. According to recent work [1], which compared fiber wall damage visualized by polarized light microscopy [7,19,22] to fiber wall damage indicated by chemically induced swelling, both methods indeed indicate cracks in the S1 fiber wall.

Conclusions

The present review shows, that considerable effort has been put on both, academic research as well as commercial development of image analysis based fiber characterization methods.

In the field of fiber morphology, there are already several commercial devices available. The measurement results for basic features like fiber length or width show sizable differences in absolute values, still correlations are high. Thus comparison of the absolute values is not possible, relative comparison can be achieved. More complex fiber characteristics like curl or coarseness can not be compared well, neither in absolute nor in relative results. It will be the challenge for the following years to achieve standardization and comparability for these fiber analyzers. Even more advanced features like fiber wall thickness, fiber flexibility, and fiber fibrillation are rarely offered yet, but without doubt these are under development by most of the fiber morphology flow cell manufacturers.

For fiber surface chemistry respectively pulp swelling and resolving behaviour no commercial analyzers are on the market yet. Still several research groups are working on such methods. To date the potential of these analytic approaches has not been fully tapped. It can be expected, that within the coming years on the one hand some existing microscopic fiber

analysis techniques will be adopted for automation. On the other hand, the fast growth of image analysis hardware and algorithmic capabilities will permit totally new methods and approaches to fiber analysis. For that reason fiber assessment has been a pronounced research focus at our institute during the last years [5,6,8,33]. Various flow cell prototypes with according image analysis software have been developed for pulp fiber quality research.

References

[1] P. Ander and D. Geoffrey. Morphology of spruce fibre dislocations as studied by balloon swelling and acid cleavage - light and electrone microscope observations. In U. Schmitt and P. Saränpää, editors, COST Action E20 - Wood Fibre Cell Walls: Methods to Study Their Formation, Strucure and Properties, Brussels, 2003. OPOCE.

[2] M.G. Carvalho, P.J. Ferreira, A.A Martins, and M.M. Figueiredo. A comparative study of two automated techniques for measuring fiber length. Tappi J., 80(2):pp. 137–142, 1997.

[3] J. Clark. Pulp Technology and Treatment for Paper. Miller Freeman Publ., San Francisco, 1978. ISBN 0-87930-066-3.

[4] T. Drnovsek and M. Perdih. Fibre surface characteristics evaluated by the method of selective staining. J. Wood Sc., 51(5):507–514, 2005.

[5] R. Eckhart. Beurteilung des Schädigungsgrades von Zellstofffasern anhand deren Quellverhalten in Kupferethylendiamin. Licentiate thesis, Graz Universtiy of Technology, 2004.

[6] R. Eckhart, U. Hirn, and W. Bauer. Fiber wall damage in the refining process - accepted for publication. In Proceedings of the Progress in Paper Physics Seminar, Oxford (Ohio) - Oct. 1-5 2006, 2006.

[7] O.L. Forgacs. Structural weakness in softwood pulp tracheids. Tappi J., 44(2):pp. 112–119, 1961.

[8] U. Hirn. New Methods in Paper Physics Based on Digital Image Analysis. PhD thesis, Graz University of Technology, 2006.

[9] B. Hortling, T. Jousimaa, and H-K. Hyvärinen. Investigation of spruce pulp fibres by swelling experiments and light microscopy. In Proceedings of the 10th International Conference CELLUCON 1998, pages 205–208. Woodhead Publishing Ltd., 2000.

[10] G. Jayme and M. Harders-Steinhäuser. Kinematografische Erfassung der bei der Auflösung von Cellulose auftretenden Querteilungsformen. Das Papier, 18(10a):pp. 606–615, 1964.

[11] B.D. Jordan and N.G. Nguyen. Curvature, kink and curl. Paperi ja Puu, 68(4):pp. 313–318, 1986.

[12] H. Karlsson, P.I. Fransson and U.B. Mohlin. STFI Fibermaster. In 1999 SPCI International Conference on New Available Technologies 1999, pages 367 – 374. Swedish Association of Pulp and Paper (SPCI), 1999.

[13] R.P. Kibblewhite. Effects of fiber kinking and pulp bleaching on wet web strength. Tappi J., 57(8):pp. 120–121, 1974.

[14] R. Klein and H. Droege. Image analysis of fibre morphology. In 3rd Symposion: Image Analysis for Pulp and Paper Research and Production. STFI, 1995.

[15] T. Kroehl, P. Lorencak, A. Gierulski, H. Eipel, and D. Horn. A new laser-optical method for counting colloidally dispersed

pitch. Nordic Pulp and Paper R. J., 9(1):pp. 26–36, 1994.

[16] J.-E. Levlin and L. Söderhjelm, editors. Pulp and Paper Testing, volume 17 of Papermaking Science and Technology. Fapet Oy, 1999. ISBN 952-5216-17-9.

[17] L. E. Lindberg, L.H. Vähäsalo, and B.R. Holmbom. Flow cytometry of bacteria and wood resin particles in paper production. Nordic Pulp and Paper R. J., 19(4):pp. 412–416, 2004.

[18] LY. Liu, R. Gustafson, and J.B. Callis. A novel method to measure fiber kappa number. Tappi J., 82(9):pp. 107 – 111, 1999. also: http://faculty.washington.edu/callis/Forest/Flow Imager A-99.htm, download 05-20-2005.

[19] C.-H. Ljungqvist, R. Lyng, and F. Thuvander. Influence of fibre damage in latewood spruce tracheids on strain to failure of wood fibres determined by weibull modelling. Nordic Pulp and Paper R. J., 19(2):pp. 164–169, 2004.

[20] P.A. Moss, I. Nyblom, A.M. Sneck, and H.K. Hyvärinen. The location and qualification of lignin in kraft pulps using clsm and image analysis. In PTS-COST E11 Workshop - Characterization Methods for Fibres and Paper, pages 2.1 – 2.7. PTS, 1999.

[21] H. Nisser and W. Brecht. Zwei neue Messkriterien von aufgeschwemmten Fasern zur Beurteilung der Blattfestigkeit. Svensk Papperstidning, 66(2):pp. 37–41, 1963.

[22] D. Page, R. Seth, B. Jordan, and M. Barbe. Curl, crimps, kinks and microcompressions in pulp fibers - their origin, measurement and significance. In Proceedings 8th Fundamental Reseach Symposium Oxford, pages 183–227, 1985.

[23] M. Pluta. Advanced Light Microscopy - Specialized Methods (Vol. 2). Elsevier, 1989. ISBN 0-444-98918-8.

[24] G. Robertson, J. Olson, and P. Allen. Measurement of fiber length, coarseness and shape with the fiber quality analyzer. Tappi J., 82(10):pp. 93–98, 1999.

[25] F.L. Simons. A stain for use in the microscopy of beaten fibers. Tappi J., 33(7):pp. 312–314, 1950.

[26] P. Stenius, editor. Forest Products Chemistry, volume 3 of Papermaking Science and Technology. Fapet Oy, 2000. ISBN 952-5216-03-9.

[27] A. Tessadro, C. Voillot, and J. Silvy. Dynamic characterization of pulp fiber morphology. In Proceedings 2nd European Symposion Image Analysis for Pulp and Paper Research and Production, pages 30–33. IFP Darmstadt, 1993.

[28] G. E. P. Tourtollet. A new tool for pulp morphology analysis. In Proceedings Conference Measurement & Control of Papermaking, Edinburgh 2000, pages 1–13. Pira, 2000.

[29] R.J. Trepanier. Automatic fiber length and shape measurement by image analysis. Tappi J., 81(6):pp. 152–154, 1998.

[30] M. Turunen, C. LeNy, T. Tienvieri, and J. Niinimäki. Comparison of fibre morphology analysers. Appita J., 58(1):pp. 28–32, 2005.

[31] E.W. Unger, H.P. Fink, and B. Philipp. Morphometrische Untersuchungen des Quell- und Lösevorgangs von Celluslosefasern in EWNN und LiCl/Dimethylacetamid. Das Papier, 49(6):297–307, 1995.

[32] L. Vähäsalo, R. Degerth, and B. Holmbom. The use of flow cytometry in wet end research. Paper Technology, 44(1):pp. 45–

49, 2003.

[33] H. Widauer. Automatisierte bildanalytische Charakterisierung des Schädigungsgrades von Zellstofffasern. Licentiate thesis, Graz University of Technology, 2003.

[34] S.C. Young. A Calibration and Maintenance Schedule for the Kajaani FS-200 Fibre Analyzer. Appita J., 46(6):pp. 435–438, 1993.

[35] L. Yu, L.H. Allen, and A. Esser. Evaluation of a laser-optical resin particle counter. Tappi J., 2(3):pp. 13–18, 2003.

Lenzinger Berichte, 86 (2006) 106-110

MAPPING OF AGING STATUS IN HISTORIC PAPERS BY FLUORESCENCE LABELING OF OXIDIZED GROUPS AND PH MEASUREMENTS

Ute Henniges, Johanna Smolle, Thomas Rosenau, Paul Kosma, and Antje Potthast

University of Natural Resources and Applied Life Sciences - Vienna (BOKU),
Muthgasse 18, A – 1190 Vienna, Austria

Aging of paper is a complex process, mainly driven by acid hydrolysis and oxidation. Yellowing and decrease of mechanical properties are two indicators for ongoing deterioration. Simple testing might also reveal a change in its wetting behavior.
In this study a more detailed insight into paper ageing was sought in order to find out what causes the differences in wettability and conservation treatment properties within the same sheet of paper. Two papers from the 20th century have been divided into 30 pieces each which have been subsequently analyzed one by one with regard to surface pH, cold extraction pH, carbonyl group content, and molecular weight distribution. The data of extract pH correlated well with carbonyl group content, but molecular weight distribution did not exhibit any correlation pattern.

Keywords: *mapping, carbonyl groups, surface pH, cold extraction pH, historic paper*

Introduction

The main causes for paper aging are acid hydrolysis and oxidation. Both are degradation processes inherent to a natural polymer, but can be considerably accelerated by using acidic sizing additives and by leaving traces of metal ions in the pulp. Paper from the mid 19th till the late 20th century has mainly been produced according to acid sulfite cooking processes with additional acid alum rosin sizing. These production parameters lead to the formation of oxidized functionalities along the cellulose chain and provide a source of acid which will lead to acid hydrolysis. As a result, paper will exhibit reduced aging resistance, namely increased brittleness and a tendency to break. Naturally occurring oxidation and traces of transition metal ions enhance oxidation processes in paper. Usually those papers from the last two centuries would contain significant amounts of lignin as well, which can be oxidized more easily. As a consequence, paper turns yellow. Besides these inherent parameters of paper aging, storing conditions will also influence the aging behavior. Light and permanent presence of oxygen will provoke oxidation, changing climate conditions can enhance cellulose degradation, high levels of humidity will promote fungal growths.
From the analytic point of view, these processes can be monitored by measuring pH and molecular weight distribution to determine the degree of acid hydrolysis, and carbonyl group content to estimate

oxidation phenomena. While the overall effects of paper degradation have been studied thoroughly, little is known about the course of acid formation, cellulose chain shortening and oxidation within a single sheet of paper. By cutting two selected papers in single fragments and analyzing them separately the question of degradation pattern within one sheet can be addressed. Basically, paper can be stored as a single document, laying or standing in a box or envelope on shelf, or bound in a book usually standing in a shelf. Access of light, oxygen, and other gaseous substances is different for both forms of storage, so that the question arises how storage influences aging parameters and if there are any detectable differences between those two types of storage.

Fluorescence labeling according to CCOA methodology provides a good means to measure the carbonyl group content of cellulosics in relation to the molecular weight, only using small quantities of paper to analyze the fragments of one sheet. Each fragment weighs about 100 mg, corresponding to a 3 g sheet of paper about the size of DIN A4. For pH measurement surface electrodes do not consume any sample material at all, and minimized extraction pH measurements have become available recently.

Experimental

Chemicals were obtained from commercial sources and were of the highest purity available. Two different papers from different origins and sources were used. CCOA labeling was performed as described earlier [1-3].

Prior to analysis, the two papers were tested for solubility in DMAc/ LiCl 9% and scanned digitally.

General analytics. Gel permeation chromatography (GPC) measurements used the following components: online degasser, Dionex DG-2410; Kontron 420 pump, pulse damper; autosampler, HP 1100 column oven, Gynkotek STH 585, fluorescence detector TSP FL2000; multiple-angle laser light scattering (MALLS) detector, Wyatt Dawn DSP with argon ion laser (λ_0 = 488 nm); refractive index (RI) detector, Shodex RI-71; Data evaluation was performed with standard Chromeleon and Astra software.

GPC method. The following parameters were used in the GPC measurements: flow, 1.00 ml min^{-1}; columns, four PL gel mixedA ALS, 20µm, 7.5 x 300 mm; fluorescence detection, λ_{ex} = 290 nm, λ_{em} =340 nm; injection volume, 100 µl; run time, 45 min; DMAc/LiCl (0.9% w/v), filtered through a 0.02 µm filter, was used as the eluant.

pH measurements. All measurements were done with the seven easy pH meter from Mettler Toledo, using a Mettler Toledo InLab 426 flat membrane electrode. Surface pH measurement was performed according to TAPPI 526_om 99. In order to measure cold extraction pH, which according to TAPPI requires an unacceptably large sample amount, a modified method was used as described in literature [4].

Results and Discussion

Comparing cold extraction pH and surface pH measurements the latter method yielded lower values than the former which is in agreement with data from literature [5]. Data for extraction pH are generally more homogenous, reflecting an overall pH of the analyzed piece. Values did not vary much, ranging from 4.9 to 5.3 in test paper "Dresden_1_4" (Figure 2). An explanation might be that in addition to acids, also alkaline fillers will have time to contribute to extraction pH, while their solubility is too low to contribute to surface pH. They do not exhibit any special pattern and cannot be interpreted in terms of differences in aging. Surface pH measurement is known to be not as precise as extraction methods, thus values vary a

lot more, ranging from 3.8 to 5.0 in test paper “Dresden_1_4”, but will certainly depict paper condition on the surface better than extraction methods where a large variety of factors will contribute to the overall pH.

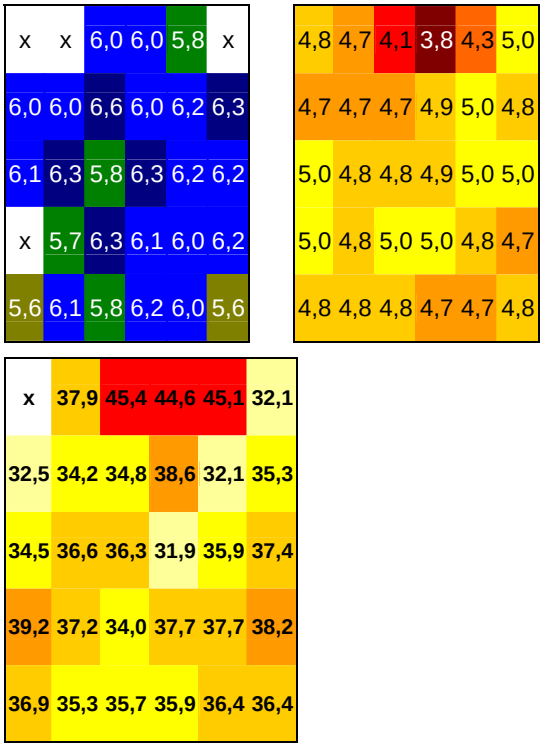

Figure 1. Test paper “T3” (taken from a bound book). left: cold extraction pH measurements, right: surface pH measurements, bottom: carbonyl group content in µmol/g, determined by the CCOA method.

In test paper “T3” which was cut from a bound book, lowest pH values were found on that piece of the sheet which belongs to the head of the book, i.e. the upper part that is exhibited to light and air when standing in a book shelf (Figure 1). Contrary to this, surface pH in test paper “Dresden_1_4” is lowest at the bottom of the document, a piece of paper which was stored in an archive, probably being kept in a map.
This might be a hint, that storing conditions contribute to acid development. Unfortunately, it is not known how test paper “Dresden_1_4” was actually stored.

Comparing surface pH with carbonyl group content, an interesting picture was revealed. Areas of low pH corresponded in both cases to areas of high carbonyl group content.

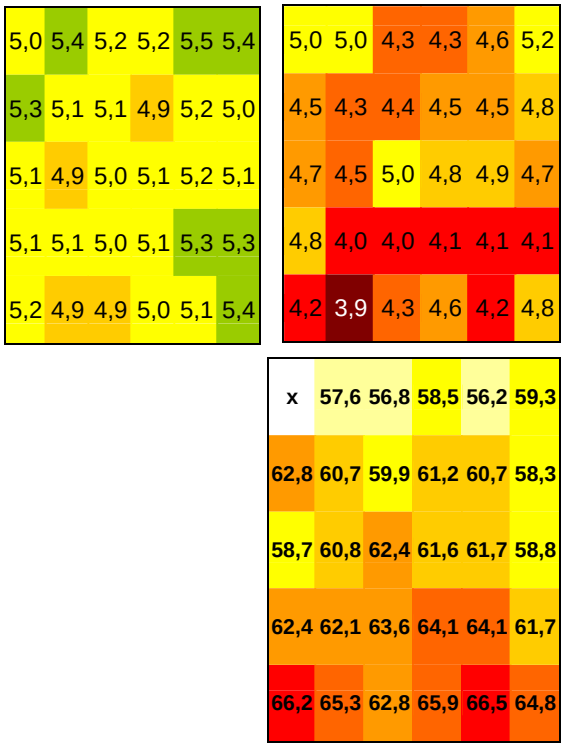

Figure 2. Test paper “Dresden_1_4” (single sheet paper document). Left: cold extraction pH measurements, right: surface pH measurements, bottom: carbonyl group content in µmol/g, determined by the CCOA method.

This contributed to the idea that on exposition to light and polluting gases, acid hydrolysis and oxidation take place at the same time. As these influencing factors attack paper from the surface, it is no surprise that surface pH measurements will response more sensitively to changes than extraction pH.
Determination of molecular weight and molecular weight distribution did not show any regular mapping pattern. Calculation of profiles in test paper T3 taken from a book revealed a zone of higher degradation in the center of the sheet, opposed to the

trend of higher oxidation and lower pH occurring at the top of the sheet (Figure 3).

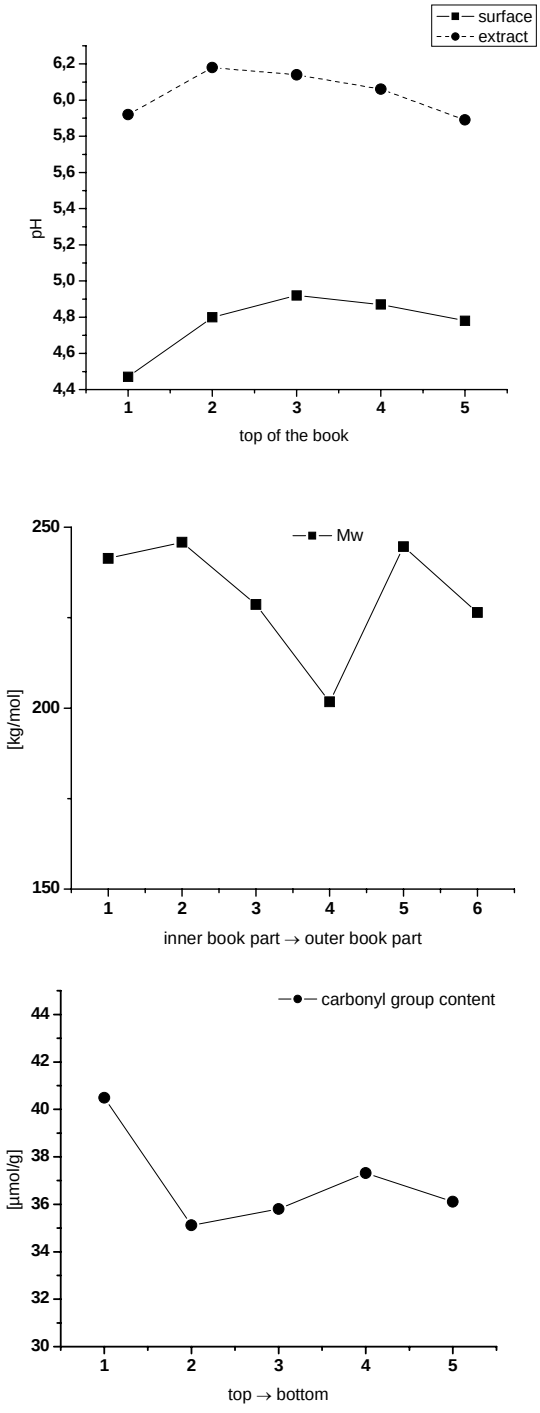

Figure 3. Profiles of pH, molecular weight (Mw) and carbonyl group content in test paper T3. To calculate the profiles, all five values for one line or all six values for one row were averaged.

Conclusions

Mapping and profiling of different aging conditions within one single sheet of paper has successfully been performed using surface and minimized cold extraction pH, as well as fluorescence labeling to determine carbonyl group content and molecular weight. The described method is very useful for the visualization of different deterioration states in paper.

As production parameters that determine aging properties of paper are expected to affect the bulk material, any degradation triggered by those factors should be distributed homogenously. This is reflected by the quite homogenous distribution of cold extraction pH. Differences occurring must thus have their origin in external aging factors such as climate impact, light or air pollution. These differences can be detected using surface pH measurements. Surface pH correlates with the expected sites of exposure for paper bound in a book standing in a shelf or documents stored in an envelope laying in a shelf. Obviously external influences lead to a decreased pH. Additionally, carbonyl group content correlated with surface pH. Fragments with low pH values had a high carbonyl group content.

As books are usually stored in a closed way, degradation products can accumulate in the center of the book. This might explain the lower Mw in the center of the test paper T3 taken from a book.

Acknowledgements

The authors would like to thank Dr. Sonja Schiehser for practical assistance and GPC measurements. Financial support by PAL GmbH, Germany, is gratefully acknowledged.

References

[1] Röhrling, J.; Potthast, A.; Rosenau, T.; Lange, T.; Ebner, G.; Sixta, H.; Kosma, P. Biomacromolecules 2003, 3, 959. A novel method for the determination of carbonyl groups in cellulosics by fluorescence labeling. Part I: Method development.

[2] Röhrling, J.; Potthast, A.; Rosenau, T.; Lange, T.; Borgards, A.; Sixta, H.; Kosma, P. Biomacromolecules 2003, 3, 969. A novel method for the determination of carbonyl groups in cellulosics by fluorescence labeling. Part II: Validation and applications.

[3] Potthast, A.; Röhrling, J.; Rosenau, T.; Borgards, A.; Sixta, H.; Kosma, P. Biomacromolecules 2003, 4, 743. A novel method for the determination of carbonyl groups in cellulosics by fluorescence labeling. Part III. Monitoring oxidative processes.

[4] Strlic, M.; Kolar, J., Kocar, D., Drnovsek, T., Selih, V.S., Susic, R., Pihlar, B. E-preservation science 2004, 1, 35. What is the pH of alkaline paper?

[5] Saverwyns, S., Sizaire, V., Wouters, J. ICOM Committee for Conservation, Graphic Documents, Prepints Vol. II of the 13th Triennial Meeting in Rio de Janeiro 2002. The acidity of paper. Evaluation of methods to measure the pH of paper samples.

Lenzinger Berichte, 86 (2006) 111-115

SEC IN CELLULOSE XANTHATE ANALYSIS

Axel Rußler,[1] Antje Potthast,[2] Thomas Rosenau,[2] Bodo Saake,[3] Jürgen Puls,[3] Herbert Sixta,[1] and Paul Kosma [2]

[1] Lenzing AG, Innovation, Lenzing, Austria,
Fax: +43-7672-918-2921, h.sixta@lenzing.com
[2] Christian-Doppler-Laboratory and Department of Chemistry, University of Natural Resources and Applied Life Sciences Vienna, Austria, Fax: +43-1-36006 6059, paul.kosma@boku.ac.at
[3] Institute for Wood Chemistry and Chemical Technology of Wood, Federal Research Centre for Forestry and Forest Products, Hamburg, Germany, Fax: +49-40-73962-599, b.saake@holz.uni-hamburg.de

After stabilisation of cellulose xanthate, the obtained derivative is suitable for SEC analysis. Also further treatments like ultrasonic or enzymatic degradation can be applied to this polymer. By detecting the samples in SEC by RI and UV detectors, the substituent distribution over the molecular weight fractions can be provided. Analyzed viscose samples showed relatively homogeneous substituent distributions over the molecular mass main fractions.

Degradation products after enzymatic treatment give further insight into the homogeneity of the substituent distribution.
SEC in combination with viscose stabilisation is also suitable for tracking transxanthation reactions within the viscose dope.

Keywords: *substituent distribution, viscose, endoglucanase, molecular weight distribution, ultrasonic degradation, transxanthation*

Introduction

Discovered in 1891 by Cross, Beavan, and Beadle, the viscose process has a long history. The transformation of unspinable wood cellulose into a spinable form by the intermediate cellulose xanthate has been used during this long time to provide a broad variety of fibers with different properties on the base of the natural polymer cellulose.
Nevertheless the viscose process is a very sophisticated process with many production parameters and complex chemical reactions and physicochemical changes. However after some 115 years of research there are still some aspects of the chemistry of cellulose xanthate that are not fully understood.
Besides the DP of the cellulose backbone and its distribution, the DS and the substituent pattern are of major interest with regard to the solvation properties of the cellulose xanthate, the spinability of the viscose dope and finally the properties of the viscose fibres. Most changes in the substituent distribution occur by different reactions during the ripening step of the dissolved cellulose xanthate. Well known are the decrease of the DS and the colloidchemical modifications of the polymer during this step.
To come to a more complex view of these processes in the viscose dope, the SEC analysis can provide important information concerning the substituent distribution between different cellulose chains and fractions of the molecular weight distribution.
The substituent pattern of this structural level of substitution is not only of great importance for the properties and processability of the viscose dope but also for the properties of the regenerated cellulose fibre.
SEC analysis of viscoses is also a good tool to look for transxanthation reactions in the viscose dope.

Stabilisation of cellulose xanthate

The xanthate groups are very unstable substituents that are very sensitive to acidic pH values and temperature changes. These drawbacks for sophisticated analysis methods could be overcome by alkylation. For this purpose a stabilisation reaction with *N*-Methyl-*N*-phenyl-2-iodoacetamide is suitable as reported elsewhere [1]. The stable product serves with good solubility and special spectroscopic properties.

SEC analysis

Stabilized cellulose xanthate could be directly applied for size exclusion chromatography. It is readily soluble in standard solvents for polymer SEC like dimethyl sulfoxide or dimethyl acetamide.

The applied SEC-System included a MALLS-, an UV- and a RI-detector. MALLS and RI-detectors allowed recognizing the molecular weight distribution (MWD) and the UV-detector allowed the detection of the substituents due to the UV-absorbing ring system in the stabilized xanthate group.

This procedure enabled the illustration of the substituent distribution over the molecular weight distribution after charging the UV-signal with the RI-signal. The profile can be lifted by multiplication to the total substitution amount (from UV integral and γ-value) and then displays the γ-value distribution.

Stabilized viscoses

On the studied viscoses, we found a very uniform distribution of the substitution over the major part of the MWD with only slight changes that are within the error of measurement.

Problems for interpretation of the signals can arise at low and very high M_W values, i.e. at the "start" and the "end" of MWD curves due to a fundamental physico-chemically caused problem. The signals can not be totally synchronized due to diffusion phenomena within the link of the RI and the UV detector. Together with the low concentration in these areas and the differences in sensitivity of the two detectors the very edges of the distribution do not supply reliable information.

Aging of the samples (24 h at room temperature) showed an equal drop of DS over all M_w fractions.

Ultrasonic degradation

Even if the state of solubility of the stabilized viscoses is sufficient for many applications such as SEC measurements, for others, like some spectroscopic measurements or further reactions an even improved solubility is desirable.

Ultrasonic degradation seemed to be a suitable method for improving this property by reducing the average chain length of the polymer.

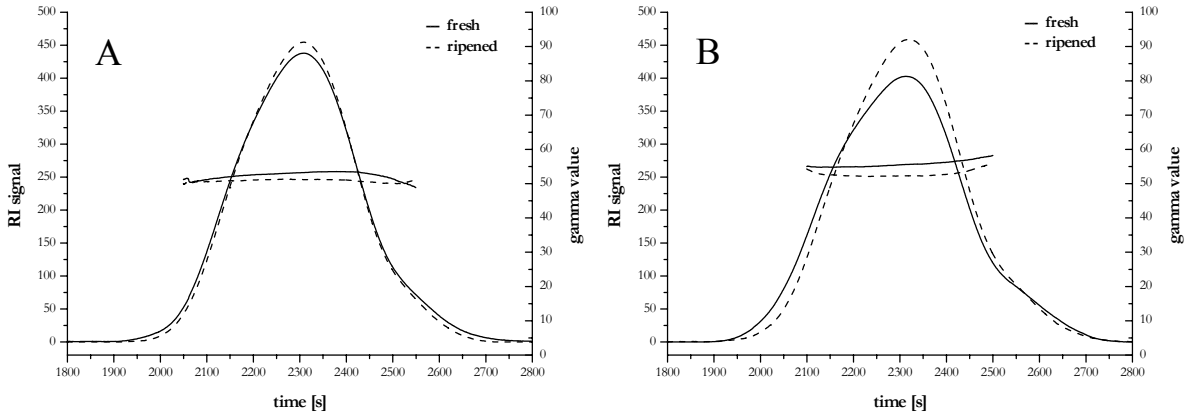

Figure 1. RI-signal and gamma value distribution on freshly stabilized viskoses (A: γ 50,6, B: γ 50,9) and the same viscoses stabilized after ripening (A: γ 49,5, B: γ 49,6).

Ultrasonic degradation led to a significant reduction of the DP in a short time period (see Figure 2).
Even if the conditions during degradation are quite harsh, the applied energy is low enough to avoid cleavage of substituents [2, 3]. This could be proved by a direct SEC analysis of a ultrasonically degraded stabilized viscose sample where no cleaved substituents could be found (see Figure 3).
Degradation by ultrasound generates no low molecular weight degradation products like e. g. monomeric sugars [4]. This is very desirable in spectroscopic analysis due to reduced end group effects and for further chemical reactions to minimize substance losses in precipitation steps.

Enzymatic degradation

Enzymatic degradation can provide further information about the distribution pattern along the molecular chains, especially of its homgeneity. An enzymatic degradation was accomplished with a pure endoglucanase preparation ((Novozym 613, NOVOZYMES A/S, DK) on two different viscose samples, one with lower and one with higher DP and DS. Both samples were degradable with the preparation.
The chromatograms (see Figure 4) show different degradation patterns of the two samples. Whereas the sample with the lower DP and DS shows a significant amount of highly substituted low molecular mass degradation products, one could only find degradation products with low substitution for the other sample. Also in the main region of the MWD significant differences are detectable. Enzyme-treated sample B showed a higher UV-response in the region of the high molecular weight shoulder, incommensurate with the RI signal. Evidently, non-substituted cellulose structures were degraded – hence the drop in RI response – while substituted structures were retained causing the observed UV signal. The degradation of the high Mw part was much more pronounced for sample B (see Figure 4, shifted RI signal), which agreed with the decreasing DS in the high DP region for sample B and an almost unchanged UV signal after degradation. Hence, the endoglucanase treatments indicated different substitution characteristics, both between samples A and B and between different Mw regions of the respective samples. The UV-characterization of the main peak and the peaks of the degradation products shows the same pattern (see Figure 4). This proves the signals to be of the same origin and not a contamination for instance by the enzyme.

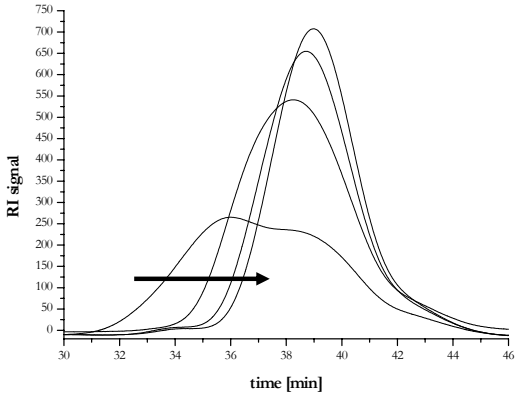

Figure 2. SEC analysis of an ultrasonically treated stabilized viscose samples with treatment times: 0, 5, 15, 30 min.

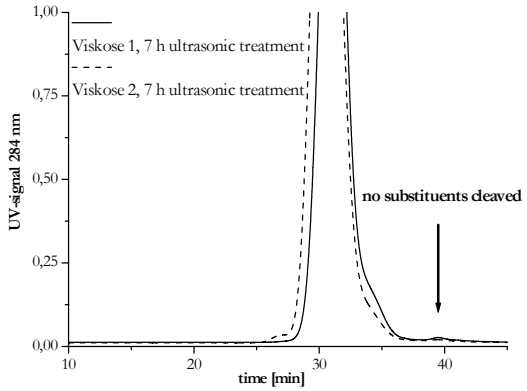

Figure 3. UV spectra of SEC of stabilized viscoses treated with ultrasound for 7 h: no significant amounts of cleaved xanthate groups are evident.

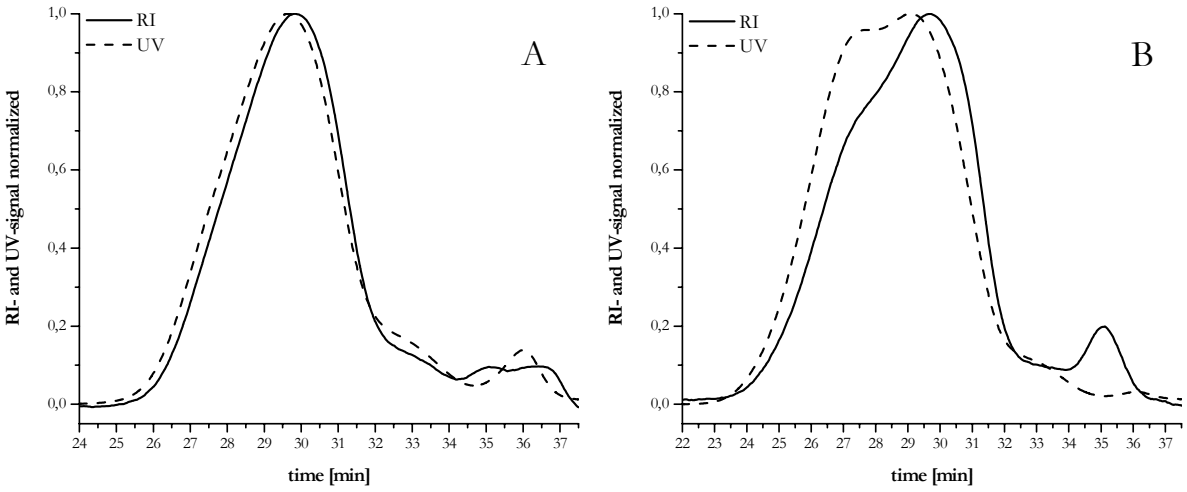

Figure 4. SEC analysis (RI and UV signal) of two different stabilized viscose samples (A and B) after endoglucanase treatment.

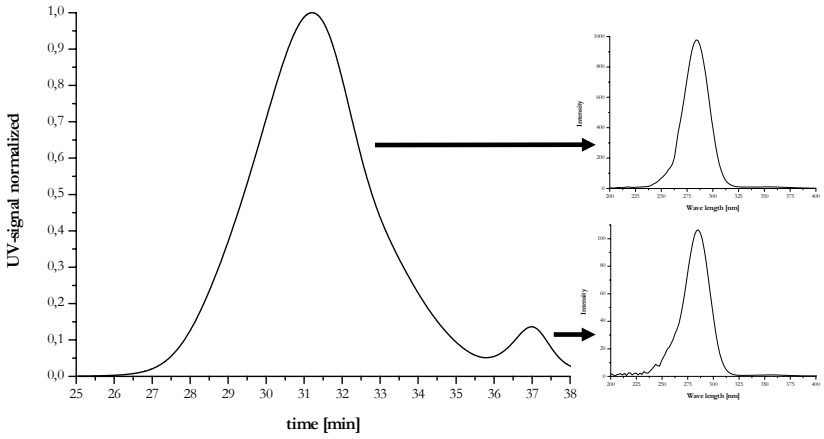

Figure 5. UV characterisation of the peaks in the UV graph of a SEC separation of enzymatically degraded stabilized viscose.

Transxanthation reactions

The transxanthation reactions, leading to a more homogeneous substitution are still not fully understood and especially not acquired concerning their amount during ripening of the viscose [5-7].

The combination of stabilization and SEC can be used to learn more about the intermolecular transxanthation reactions occurring in the viscose dope.

For this purpose a fresh high molecular mass viscose is mixed with a low molecular mass alkali cellulose and the mixture is ripened for at least one day at room temperature. After the ripening, the viscose is diluted, filtrated and subsequently stabilized. If transxanthation occurs the UV profiles of the SEC separation change and an increase in the low molecular mass region can be observed due to xanthated small alkali cellulose chains. In combination with the RI profiles the amount of transxanthation reaction can be assigned.

Results of this assay will be presented in detail elsewhere.

Conclusions

Stabilized “anilid” viscoses are capable for SEC analysis. SEC analysis showed a relatively homogeneous substituent distribution over the main part of the molecular weight distribution. The polymer is also accessible to ultrasonic and enzymatic degradation without loss of substituents. An enzymatic degradation with an endoglucanase preparation shows significant differences in the degradation products of viscoses with different degrees of substitution and polymerisation.

References

[1] Rußler, A.; Lange, T.; Potthast, A.; Rosenau, T.; Berger-Nicoletti, E.; Sixta, H.; Kosma, P., A Novel Method for Analysis of Xanthate Group Distribution in Viscoses. Macromol. Symp. **2005,** 223, (1), 189-200.

[2] Schittenhelm, N.; Kulicke, W.-M., Producing homologous series of molar masses for establishing structure-property relationships with the aid of ultrasonic degradation. Macromol. Chem. Phys. **2000,** 201, (15), 1976-1984.

[3] Kulicke, W.-M.; Otto, M.; Baar, A., Improved NMR characterization of high-molecular-weight polymers and polyelectrolytes through the use of preliminary ultrasonic degradation. Die Makromolekulare Chemie **1993,** 194, (3), 751-765.

[4] Czechowska-Biskup, R.; Rokita, B.; Lotfy, S.; Ulanski, P.; Rosiak, J. M., Degradation of chitosan and starch by 360-kHz ultrasound. Carbohydr. Polym. **2005,** 60, (2), 175-184.

[5] Bär, H. J.; Dautzenberg, H.; Philipp, B., Kinetische Untersuchungen zur Umxanthogenierung von Cellulosexanthogenat. Faserf. Textiltech. **1966,** 17, (12), 551-558.

[6] Philipp, B.; Dautzenberg, H., Untersuchungen zum Mechanismus der Umxanthogenierung bei Cellulosexanthogenat. Faserf. Textiltech. **1966,** 17, (1), 1-7.

[7] Phifer, L. H.; Dyer, J., Cellulose Xanthic Acid. II. Studies of Cellulose Xanthate. Macromolecules **1969,** 2, (2), 118-122.

Lenzinger Berichte, 86 (2006) 116-123

SPUNBOND CELLULOSE*

MJ Hayhurst

Lenzing AG, Werkstrasse 1, A-4860, Lenzing, Austria
E-mail: m.hayhurst@lenzing.com

*This work was presented during the 45th Dornbirn Man-Made Fibers Congress, September 2006

The benefits which cellulose fibres bring to nonwoven products are well-known. Fibre suppliers are continuously working to improve the benefit and cost-effectiveness of the cellulose contribution. As part of this strategy, direct formation of cellulose webs has long been a subject of research, but this approach has not so far delivered products with a significant commercial impact.

Lyocell is a relatively new technology, used for the commercial production of cellulose staple fibre (TENCEL®, from Lenzing). The fibre offers a broad range of benefits and has gained wide acceptance for both textile and nonwoven applications.

In principle, lyocell technology should also be well-suited to the requirements of a direct cellulose web formation process. Results from initial laboratory-scale investigations were published several years ago. These indicated technical viability, but the work was not pursued due to uncertainties over cost-effectiveness.

The recent integration of Lenzing and TENCEL® has provided the opportunity to combine expertise and re-evaluate interesting projects. This paper presents results which demonstrate the potential to produce, directly from lyocell spinning solutions, a wide range of web attributes.

Keywords: *lyocell, cellulose, nonwoven, web, spunbond, meltblown*

Introduction/Background

This paper will discuss the latest developments in a new fibre formation technology which, potentially, could deliver directly-formed cellulose webs with attractive, spunbond-like, properties.

The benefits of cellulose in nonwoven web applications are well known. These include absorbency, purity, softness, opacity and biodegradability. In addition, man-made cellulose fibres as feedstock offer a very high degree of product consistency.

A key question is how to maximise the benefit and cost-effectiveness of the cellulose fibre contribution. The two main approaches are:

- Develop fibre engineering/staple conversion efficiency to web
- Direct web formation

Considerable advances have been made in cellulose fibre engineering/conversion efficiency in recent years**,** but there has been relatively little published activity on direct web formation. This paper will focus on direct formation of cellulose webs. The new technology to be described could deliver new property/performance ranges for cellulose webs & hence open up new product application areas.

Direct formation of cellulose webs is not a new idea. For example, the British company Courtaulds experimented with viscose-based spun laid technology during a 10 year period some 35 years ago:

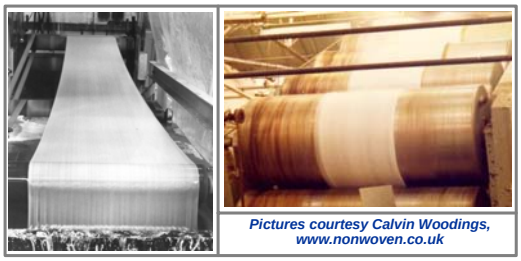

Pictures courtesy Calvin Woodings, www.nonwoven.co.uk

1m webs were successfully produced at pilot scale, but the project was not pursued as production cost estimates were not favourable.

Some successful niche businesses have been developed for directly-formed cellulose webs, in particular, Asahi's range of Bemcot webs, derived from a cupro filament process. However, the overall impact on the nonwovens industry has been limited.

By contrast, direct web formation from synthetic polymers, via technologies such as meltblow and spunbond, has developed into a major business.

SYNTHETIC MELTBLOWN	SYNTHETIC SPUNBOND
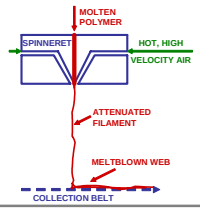	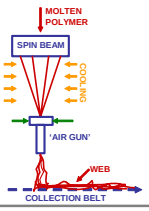
Attenuation of filaments by high velocity, (usually) hot air	Cooling of as-formed filaments, subsequent stretch
Generally microfibre/low basis weight and high bonding. Applications such as filtration and insulation. Low filament strength.	Generally stronger with 'textile' aesthetic. Used in broad range of applications, eg coverstock, geotextiles

The market size for directly formed synthetic webs was estimated at approximately 1.8m tonnes in 2004, ~40% of the 4.4m tonne total rolled goods market. There is increasing use of spunbond/meltblown composite webs to take advantage of product benefits from both technologies

Could there be similar potential for directly formed cellulose webs? This paper will consider the potential of adapting lyocell technology for direct cellulose web production.

The Potential of Lyocell Technology

TENCEL®

The production of lyocell staple fibre has been commercial for over 15 years. It is better known as TENCEL®, from Lenzing AG. The product benefits, for both textile and nonwoven applications are well established. For example:

- **Aesthetic**: comfort, softness, breathability, purity
- **Performance**: strength (especially wet), moisture management, controllable fibrillation, sensitive skin applications
- **Environment**: biodegradable, sustainable raw materials & production route

The manufacturing route involves the direct dissolution of cellulose woodpulp in a special solvent, N-

methylmorpholine N-oxide, followed by extrusion & stretching of the hot filaments in a short 'air-gap'. This is followed by removal of residual solvent and final preparation of the staple fibre. The manufacturing route has low impact on the environment, particularly due to the very high levels of solvent recovery achieved.

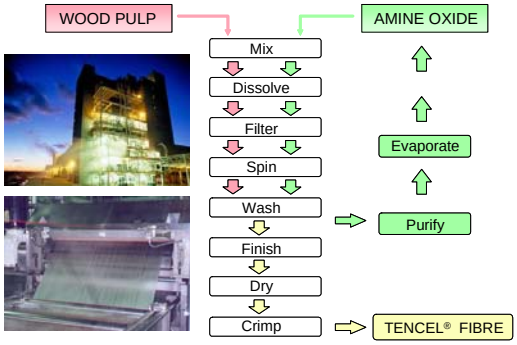

The spinning solution is a clear, pale brown, thermoplastic material. It has similarities in flow properties with polymer melts. In principle, therefore, it should be possible to use this material, modified if necessary, as a feedstock for direct web formation technologies such as meltblow.

Previous studies of lyocell technology for web formation

In the period 1996-2001, TENCEL® and others (e.g. Spontex, Weyerhaeuser & TANDEC) published the results of initial feasibility studies on meltblowing lyocell solutions. The technology is similar to that employed for synthetic polymers, but with the addition of a 'filament coagulation' step. (Only up to ~15% of the spinning solution is cellulose. Solvent must be removed to form filaments).

The key findings *(reference 1)* were:

- Potential to produce fine microfibre cellulose webs directly
  - Predicted good web opacity, thermal properties, filtration performance, moisture management, comfort/ softness
- Filaments stronger than meltblown synthetics
  - Cotton like morphology: natural crimp, variable diameter, pebbled surface
  - 'Continuous' filaments: low linting
- Effect of process variables on product properties similar to that seen with synthetics
- Potential to modify web properties via filament coagulation

It was concluded that the technology produced very interesting products at laboratory scale, in particular the ability to produce fine microfibre webs. However, in-house estimates by TENCEL® of scale-up and implementation costs suggested that products would not be economically attractive. So, in 2001, the project was suspended. Following this, there has been little published activity in this field until recently.

Current Research

Published Activity

There is now significant new published information Worldwide *(reference 2)*. Several manufacturers of web forming machinery have recently announced that they are developing meltblow-type equipment suitable for use with lyocell dope and have pilot-scale facilities:

- Reicofil, with Weyerhaeuser & Fraunhofer Institute
- Nanoval, with TITK
- Biax Fiberfilm

Some of these systems incorporate innovative variations on 'benchmark' technology. This activity suggests a

broad-based belief that the technology could become commercially viable.

Overview of Lenzing Research

In parallel, TENCEL® joined Lenzing AG in 2004. This provided the opportunity to combine expertise and re-evaluate interesting projects. For meltblown lyocell technology, Lenzing has implemented a programme to better understand the process fundamentals and characterise product opportunities.

The studies have demonstrated that a remarkable range of web properties can be achieved via relatively minor changes to process conditions. In particular, although the process has much in common with traditional meltblow technology, products more associated with **spunbond** technology can readily be produced. Benefits of a cellulose substrate are retained.

Filament Properties

It is well-known that individual filament tensile strength of synthetic meltblown fibres is lower than equivalent staple fibres. It has also been reported that cellulose filaments based on meltblown lyocell technology have lower strengths than equivalent TENCEL® staple. Whilst this is certainly generally true (filament tensiles around 25cN/tex/25% typical from lab-scale results at 1.5dtex), Lenzing's studies have shown that, by modification of process conditions, a wide range of strength/extension combinations can be accessed. For ease of comparison with staple fibres, results below are for filaments around ~1.5dtex:

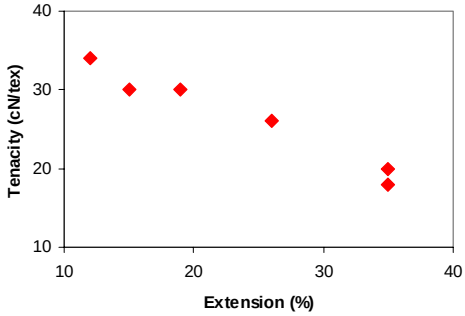

Good tensile performance has also been obtained for microfibres, eg. 30cN/tex tenacity at 20% extension for 0.6dtex filaments.

Clearly, there are difficulties in obtaining precise single filament data from inherently variable meltblown fibres in webs, but the data illustrates interesting trends.

Another 'generic' feature of synthetic meltblown webs is high variability in filament diameters. Again, this is also often the case with the meltblown lyocell product, although Lenzing's results suggest there are process conditions where very good uniformity may be obtained:

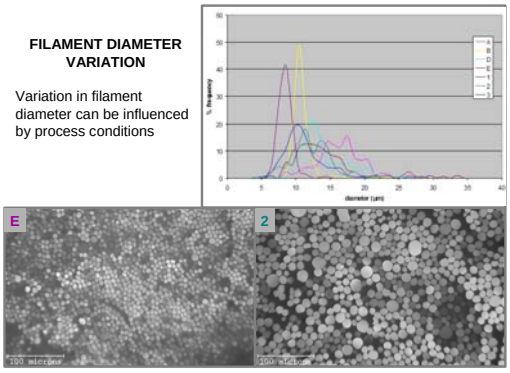

As might be expected, the process conditions which favour improved strength and filament uniformity also tend to reduce productivity.

Web Properties

Of course, the key product indicator is web performance. For ease of comparison with known products, data for webs based on ~1.5dtex/50gsm is presented. Tensile data:

	Meltblown Lyocell	Spunlaced TENCEL®
Web Strength, dry. MD/CD (N)	~75/60	~85/95
Web Extension, dry. MD/CD (%)	~20/20	~30/35
Web Strength, wet. MD/CD (N)	~65/55	~85/80
Web Extension, wet. MD/CD (%)	~25/30	~30/35

Web tensiles are lower than achieved for equivalent spunlaced TENCEL®, but are sufficient for practical applications.

Moisture management properties of meltblown lyocell webs seem close to those of equivalent spunlaced TENCEL®:

	Meltblown lyocell	Spunlaced TENCEL®
Maximum Absorbency Rate (g/s)	~0.3	~0.3
Dynamic Absorbency Capacity (g/g)	~7	~7.5
Water Sorption under pressure (front/back, g/g). GATS	6.5/6.5	8/8
Wicking (MD/CD, mm, 300s) DIN53924	120/120	120/120

GATS = Gravimetric Absorbency Test

The first two methods in the table are in-house tests, developed to provide an indication of performance when only small sample sizes are available.

Influence of Filament Coagulation Conditions

To illustrate the flexibility of the technology, results from 3 variations in process conditions will be presented. As mentioned earlier, a key difference between lyocell and melt polymer systems is that, for lyocell, only a minority component of the spinning solution is the polymer of interest (cellulose). Most of the remainder is solvent, which must be removed and recycled.

There are several options as to how and where the initial solvent removal step can be carried out:

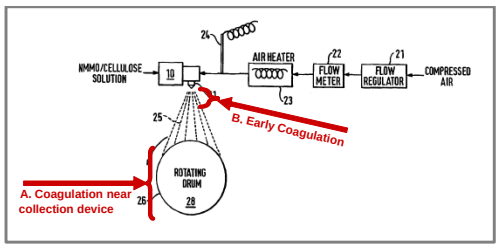

In example A, initial solvent removal occurs on or near the web collection device, allowing a high degree of filament bonding. By contrast, in example B, at least part of the solvent removal occurs early between filament formation and web collection, producing a low degree of filament bonding. Finally, example C is an 'intermediate coagulation' product, between A and B.

All three examples are fine microfibre webs. For comparison, results from a 1.7dtex staple/50gsm commercial TENCEL® web are included:

Trial Set	Degree of filament bonding	Web weight (gsm)	Equivalent average filament decitex
A	High	30	0.2
B	Low	30	0.2
C	Medium	15	0.1
Spunlaced Tencel staple	'Low'	50	1.7

Solid-state NMR techniques have been used to characterise cellulose crystallinity (Bruker Avance 300mHz NMR multinuclear spectrometer, equipped with Cross-Polarisation Magic Angle Spinning accessory). The NMR spectrum shows peaks due to the different atom positions around the glucose ring. Some of these peaks, particularly C4, exhibit secondary shifts characteristic of crystal type. A detailed explanation of the technique is beyond the scope of this paper, interpretation of spectra is a subject of continuing debate in academic literature. However, key findings so far for the cellulose web samples can be summarised:

FIBRE CRYSTALLINITY
Solid state NMR

Sample	Crystallinity Index (%)
A – meltblown lyocell, high bond	30
B – meltblown lyocell, low bond	33
TENCEL®	34
Viscose	20

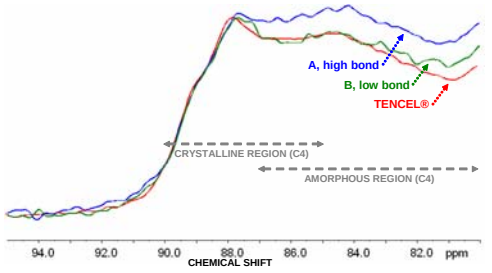

As can be seen, the 'low bond' sample has crystallinity very similar to

TENCEL®, whereas the 'high bond' sample has a significantly lower 'Crystallinity Index'. Such a result might be expected from the differences in attenuation/coagulation conditions.

The webs have very different appearance and aesthetic. A (high bond) has a shiny surface and a crisp, paper-like texture whereas B (low bond) looks and feels much more like a textile fabric. Sample C (intermediate bond) also looks and feels like a textile product.

Examining the web samples via scanning electron microscopy (Hitachi S-4000 SEM, acceleration voltage 5keV) provides a good explanation of the product differences and illustrates the profound influence of manufacturing conditions very well.

The first set of pictures, at relatively low magnification, clearly shows how surface filaments on the 'high bond' sample have fused, forming a surface film in some areas. This effect has been reported by several other research groups. By contrast, the 'low bond' and 'medium bond' samples are composed of discrete filaments. The pictures show the microfibres very well, in comparison with existing commercial product. The ability of microfibres to deliver high uniformity of cover can clearly be seen:

1) 'Overview' (500 micron scale)

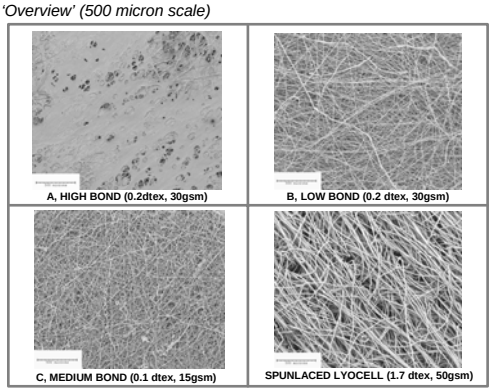

At higher magnification, differences in filament 'interactions' can be seen. For the 'high bond' sample, below the surface 'film', there appears to be a network of highly cross-linked filaments. The filaments in the 'low bond' sample are generally unfused. In this picture, there is some suggestion of twisted filaments. As might be expected, the 'medium bond' sample appears to be intermediate: discrete filaments fixed by fusion at connection points. Of course, there is no fusion on web sample derived from staple fibre:

2) Web structure (50 micron scale)

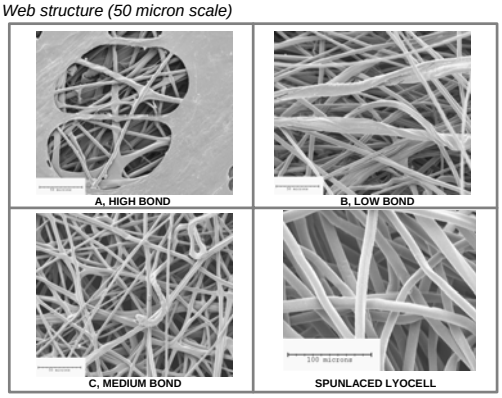

At the highest magnification, filament surfaces may be examined. All the meltblown samples seem to offer the smooth, generally round cross-section characteristic of lyocell staple fibre. This compares with the crenulated cross-section found with viscose:

3) Filaments (10 micron scale)

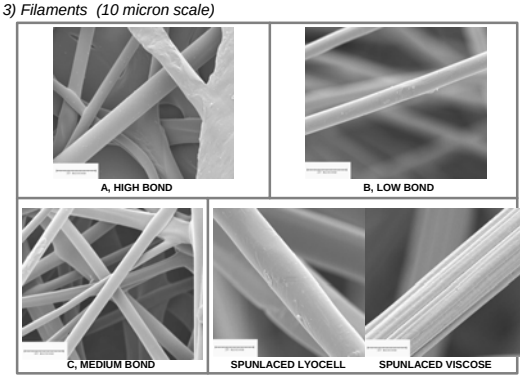

Overall, these seem very interesting results which emphasise the potential flexibility of the technology.

Conclusions

Product Features

- Performance normally associated with spunbond products can be achieved
- Microfibre webs at low basis weights may be produced, delivering high coverage & consistency
- A wide range of web performance may be delivered. This includes variations in tensiles, cohesiveness, aesthetic and porosity. Manipulation of the initial coagulation step is a particularly effective route to modify web performance
- Expected cellulose continuous filament benefits are obtained. These include hydrophilicity, absorbency, fast wicking, wet strength and very low linting
- Acceptable web tensile performance is achieved

In comparison with other web products the technology offers a number of potential complementary feature, eg:

Compared to synthetics:

- Comfort/softness, moisture management/wet strength, temperature stability

Compared to staple-based webs

- Low lint, excellent coverage/low basis weight

The Future

Considering the future commercial potential, meltblown lyocell technology is still embryonic, but the products so far obtained are very interesting.

The key to success will be the price at which attractive new products can be delivered on a commercial basis. This assessment is currently being carried out. Factors to consider include:

- Current cellulose fibre production and conversion routes are very efficient
- New technology will be capital intensive

Although pilot scale research facilities are now operational, there remains a very large amount of development work to assess whether this promising technology can be cost-effective.

The most likely route to implement would take advantage of the fine microfibre web capability.

Lenzing is well placed to implement the technology, should current assessments prove successful, by offering a blend of lyocell expertise/rights/capacity and fundamental product knowledge combined with nonwovens market experience.

Acknowledgements

Dr T Steindl, Dr M Einzmann, Dr M Fasching, Dr G Kandioller of Lenzing AG for analytical measurements/ interpretation & advice.
Mr C Woodings, for providing information concerning history of directly formed cellulosic webs (www.nonwoven.co.uk).
Dr S Law, now of ConvaTec, for helpful discussions concerning original TENCEL® feasibility assessments.

References

1) *For example:*
WO9701660 (Spontex/Lenzing)
WO9826122/WO9964649
(Tencel/Lenzing)

US6306344/6596033/6511930/ 6221487 (Weyerhaeuser).
Meltblowing of amine-oxide based lyocell solutions: a preliminary investigation, S Lam. J Textile Inst, 2001, 92 part 1, no.4

2) *For example:*
US20050056956,WO20051060085, Nonwoven Markets 19/17 (Biax Fiberfilm)
WO02052070, Tech. Textilien 1/2006, 7th Int. Symposium 1 "Alternative Cellulose" TITK Sept '06 (Nanoval/Gerking/TITK)
Nonwovens Markets 13/7/06, Chemical Fibers International 4/2006, US7067444, 7th Int. Symposium "Alternative Cellulose" TITK Sept '06 (Reicofil/Weyerhaeuser/ Fraunhofer Institute)
Meltblown lyocell: influence of solution characteristics on fibre properties, S Lam J Textile Inst, 2006, 97, no.

Lenzinger Berichte, 86 (2006) 124-131

CELLULOSE MELTBLOWN NONWOVENS USING THE LYOCELL-PROCESS

H. Ebeling[1], H.-P. Fink[1], M. Luo[2], and H.-G. Geus[3]

[1] Fraunhofer-Institute for Applied Polymer Research, Potsdam-Golm, Germany
[2] Weyerhaeuser Comp., Federal Way, WA, USA
[3] REICOFIL GmbH & Co. KG, Troisdorf, Germany

Lecture given at the 7th International Symposium "Alternative Cellulose – Manufacturing, Forming, Properties", September 06-07, 2006, Rudolstadt, Germany

Today, cellulosic nonwovens are mainly produced from viscose and lyocell staple fibres using various bonding processes. The meltblow process as an alternative technology has been used so far for the production of nonwovens from synthetic polymers. Progress in the development of the lyocell technology made it possible to produce meltblown nonwovens from cellulose as well. Recently, the Weyerhaeuser Comp. has patented an appropriate meltblowing method with high hemicellulose (hemi) pulp as raw material. The scale-up of the process was carried out in close collaboration between the Fraunhofer IAP, the Weyerhaeuser Comp., and the REICOFIL GmbH. The results which were obtained at Weyerhaeuser's on a laboratory scale were transferred to a pilot plant scale at the Fraunhofer IAP. The pilot line had a working width of 60 cm and a dope throughput of approx. 40 kg/h. Experiments were carried out with regard to the quality of the pulp and the characteristic parameters of the meltblow process. The structure of the single fibres and the mutual bonding are illustrated by SEM. Finally, the absorption and the strength of the nonwoven webs are determined using single fibres with diameters in the micro range.

Keywords: *meltblown nonwoven, lyocell, hemicellulose, electron microscopy, absorption, strength*

Introduction

Today, nonwovens have achieved an excellent position among the products of daily use (hygenics, medicine, household…). Due to excellent usage properties, such as adsorption, softness, strength, cellulose fibres play an important role as basic material. Cellulosic nonwovens are mainly produced from viscose and lyocell staple fibres through dry or wet fleece processes with different bonding procedures. The production of fibres and nonwoven fabrics are separate processes.

Since its beginnings at the end of the sixties the meltblow process has become an alternative to the classic fleece forming processes. It is used for the production of microfibre nonwovens based on synthetic polymers, such as polypropylene and polyester. An outstanding characteristic is the single-step process including polymer dosage as well as packaging of the nonwoven. Figure 1 shows the cross section of a meltblown die (Exxon type).

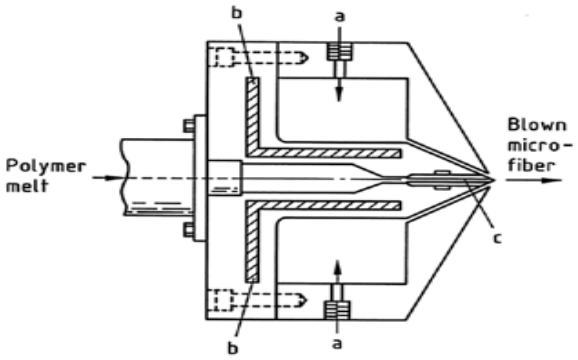

Figure 1. Meltblown die – Exxon type [Ullmann's Enzycl. Ind. Chemistry].
a) hot air inlet; b) heating plate; c) capillary tube

The so-called „Bemliese" process with direct fleece formation from cotton linters using the cupro-ammonium-process is one of the first spin fleece processes for the production of cellulosic nonwovens from continuous filaments [1].
From the early nineties, much endeavour has been made to develop a technical process for the production of meltblown nonwovens based on the lyocell process, and many patents have been filed in this field [2-5].
In recent publications, the companies Biax Fiberfilm [6] and Nanoval [7] have reported on planned and existing pilot plants for the preparation of cellulosic nonwovens based on the meltblown technology. They used working width of 30 – 40 cm.
The present paper reports on the development of a meltblown process on a pilot plant scale where the dope preparation is based on the lyocell process. The patented Weyerhaeuser technology [2] was used for the experiments which were carried out in close collaboration between the Fraunhofer IAP, the Weyerhaeuser Company, and the REICOFIL GmbH. Thus, three specialists in this field combined their know-how to scale-up and develop an industrial cellulose meltblown nonvowens technology: the pulp producer Weyerhaeuser, REICOFIL as an experienced company in the field of melt blown technology with more than 100 lines sold worldwide, and the Fraunhofer IAP with its experience in lyocell research. The experiments were carried out at the Fraunhofer IAP using the existing lyocell pilot plant which was modified by an additional meltblown nonwovens line.
In the following, the transition from the lab scale to the pilot plant scale is described, also the optimisation of crucial process parameters and the effect of pulp quality. The obtained material is characterised with regard to fleece structure, absorption and strength

Meltblown Pilot Plant

Figure 2 gives an overview of the equipment and performance parameters of the plant working in the Fraunhofer IAP.

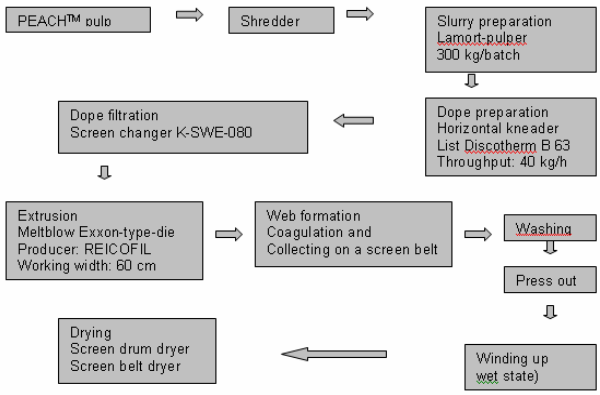

Figure 2. Steps and equipment of the lyocell meltblown nonwoven plant.

The basic principle for the dope preparation including shredding, swelling, dissolving, and filtration is the lyocell technology. In the continuous process up to 40 kg/h of dope can be produced. The pilot plant is combined with a two-stage solvent recovery.

Figures 3 and 4 show the meltblown die and the winding-up equipment for the wet (never dried) fleece.

Figure 3. Meltblown-die.

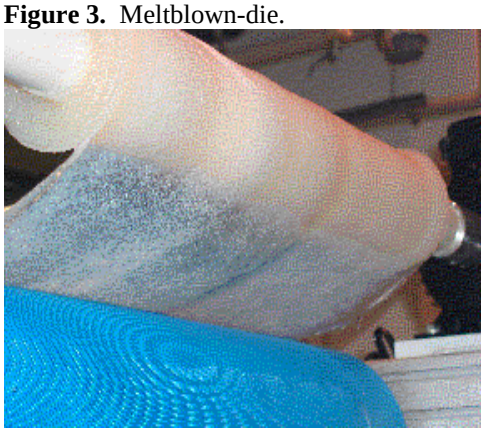

Figure 4. Running meltblown plant winding up the wet nonwoven web.

Scale-up of the Die

Prior to all experiments the following questions had to be answered:
(1) Is the process behaviour of a lyocell dope comparable to that of a PP melt?
(2) Does the die work with the same space between the holes?
Basic tests were carried out with a 12 cm die and a low hole density. Scale–up finally resulted in a die from REICOFIL with high hole density and a working width of 60 cm.
The following results were obtained from experiments with different dies:
(1) There is a suitable adjustment of the geometric parameters where the dies run steady and independent of the space between the holes.
(2) With decreasing space between the holes a clear tendency to adhesion of the fibres is observed. The tendency to adhesion increases with the throughput. The diameters of the adhered fibres are many times higher than the lowest values obtained for single fibres.
A possible reason for the adhesions might be die swelling at the outlet of the die.
In order to assess the die swelling under process conditions, a 7.5 % lyocell dope was extruded through a 400 µm die hole with a ratio of l:d = 6. The throughput was varied from 0.25 to 2.0 g/hole/min and the die swelling was observed. Figure 5 shows a 4 mm filament section just behind the die.
Figure 6 shows the fibre diameter as a function of the dope throughput.
For high throughputs the diameter of the single fibre is almost twice the hole diameter of the die.

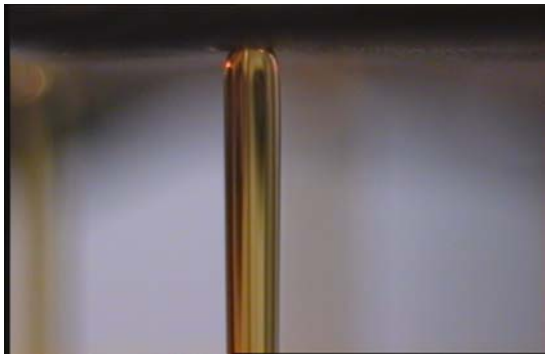

Figure 5. Die swelling during the extrusion of a NMMO dope.

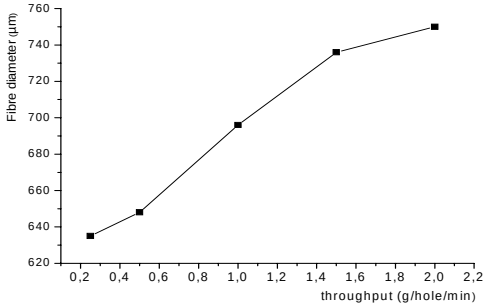

Figure 6. Die swelling as a function of the throughput.

PEACH^{TM} – the Tailor-made Pulp

The pulps for the lyocell process are commercially available from Weyerhaeuser (PEACH^{TM} pulp, [12]). They are characterised by higher

contents of hemicellulose compared to traditional dissolving pulps.

The main advantages of the novel PEACH™ pulp are:
(1) high yield in the pulp production process
(2) high content of hemicellulose which leads to special properties
(3) low cost

The degree of polymerisation (DP) should be low for processes using the meltblow technology to keep down the dope viscosity. PEACH™ pulps were tested with reference to a softwood PHK dissolving pulp.

Table 1. Parameters of the tested pulps.

pulp parameter	softwood PHK (ref.)	Peach A	Peach B	Peach C
DP (cuen)	844	862	754	673
R 18 [%]	97.3	88.4	88	85.6
R 10 [%]	91.9	84	82.5	81.3
nonwovens				
DP (cuen)	775	785	689	613
R 18 [%]	97.1	87.6	-	-

There was no significant difference between the dissolving pulp and the PEACH™ pulp. Pulps B and C show lower dope viscosities, which allows the use of higher concentrations.
Hemicellulose components could be observed in the fibres in the same order of magnitude as in the PEACH™ pulp.

Process Conditions

Parameter

One purpose of the meltblown process is the production of nonwovens based on very low denier fibres, i.e. fibres with a diameter < 10 µm and < 1dtex, respectively. Spinning such cellulose fibres makes heavy demands on the process of fibre production.
In the meltblown process fine fibres are obtained under the following conditions:

- Low cellulose concentration in the dope
- High dope temperature
- Low DP
- Low throughput per orifice
- High temperature and flow speed of the hot blow air

The first three items decrease the dope viscosity. In combination with a high temperature of the blown air this supports filament drawing and thus the spinning of micro fibres. Low cellulose concentrations and a low throughput per orifice, however, reduce the capacity of the nonwoven line.
Due to the decomposition of cellulose/NMMO spinning solutions which is described in [8], the increase of the dope temperature is limited.

Coagulation and Structure

Coagulation between die and conveyor belt is also a process parameter which affects the properties of the single fibres and non-woven fabric. Using melted polymers the cooling-down of the dope strand is caused by the ambient air, the solidified filaments are collected on the conveyor belt as random web.
The structure formation for lyocell meltblown nonwovens should be comparable to the dry/jet-wet process for the preparation of lyocell fibres [9]. The extruded filament is drawn to a multiple by the hot blow air, subsequently it is coagulated by spraying water or a mixture of water and NMMO. In this stage, a part of the solvent is washed out. Practical tests have shown that films are formed when the dope strand is not sprayed with water. The objective must be to coagulate the dope strand in such a way that a self-bonded nonwoven is formed without distinct adhesions of single fibres.
The effect of the coagulation conditions on structure formation was investigated by electron microscopy.

Various cellulosic meltblown nonwovens were examined with regard to the variation of the coagulation parameters.

Experimental

Scanning electron microscope (JSM 6330F, Jeol): Dried samples were examined. To avoid electrical charging of the samples, the fleeces were coated with a thin Pt – layer (thickness 4 nm). The micrographs were taken at an acceleration voltage of 5 kV.

Transmission electron microscope (CM 200, Phillips): Never dried fibres were embedded after the exchange of water by ethanol into a matrix of methyl/butyl-methacrylate. After polymerisation of the matrix, ultra-thin cross sections (thickness approx. 60 nm) were prepared (Ultra-cut S, Leica) and investigated at 120 kV.

Results

The EM-micrographs show that

- fibre diameters scatter considerably. The higher values for the diameters can be explained by the adherence of single fibres (Figure 7 and 8).
- A skin-core structure was observed (Figure 9). The skin gets thicker with increasing coagulation: for intensive coagulation 300 nm and for weak coagulation 0-125 nm
- The pore diameter increases in both, the skin and the core region, with increasing coagulation:

intensive coagulation:

skin 30 – 80 nm
core 30 – 130 nm

weak coagulation:

skin 10 – 50 nm
core 20 – 50 nm

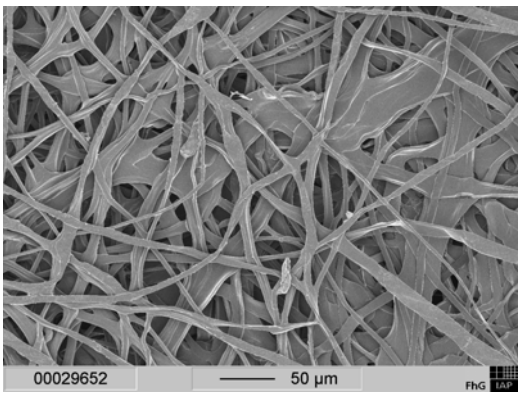

Figure 7. SEM–micrograph of a meltblown fibre fleece.

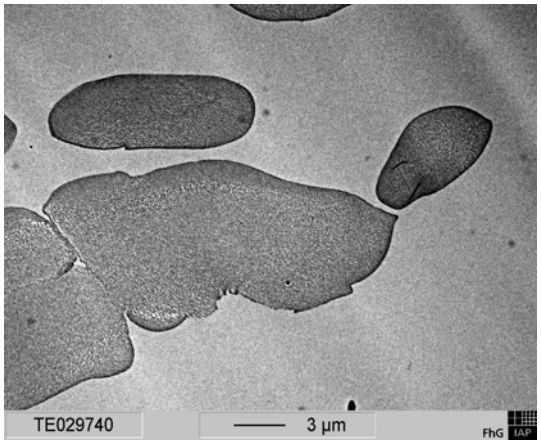

Figure 8. TEM–micrograph of adhered single fibres.

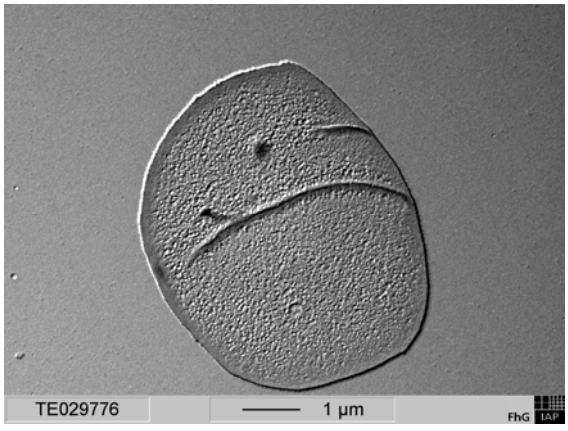

Figure 9. TEM–micrograph of a cellulose MB-fibre with a skin-core structure.

Properties of the Nonwovens

Tensile strength and absorption were chosen as characteristic parameters to describe the properties of the fleece. The determination was carried out using the recommended nonwoven test methods of EDANA:

Nonwovens tensile strength 20.2 – 89

Nonwovens absorption 10.4 – 02

Tensile strength

To characterise the behaviour throughout the production process, the wet initial samples were tested, further measurements were carried out using dried and rewetted samples after conditioning. The Universal Test Device ZWICK 1445 was used for the determinations for both samples in machine (MD) and cross (CD) direction.

For the wet initial fleeces with different mass units per area the following strength and elongation values were obtained (diameter of a single fibre: 8 – 12 µm).

Table 2. Strength and elongation of wet initial fleeces.

Weight (g/m²)	Strength (N/m)		Elongation (%)	
	MD	CD	MD	CD
22	110	95	19	36
45	140	124	21	45
65	175	156	25	29

The strength of the wet initial fleeces is sufficient for the transport through the production line. Also with water contents in the range of 1000 % winding-up was still possible without tearing the web.

Figure 10 shows the strength of dried and rewetted samples for different basic weights.

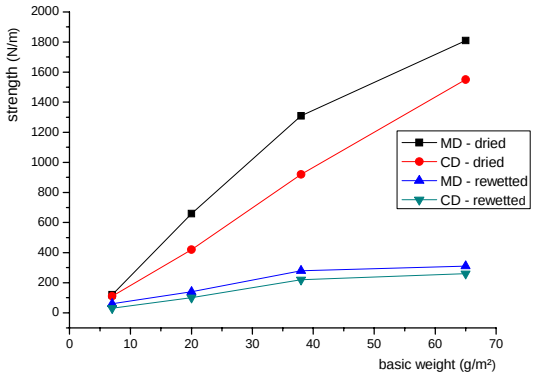

Figure 10. Strength of nonwovens as a function of basic weight.

The production of wipes (Durables) requires a maximum tensile strength of 1600 N/m for basic weights > 100 g/m² [10]. This quality can also be attained by cellulose meltblown nonwovens as is shown in Figure 10.

The elongation of the dried fleeces was between 10 and 20 %. Measurements in cross direction show a trend to higher values. In the rewetted state the same samples show elongations of about 25 % in machine direction and in cross direction of about

30 – 40 %.

Absorption

The absorption of water into fibres and the respective formed fabrics is mainly affected by the polymer matrix and the process conditions.

Until now, microfibre nonwoven fabrics have been produced from synthetic polymers using the meltblow technology. As regards absorption these fabrics are inferior to cellulosic fabrics.

The absorbencies of the obtained cellulose meltblown nonwovens were characterised using the recommended methods of EDANA:

- Liquid absorptive capacity: ISO 9073-6:2000
- Liquid wicking rate: ISO 9073-6:2000
- WRV: DIN 53814

The water retention of all produced nonwoven webs is in the range of 120 – 170 %.
In Figure 11 the water liquid absorptive capacity of cellulose meltblown nonwovens is compared to values for hydroentangled nonwovens taken from the literature [11]. The values are similar to those of fabrics which were obtained from viscose or lyocell staple fibres through the classical procedures of fleece formation.
A similar coincidence was found comparing the liquid wicking rates of the different cellulosic nonwoven fabrics [11] (Table 3).

Table 3. Liquid wicking rates of cellulosic nonwoven (NW) fabrics.

	Wicking rate 300 s (mm)
Cellulose MB-NW	120
Hydroentangled viscose NW	120
Hydroentangled lyocell fibre NW	105

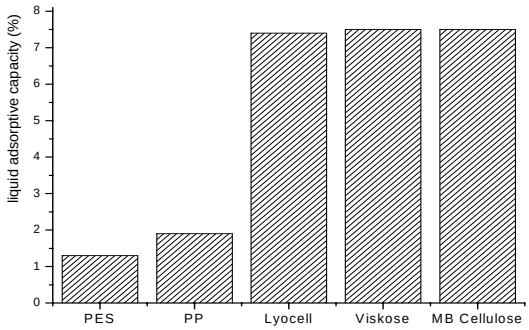

Figure 11. Liquid absorptive capacity of cellulose meltblown nonwovens compared to various hydroentangled nonwovens.

Figure 12 shows the wicking rate as a function of the coagulation conditions. The coagulation in the dope strand is compared to the coagulation on the conveyor belt.

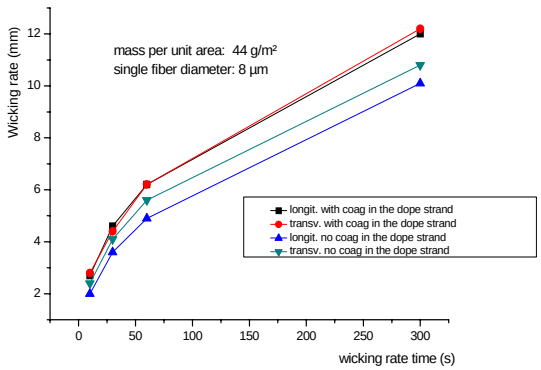

Figure 12. Liquid wicking rate as a function of coagulation.

The more intensely coagulated samples show significantly higher wicking rates. This is confirmed by the values for the liquid absorptive capacity. The value for the samples coagulated in the dope strand is higher by 115 % (from 630 to 745 %).

Conclusions

In close collaboration the Fraunhofer IAP, the Weyerhaeuser Company, and the REICOFIL GmbH developed a technology for the production of lyocell based cellulose meltblown nonwovens. Scale-up was carried out up to a pilot plant scale. The pilot plant with equipment for dope preparation (List-technology), Exxon type die (Reifenhäuser), washing and winding up equipment had a working width of 60 cm. The production period from pulp feeding up to the final product was approx. 3 hours. The properties of the novel cellulose meltblown nonwovens from Kraft PEACH^{TM} pulp are comparable to classic cellulose nonwoven fabrics deriving from staple fibres. Cellulosic microfibre nonwovens can now be produced by means of the meltblow process.

Acknowledgements

The authors would like to thank the Fraunhofer-Gesellschaft for financial support in the initial stage of this project via the MAVO program. Subsequent financial support (FKZ 22010204) of the German Agency for Renewable Resources (FNR) is also gratefully acknowledged. The authors are grateful to Dr. Pinnow from the Fraunhofer IAP for the TEM and SEM investigations.

References

[1] K. Nishiyama, Proceedings „Cellulosic Man-made Fibers“, Singapore 1997.
[2] EP 0920548 (Weyerhaeuser).
[3] US 6358461 (Accordis).
[4] DE 10065859 (L. Gerking).
[5] US 2005/0056956 (Biax Fiberfilm Corp.).
[6] Nonwoven Markets 19, Nr.17 (2004).
[7] Techn. Textilien 1/2006 S. 41.
[8] T. Rosenau, A. Potthast, H. Sixta, P. Kosma: Progr. Polymer Sci. 26 (2001) 1763-1837.
[9] H.-P. Fink, P. Weigel, H.J. Purz, J. Ganster: Prog. Polym. Sci. 26 (2001) 1473-1524.
[10] W. Albrecht, H. Fuchs, W. Kittelmann, in Vliesstoffe (Wiley-VCH) (2000), S. 507.
[11] J. Schmidbauer, M. Einzmann, B. Schachtner: Techn. Textilien 1/2006, S. 20.
[12] U.S. 6692827 (Weyerhaeuser).

Lenzinger Berichte, 86 (2006) 132-136

CRYSTALLINITY DETERMINATION OF MAN-MADE CELLULOSE FIBERS – COMPARISON OF ANALYTICAL METHODS*

Thomas Röder[1], Johann Moosbauer[1], Mario Fasching[2], Andreas Bohn[3], Hans-Peter Fink[3], Thomas Baldinger[1], and Herbert Sixta[1]

[1]Department Zellstoff-Forschung, Lenzing AG, Werksstrasse 1, A-4860 Lenzing, Austria
Phone: (+43) 07672-701-3082; Fax: (+43) 07672-918-3082; E-mail: t.roeder@lenzing.com
[2]Kompetenzzentrum Holz GmbH, St.-Peter-Str. 25, A-4021 Linz, Austria
[3]Fraunhofer-Institute for Applied Polymer Research, Geiselbergstraße 69, D-14476 Potsdam-Golm, Germany

* This work was presented during the 9th European Workshop on Lignocellulosics and Pulp (EWLP) 28th-30th August, Vienna, Austria

Fiber properties (tenacity, elongation, and modulus) of man-made cellulose fibers are depending on their inner structure. Changes in fiber structure result in changes in fiber properties and vice versa. The crystallinity is one of these structural parameters. Native cellulose (e.g., wood, pulp, cotton, kenaf, bacteria cellulose) consists of the cellulose I, regenerated cellulose consists of the cellulose II modification.
WAXS (wide angle X-ray scattering) is the standard method for the determination of crystallinity of man-made cellulose fibers. This method was established by Hermans and Weidinger in 1949 [1].
Nowadays the information concerning crystallinity of cellulose II can be obtained by other methods as well, e.g. Fourier Transform (FT) Raman, FT-infrared (IR), or solid state ^{13}C NMR (nuclear magnetic resonance) Spectroscopy.
An extensive matrix of cellulose II samples from different sources was investigated using the methods mentioned above. The results were compared with those of the standard WAXS method.

Keywords: *FT-Raman, cellulose fiber, crystallinity, NMR, WAXS, FT-IR*

Introduction

Cellulose deformation without strong degradation needs a dissolution/ derivatization with a subsequent regeneration step. The resulting cellulose changed crystalline modification from cellulose I into cellulose II. Depending on the solvent system and on the regeneration process parameters the ratio of crystalline and amorphous regions in the cellulose can vary within a wide range. This ratio is an important parameter correlated with accessibility, reactivity, and mechanical properties, i.e. the processability of cellulose fibers.

In 1949 Hermans and Weidinger [1] published their procedure for crystallinity determination from WAXS data. Up to now quite a number of methods are available for the determination of cellulose crystallinity based on WAXS experiments [2-4]. Today WAXS is still used as the standard method. Nevertheless, WAXS is expensive, time-consuming, and needs well maintained equipment. The information concerning crystallinity of cellulose can be obtained by other methods as well: solid state ^{13}C NMR spectroscopy [5], IR spectroscopy [6], and Raman spectroscopy [7].

Experimental

Methods

WAXS measurements were done in symmetric transmission with a two-circle diffractometer D5000 (Fa. Bruker-AXS, Germany). Cu-K_α radiation (with Ge(111) as monochromator) was used (30 mA, 40 kV, 2theta with 4-104° in 0.2° steps). The scattering curves were corrected concerning absorption, polarization, Compton, and parasitic scattering [3, 4].

NMR Experiments were performed on a Bruker 300 MHZ DPX spectrometer equipped with a 7 mm CP-MAS probehead. For ^{13}C CP-MAS experiments 1000 scans with 2k time domain data points were acquired at 26 °C using a contact time of 1 msec, a recycle delay of 3 sec, and a spinning rate of 4000 Hz. The high field peak of adamantan at 29.5 ppm was used for referencing. Prior to Fourier transformation a line broadening of 20 Hz was applied. Cellulose II samples (fibers) were measured without any sample pretreatment by rolling the fibers into small balls and packing them into a 7 mm zirconia MAS rotor. The crystallinity index CrI was calculated from the spectral region representing the C-4 carbon in the anhydroglucose units using a spectral subtraction procedure: A synthetic peak (center = 83.3 ppm, width at half height = 490 Hz) was interactively subtracted from the carefully phased and base-line corrected spectrum to obtain (for the C-4 area) a pure crystalline spectrum. CrI was then calculated from area crystalline / (area crystalline + area amorphous). Shape and line width of the used synthetic peak were obtained by comparison with amorphous fiber samples prepared by derivatisation and ball milling.

The IR measurements were done in transmission mode (with KBr press technique) in a Bruker IFS 66 (4000 - 550 cm^{-1}, resolution 2 cm^{-1}). Cellulose samples were cut with a scissor (<0.5 mm length). 1.5 g KBr and 5 mg sample were levigated and four pellets of 300 mg were produced and measured [6]. The area ratio of the two peaks at 1370 cm^{-1} and 2900 cm^{-1} (A1370/A2900) was used to generate the so-called IR-index. Additionally, all samples were investigated via IR measurements in ATR mode.

FT-Raman measurements were done with a Bruker IFS66 with Raman module FRA106, Nd:YAG Laser 500 mW; Laser wavenumber 9394 cm^{-1} (1064 nm), liq. N_2 cooled Ge-Detektor, 3500-100 cm^{-1}, resolution 4 cm^{-1}, 100 scans, four measurements of each sample. Two methods of calibration were used: (1) vector standardization 3500-250 cm^{-1} and (2) vector standardization over the common spectral area 3500-100 cm^{-1}.

Materials

Man-made Cellulose fibers from different sources were investigated: 9x lyocell, 9x viscose, 4x modal, 2x polynosic, 1x cupro, 1x fortisan, and 1x celsol fiber. A few samples were experimental fibers, all the others were commercial standard fibers (viscose and viscose tire cord, lyocell, polynosic, modal, and cupro) from different companies.

Results and discussion

WAXS data were used as standard for calibration and comparison. The degree of crystallinity $x_{c(WAXS)}$ was determined by the method of Ruland-Vonk with the IAP software WAXS 7. Raman and IR data were calibrated with WAXS data.

In general the calibration of IR-data (in KBr technique, Figure 1a) with WAXS showed a good correlation, except in two cases: (1) when fibers with chemical modifications on the surface were used and (2) when fibers with a higher diameter were measured (above 2.8 dtex). In case (1) IR bands of the chemical modifications were visible in the same regions used for the analysis. Therefore, an apparent increase in crystallinity was observed. In

case (2) the milling, normally used for standard pulp analysis, destroyed the fiber structure mostly perpendicular to the fiber axis. Consequently, the milling of the thicker fibers led to larger pieces.

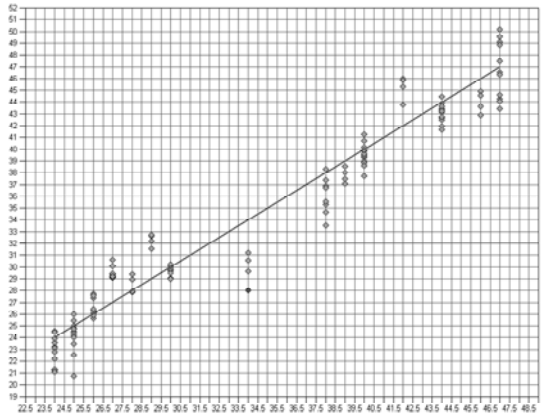

Figure 1a. Calibration of IR (KBr) crystallinity, rank 8, R^2=94.34, RMSECV=1.99.

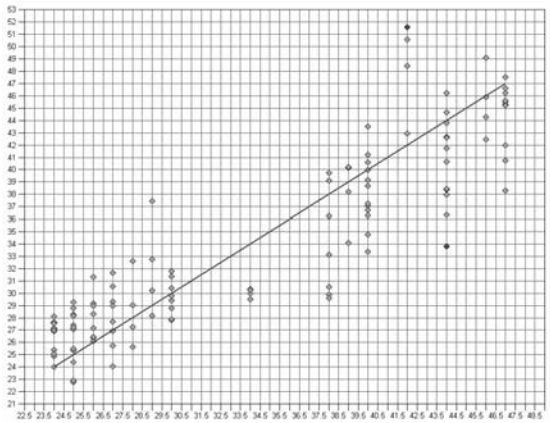

Figure 1b. Calibration of IR (ATR) crystallinity, rank 7, R^2=80.9, RMSECV=3.66.

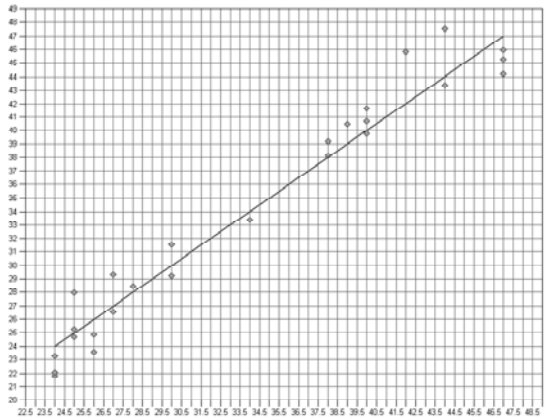

Figure 1c. Calibration of Raman crystallinity, rank 11, R^2=95.44, RMSECV=1.76.

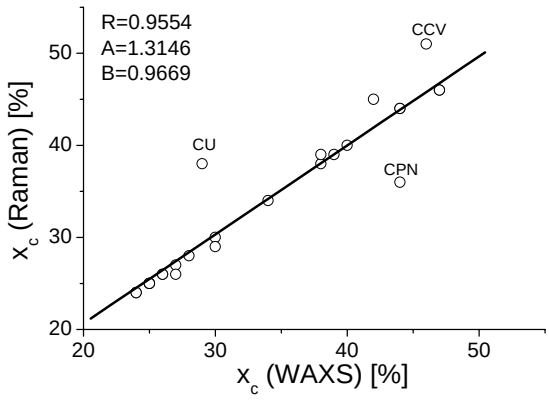

Figure 2. WAXS versus FT-Raman crystallinity.

The correlation of IR data in ATR technique with WAXS results is worse, especially for chemical modified samples (Figure 1b).

Solid state ^{13}C NMR (nuclear magnetic resonance) spectroscopy is a second method to determine the crystallinity of cellulose II without a calibration based on other methods. The NMR and WAXS methods show acceptable correlation, with WAXS typically returning higher values for the lower crystallinity materials, such as viscose. The fixing of the amorphous peak subtraction position means that surface crystalline polymer will be included in the NMR crystalline integral, which would also be included within the WAXS crystalline diffraction peak. However, there may be material of slightly lower conformational order, which appears as disordered by NMR and yet still diffracts at the crystalline peak position.

WAXS crystallinity includes all crystal material also on the surface. This leads to the decision to use WAXS as a reference. In this study NMR was used only for comparison and to get additional information.

The best correlation was observed by calibrating the FT-Raman data with WAXS results (Figure 1c and 2). In contrary to IR, effects of water content are not visible in Raman. Likewise the chemical modifications on some of the investigated fibers had no significant influence on the Raman results.

Table 1. Cellulose II matrix – fiber properties and the results of several methods of crystallinity determination with WAXS as the reference method.

Sample	titre	Tenacity (cond)	Elongation (cond)	x_C IR (KBr)	x_C IR (ATR)	x_C Raman	CrI NMR (Lenzing)	x_c WAXS (Golm)	Fiber type		
	[dtex]	[cN/tex]	[%]	[%]	[%]	[%]	[%]	[%]	Exp…experimental Com…. commercial		
1	4.86	31.3	16.6	20	56	39		39	CLY	Filament	Exp
2	2.47	38.4	13.2	34	57	38		38	CLY	Filament	Exp
3	1.03	42.6	11.4	41	57	40	34	40	CLY	Filament	Exp
4	0.73	44.2	11.7	42	58	40		40	CLY	Filament	Exp
5	1.3	40	15	46	51	40	34	40	CLY	Staple	Com
6	1.4	23.2	7.3	61	69	45		42	CLY	Staple	Exp
7	1.3	34.7	11	65	66	46		47	CLY	Staple	Exp
8	1.3	24	6	65	72	46		47	CLY	Staple	Exp
9	1.3	36	13	36	53	44		44	CLY	Staple	Com
10	1.63	17.6	24.5	25	56	34		34	CMD	Staple	Com
11	1.37	38.5	13.4	34	52	30	22	30	CMD	Staple	Com
12	1.32	42.8	15.5	28	53	27		27	CMD	Staple	Com
13	1.23	35.9	11.9	37	49	28		28	CMD	Staple	Com
14	1.43	36.9	10.9	35	54	36		44	CPN	Staple	Com
15	1.43	27.3	13.7	29	45	25	13	25	CPN	Staple	Com
16	1.8	38.2	9.7	42	51	44		44	CPN	Staple	Com
17	1.5	23.4	17.4	33	46	26		26	CV	Staple	Com
18	1.38	29	15.9	32	46	25		25	CV	Staple	Com
19	1.36	29.1	15.8	34	44	29	19	30	CV	Staple	Com
20	1.86	45.7	14.5	25	43	24		24	CV	Filament	Com
21	1.85	51.5	12.6	24	48	24		24	CV	Filament	Com
22	1.43	25.9	14.5	31	46	26		27	CV	Staple	Com
23	1.89	52.3	15.1	29	48	24		24	CV	Filament	Com
24	1.89	49	15	29	45	26	10	26	CV	Filament	Com
25	1.85	41.8	14.2	27	47	25		25	CV	Filament	Com
26	2.52	22.3	24.3	29	48	38	26	29	CU	Filament	Com
27	3.32	17	7.8	26	46	39		38	CS	Filament	Exp
28	2.85	19.8	7.7	36	50	51		46	CCV	Filament	Exp
29	0.68	23.9	3.2	46	48	46	50	47	CFN	Filament	Exp

CLY… lyocell CMD … modal CV… viscose, rayon CPN … polynosic CU… cupro

CS… celsol CCV… hydrolyzed carbamate CFN… fortisan

Conclusions

In this study, common spectroscopic methods for crystallinity determination of cellulose II, i.e. FT-Raman, FT-IR, and NMR, were evaluated and compared with the classical WAXS method. NMR was used on a few examples for comparison only. The best correlation with WAXS data was found by using FT-Raman spectroscopy. An easy sample preparation, low measuring time, and a rugged calibration with only a few outliers (no viscose, modal, or lyocell, i.e. for fibers produced by the Lenzing AG the calibration works very well) are additional benefits of this method. Therefore, FT-Raman spectroscopy is the fastest,

cheapest, and therefore for our purpose the best method to determine the crystallinity of cellulose II.

Acknowledgements

We thank Prof. H. Chancy (Grenoble, France) for the donation of the fortisan sample, Dr. F. Hermanutz (Denkendorf, Germany) for the hydrolyzed carbamate fiber.

References

[1] P.H. Hermans, A. Weidinger. X-ray studies on the crystallinity of cellulose, *J. Polymer Sci.* 4 (1949) 135-144.

[2] W. Ruland. X-ray determination of crystallinity and diffuse disorder scattering, Acta Crystallogr. 14 (1961) 1180-1185.

[3] H.-P. Fink, D. Fanter, and B. Philipp. Wide angle X-ray study of the supermolecular structure at the cellulose I – cellulose II phase transition, Acta Polym. 36 (1985) 1-8.

[4] H.-P. Fink and E. Walenta, X-ray Diffraction Investigations of Cellulose Supermolecular Structure at Processing, Das Papier 12 (1994) 739-748.

[5] W.-D. Herzog, M. Messerschmidt. NMR-Spektroskopie für Anwender, VCH Verlagsgesellschaft, Weinheim, New York, Basel, Cambridge, Tokyo (1995).

[6] T. Baldinger, J. Moosbauer, H. Sixta. Supermolecular structure of cellulosic materials by Fourier Transform Infrared Spectroscopy (FT-IR) calibrated by WAXS and ^{13}C NMR, Lenzing Berichte, 79 (2000) 15 - 17.

[7] K. Schenzel, S. Fischer, and E. Brendler. New method for determining the degree of cellulose I crystallinity by means of FT Raman spectroscopy, Cellulose 12 (2005) 223-231.

Lenzinger Berichte, 86 (2006) 137-143

AEROCELL
AEROGELS FROM CELLULOSIC MATERIALS*

Josef Innerlohinger, Hedda K. Weber, and Gregor Kraft

Lenzing AG, Werksstrasse 1, A-4860 Lenzing, Austria
Phone: (+43) 07672-701-3776; Fax: (+43) 07672-918-3776; E-mail: j.innerlohinger@lenzing.com

* This work was presented during the 9th European Workshop on Lignocellulosics and Pulp, 28th-30th August 2006, Vienna, Austria

Within the 6th Framework Program of the European Union the AeroCell project deals with the preparation of aerogels and aerogel-like materials from the renewable resource cellulose. The highly porous cellulosic materials are produced via the well known aerogel-path: preparation of a gel, solvent exchange and supercritical drying. However, the different cellulosic materials and cellulose derivatives that can be used and also the huge number of parameters that can be altered give rise to a vast scientific field. This work presents the results from the first two years of the AeroCell project. The key features of the different ways of production are described as well as the properties of the porous materials and their relation to the production process. Finally some possible applications are presented.

Keywords: *aerogel, nano- and microporous structure, supercritical CO_2, N_2-adsorption/desorption*

Introduction

Aerogels have been synthesised for the first time in the 1930s [1]. During the last years the interest in these materials has reoccurred and a lot of scientific research efforts have been dedicated to them. Aerogels based on silica are most commonly known. These are used in rather exotic applications like detectors for Cherenkov radiation or the capture of cosmic dust in space, but also in more common ones like sound or thermal insulation. In addition to the aerogels made from Silica there is also a variety of aerogels made from organic compounds. The later yield carbon aerogels after a pyrolysis step. The main route for the production of organic aerogels is a sol-gel synthesis from resorcinol and formaldehyde [2] and their derivatives. No extended research in cellulose aerogels exists so far although they are an interesting class of material made from a renewable resource, a fact that is gaining more and more importance nowadays [3]. The project deals with the preparation and possible applications of aerogels and aerogel-like materials based on different cellulosic starting materials (Figure 1). The consortium consists of ten partners from five different countries, who focus on various aspects of the production and the application of this new class of materials. Cellulose aerogels are highly porous and light weighted, yet mechanical stable. They possess a high internal surface and a complex pore structure, which makes them

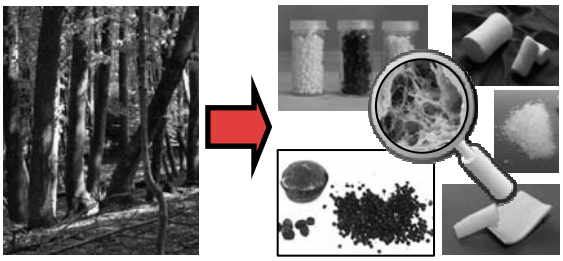

Figure 1. Different aerogel-materials that were produced from cellulosic starting materials.

an ideal candidate for various applications like packaging, controlled release and delivery systems or thermal and acoustic insulation.

AeroCell Production

Different routes for the production of the cellulose aerogels are investigated in this project. For the production of the wet gel precursors cellulose is either directly dissolved (NMMO or NaOH) or derivatives (acetate or carbamate) are used. These four ways are shortly described below followed by the other steps necessary to produce aerogels from these precursors.

Cellulose-NaOH
It has been known for some time that cellulose can be dissolved in aqueous NaOH-solutions in a rather narrow temperature and concentration range. CEMEF[1] is investigating this way in the AeroCell project. Solutions of celluloses with a DP ranging from 170 to 500 were prepared at different concentrations at -6°C and a fixed NaOH concentration of 7.6%. They were gelled by increasing the temperature and finally regenerated, mostly in water, but other solvents (alcohols and acids) were also tested. The influence of the DP and the cellulose concentration on the gel-formation and the properties of the subsequently produced materials have been studied.

Cellulose-NMMO
N-methylmorpholine-N-oxide (NMMO) is a solvent that can completely dissolve cellulose without prior derivatisation. The region in the NMMO/water/cellulose phase diagram, where complete dissolution is possible, is still rather small. However, a wider range of cellulosic materials can be dissolved compared to NaOH.
Cellulose-NMMO solutions were prepared in the following way [4]. Pulp, NMMO (50% - 75%) and stabilizer were placed in a kneader. The pulp was soaked and afterwards the temperature was increased and the excess water was removed by applying low pressure. The kneader was kept under these conditions until all the excess water was removed. Normally during this time the pulp will be dissolved completely. Then the pressure was raised and the solution was kneaded until the pulp was completely dissolved if necessary.
Cellulosic materials in a wide variety can be easily dissolved in NMMO. We were able to dissolve commercial paper pulp and unbleached pulp in NMMO, without any difficulties. The DP of the used materials ranges from 180 to 6200. The addition of other substances (fibres, polymers, soot) to the solution is also possible as long as they fulfil some basic requirements (e. g. stable in NMMO-solution).

Cellulose-acetate
The sol-gel synthesis carried out by CEP[2] is based on the formation of urethane bondings through addition reactions between cellulose acetate and isocyanate [5] – namely the reaction of cellulose acetate with a poly-functional isocyanate (MDI, functionality = 2.7). For this purpose, we dissolved commercial cellulose acetate (from Aldrich, Mn = 50000) with an acetyl substitution degree (DS) equals to 2.4 in acetone. In solution, the unreacted hydroxyl groups can further react with MDI to cross-link. Extra-dry acetone (water content <0.02%) was used in order to prevent any reactions between isocyanate groups and water. Gelation requires the use of a catalyst. Dibutyltin dilaurate was chosen for its adequate catalytic activity towards urethane bondings formation. The associated sol-route process was performed at room

[1]Centre de Mise en Forme des Matériaux, Ecole des Mines de Paris, Sophia-Antipolis, France

[2] Center for Energy and Processes, Ecole des Mines de Paris, Sophia Antipolis, France

temperature under slow mechanical stirring.
The cellulose acetate concentration (mass ratio cellulose acetate - solvent) was fixed to 10% and catalyst concentration (mass ratio catalyst - reagents) to 5%. In addition we have varied the mass ratio between cellulose acetate and isocyanate. During the syneresis stage, the gels were washed three times with pure acetone.

Cellulose-carbamate
AeroCell precursors based on cellulose carbamate (CC) were prepared by FhG-IAP[3]. Cellulose carbamate was synthesized from activated dissolving pulp and urea at elevated temperatures. The resulting cellulose carbamate has a DP of 300-400 and a DS of 0.2-0.6. The cellulose carbamate was dissolved in caustic soda at an appropriate temperature and NaOH concentration. For precipitation and shaping two precipitation routes are available: chemical precipitation (acidic precipitation medium with additives) and thermal precipitation (via a suitable temperature regime). Cellulose carbamate solutions with 1%, 3%, 5% and 9% were prepared and tested with respect to the effects of the chemical and thermal precipitation.

Shaping of the precursors
In most cases the liquid solutions were poured in a (cylindrical) mould and then gelled/solidified. In addition there are some more shaping methods to produce cellulose aerogels of different sizes and forms. GeniaLab[4] used the JetCutter technology [6] to produce beads with a size of 400µm to 1200µm from the cellulose solutions. The bead generation is achieved by cutting a solid jet of fluid coming out of a nozzle by means of rotating cutting wires into cylindrical segments, which then form beads due to surface tension on their way to a hardening device.
By dripping the molten cellulose-NMMO solution through a hole into the regeneration bath small spheres can were produced. The cellulose-NMMO solutions can also be cast into films or spun into fibres, which offers the possibility of continuous production.

Cross-linking
The regenerated hydrogels can be cross-linked to further influence the properties (pore size, mechanical stability) of the finally obtained aerogels. The School of Materials[5] developed several methods (two- or one-stage) to produce cross-linked hydrogels. A variety of cross-linking agents were investigated (an example is shown in Figure 2) as well as the distribution of the cross linkers inside the gels.

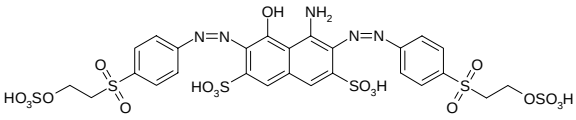

Figure 2. C.I. Reactive Black 5 – one of the cross-linking agents used for the hydrogels.

Solvent exchange
For those wet gels, which are not in a solvent suited for drying with supercritical CO_2, one or more solvent exchange steps are necessary. One solvent is replaced by the following via several solvent exchanges. This has to be done very carefully, because even very small residues of H_2O can greatly interfere with the SC-drying process. The kinetics of the solvent exchange (as well as those of regeneration) have been studied by CEMEF and Lenzing AG [7]. During regeneration and solvent exchange a severe shrinkage of the cellulosic bodies was observed sometimes. This behaviour can be influenced partly by choosing

[3] Frauenhofer Gesellschaft – Institut für angewandte Polymerforschung, Golm, Germany
[4] GeniaLab Biotechnologie GmbH, Braunschweig, Germany
[5] School of Materials, University of Manchester, Manchester, England

appropriate preparation parameters (e.g. higher cellulose concentration results in lower shrinkage).

Supercritical drying

If the wet gels are dried at ambient conditions the occurring strong capillary forces will cause the porous structure to collapse. To prevent this, a more sophisticated method of drying the acetone or alcohol gels is necessary. The samples are dried under supercritical conditions using CO_2 to displace the solvent. The dryings were performed by CEP at laboratory scale and by NATEX[6] at larger scale with a 5l/1000bar plant.

The wet gels were filled into a high-pressure vessel and were soaked in the organic solvent before the extractor was closed. Liquid CO_2.(at about 60 bar) from a storage vessel was pressurized to between 90 and 200 bar and heated up to 40°C before entering into the extractor. After the drying conditions were reached the samples remained in the extractor without CO_2 flow and the CO2 was able to penetrate into the sample and to form a homogeneous mixture with the organic solvent inside and outside the sample. Then the CO_2 flow started and diluted the organic solvent-CO_2 mixture. After the extractor the loaded CO_2 was depressurized in order to separate the organic solvent from the gaseous CO_2. CO_2 flow was maintained until the organic solvent is completely removed from the samples. In the final step the extractor was depressurized to atmospheric pressure according to a certain pressure-time gradient and the dried samples were unloaded.

As mentioned above small residues from chemicals can worsen the result of the SC-drying. But also the drying procedure itself has a big influence on the properties of the obtained aerogels. Figure 3 compares the results of different drying runs (A-E) of acetone gels with varying cellulose content

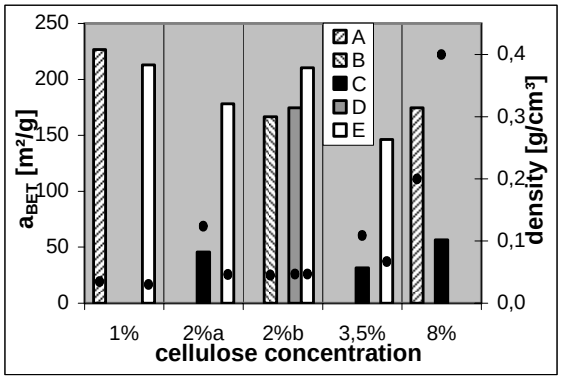

Figure 3. Influence of SC-drying (A-E) on the AeroCell-properties Bars show the BET-surface (left) and the dots the corresponding density (right).

obtained from the NMMO-route. Changed was the temperature ramp, which was used to bring the extractor vessel to the desired supercritical conditions. The temperature and pressure used for the drying were the same, but already the changes in the temperature ramp can have quite big effects.

Pyrolysis

Organic aerogels can be pyrolysed to yield aerogels consisting completely of carbon. This pyrolysis is performed by CEP under inert atmosphere (nitrogen flow) at 800°C.

Figure 4. Different carbon aerogels - precursors (left to right): cross-linked, cellulose-acetate, cellulose-carbamate, NaOH/cellulose and NMMO/cellulose.

Various pyrolysis programs have been investigated in order to reduce the high mass loss during this step. The theoretical mass loss for cellulose is about 60%, but literature reports 80% - 85% [8]. The mass loss in this project so far is between 83% and 99% for the pure cellulose aerogels, for the cellulose acetate aerogels values between 70% and 83% are achieved. Figure 4 shows some of the about 30g carbon aerogels produced so far.

[6] NATEX Prozesstechnologie GesmbH, Ternitz, Austria

Properties and Applications

A thorough characterisation of the aerogels as well as the precursors is vital to understand and finally to control the structures and the thereof resulting properties of the materials that are produced via the different routes and by varying the numerous parameters. The characterisation of highly porous materials is no trivial problem [9]. A whole work package of the AeroCell project is dedicated to this task. In the following some of the research findings are presented.

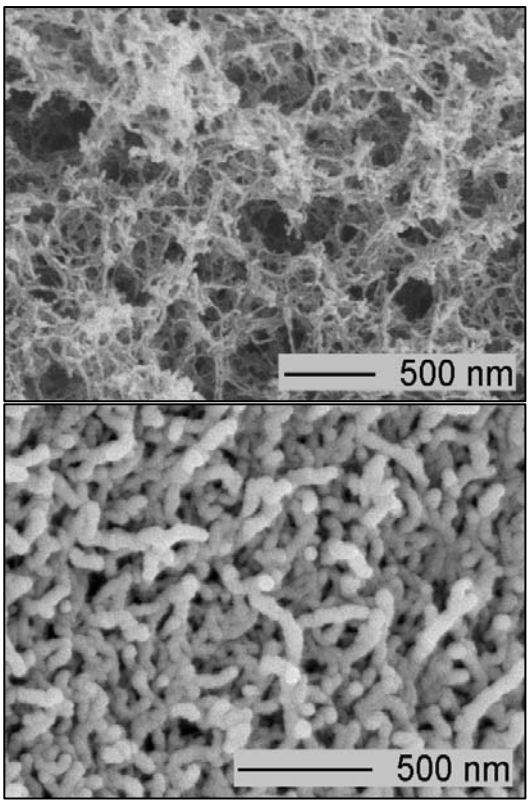

Figure 5. Top: interior of aerogel monolith from NaOH/cellulose. Bottom: surface of aerogel JetCutter-beads from NMMO/cellulose.

Depending on the way of production the internal structure of the aerogels can be quite different. Figure 5 shows electron micrographs (SEM by FhG-IAP) of two such examples: the sponge-like structure, which is found for most cellulose aerogels, and a more worm-like structure, which was observed on the surface of beads produced with the JetCutter.

Due to their highly porous structure the cellulose aerogels possess good sound and thermal insulating properties. The thermal conductivity was measured at CEP via a hot-wire method under variable partial vacuum of air (from secondary vacuum to atmospheric pressure). As for the thermal conductivity measurement a sample volume of approximately 500cm³ is necessary (which is quite a lot at this stage of the project), only a few measurements have been performed so far. Figure 6 shows one of the first results obtained with a cellulose aerogel (from NMMO/ cellulose, ρ=0.08g/cm³) compared with commercial PU-foam (ρ=0.1g/cm³) and with a silica aerogel (ρ=0.2g/cm³) synthesised at CEP. Already this first result with a non-optimized sample formulation/preparation shows the great thermal insulating properties.

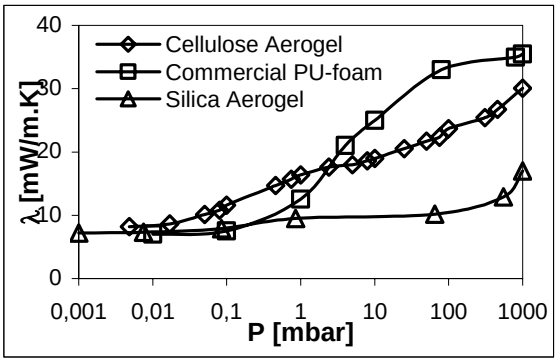

Figure 6. Thermal conductivity of AeroCell compared with PU-foam and a Silica aerogel.

Another parameter, which is important for some applications, is the biodegradability of the aerogel samples. This was investigated by Novamont[7] (using the international standard ISO14851). Figure 7 shows the results from these tests for a cellulose aerogel compared to other materials. The lower, but still good, biodegradability of the AeroCell sample could arise from small traces of chemicals used during the production chain still inside the sample or could be due to the special material properties. This point still has to be clarified in future experiments

[7] Novamont S. p. A., Novara, Italy

with more samples and also the starting materials.

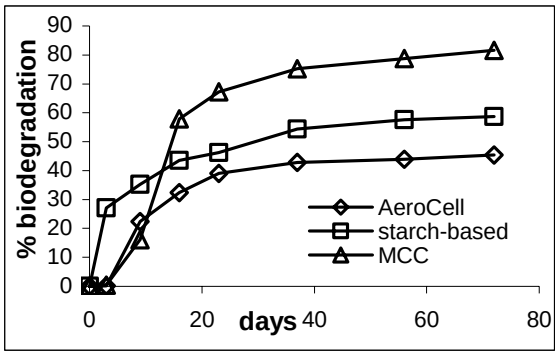

Figure 7. Biodegradation of AeroCell compared to a starch-based material by Novamont and to microcrystalline cellulose.

Their unique properties like high internal surface, high porosity and low density and the fact that they are produced from the natural renewable resource cellulose makes the cellulose aerogels an interesting candidate for various applications. Some of the partners within the AeroCell consortium focus on evaluating applications for the different aerogels. Cognis[8] is investigating the possibilities of using the cellulose aerogels as carrier systems for controlled release applications in the cosmetic and nutritional field. Packaging applications and the necessary requirements therefore are tested by Novamont.

The usability of the carbon aerogels for electrochemical applications is investigated by LEPMI[9] and by SAFT[10]. Carbon aerogels have been characterised at LEPMI for use in proton exchange membranes fuel cells. Preliminary results for the samples obtained after pyrolysis of cellulose-acetate aerogels have been recently published [10].

Conclusions

Although cellulose aerogels are a class of highly interesting materials no extended research about them existed so far. The AeroCell project now succeeded in producing a wide variety of different aerogels from cellulose and its derivatives and to characterise them in detail. Some relations between the production conditions and the properties of the finally obtained aerogels were successfully established. The different manufactured aerogels show promising properties for the applications evaluated so far, but much more research is necessary before commercialisation.

Acknowledgements

The described work is supported by the EC 6th framework program, contract number NMP3-CT2003-505888 (project acronym: AeroCell). The authors thank the partners for the good cooperation, stimulating discussions and for supplying data for this publication.

References

[1] S. S. Kistler, Coherent expanded aerogels, J. Phys. Chem. 1932, 36, 52-64.

[2] R. W. Pekala, Organic aerogels from the polycondensation of resorcinol with formaldehyde, J. Mater. Sci., 1989, 24, 3221-3227

[3] Busch, R., T. Hirth, A. Liese, S. norhoff, J. Puls, O. Putz, D. Sell, C. Syldatk, R. Ulber, Nutzung nachwachsender Rohstoffe in der industriellen Stoffproduktion, Chem. Ing. Tech., 2006, 78(3), 219-228

[4] J. Innerlohinger, H. K. Weber, G. Kraft, Aerocellulose, Aerocellulose: Aerogels and Aerogel-like Materials made from Cellulose, submitted to Macromol. Symp.

[5] F. Fischer, A. Rigacci, R. Pirard, S. Berthon-Fabry, P. Achard, Cellulose-based aerogels, Polymer

[8] Cognis Deutschland GmbH & Co. KG, Düsseldorf, Germany

[9] Laboratoire d'Electrochimie et Physico-chimie des Matériaux et des Interfaces, Institut National Polytechnique de Grenoble, Grenoble, France

[10] SAFT S. A., Bordeaux, France

(in press)
[6] U. Prüße, J. Dalluhn, J. Breford, K.-D. Vorlop, Production of spherical beads by JetCutting, Chem. Eng. Technol., 2000, 23, 1105-1110
[7] G. Kraft, in preparation
[8] D.-Y. Kim, Y. Nishiyama, M. Wada, S. Kuga, Graphitization of highly crystalline cellulose, Carbon, 2001, 39, 1051-1056
[9] G. W. Scherer, Characterization of aerogels, Adv. Colloid Interface Sci., 1998, 76-77, 321-339
[10] F. Fischer, E. Guilminot, M. Chatenet, A. Rigacci, S. Berthon-Fabry, E. Chainet, P. Achard, Nanostructured carbons from cellulose aerogels for PEM-FC electrodes: elaboration and electrochemical characterization, Proceedings 7th European Symposium on Electrochemical Engineering, 2005, Toulouse (France)

Lenzinger Berichte, 86 (2006) 144-153

BEITRAG ZUR STRUKTUR VON LYOCELLFASERN, ERSPONNEN AUS AMINOXIDHYDRATEN BZW. IONISCHEN FLÜSSIGKEITEN

Christoph Michels und Birgit Kosan

Thüringisches Institut für Textil- und Kunststoff- Forschung e.V., Breitscheidstr. 97, D-07407 Rudolstadt, Germany, Tel.: (+49) 0 36 72 – 37 92 20, Fax: (+49) 0 36 72 – 37 93 79, E-mail: kosan@titk.de

Ausgehend von Modellversuchen zur Fadenbildung aus Lösungen mit Cellulosen unterschiedlicher Provenienz, Molmasse und Molmassenverteilung allein oder in Mischung mit löslichen bzw. nichtlöslichen Zweitkomponenten und wasserhaltigem NMMO bzw. wasserfreiem BMIM-Cl als Lösungsmittel wurde der Einfluss des Wassers, der Cellulose und der Zusatzkomponenten auf die binodale und / oder spinodale Entmischung während der Fadenbildung, das Entstehen des Kapillar- / Porensystems sowie die Eigenschaften der Lyocellfasern untersucht.

Keywords: *Aminoxidhydrat, Cellulosefaser, Faserstruktur, Ionische Flüssigkeit, Lyocellfaser*

Einleitung

In einem früheren Beitrag [1] berichteten wir über das Lösen und den Lösungszustand von Cellulose in Aminoxidhydraten und ionischen Flüssigkeiten. Im Folgenden sollen nun die strukturellen Änderungen während der Fadenbildung und Nachbehandlung im Vordergrund stehen. Als Lösungsmittel wurde stellvertretend für die Aminoxide das N-Methylmorpholin-N-Oxidhydrat (NMMO) und für die ionischen Flüssigkeiten das 1-Butyl-3-Methylimidazoliumchlorid (BMIM-Cl) eingesetzt. Beide Verbindungen gehören zur Klasse der EDA-Lösungsmittel [2], wirken auf die Cellulose weder derivatisierend noch komplexierend, bewirken eine Umwandlung von Cellulose I in II vor dem Lösen, unterscheiden sich aber signifikant im Wassergehalt und in der Leitfähigkeit. Während das reine NMMO als „innerer Dipol“ praktisch einen Isolator (< 2 µS) darstellt, besitzt das wasserfreie BMIM-Cl eine echte Ionenleitfähigkeit (> 2 mS). Beide Lösungsmittel scheinen unabhängig von ihrem chemischen Aufbau und ihrer physikalischen Struktur zu einem vergleichbarem Lösungszustand zu führen, da nach den Ergebnissen in Tabelle 1 Cellulosen gleicher Molmasse und Molmassenverteilung bei gleichen Molverhältnissen zu gleichen Nullscherviskositäten führen [1].

Tabelle 1. Nullscherviskositäten verschiedener Celluloselösungen.

Datei	Cellulose	Lösungsmittel	DP_Z / DP_L [1)]	Molverhältnis	$c_{Cell.}$ [%]	η_0 (85°C) [Pas]
VR04041	BW-Linters	BMIM-Cl	454/442	1 : 7,9	10,5	2 500
VR04048	BW-Linters	NMMO-MH	454/445	1 : 7,9	13,2	2 470
VR04042	BW-Linters	BMIM-Cl	454/444	1 : 6,0	13,4	12 610
VR04009	BW-Linters	NMMO-MH	454/434	1 : 6,0	17,0	11 470
VR04007	Vorh.-Sulfat	BMIM-Cl	569/533	1 : 7,1	11,5	20 500
VR04004	Vorh.-Sulfat	NMMO-MH	569/537	1 : 7,1	14,4	21 160

[1)] $DP_{Z/L}$ Cuoxam DP vom Zellstoff bzw. der Cellulose nach dem Lösen

Damit sollte ein Vergleich der Lösungen aus wasserhaltigem NMMO und wasserfreiem BMIM-Cl Aussagen zum Einfluss des Lösungsmittels und des Wassers auf die Struktur der Cellulose und des Porensystems bei der Fadenbildung und Nachbehandlung ermöglichen. Im Gegensatz zu den EDA-Lösungsmitteln besteht beim Lösen des Cellulosexanthogenates in verdünnter Natronlauge (Viskoseprozess) bzw. des Cellulose-2,3-Kupfertetraminkomplexes in verdünntem Ammoniak (Cuoxamverfahren) das Lösungsmittel vorwiegend aus Wasser und das Molverhältnis Cellulose / Lösungsmittel ist um den Faktor 1 : ~10 signifikant größer.
Die fehlende Derivatisierung und Komplexierung des NMMO bzw. BMIM-Cl sowie das geringe Molverhältnis zur Cellulose haben wahrscheinlich zur Folge, dass die lateralen Bindungen zwischen den Celluloseketten und damit die Kristallinität der Cellulose verloren geht, eine freie Beweglichkeit der Celluloseketten aber nicht vorliegt und damit eine Nahordnung, vergleichbar einer flüssig-kristallinen (smektischen) Phase, in der Lösung oder besser Spinnmasse erhalten bleibt. Diese Nahordnung dürfte auch dafür verantwortlich sein, dass die Orientierung und Kristallisation beim Lyocellprozess immer räumlich und zeitlich getrennt ablaufen.

Weiterhin gilt als Arbeitshypothese, dass die Spinnmasse während der Fadenbildung eine binodale und/oder spinodale Phasentrennung erfährt und diese zum Entstehen einer durchgehenden Cellulose- und einer durchgehenden Lösungsmittelphase führt. Letztere zeichnet für die Ausbildung der Poren- bzw. Kapillarstruktur verantwortlich und determiniert weitgehend die hydrophilen Eigenschaften der Lyocellfaser. Das experimentell leicht zugängliche Wasserrückhaltevermögen korreliert mit dem Poren-/Kapillarvolumen und die Faserparameter feinheitsbezogene Reißfestigkeit, Reißdehnung und Schlingenreißfestigkeit korrelieren mit der Cellulosestruktur.

Experimentelles

Für die Untersuchungen wurden Vorhydrolysesulfat-, Sulfit- und Baumwoll-Linters- Zellstoffe unterschiedlicher Provenienz (Tabelle 2) als Hauptkomponente verwendet, deren wesentliche analytische Parameter in Tabelle 3 enthalten sind.
Zum Verspinnen gelangten sowohl mikroskopisch einphasige Lösungen aus Cellulose und Lösungsmittel, als auch mehrphasige Lösungen aus Cellulose, Zusatzkomponente und Lösungsmittel.

Tabelle 2. Herkunft der eingesetzten Zellstoffe.

- Sai - Lyo	Eukalyptus - Sulfitzellstoff (Sappi Saiccor SA)
- Bacell (Solucell 400)	Eukalyptus - Vorhydrolysesulfatzellstoff (Lenzing AG)
- Viskokraft - LV	Buche - Vorhydrolysesulfatzellstoff. (IP Natches USA)
- Alistaple - LD	Fichte - Sulfitzellstoff (Western Pulp CA)
- CHN - BWL	Baumwoll-Linters-Zellstoff (Shanghai CHN)

Tabelle 3. Analytische Parameter eingesetzter Zellstoffe.

Zellstofftyp / Kurzbezeichnung	Cell.$_{atro}$ [%]	$[\eta]_{Cuen}$ [1)] [ml/g]	DP_{Cuoxam}	α-Cell. [%]	$COOH$ [µmol/g]	$\succ CO$ [µmol/g]	Fe [2)] [ppm]	Cu [2)] [ppm]
Sai Lyo (S-556)	92,3	383	556	93,8	22,5	22,2	1,4	3,9
Bacell (B-569)	92,7	365	569	96,0	4,2	16,5	2,3	0,7
Viskokraft (VK-389)	93,4	238	389	94,9	0,0	36,9	3,5	0,8
Alistaple (AS-1168)	93,8	781	1168	94,9	6,2	21,2	2,6	1,9
BWL (BWL-454)	92,6	367	454	95,2	0,0	11,7	8,4	0,3

[1)] nach DIN 54270 (Teil 2); [2)] nach DIN EN ISO 11885 (E22)

Als Zusatzkomponenten dienten einerseits im Lösungsmittel lösliche Stoffe, wie Cellulose, Cellulosederivate, Stärke und Stärkederivate und andererseits im Lösungsmittel unlösliche Komponenten wie PP, PTFE und hydrophobierte Kieselsäure mit Dimensionen im Nano- bzw. Mikrometerbereich.
Die Lösungsherstellung im Vertikalkneter sowie die Charakterisierung von Lösungsqualität durch Partikelanalyse und Lösungszustand durch rheologische Messungen wurde mehrfach beschrieben [1,3,4].
Zum Verspinnen der Polymerlösungen diente eine Kolbenspinnapparatur, bestehend aus einem temperierbaren Zylinder, einem Spinnkopf, einem klimatisierten Luftspalt, einem Spinnkasten, einer Umlenk- und einer Abzugsgalette. Über einen Präzisionsvortrieb des Kolbens wird die Spinnmasse definiert dem Spinnkopf zugeführt. Der Spinnkopf dient zur Aufnahme einer Filterpackung, eines beheizbaren Wärmetauschers und einer Spinndüse. Der Wärmetauscher gestattet, neben einer Vergleichmäßigung der Spinnmassetemperatur, bei geringen Verweilzeiten unmittelbar vor der Spinndüse ein stufenloses Anheben der Spinnmassetemperatur von 80 auf bis zu 150°C. Eine notwendige Voraussetzung, um mit der gleichen Ausrüstung unter vergleichbaren Bedingungen Cellulosespinnmassen mit NMMO bzw. BMIM-Cl als Lösungsmittel verspinnen zu können. Am Spinnkopfeingang befindet sich ein Massedruck- und ein Massetemperatur- und zwischen beheizbarem Wärmetauscher und Spinndüse ein Massetemperatursensor. Der Luftspalt zwischen Spinndüse und Fällbad kann räumlich getrennt von der Außenatmosphäre betrieben werden, ist durch vertikale Bewegung des Spinnkastens und/oder Fällbades stufenlos zwischen 10 und 150 mm einstellbar und gestattet eine Klimatisierung mit gasförmigen Medien definierter Temperatur und Feuchte. Das Fällbad, in der Höhe zwischen 10 und 100 mm stufenlos einstellbar, passiert den Spinnkasten über eine Pumpe im Kreislauf und kann in Temperatur und Durchflussmenge in weiten Grenzen variiert werden. Fällbad und Fadenschar trennen sich beim Verlassen des Spinnkastens über eine Bodenöffnung. Eine Umlenkgalette erfasst die Fadenschar und transportiert sie über eine Changierung zur Abzugsgalette. Die Nachbehandlung erfolgt diskontinuierlich in Stapeln oder kontinuierlich im Strang.
Die Bestimmung des Wasserrückhaltevermögens der spinnfeuchten und/oder gewaschenen ($WRV_{ng.}$) und der getrockneten (WRV) Lyocellfaser erfolgte nach DIN 53814 und die der textilphysikalischen Faserparameter Faserfeinheit (T_{10}) nach DIN EN ISO 1973, feinheitsbezogene Reißfestigkeit trocken ($\sigma_{kond.}$) und Reißdehnung ($\varepsilon_{kond.}$) nach DIN EN ISO 5079 und die feinheitsbezogene Schlingenreißkraft ($\sigma_{Schl.}$) nach DIN 53843 Teil 2.

Versuchsergebnisse und Diskussion

Zur experimentellen Bestätigung der in der Einleitung aufgestellten Arbeitshypothese wurden 3 verschiedene Typen von Lösungen hergestellt, versponnen und die Fasern im spinnfeuchten und/oder gewaschenen und getrockneten Zustand charakterisiert. Eine Zusammenstellung der Spinnversuche enthalten die Tabellen 4 und 5.

Tabelle 4. Lösungen aus Cellulose und Lösungsmittel.

Nr.	Cellulose-provenienz	Cell. [%]	LM	Fällbad	T_{10} [dtex]	$\sigma_{kond.}$ [cN/tex]	$\varepsilon_{kond.}$ [%]	$\sigma_{Schl.}$ [cN/tex]	WRV_{ng} th. [%]	WRV_{ng} gef. [%]	WRV [%]
1	S-556	12,0	NMMO	Wasser	1,30	45,7	17,1	19,5	195	197	73
2	B-569	12,9	NMMO	Wasser	1,29	48,1	15,7	29,1	180	181	68
3	VK-389	15,2	NMMO	Wasser	1,25	54,5	13,8	15,9	148	---	68
4	BWL-454	17,0	NMMO	Wasser	1,61	46,3	13,2	18,0	130	218 [1)]	62
5	BWL-454	17,0	NMMO	Ethanol	1,59	45,9	13,2	15,8	316	354 [1)]	67
6	BWL-454	17,0	NMMO	Isoprop.	1,59	40,8	12,1	9,0	390	503 [1)]	67
7	B-569	9,6	BMIM-Cl	Wasser	1,68	38,6	13,2	20,0	193	185	84
8	B-569 [2)]	10,4	BMIM-Cl	Wasser	1,70	38,2	15,2	18,7	177	175	82
8a	B-569 [3)]	10,4	BMIM-Cl	Wasser	1,68	43,8	15,3	18,8	177	154	74
8b	B-569 [4)]	10,4	BMIM-Cl	Wasser	1,57	44,7	12,0	24,3	177	143	69
9	B-569	13,7	BMIM-Cl	Wasser	1,73	51,4	13,5	28,6	129	131	67
10	B-569	14,8	BMIM-Cl	Wasser	1,73	48,8	14,3	30,3	118	119	67

[1)] Probe spinnfeucht, NMMO-haltig ohne Wäsche in Wasser bzw. Alkohol [2)] SV_a = 2,9; D_A = 70 µm
[3)] SV_a = 6,0; D_A = 100 µm [4)] SV_a = 10,9; D_A = 130 µm

Tabelle 5. Lösungen aus Cellulose /-derivat, Zusatzkomponente und NMMO.

Nr.	Cellulose-proven.	Zusatzkomponente	Anteil	Cell. [%]	T_{10} [dtex]	$\sigma_{kond.}$ [cN/tex]	$\varepsilon_{kond.}$ [%]	WRV_{ng} th. [%]	WRV_{ng} gef. [%]	WRV % [1)]
1	S-556	K^+ 2,3 µmol/g [K)]	100	11,4	1,15	48,7	17,0	207	---	92
2	S-556	K^+ 64 µmol/g	100	12,6	1,28	44,6	16,8	185	---	116
3	S-556	K^+ 220 µmol/g	100	12,0	1,37	40,5	14,3	195	---	161
4	VK-389	Cell.-200	95:5	14,0	1,27	38,8	11,8	163	175	76
5	VK-389	Avicel-155	90:10	13,4	1,34	37,1	13,8	172	179	77
6	VK-389	AS-1168	85:15	14,3	1,34	32,5	18,2	172	187	80
7	S-556	CMC A^-: 403 µmol/g	90:10	13,2	1,30	37,9	12,1	175	----	173
8	S-566	Kartoffelstärke [2)]	83:17	12,2	1,29	32,4	13,7	191	----	113
9	S-556	Fibraffin K-75 [3)]	80:20	12,1	1,20	32,9	13,7	193	----	130
10	S-556	Fibraffin 2285 [4)]	70:30	10,0	1,19	27,6	12,1	239	----	176
11	S-556	Aerosil R 104 [5)]	90:10	12,0	1,36	40,1	17,5	195	----	64
12	S-556	WAX-PP [6)]	90:10	11,8	1,23	37,7	17,1	199	----	81
13	S-556	PTFE-2-Emulsion [7)]	97: 3	12,0	1,22	44,7	16,5	195	----	72
13a	(13)10 Min. bei 90°C gewaschen u. getrocknet				1,22				----	54
14	S-556	PTFE-3-Emulsion [8)]	97: 3	12,1	1,21	37,4	14,1	193	----	76
14a	(14)10 Min. bei 90°C gewaschen u. getrocknet				1,23				----	56

[K)] kationisiert mit Glycidyltrimethylammoniumchlorid; [1)] WRV korrigiert auf den Celluloseanteil; [2)] Raisio Chemicals Finnland; [3)] Kationische Kartoffelstärke mit 0,25 % Stickstoff Südstärke GmbH; [4)] Kationische Kartoffel stärke mit 0,52 % Stickstoff; [5)] hydrophobierte Kieselsäure ∅ 12 nm Degussa; [6)] micronisiertes PP 0,5 - 21 µm ; [7)] Verteilung 60-1000 nm, Max. 315 nm; [8)] Verteilung 30-800 nm, Max. 250 nm

Die Celluloselösungen unterscheiden sich dabei wie folgt:

1. Cellulose bzw. Cellulosederivat und das Lösungsmittel bilden eine homogene, einphasige Lösung. Da keine separaten Phasen existieren, können auch keine Grenzflächenspannungen bestehen [$\sigma_{Gr.} \equiv 0$]. Das Verformen im Spinndüsenkanal bei konstanter Temperatur erfolgt ohne Phasentrennung. Offen bleibt die Frage, ob im Luftspalt unter Abkühlung eine binodale Entmischung der Lösung stattfindet oder ob der orientierte Lösungsstrahl erst beim Eintritt in das Fällbad eine spinodale Entmischung in eine durchgehende Cellulose- und eine durchgehende Lösungsmittelphase erfährt.

⇒ Lösungen Tabelle 4 (1 – 10) und Tabelle 5 (1 – 3)

2. Cellulose oder Cellulosegemisch, Lösungsmittel und gegebenenfalls Zusatz-

stoffe bilden mikroskopisch homogene, mehrphasige Lösungen. In diesem Fall gilt für die Grenzflächenspannung die Bedingung $\sigma_{Gr.} > 0$ und die Verteilung der Phasen ist so fein, dass ihr Durchmesser D_λ die Wellenlänge des sichtbaren Lichtes [$\lambda \sim 320$ nm] deutlich unterschreitet. Dieser Fall gilt wahrscheinlich für Mischungen aus Cellulose/-derivaten und Stärke -derivaten, wenn alle Komponenten bei erhöhter Temperatur im Lösungsmittel löslich sind, aber beim Abkühlen eine binodale Entmischung erfahren. Für Aminoxidlösungen, die 12,2 % einer Mischung aus 83 % Cellulose und 17 % Stärke enthalten, konnte ein solches Verhalten beobachtet werden. Die mikroskopische Querschnittsaufnahme der binodal entmischten Lösung zeigt Abbildung 1.

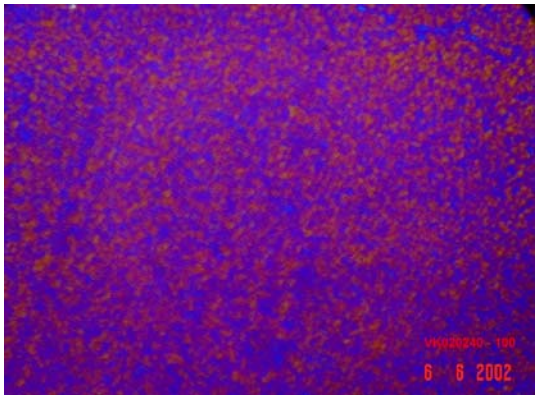

Abbildung 1. Cellulose / Stärke-Mischung in NMMO nach binodaler Entmischung.

Bei derartigen Lösungen erfolgt der Düsenverzug aus homogener Lösung, während die Orientierung im Luftspalt bei abnehmender Temperatur mit einer binodalen Entmischung einhergeht.

⇒ Lösungen Tabelle 5 (4 – 10)

3. Cellulose, Lösungsmittel und Zusatzkomponente bilden mikroskopisch mehrphasige Lösungen, d.h. es gelten die Bedingungen $\sigma_{Gr.} > 0$ und $D_\lambda > 320$ nm. D.h., das Verformen im Düsenkanal und Luftspalt erfolgt durchgängig in getrennten Phasen. Die Zusatzkomponente ist von Anfang an Bestandteil der Lösungsmittelphase und befindet sich später als „Einlagerung“ im Poren-/ Kapillarsystem.

⇒ Lösungen Tabelle 5 (11 – 14)

Unabhängig davon, welcher Lösungstyp versponnen wird, erfährt der aus der Spinndüse austretende Lösungsstrahl im Luftspalt eine Querschnittsreduzierung unter gleichzeitiger Orientierung der Cellulose- und Lösungsmittelphase entsprechend dem Verzugsverhältnis. Der spinnfeuchte Faden besteht in jedem Fall aus einer durchgehenden, orientierten Cellulosephase und einer durchgehenden, orientierten Lösungsmittel-/Fällbadphase, die gegebenenfalls die Zusatzkomponente als Einlagerung enthält. Der Lösungsmittelaustausch beim Passieren des Fällbades und bei der anschließenden Wäsche ist mit einer weiteren Querschnittsverminderung verbunden. Nach vollständigem Lösungsmittelaustausch sollte das Wasserrückhaltevermögen der Lyocellfaser ein Maximum betragen und berechenbar sein. Im nachfolgenden Trocknungsprozess bewirkt die Wasserverdampfung ein irreversibles Kollabieren des Porensystems unter weiterer Querschnittsverminderung bis zur beginnenden Kristallisation der orientierten Cellulosephase unter gleichzeitiger Fixierung des noch vorhandenen Poren-/Kapillarsystems.

Betrachtet man z.B. eine Spinnmasse aus 13 % Cellulose und 87 % NMMO, die zu einer Faser der Feinheit 1,7 dtex versponnen wird, so ergibt sich folgender Ansatz (Abbildung 2):

Celluloselösung:	M% Cell. + M% NMMO + M% H_2O	$\Rightarrow$ 13 + 75,4 + 11,6
Molverhältnis:		$\Rightarrow$ 1 : 8 : 8
Molmasse.	162 / 117 / 18	$\Rightarrow$ 162 + 936 + 144
Verhältnis Lösungsmittel : Cellulose		$\Rightarrow \frac{936+144}{162}\cdot 100 = 667\,\%$
Austausch NMMO gegen Wasser		$\Rightarrow$ 162 + 144 + 144
Verhältnis Wasser : Cellulose (WRV_{ng})		$\Rightarrow \frac{144+144}{162}\cdot 100 = 178\,\%$

Abbildung 2. Kalkulation des zu erwartenden Wasserrückhaltevermögens einer nie getrockneten Faser (WRV_{ng}), ersponnen aus einer 13%igen Celluloselösung in NMMO.

Tatsächlich werden diese Werte für das WRV_{ng} der niemals getrockneten Faser von ca. 178 % durch das Experiment bestätigt (siehe Lösungen 1+2 in Tabelle 4). Untersucht man Fasern vor einem vollständigen Lösungsmittelaustausch, so findet man Werte zwischen 178 und 667 %, was ebenfalls durch die Praxis (siehe Lösung 4 in Tabelle 4) bestätigt wurde. Allgemein lässt sich das WRV_{ng} der niemals getrockneten Faser nach vollständigem NMMO-Austausch entsprechend der Beziehung (1)

$$WRV_{ng.}^{NMMO} = 26{,}6 \cdot \frac{100 - \%Cell.}{\%Cell.} \qquad (1)$$

berechnen.

Ersetzt man das Lösungsmittel NMMO durch BMIM-Cl, so führt die Berechnung für die gleiche Spinnmassezusammensetzung zu einem analogen Ansatz (Abbildung 3):
Auch dieses Ergebnis wird durch das Experiment bestätigt (siehe Lösungen 7-10 in Tabelle 4). Allgemein gilt nach vollständigem BMIM-Cl-Austausch für das WRV der niemals getrockneten Lyocellfaser die Beziehung (2):

$$WRV_{ng.}^{BMIMCl} = 20{,}5 \cdot \frac{100 - \%Cell.}{\%Cell} \qquad (2)$$

Verwendet man keine wässrigen, sondern alkoholische Bäder, so muss das Rückhaltevermögen der Faser nach vollständigem Austausch des Lösungsmittels gegen einen Alkohol deutlich höher liegen. Für die gleiche Celluloselösung ergibt sich beim Austausch gegen Ethanol 316 % und beim Austausch gegen Isopropanol 390 % (siehe Lösungen 5+6 in Tabelle 4).
Das bedeutet aber, dass das Rückhaltevermögen der spinnfeuchten, gewaschenen Faser und damit ihr Porenvolumen von der Cellulosekonzentration der Spinnlösung, der Molmasse des Lösungsmittels, und der Molmasse des Fällbades abhängig ist.

Celluloselösung:	M% Cell. + M% BMIM + M% Cl	$\Rightarrow$ 13 + 69,4 + 17,6
Molverhältnis:		$\Rightarrow$ 1 : 6,2 : 6,2
Molmasse.	162 / 140 / 35,5	$\Rightarrow$ 162 + 865 + 219
Verhältnis Lösungsmittel : Cellulose		$\Rightarrow \frac{865+219}{162}\cdot 100 = 669\,\%$
Austausch NMMO gegen Wasser		$\Rightarrow$ 162 + 111 + 111
Verhältnis Wasser : Cellulose (WRV_{ng})		$\Rightarrow \frac{111+111}{162}\cdot 100 = 137\,\%$

Abbildung 3. Kalkulation des zu erwartenden Wasserrückhaltevermögens einer nie getrockneten Faser (WRV_{ng}), ersponnen aus einer 13%igen Celluloselösung in BMIM-Cl.

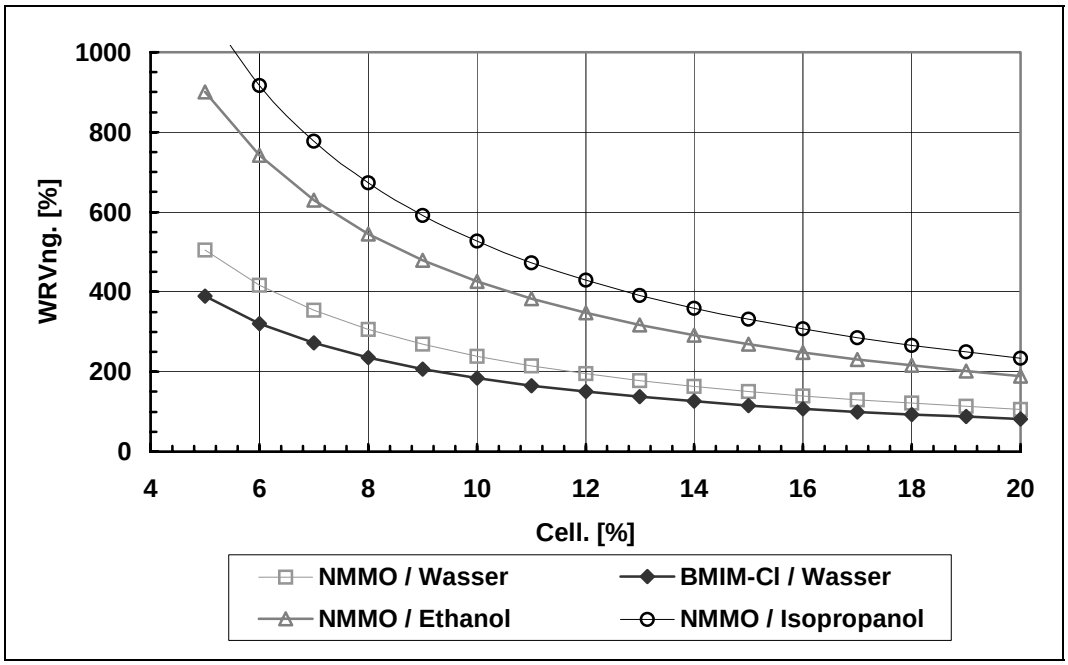

Abbildung 4. WRV_{ng} einer Lyocellfaser nach vollständigem Lösungsmittelaustausch in Abhängigkeit vom Cellulosegehalt für unterschiedliche Lösungsmittel und Fällbäder (berechnet).

In Abbildung 4 sind die berechneten Abhängigkeiten für einen Cellulosekonzentrationsbereich von 4 – 20 % dargestellt. Der Spinnverzug wurde als konstant vorausgesetzt.

Vergleicht man die homogen einphasigen Lösungen 1-10 in Tabelle 4, so findet man bei Spinnverzügen $SV_a \sim 3$ eine sehr gute Übereinstimmung zwischen den theoretisch berechneten und experimentell bestimmten Werten des WRV_{ng}, während bei erhöhten Spinnverzügen (siehe Tabelle 4 / 8-8b) eine Abnahme des WRV_{ng} zu beobachten ist. Obwohl die Werte der spinnfeuchten Faser um ca. 300 % differieren, findet man für die getrocknete Faser nahezu gleiche Werte für das WRV, d.h. durch die Trocknung werden die Unterschiede weitgehend aufgehoben. Nach WAXS-Streukurven, aufgenommen während der Trocknung, erfolgt nahezu unabhängig vom Ausgangswert eine Wasserverdampfung unter irreversiblem Kollabieren des Porensystems bis zu einem WRV von ~75 % (entspricht einem Volumenverhältnis Cellulose : Wasser von ca. 50:50). Ab diesem Zeitpunkt beginnt die Kristallisation der orientierten Cellulosephase unter gleichzeitiger Fixierung des noch vorhandenen Poren-/Kapillarsystems.

Ein Vergleich der Lösungen 1 (Tabelle 4) und 1-3 (Tabelle 5) macht deutlich, dass eine Kationisierung der Cellulose zu homogenen einphasigen Lösungen führt, deren Verspinnung Lyocellfasern mit erhöhtem WRV und vergleichbaren textilphysikalischen Parametern liefert, wobei das WRV erwartungsgemäß mit zunehmenden Kationisierungsgrad ansteigt.

Ein Verspinnen von Lösungen aus Cellulosemischungen (siehe Tabelle 5, Beispiele 4-6) im Vergleich zur reinen Cellulose-lösung (Beispiel 3 in Tabelle 4) macht deutlich, dass bei großen Unterschieden in der Molmasse und Molmassenverteilung die Spinnmassen zwar mikroskopisch homogen erscheinen, aber mehrphasig mit einer Partikelgröße < 320 nm sind. Man findet für die Cellulosemischungen deutlich geringere Festigkeiten, die mit steigendem Zumischungsanteil weiter abnehmen. Das WRV liefert leicht erhöhte Werte. Die cellulosische Zusatzkomponente leistet keinen Beitrag zur Festigkeit, wirkt als Störstelle und lässt möglicherweise die Kristallisation früher einsetzen.

Die Spinnmassen 7-10 in Tabelle 5 sind mikroskopisch homogene, mehrphasige Lösungen, die beim Abkühlen zur binodalen Entmischung neigen. Der Vergleich mit der reinen Celluloselösung 1 (Tabelle 4) zeigt, dass die Faserfestigkeiten entsprechend dem Zumischungsanteil abnehmen und das WRV deutlich ansteigt. Nach Untersuchungen von Nicolai [5] sind die Eigenschaften dieser Fasern (enzymatische Hydrolysierbarkeit, Sorption großvolumiger Säurefarbstoffe, WRV usw.) nicht stabil, sondern ändern sich mit wiederholten Wasch- und Trockenzyklen. Offensichtlich wird die im Kapillarsystem eingelagerte Zusatzkomponente Cellulosederivat, Stärke/-derivat nach und nach herausgelöst. Dies ist ein Beweis dafür, dass in der mikroskopisch homogenen Spinnmasse keine Mischbarkeit der Komponenten im thermodynamischen Sinne vorlag.

Vergleicht man schließlich die Spinnversuche der Lösung 1 (Tabelle 4) mit den Versuchen 11-14 in Tabelle 5, d.h. der Zumischung nicht löslicher, hydrophober Stoffe, so befindet sich diese Komponente erwartungsgemäß als Einlagerung im Kapillarsystem, führt zu einer Abnahme der Faserfestigkeiten ohne einen signifikanten Rückgang des WRV zu bewirken. Erkennbar ist eine Abhängigkeit von der Größenverteilung der Zusatzkomponente. Während micronisiertes PP mit ∅ 11 µm das WRV um ~10 % erhöht, führt die hydrophobierte Kieselsäure mit ∅ 12 nm zu einer Abnahme um ~12 %. Beim Zumischen einer „nanoskaligen“ PTFE-Emulsion erreicht man erst nach zusätzlicher Wäsche der getrockneten Lyocellfaser (Versuche 13a und 14a in Tabelle 5) eine Abnahme des WRV um ~25 %. Man stößt hier auf ein generelles Problem bei der Verarbeitung „nanoskaliger“ Emulsionen, da zur Partikelstabilisierung Tenside zugesetzt werden müssen und diese eine hydrophile Grenzschicht erzeugen, d.h. die Hydrophobie des PTFE wird überkompensiert und erst durch die nachträgliche Wäsche mehr oder minder zurückgewonnen. Die Zumischung von echt hydrophoben Partikeln, deren Größenverteilung der des Kapillarsystems entspricht, sollte durch mehr oder minder starkes „Verstopfen“ des Kapillarsystems eine deutliche Abnahme des WRV der Lyocellfaser ermöglichen.

Die Querschnittsänderungen beim Verspinnen einer Spinnmasse aus 13 % Cellulose und 87 % NMMO zu einer Lyocellfaser der Feinheit 1,7 dtex zeigt in einer maßstabsrelevanten Darstellung Abbildung 5.

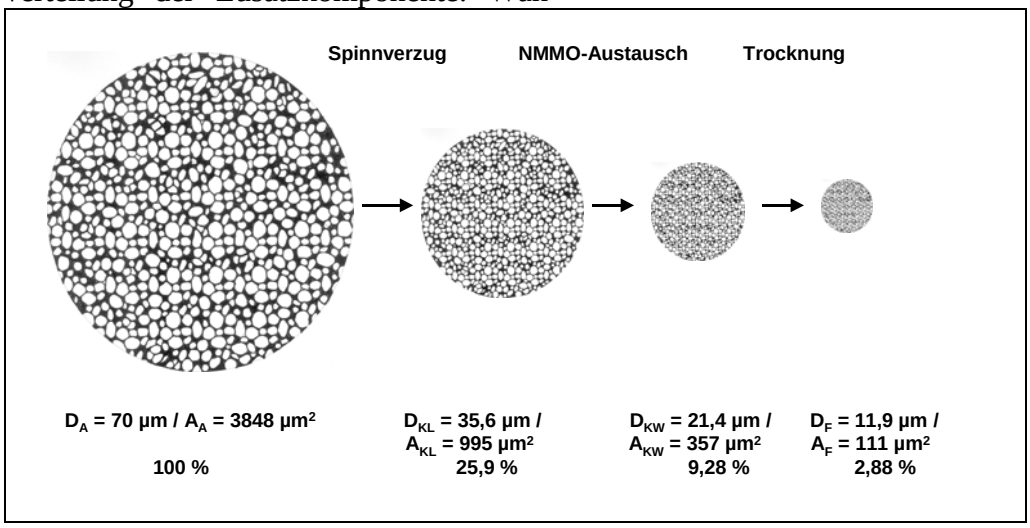

Abbildung 5. Querschnittsflächenänderung beim Verformen, Lösungsmittelaustausch und Trocknen einer Lyocellfaser 1,7 dtex aus einer Lösung mit 13 % Cellulose und 87 % NMMO.

Die Spinnmasse passiert den Spinndüsenkanal mit dem Austrittsdurchmesser D_A = 70 µm, wird im Luftspalt im Verhältnis 1: 3,9 auf einen Kapillardurchmesser D_K = 35,6 µm verzogen, erfährt durch Lösungsmittelaustausch einen Querschrumpf auf einen Kapillardurchmesser von D_{KW} = 21,4 µm, um dann während des Trocknens unter weiterem Querschrumpf einen endgültigen Durchmesser der konditionierten Faser von D_F = 11,9 µm zu erreichen. D.h., setzt man die Austrittsfläche der Spinnkapillare gleich 100 %, so ist die Fadenbildung und Nachbehandlung mit einer Verminderung der Querschnittsfläche > 98 % verbunden.

Eine maßstabsrelevante Darstellung der analogen Vorgänge im Längsschnitt wurde versucht, in Abbildung 6 wiederzugeben.

Der Ausschnitt einer durchgehenden Cellulose- und Lösungsmittelphase, ihre Orientierung beim Düsen- (SV_D = 17,2) und Spinnverzug (SV_a = 3,9), sowie das „Zusammenrücken“ der Cellulosephasen / -fibrillen während des Lösungsmittelaustausches und der Trocknung soll stellvertretend für die ganze Faser stehen.

Diese Modellvorstellung führt zwangsläufig zu einer fibrillären Struktur der Lyocellfaser. Sie besteht aus einer durchgehenden orientierten Cellulosephase, die ein zusammenhängendes System sehr feiner Poren/Kapillaren durchzieht.

Die Cellulosephase sollte weitgehend die mechanischen Fasereigenschaften bestimmen, während das Poren-/Kapillarsystem für die hydrophilen und hydrophiliebedingten Fasereigenschaften wie die Nassscheuerbeständigkeit verantwortlich zeichnet.

Die Cellulosephase ist aus weitgehend parallel angeordneten morphologischen Einheiten, den Mikrofibrillen, aufgebaut. Bedingt durch die bestehende Nahordnung in der Spinnmasse, die Orientierung im Spalt ohne Kristallisation und die Kristallisation

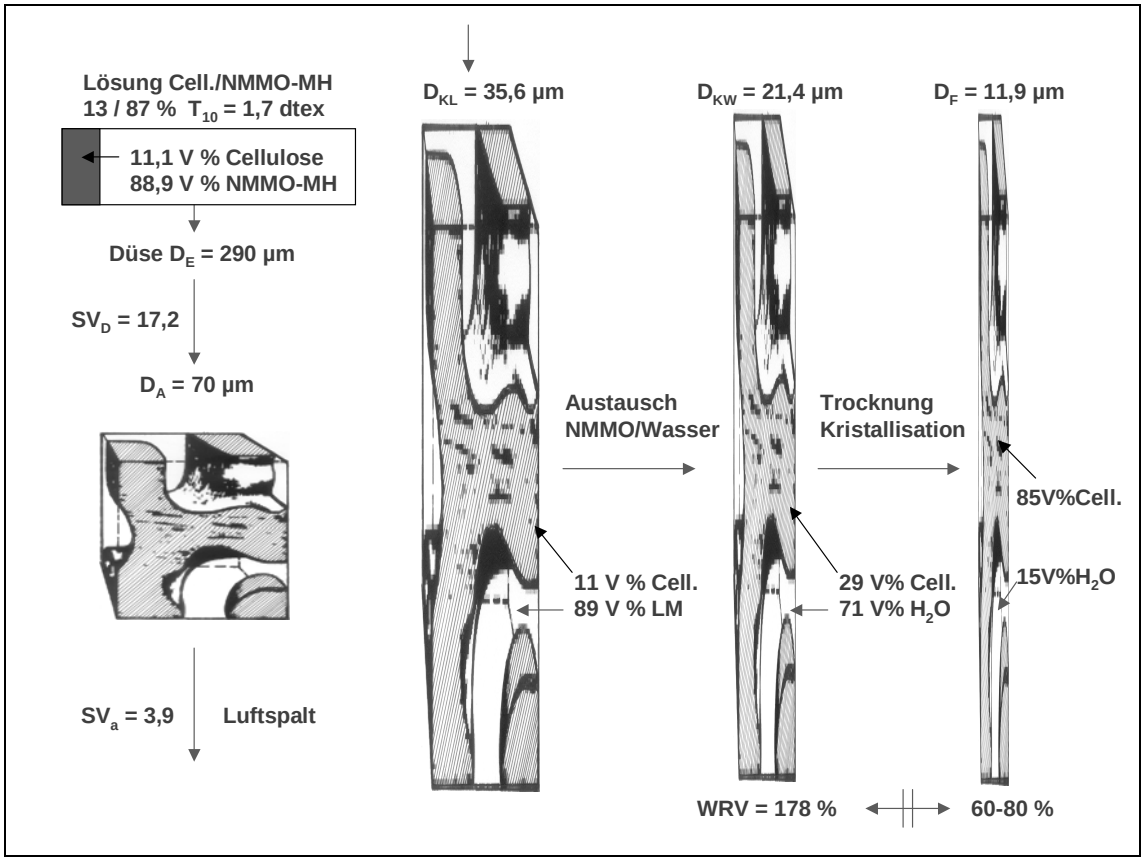

Abbildung 6. Phasendeformation beim Verformen, Lösungsmittelaustausch und Trocknen einer Lyocellfaser 1,7 dtex aus einer Lösung mit 13 % Cellulose/87 % NMMO.

ohne Längsorientierung während der Trocknung, bilden sich die morphologischen Einheiten aus langen kristallinen und kurzen amorphen Bereichen. Der laterale Zusammenhalt zwischen den Fibrillen ist ausschließlich durch Kohäsion bedingt. Die morphologische Struktur der Lyocellfaser bedingt eine hohe Längsfestigkeit und Flexibilität, ausgedrückt durch Schlingenreißfestigkeiten > 50 % der Längsfestigkeit. D.h., Lyocellfasern sind nicht spröde.
Die Kapillaren mit Durchmessern von wenigen Nanometern erzeugen in Gegenwart von Quellmitteln wie Wasser hohe Kapillardrucke und führen unter Wasseraufnahme zu einem mehr oder minder starken Abbau der Kohäsionskräfte zwischen den Fibrillen. Dieses Verhalten erklärt einerseits die Hydrophilie der Lyocellfasern und anderseits ihre geringe Nassscheuerbeständigkeit.
Die simultane Verspinnung von Cellulose und Zusatzkomponenten führt in der Regel zu einem erhöhten WRV der Lyocellfaser. Das kann bedingt sein durch die Hydrophilie der Zusatzkomponente selbst, durch teilweises Verhindern des Kollabierens der Poren/Kapillaren während der Trocknung durch Ablagern der Komponente in den Poren/Kapillaren oder durch eine kristallisationsfördernde Wirkung der Zusatzkomponente und damit früher einsetzende Kristallisation während der Trocknung. Eine Verminderung des WRV erscheint gegenwärtig nur möglich, wenn die Poren/ Kapillaren durch hydrophobe Partikel gleicher Größenordnung bleibend „blockiert“ werden. Der Rückgang des WRV führt in diesem Fall aber zu keiner abnehmenden Fibrillierneigung, da die lateral zwischen den Fibrillen wirkenden Kohäsionskräfte ebenfalls geschwächt sind.

Zusammenfassung

Anhand von Untersuchungen zur Fadenbildung aus Lösungen mit Cellulosen unterschiedlicher Provenienz, Molmasse und Molmassenverteilung allein oder in Mischung mit löslichen bzw. nichtlöslichen Zweitkomponenten und wasserhaltigem NMMO bzw. wasserfreiem BMIM-Cl als Lösungsmittel wurde der Einfluss des Wassers, der Cellulose und der Zusatzkomponenten auf die binodale und/oder spinodale Entmischung während der Fadenbildung, das Entstehen des Kapillar-/ Porensystems sowie die Eigenschaften der Lyocellfasern untersucht.
Unabhängig vom Lösungsmittel besteht die Lyocellfaser aus einer durchgehenden, orientierten Cellulosephase, die die mechanischen Fasereigenschaften bestimmt und einem durchgehenden anisotropen Porensystem, das die Hydrophilie und die hydrophiliebedingten Eigenschaften der Lyocellfaser determiniert.
Zweitkomponenten vermindern die mechanischen Fasereigenschaften, meistens proportional zur zugesetzten Menge, während das Wasserrückhaltevermögen in der Regel ansteigt.

Danksagung

Die Arbeiten wurden im Rahmen eines durch das Bundesministerium für Wirtschaft und Arbeit geförderten Projektes (BMWi – Projekt - Nr. 1077/03) durchgeführt. Außerdem danken die Autoren der Lenzing AG (Austria) für die finanzielle Unterstützung.

Literatur

[1] Michels, Ch.; Kosan, B. Lenzinger Berichte **84** (2005**)** 62-70
[2] Philipp, B.; Schleicher, H.; Wagenknecht, W. Chem. Technol. (1977) 702
[3] Kosan, B. Michels, Ch. Chemical Fibers Int. **49** (1999) 50-54
[4] Michels, Ch.; Kosan, B. Chemical Fibers Int. **50** (2000) 566-561
[5] Nicolai, M. Forschungsbericht AiF Vorhaben 13104 B 2004/2

Lenzinger Berichte, 86 (2006) 154-161

CELLULOSE PROCESSING WITH CHLORIDE-BASED IONIC LIQUIDS

Gino Bentivoglio[1,2], Thomas Röder[3], Mario Fasching[1], Mario Buchberger[3], Herwig Schottenberger[2], and Herbert Sixta[3].

[1] Kompetenzzentrum Holz GmbH, St.-Peter-Str. 25, 4021 Linz, Austria;
Phone: +43 512 507 5117; Fax: +43 512 507 2934; E-mail: g.bentivoglio@kplus-wood.at
[2] Faculty of Chemistry and Pharmacy, University of Innsbruck, Innrain 52a, 6020 Innsbruck, Austria
[3] Lenzing AG, Department of Pulp Research, Werkstrasse 1, 4860 Lenzing, Austria

Ionic liquids (ILs, salts with a melting point below 100 °C) are discussed as solvents for cellulose with a potential for industrial applications. Several chloride containing ILs have been tested for their cellulose dissolving properties. Partly, strong cellulose degradation was observed, but could be prevented in some cases by addition of stabilisers. Cellulose degradation was compared for five chloride ILs.
For three solvents, 1-butyl-3-methyl-imidazolium chloride, 1-allyl-3-methyl-imidazolium chloride and 1,3-diallyl-imidazolium chloride the temperature effect on degradation was studied. Fibres could be obtained by spinning the IL solutions into water; fibre characteristics are presented. The experimental cellulose spinning process with chloride containing ILs is compared to the well-known NMMO-based Lyocell process.

Keywords: *cellulose, ionic liquids, degradation, fibres, Lyocell process*

Introduction

Ionic liquids [1a,b]

Liquids consisting only of ions are called ionic liquids (ILs). In the broader sense, this term includes all kind of salt melts, like sodium chloride at temperatures above its melting point of 800 °C. Today, the term “ionic liquid” refers particularly to salts with a melting point below 100 °C. Salts with a melting point below 25 °C are called “room-temperature ionic liquids” (RTILs).
Usually, ionic liquids consist of a bulky, asymmetric organic cation, like 1-alkyl-3-methylimidazolium, 1-alkylpyridinium, 1-methyl-1-alkylpyrrolidinium or ammonium ions. A wide range of anions is employed, from simple halides which inflect high melting points, to inorganic anions such as tetrafluoroborate and hexafluorophosphate and to large organic anions like bis(trifluorosulfonyl)amide, triflate or tosylate. The notable characteristics of ionic liquids are their non-measurable vapor pressure, thermal stability, wide liquid range, electric conductivity and solvating properties for diverse kinds of materials. Another important feature of ionic liquids is their designability: miscibility with water or organic solvents can be tuned through sidechain lengths on the cation and choice of anion. Furthermore, their properties can be varied by introduction of functional groups.
Because of their specific properties, ionic liquids have found to be useful in many fields, like as reaction media in organic synthesis or electrolytes for electrochemical applications. In addition, their non-volatility results in low impact on the environment and human health advantaging them in comparison to conventional organic solvents, and they

are recognized as "green solvents". However, this term is misleading, as many ILs show aquatic toxicity [2] and spilling into waterways should be avoided.

Ionic liquids as solvents and reaction media for biomacromolecules

The search for suitable cellulose solvents was and is still of great importance in cellulose research, as shaping of cellulose can only be achieved by dissolution and regeneration. The fact that cellulose is earth's most abundant renewable biomacromolecular resource will encourage further development of cellulose-based materials, whose production will require suited solvents.

Today, only one solvent system with structural analogies to ionic liquids is used commercially on large scale, namely *N*-methylmorpholine-*N*-oxide monohydrate (NMMO, Figure 1). The cellulose is dissolved without derivatisation and subsequently spun (Lyocell-process). This system has already been extensively described in the literature. [3] As many ILs, NMMO possesses a quaternized nitrogen atom. Contrarily to ionic liquids, introduction of alkyl substituents into the heterocyclic ring of NMMO decreases the solubility of cellulose.

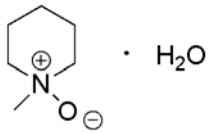

Figure 1. NMMO-monohydrate.

The application of low-melting quaternised nitrogen bases as solvents for cellulose was first proposed by Graenacher in 1934. [4] In his patent, he describes the preparation of cellulose solutions in benzyl pyridinium chloride in the presence of nitrogen bases, possibly derivatisation and subsequent regeneration of the cellulose (e.g. as threads or films) by precipitation in water or alcohols. However, these results were thought to be of little practical value and the invention found no application.

In 2002, the term "ionic liquid" was first mentioned in the context of cellulose. Rogers & coworkers investigated the cellulose dissolving ability of several dialkylimidazolium-based ILs. [5] With 1-butyl-3-methylimidazolium chloride (BMIM-Cl, Figure 2), using a pulp with polymerisation degree of ~ 1000, cellulose solutions up to 10 % could be obtained. The dissolved cellulose was subsequently precipitated in water or organic solvents like ethanol or acetone. Water in concentrations above 1 % prevents the cellulose from being dissolved. By microwave irradiation solutions with 25 % cellulose were prepared. This high solubility under microwave irradiation suggests that decomposition takes place; unfortunately, no information regarding the degradation of the cellulose was given by the authors.

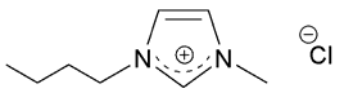

Figure 2. BMIM-Cl.

Since then, a number of cellulose dissolving ionic liquids based on imidazolium cations have been found. In 1-allyl-3-methylimidazolium chloride (AMIM-Cl) cellulose concentrations of 14.5 % (DP of dissolving pulp of ~ 650) and 8 % (DP ~ 1600) could be achieved. [6] 1-Allyl-3-butylimidazolium chloride (ABIM-Cl) and 1,3-diallylimidazolium chloride (AAIM-Cl) are solvents for cellulose as well. [1a]

Among the multitude of tested ILs, especially the chlorides have shown outstanding cellulose dissolving abilities. The exact dissolution mechanism is still unknown; however, it is assumed that the unhydratised chloride anions present in the ionic liquid are able to disrupt the strong intra- and intermolecular hydrogen bonds between the cellulose chains. This assumption is supported by the fact that the dissolving ability increases with the chloride ion concentration. [7]

A number of publications deal with the derivatisation of cellulose in ionic liquids. Cellulose acetate with a substitution degree of 0.9 – 2.7 can be produced in a homogeneous reaction with AMIM-Cl as solvent. [8] In ionic liquids, acylations with various acid chlorides and

carbanilations are possible under mild conditions without the need of a catalyst and in short reaction times. [9] Cellulose ethers can be synthesised in ionic liquids with slight excess of reagents under mild conditions in a water free environment. [10]

Besides cellulose, other biopolymers can be dissolved in ionic liquids, as it is known from NMMO. Lignocellulosic material like straw or wood in the form of chips or sawdust can be dissolved in BMIM-Cl under microwave irradiation. This opens an easy way to isolate individual wood components, for instance by fractional precipitation. [11] Wool (keratin) could be dissolved in BMIM-Cl with concentrations up to 11 % and regenerated by precipitation into water or alcohols. By adding a solution of cellulose in BMIM-Cl prior to precipitation, wool-cellulose composites in form of fibres or membranes were obtained. [12] Ionic liquids have also proven to be good solvents for silk. For instance, the saturation concentration of silk fibroin in 1-ethyl-3-methylimidazolium chloride (EMIM-Cl) at 100 °C is about 23 %. [13] By spinning 10 % solutions into methanol regenerated silk fibres were obtained. [14]

Ionic liquids as solvents in the spinning process

A method for the production of cellulosic moulds like fibres or films from ionic liquids was described by the Thuringian Institute of Textile and Plastics Research. [15] After dispersion in water, the moist cellulose is mixed with aqueous BMIM-Cl solution under addition of stabilizers like sodium hydroxide and propyl gallate. Under shear strain, temperature, and vacuum the suspension is transformed into a homogeneous, nearly water free dope. By passing through a spinneret and an air gap, the solution is shaped into fibres or foils. The cellulose is regenerated by precipitation in an aqueous spinning bath. To regenerate the solvent, the spinning bath is treated with alkaline hydrogen peroxide solution, metal ions are removed with the aid of an ion exchanger and the water is finally removed by distillation. According to the Bisfa-Definition, this process is a Lyocell-process. [16] Fibres obtained by this procedure are very similar to Lyocell fibres obtained by the NMMO-process, due to the comparable dissolution step, the similar solution structure, and the same regeneration conditions. The so called working capacity (tenacity* elongation) in dry conditions is the same. The tendency to fibrillation is comparable, too.

Other patents concerning the production of cellulose fibres from ionic liquids have been applied by Chinese groups. [17, 18]

Experimental

Ionic liquids

Ionic liquids were synthesised according to known procedures. [1a, 19, 20, 21]

Synthesis of 1-Allyl-2-methylpyridinium chloride

To 20.0 ml of 2-picoline (18.9 g, 0.20 mol, 1 eq.) was added an excess of allyl chloride (20.0 ml, 18.6 g, 0.24 mol, 1.2 eq.). The reaction mixture was refluxed for 48 h. After 1 h, a dark brown, heavier phase began to separate. TLC analysis (Merck silica gel, ethyl acetate) showed traces of starting material. After refluxing for additional 24 h, excess allyl chloride was removed by means of an oil pump leaving behind a brown solid. The crude product was washed with 50 ml of diethyl ether and finally dried on a high vacuum line giving 17.4 g of 1-allyl-2-methylpyridinium chloride (brown powder, 51 % of theory). Analytical data: ^{1}H NMR ($CDCl_3$): δ 2.93 (3H, s), 5.10 (1H, d, J 17.2 Hz), 5.35 (1H, d, J 10.6 Hz), 5.66 (2H, d, J 5.6 Hz), 6.00 (1H, m), 7.92 (1H, t, J 6.8 Hz), 8.00 (1H, d, J 7.9 Hz), 8.41 (1H, t, J 7.6 Hz), 9.70 ppm (1H, d, J 5.9). ^{13}C NMR ($CDCl_3$): δ 20.5, 60.0, 120.9, 126.2, 130.0, 130.1, 145.5, 146.9, 155.0 ppm. IR (neat, ATR): 3009, 2921, 2438, 1622, 1573, 1503, 1478, 1455, 1421,

1296, 1158, 1141, 1053, 1004, 930, 829, 794, 770, 710, 663 cm^{-1}. Mp.: 91-94 °C.

Dissolution experiments

Chloride based ionic liquids have been tested in the face of their cellulose-dissolving ability. For this, the preparation of 3 % solutions of cellulose in the ionic liquid was attempted. Beech sulfite pulp was hackled in a kitchen blender, mixed with the ionic liquid, and stirred magnetically in a teflon coated reaction vessel at 100 °C for 2 h. If no dissolution took place under these conditions, stirring was continued for another 2 h at 110 °C. Then, the solution was examined under a light microscope to reveal undissolved fibres. To determine the degradation, 3 % cellulose solutions were prepared and the dissolved cellulose reconstituted by contacting with water. The molecular mass distribution of the reconstituted cellulose samples was determined by gel permeation chromatography using DMA/LiCl as eluent. The method was described in detail earlier. [22]

Spinning experiments

Spinning dopes with concentrations over 10 % were prepared in a vertical kneader. For this, the dry pulp was added to the solvent under optional addition of propyl gallate and/or sodium hydroxide as stabilisers and transformed into a homogenous solution under shear strain, temperature, and vacuum.

Results and discussion [23]

Besides the well-known cellulose solvents AMIM-Cl and BMIM-Cl, new solvents with imidazolium- and methylpyridinium-cations were found (Table 1).

The assumption, that a N-O-bond in the cation would be favorable for cellulose dissolution (structural analogy to *N*-methylmorpholine-*N*-oxide), proved to be false. Cellulose was insoluble in the tested N-alkyloxyimidazolium salts. Ionic liquids functionalised with hydroxyl groups didn't dissolve cellulose as well.

Table 1. Solubility of 3% cellulose in ILs (chlorides).

Ionic liquid	
1-Butyl-3-methylimidazolium chloride (BMIM-Cl)	+
1-Allyl-3-methylimidazolium chloride (AMIM-Cl)	+
1-Allyl-3-butylimidazolium chloride (ABIM-Cl)	+
1,3-Diallylimidazolium chloride (AAIM-Cl)	+
1-Allyl-2-methylpyridinium chloride (A2Pic-Cl)	+
1-Butyl-2,3-dimethylimidazolium chloride	+
1-Allyl-3-propargylimidazolium chloride	reacts
1-Allyloxy-3-methylimidazolium chloride	–
1-Allyl-3-Hydroxyethylimidazolium chloride	–
1-Methyl-3-Hydroxyethylimidazolium chloride	–

Degradation behaviour

The degradation of the dissolved polymer is of great importance to determine the suitability of a solvent system. Rogers & coworkers describe the dissolution of 25 % cellulose in BMIM-Cl with the aid of microwave irradiation. By means of a vertical kneader, 25 % solutions are feasible, too. However, the cellulose is subjected to strong degradation (Figure 7). These results point out the need of a stabiliser to prevent cellulose degradation. With conventional dissolving pulps, cellulose concentrations in the spinning dope of more than 15 % are not within reach due to the high viscosity of such solutions. Higher temperatures lead to stronger degradation; therefore it has no advantage to the NMMO-process.

It was found, that the stability of the cellulose depends clearly on the used cation (Table 2). All of the tested solvents based on chloride showed conspicuous degradation of the cellulose at 100 °C. The degradation was exceptionally strong in AMIM-Cl and A2Pic-Cl, whereas cellulose regenerated from ABIM-Cl and AAIM-Cl showed relatively high molar masses.

Table 2. Molecular masses of cellulose after dissolution in various ILs.

Solvent	M_n (x 10^3)	M_w (x 10^3)
pulp: Euca-PHK (1)	68.8	200.2
BMIM-Cl	37.9	100.8
AMIM-Cl	19	31.4
A2Pic-Cl	14.8	24
AAIM-Cl	43.1	117.2
ABIM-Cl	48.2	150.5

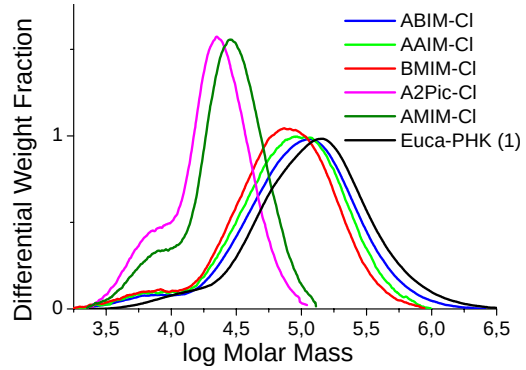

Figure 3. Molecular mass distribution of cellulose after regeneration from ILs.

The effect of the temperature on degradation was examined on the well-known solvents BMIM-Cl and AMIM-Cl and on the new solvent AAIM-Cl. At the same time, the effect of propyl gallate, a stabiliser with antioxidative action used in the NMMO-process, was investigated.

BMIM-Cl: As expected, the extent of degradation increased with the temperature. Above 90 °C, drastic degradation occurred. Propyl gallate had no stabilising effect under these conditions.

Table 3. Molecular masses in BMIM-Cl at various temperatures, with/without propyl gallate.

	Not stabilised		propyl gallate	
	M_n	M_w	M_n	M_w
	(x 1000)	(x 1000)	(x 1000)	(x 1000)
80 °C	48.2	160.3	49.7	164.4
90 °C	48.1	149.6	46.7	148.6
100 °C	37.9	100.8	39	98.2

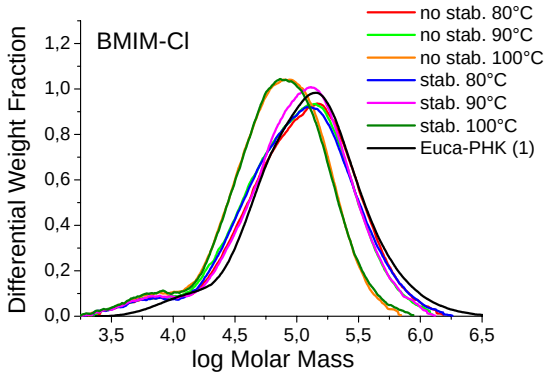

Figure 4. BMIM-Cl at various temperatures, with/without propyl gallate.

AMIM-Cl: A distinct temperature effect could be observed. The degradation was pronounced even at 80 °C. Propyl gallate showed no significant influence on the degradation behaviour.

Table 4. Molecular masses in AMIM-Cl at various temperatures, with/without propyl gallate.

	Not stabilised		Propyl gallate	
	M_n	M_w	M_n	M_w
	(x 1000)	(x 1000)	(x 1000)	(x 1000)
80 °C	38.7	98.8	38.5	100
90 °C	28.3	57.3	29.2	62.2
100 °C	19.4	32.9	19	31.7

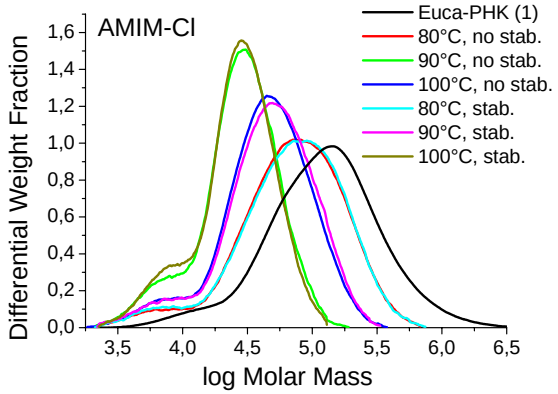

Figure 5. AMIM-Cl at various temperatures, with/without propyl gallate.

AAIM-Cl: This solvent showed temperature dependent degradation, too. However, compared to the other two solvents, the degradation occurred to a much lesser extent. Propyl gallate had no stabilizing effect.

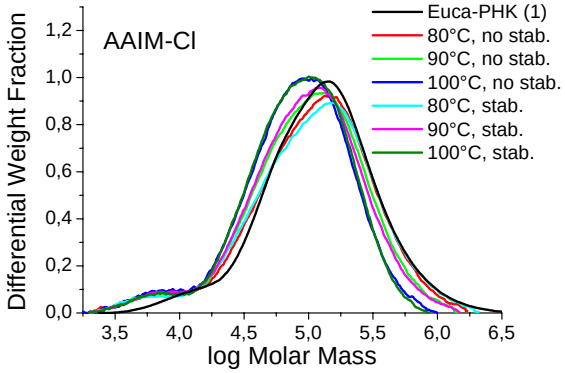

Figure 6. AAIM-Cl at various temperatures, with/without propyl gallate.

The experiments showed clearly, that the substituents on the cation have an effect on the stability of the dissolved cellulose. Propyl gallate was useless under these conditions.

Table 5. AAIM-Cl at various temperatures, with/without propyl gallate.

	Not stabilised		Propyl gallate	
	M_n	M_w	M_n	M_w
	(x 1000)	(x 1000)	(x 1000)	(x 1000)
80 °C	49.5	174.4	50.6	182.2
90 °C	49.5	152.9	47.6	145.5
100 °C	43.1	117.2	45.2	114.2

Spinning experiments

BMIM-Cl: The addition of propyl gallate in conjunction with sodium hydroxide has a stabilising effect. [15] Fibres could be spun from 11 % stabilised solutions.

Table 6. Stabiliser effect on the molecular masses of cellulose in BMIM-Cl.

	M_n [10^3 g/mol]	M_w [10^3 g/mol]
Euca-PHK (2)	67	170
stabilised	52.3	148.9
not stabilised	10	27

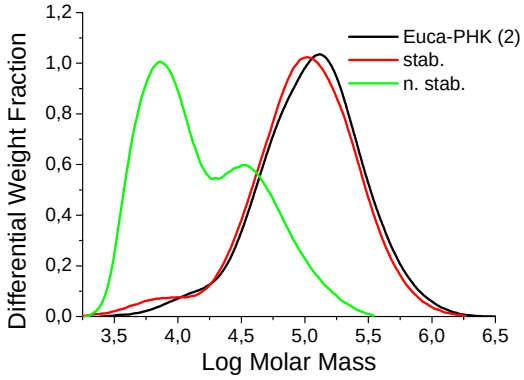

Figure 7. Molecular mass distribution of reconstituted cellulose out of stabilised 11 % solution (red) and not stabilised 25 % solution (green) in BMIM-Cl. 100 °C, stirring time 3-4 h.

AMIM-Cl: 15 % solutions could be obtained at 100 °C within 2 h. However, the cellulose was strongly degraded by this procedure to an extent which affected the spinnability of the solution. By stirring for 5 h at a temperature of 70 °C, 11 % solutions were obtained. Due to the lower temperature, the degradation remained on a reasonable scale and spinning was possible.

Table 7. Temperature effect on molecular mass of cellulose in AMIM-Cl dopes.

	Mn (x1000)	Mw (x1000)
Euca-PHK (2)	67	170
70 °C	45.6	127.6
100 °C	8.5	14.5

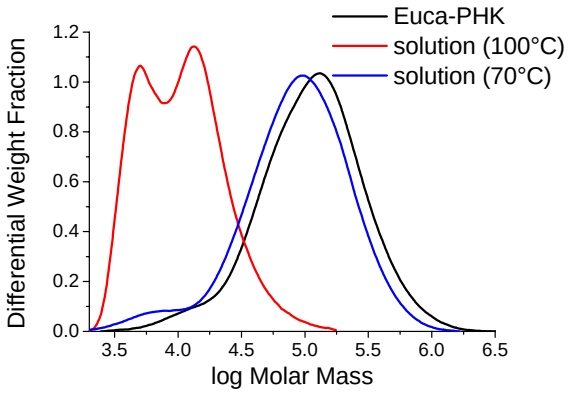

Figure 8. Molecular mass distribution of reconstituted cellulose out of 15 % solution (red, 100 °C, stirring time 2 h) and 11 % solution (blue, 70 °C, stirring time 5 h) in AMIM-Cl.

Fibre characteristics

The spinning conditions in our experiments are similar to the spinning conditions in the NMMO-process. The resulting fibres show comparable characteristics, like a round profile, smooth surface, similar fibrillation behaviour and the same "working capacity". The observed, somewhat higher tenacities are compensated by lower elongation values. Advantages of IL-Lyocell-fibres over NMMO-Lyocell-fibres could not be observed. From our point of view, there is no significant difference in the physical and chemical characteristics.

Cellulose dissolution: Chloride containing ionic liquids compared to NMMO

A comparison with the NMMO-process shows no improvement of the fibre characteristics, especially of the fibrillation tendency. The similar processes lead to similar fibre properties. ILs have a lower melting point than NMMO, which simplifies handling of the solvents. However, the required processing temperatures are the same in both cases.

Table 8. Comparison of fibre data for the solvents BMIM-Cl, AMIM-Cl, and NMMO

Fibre	Titre	Tenac. (cond)	Elong. (cond)	Tenac. (wet)	Elong. (wet)	Working capacity (cond)
	dtex	cN/tex	%	cN/tex	%	%cN/tex
BMIM-Cl*	0.9	51.2	8.5	45.3	11.6	435
BMIM-Cl*	2.1	45	7.5	32.8	8.1	338
AMIM-Cl*	2.2	41.6	12.2	33.4	17.6	508
TENCEL (NMMO)**	0.9	38	14	31	18	532
TENCEL (NMMO)**	1.3	37	13	30	15	481

* experimental fibre; **standard fibre

Stabilisers are required in both cases. The preparation of the spinning dopes is more expensive than in the NMMO-process, because of the required nearly complete removal of water. An advantage is the thermal stability of the system, no auto-catalytically initiated exothermic run-away-events were observed. The degradation of the cellulose is higher than in NMMO. Little is known about the reaction mechanisms, except that they differ from those in the NMMO-system. As for the solution process, the recovery of the solvent from the aqueous spinning bath is more energy-consuming because of the need for complete water removal. For industrial processes, the high corrosivity of chloride melts to steel may be of further concern. The potential toxicity of the ILs is also a disadvantage. For this reasons, we don't consider the tested chloride-based ILs to be an alternative to the NMMO system.

Conclusions

Chloride-based ionic liquids are suitable solvents for cellulose dissolution and for fibre spinning. The resulting fibres belong to the class of Lyocell-fibres and show comparable or same characteristics as fibres obtained from NMMO solutions. The advantages of ionic liquids, like their non-volatility, thermal stability, chemical modifiability, and low melting points are countervailed by their numerous disadvantages: the need for stabiliser use, potential (aquatic) toxicity, corrosivity, and a higher energy input for dope preparation and solvent recovery due to the required complete removal of water.
In their textile quality, IL-fibres are virtually indistinguishable from conventional Lyocell-fibres on NMMO-basis.
Up to now, an industrial application of the tested IL-systems for the production of man-made cellulosic fibres is not useful. Firstly, none of these systems showed significant advantages in comparison to already used technologies; secondly, the recovery of the solvent is more expensive than in the NMMO process.

Acknowledgement

Financial support was provided by the Austrian government, the provinces of Lower Austria, Upper Austria and Carinthia as well as by the Lenzing AG. We also express our gratitude to the Johannes Kepler University, Linz, the University of Natural Resources and Applied Life Sciences, Vienna, and the Lenzing AG for their in kind contributions.

References

[1] a) Laus, G.; Bentivoglio, G; Schottenberger, H; Kahlenberg, V.; Kopacka, H.; Röder, T.; Sixta, H.; Lenzinger Berichte, 2005, 84, 71-85; ref. cit.; b) Zhu, S.; Wu, Y.; Chen, Q.; Yu, Z.; Wang, C.; Jin, S.; Ding, Y.; Wu, G.; Green Chemistry, 2006, 8, 325-327.

[2] C. Pretti, C. Chiappe, D. Pieraccini, M. Gregori, F. Abramo, G. Monnia, L. Intorre; Green Chem., 2006, 8, 238–240.

[3] Rosenau, T.; Potthast, A.; Sixta, H.; Kosma, P. Prog. Polym. Sci. 2001, 26, 1763-1837.

[4] Graenacher, C. Cellulose Solution. U.S. Pat. 1,943,176, 1934.

[5] Swatloski, R. P.; Spear, S. K.; Holbrey, J. D.; Rogers, R. D. J. Am. Chem. Soc. 2002, 124, 4974-4975.

[6] Zhang, H.; Wu, J.; Zhang, J.; He, J. Macromolecules 2005, 38, 8272-8277.

[7] Remsing, R.; Swatloski, R.; Rogers, R.; Moyna, G.; Chem. Commun., 2006, 1271-1273.

[8] Wu, J.; Zhang, J.; He, J.; Ren, Q.; Guo, M. Biomacromolecules 2004, 5, 266-268.

[9] Barthel, S.; Heinze, T.; Green Chemistry, 2006, 8(3), 301-306.

[10] Myllymaeki, V.; Aksela, R.; Int. Pat. Appl. WO 2005054298 A1 20050616 (2005); Chem. Abstr. 143:28326.

[11] Myllymaeki, V.; Aksela, R.; Int. Pat. Appl. WO 2005017001 A1 20050224 (2005) Chem. Abstr. 142:242565.

[12] Xie, H.; Li, S.; Zhang, S. Green Chem. 2005, 7, 606-608.

[13] Phillips, D. M.; Drummy, L. F.; Conrady, D. G.; Fox, D. M.; Naik, R. R.; Stone, M. O.; Trulove, P. C.; De Long, H. C.; Mantz, R. A. J. Am. Chem. Soc. 2004, 126, 14350-14351.

[14] Phillips, D. M.; Drummy, L. F.; Naik, R. R.; De Long, H. C.; Fox, D. M.; Trulove; P. C.; Mantz, R. A. J. Mater. Chem. 2005, 15, 4206–4208.

[15] Michels, C.; Kosan, B.; Meister, F; Verfahren und Vorrichtung zur Herstellung von Formkörpern aus Cellulose. Int. Pat. WO2006000197, 2005.

[16] http://www.bisfa.org/booklets/Terminology%202006.doc, aufgerufen am 22.08.2006.

[17] Wang, H.; Liu, W.; Li, D.; Tu, X.; Zhao, T.; Yang, B.; Zhang, Y.; Yu, M.; Chinese patent CN 1804161 A 20060719 (2006) Chem.Abstr. 145:212470.

[18] Wang, H.; Liu, W.; Li, D.; Tu, X.; Zhao, T.; Yang, B.; Zhang, Y.; Yu, M.; Chinese patent CN 1818160 A 20060816 (2006) Chem.Abstr. 145:273168.

[19] Zhang, H.; Wu, J.; Zhang, J.; He, J. Macromolecules 2005, 38, 8272-8277.

[20] Mizumo, T.; Marwanta, E.; Matsumi, N.; Ohno, H. Chem. Lett. 2004, 33, 1360-1361.

[21] Andre, M.; Loidl, J.; Laus, G.; Schottenberger, H.; Bentivoglio, G.; Wurst, K.; Ongania, K.-H. Analytical Chemistry 2005, 77, 702-705.

[22] Schelosky, N.; Röder, T.; Baldinger, T. Das Papier 1999, 53, 728-738.

[23] Results presented in part as a poster at the 231st ACS National Meeting, March 26-30, 2006 Atlanta, GA.